Vindkraftskonsortiet
FFA MIUU CTH

Sammanställning av föredrag vid

EUWEC'96, i Göteborg, maj 1996

sammanställt av S-E Thor

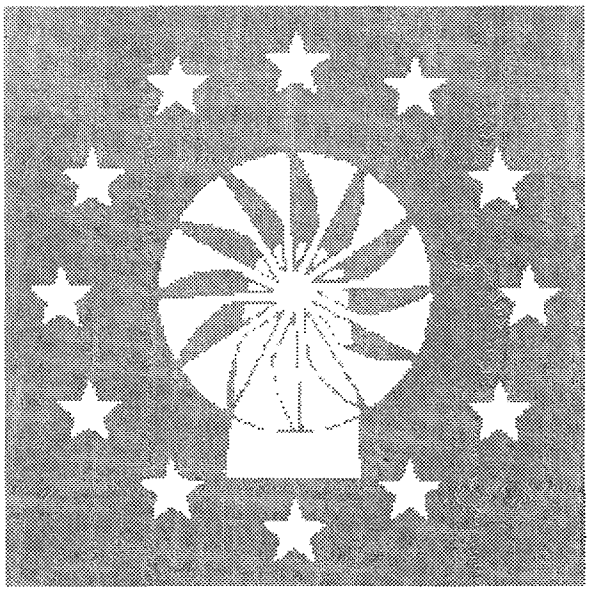

FFA FLYGTEKNISKA FÖRSÖKSANSTALTEN
THE AERONAUTICAL RESEARCH INSTITUTE OF SWEDEN

FFA i Bromma är landets centrala instans för flygteknisk forskning och provning. Verksamheten startade 1940, är uppdragsfinansierad och sorterar förvaltningsmässigt under försvarsdepartementet.

FFA utför forsknings- och provningsverksamhet som stöd för svensk flygindustris utveckling av militära och civila flygplan samt för att tillgodose svenska flygmyndigheters behov av särskild kompetens i samband med upphandling, certifiering och användning av flygmateriel. Andelen utländska kunder inom flyg- och rymdbranschen ökar. FFAs kunder finns också inom andra branscher, t ex energi, miljö och transporter.

FFAs verksamhetsområden är aerodynamik, hållfasthet, akustik och flygsystemteknik. De olika kompetenserna utnyttjas också inom det svenska vindenergiprogrammet. FFA är riksmätplats för tryck.

Vid FFA finns vindtunnlar för olika hastighetsområden – upp till sju gånger ljudhastigheten. Den senast byggda transsoniska vindtunneln – T1500 – är en av de modernaste i Europa. FFAs anläggningar omfattar också ett hållfasthetslaboratorium, en flygforskningssimulator och ett strukturakustiskt laboratorium med landets största ekofria rum.

Vindkraftskonsortiet
FFA MIUU CTH

Sammanställning av föredrag vid

EUWEC'96, i Göteborg, maj 1996

sammanställt av S-E Thor

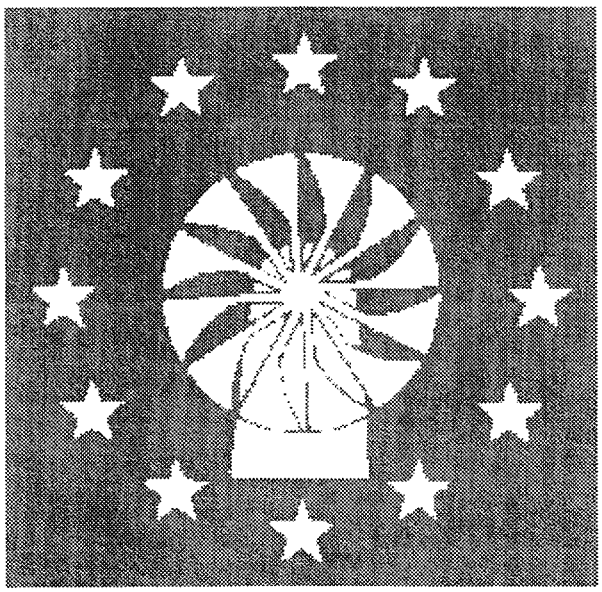

FFA FLYGTEKNISKA FÖRSÖKSANSTALTEN
THE AERONAUTICAL RESEARCH INSTITUTE OF SWEDEN

FLYGTEKNISKA
FÖRSÖKSANSTALTEN
THE AERONAUTICAL RESEARCH INSTITUTE OF SWEDEN
B.O.Box 11021, S-161 11 Bromma, Sweden
Phone +46 8 634 1000, Fax +46 8 25 34 81

Sammanfattning

Den Europeiska Unionen arrangerar vart tredje år en konferens och utställning, European Union Wind Energy Conference and Exhibition, EUWEC. I år, 1996, arrangerades EUWEC´96 i Göteborg. Vart tredje år arrangerar dessutom European Wind Energy Association, EWEA, sin vindenergikonferens. Konferenserna är förskjutna ett och ett halvt år inbördes. Det innebär att det i Europa arrangeras vindkonferenser var 18:e månad.

Konferensen var mycket lyckad och uppskattad av deltagarna. Detta berodde till stor del på de ändamålsenliga lokalerna (Svenska Mässan), bra organisation samt ett bra stöd från de svenska sponsorerna - Göteborg Energi, Vattenfall, Nutek, Elforsk, NWP, Kvaerner, Teknikgruppen AB, Nordic Wind Power och FFA. Vädrets makter var dock inte de bästa under veckan. Regn och rusk gjorde dock att det inte kändes som någon uppoffring att sitta inomhus.

Kommande europeiska vindenergikonferenser arrangeras i Dublin EWEC'97 och i Nice EUWEC'99.

I denna rapport redovisas de svenska föredrag som har anknytning till vindkraftskonsortiet.

Innehållsförteckning

1 Inledning

Den 20-24 maj 1996 arrangerades Europeiska Unionens Vindenergikonferens i Göteborg. Konferensen samlade cirka 600 deltagare. Detta var en ökning med 15% i jämförelse med föregående EU-konferens i Travemünde 1993. VKK presenterade 17 olika föredrag och "posters". En av dessa fick pris för bra innehåll och tydlig presentation.

Erfarenheter som presenterades på konferensen visar att vindkraften ökar kraftigt i de olika europeiska länderna. Under det senaste året, 1995, har utbyggnaden varit mycket kraftig i ett flertal länder, speciellt i Indien och Tyskland. Under 1995 ökade den installerade vindkraften [MW] med 40% och vid slutet av 1995 fanns det totalt i hela världen ungefär 5100 MW. Produktionen av el från dessa vindkraftverk motsvarar ungefär produktionen från två stora kärnkraftverk.

Tyskland är det land som har mest vindkraft i världen. Danmark ligger på andra plats och Sverige finns på sjunde plats med 80 MW installerad effekt.

2 Konferensen

ALLMÄNT

Årets konferens hade samlat ungefär så många deltagare som man kalkylerat med i den budget som hade upprättats inför konferensen.

Antal deltagare	527
Utställarrepresentanter	69

Det var 38 olika länder var representerade. Nedan deltagarantal från några olika länder:

Sverige	89	Finland	21
Danmark	86	Frankrike	14
Tyskland	77	Japan	14
Holland	49	Italien	13
Storbritannien	49	USA	12
Spanien	21	Övriga länder	70
Grekland	20		

Totalt presenterades 91 muntliga föredrag och 260 "posters". Dessutom fanns en utställning i anslutning till konferenslokalerna. Det fanns 31 utställare i den 600 m² stora lokalen.

Invigningen av konferensen var planerad att genomföras av Energiminister Anders Sundström, denne fick förhinder och invigningen genomfördes därför av Göran Bengtsson från Länsstyrelsen i Göteborg och Bohuslän. Invigningsprogram framgår av figur 1. Nutek representerades vid invigningen av generaldirektör Birgit Erngren. Hennes tal återges i Appendix 0.

På konferensens sista dag delades Paul la Cour priset ut till Aloys Wobben. Motiveringen lyder fritt översatt - för hans utomordentliga insatser för den europeiska vindenergiindustrin och speciellt för hans insatser att utveckla och kommersialisera innovativ teknik som en del av hans vision om en renare framtid.

Utställningen av "posters" fick speciell uppmärksamhet vid konferensen genom det "poster award" som delades ut till bästa "poster". Dessutom utdelades priser i fem olika delgrupper. Sverige erövrade här ett av prisen genom CAN-projektet, se föredrag nummer 19 nedan.

REGLERTEKNIK

Denna avdelning omfattade 6 muntliga och 17 poster presentationer. Ur reglersynpunkt var 3 muntliga presentationer intressanta (OR14.1, OR14.2, OR14,6). Den första behandlade en regulator för variabelt varvtal och bladvinkel som beräknades för att minska utmattning. Inga resultat som visade att så verkligen var fallet visades dock. Invändningar finns också mot deras evaluering av modellerna, där man jämför simulering med uppmätta värden. I simuleringen används estimerad vind, och estimatet är grundat på mätningar av samma variabler som man sedan använder i jämförelsen. Den andra var en sammanfattning av den rapport som Garrad & Hassan skrev om stallreglering av aggregat med variabelt varvtal. Den sista muntliga presentationen handlade om hur man skall ta fram realiseringar av vindbyar. Metoden bygger på resultat som är gamla och välkända inom stokastiska processer. Verifikation efterlyses dock. Garrad & Hassans windowsversion av BLADED demonstrerades. Programmet föreföll vara en användarvänlig version av VIDYN. Invändningarna var huvudsakligen att man hade begränsade valmöjligheter när det gällde design. Man kunde till exempel inte simulera en direktdriven maskin. Regleringen var inte heller särskilt generell, men här fanns det möjlighet att kommunicera med en extern, egenhändigt framtagen, regulator.

ELSYSTEM

Variabelt varvtal har kommit på bred front. I stort sett alla stora vindkraftsproducenter har nu prototyper eller försöksanläggningar i drift med variabelt varvtal. Även problematiken med nätåterverkan har kommit i fokus, då vindkraftsinstallationerna blir större och större.

Ett flertal artiklar och föredrag berörde direktdrivna generatorer, resultat och slutsatser från några dem kommenteras här. S. Jöckel har visat att permanentmagneter, trots sitt höga pris, är ett billigare alternativ än elektrisk magnetisering. Han har gjort en konstruktionsstudie av en 750 kW generator och visade att en direktdriven generator ledde till lägre pris på den producerade elektriciteten än en konventionell generator med växel. P. Lampola hade en poster som diskuterade olika alternativ till likriktare för en direktdriven generator. Han visade att diodlikriktare leder till lägre uteffekt från generatorn samt en lägre verkningsgrad. A. Veltman et al. presenterade i sin artikel en studie som jämförde olika generatortyper. Till exempel visas att en asynkron axialflödesgenerator kommer att få en orimligt låg verkningsgrad (<50%). Resultaten som visas för en reluktansgenrator tyder på att den skulle bli större och ha lägre verkningsgrad än en permanentmagnet generator, någon sådan slutsats dras dock inte. Enercon visade bilder från sin 1.5 MW prototyp med direktdriven generator. Generatorn är elektriskt magnetiserad vilket skiljer sig från vad som föreslagits i ovan nämnda artiklar. Det konstaterades att Enercons generator har en väldigt stor diameter (ca 7m) och är mycket tung (48 ton).

3 Svenska föredrag

3.1 Inledning

VKK var representerade vid konferensen med 17 föredrag och posters. I denna rapport finns en sammanställning av dessa. Dessutom bifogas några föredrag med anknytning till VKK:s verksamhet.

Samtliga föredrag kommer senare att presenteras i proceedings från konferensen. Översiktligt program för konferensen framgår av Figur 2.

3.2 VKK:s föredrag

Följande presentationer har tagits fram med stöd från VKK. Numret framför hänvisar till det Appendix där föredraget finns.

1. Measured and Modelled Local Wind Field in Mountainous Terrain Ann-Sofi Smedman, Hans Bergström, Ulf Högström
2. Do Simple Models Give a Correct Description of the Wind Condition in a Coastal Area? Birgitta Källstrand
3. High Resolution Climatological Wind Measurements for Wind Energy Applications. Hans Bergström
4. Wind Characterisation for Design and Comparison with Standards, an Example from Lyse at the Swedish West Coast. Hans Ganander, Ingemar Carlen, Hans Bergström
5. Wake Effects in Alsvik Wind Park: Comparison Between Measurements and Predictions. Mikael Magnusson, K. Rados, K. Pothou
6. A New Approach for Evaluating Measured Wake Data. Mikael Magnusson.
7. Calibration Procedures for Improved Accuracy of Wind Turbine Load Measurements. Jan-Åke Dahlberg och Hjalmar Johansson
8. Load Prediction of Stall Regulated Wind Turbines. Anders Björck, Jan-Åke Dahlberg, Ingemar Carlén, Hans Ganander
9. Aerodynamical Errors on Tower Mounted Wind Speed Measurements due to the Presence of the Tower. Hans Bergström, Jan-Åke Dahlberg
10. Methods to Predict Fatigue Lifetimes of GRP Wind Turbine Blades and Comparison with Experiments. Andreas Echtermeyer, C. Kensche, P. Bach, Maria Poppen, L. Lilholt, S. Andersen, P. Brøndstedt
11. Joule II - Dynamic Stall and 3D Effects. Anders Björck, Sven-Erik Thor
12. Survey of variable speed operation of wind turbines. Ola Carlson, Jonny Hylander, K. Thorborg
13. Generators for Gearless Wind Energy Converters. Anders Grauers
14. Rotating Transformers in Wind Turbine Applications. Jonny Hylander
15. Possibilities by Using a Self-Commutated Voltage Source Inverter Connected to a weak grid in Wind Parks. Jan Svensson
16. Torque Control of Synchronous and Induction Generators for Variable Speed Operation of Wind Turbines. Ola Carlson, Eskil Ulén
17. Yaw Control for Active Damping of Structural Dynamics. Tommy Ekelund

3.3 Övriga

Övriga svenska presentationer av FoU karaktär:

18. Improving Acceptance in Wind Power Planning. Karin Hammarlund
19. Comparison of Power Performance and Noise between Aeolus II and Näsudden II. A. Albers, C. Hinsch, J. Gabriel, H. Klug, G. Ronsten, B. Simonsson. **POSTER AWARD**
20. National Evaluation of Näsudden II, NEON. G. Tunell, A. Andersson, G. Olsson, G. Ronsten, H. Ganander, B. Göransson, B. Simonsson

4 EWEA Annual General Meeting

Under konferensen höll Europeiska vind energiföreningen, EWEA, sitt "annual general meeting". S-E Thor var svensk representant vid mötet.

1996 European Union Wind Energy Conference and Exhibition

20-24 May 1996 - Svenska Mässan Congress Centre, Göteborg, Sweden

OPENING SESSION

Monday, 20 May 1996
10:15 - 12:30
Svenska Mässan Congress Centre,
Göteborg, Sweden

Panelists:

Conference Chairman
Prof. Arthouros Zervos
National Technical Unversity of Athens, Greece

Göran Bengtsson
Governor and Representative of the Swedish Government in the Western Part of Sweden

Hendrik Tent
Deputy Director General, DG XII, Brussels

Joanna Tachmintzis
Member of the Cabinet of Commissioner C. Papoutsis, Brussels

Birgit Erngren
Director General of NUTEK, Stockholm, Sweden

Dr. Hermann Scheer
President of Eurosolar, Bonn, Germany

Ian Mays
President, European Wind Energy Association

WIP-Munich, 13 May 1996

Figur 1. EUWEC'96 Invigningsprogram

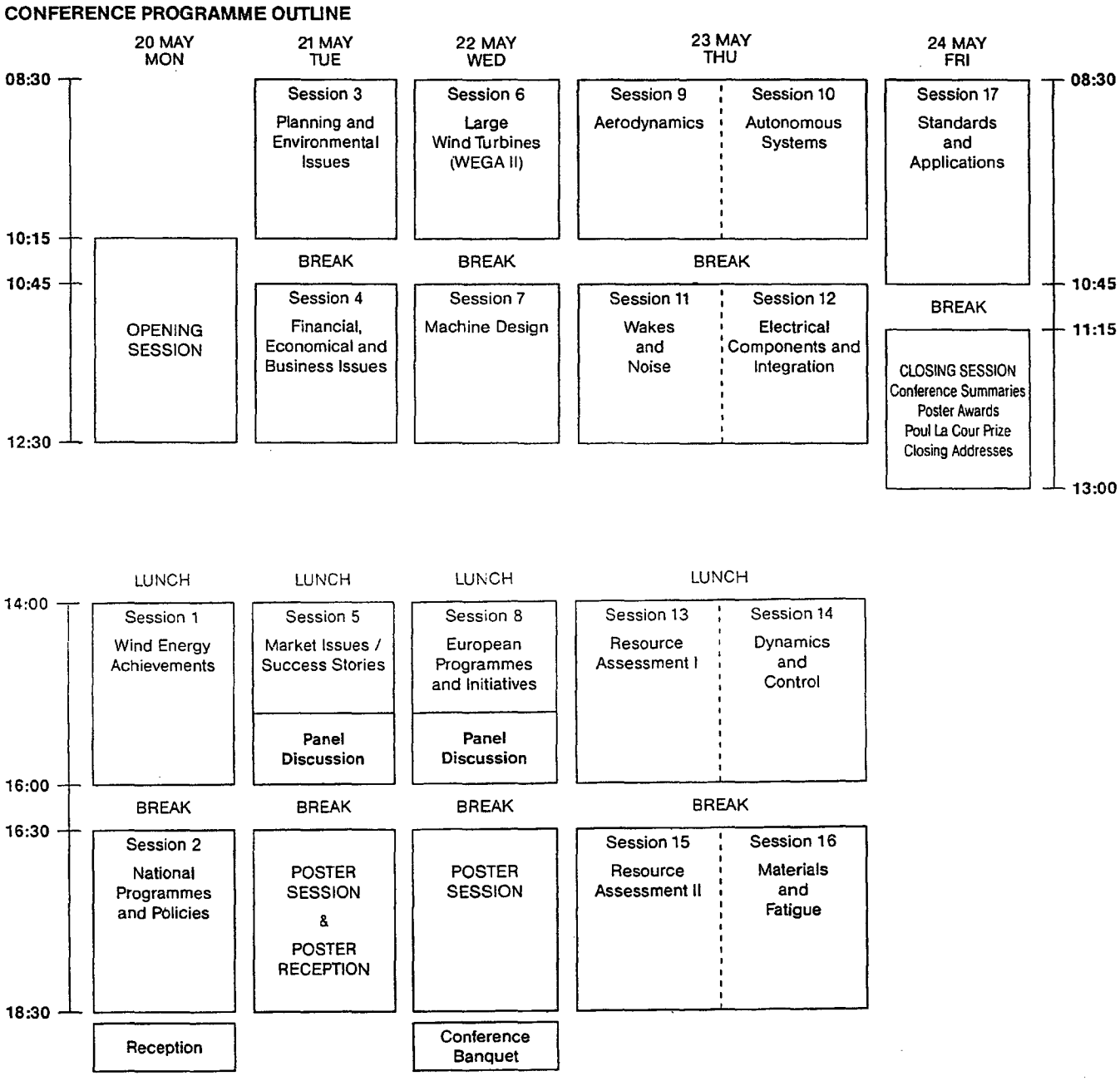

Figur 2. Översiktligt konferensprogram

Appendix 0, Nutek Invigningstal EUWEC'96

EUWEC96

Birgit Erngren

Director General of NUTEK

Swedish National Board for Industrial and Technical Development

It is with great pleasure I on the behalf of The Swedish National Board for Industrial and Technical Development, NUTEK welcome you all to this conference in Gothenburg. The city of Gothenburg has for 20 years been an important city for the Swedish Wind Energy programme. Wind energy research was initiated at Chalmers University of Technology as early as in the mid-seventies. Ever since, Chalmers is an important part of the Swedish wind energy society.

The local power distribution company in Gothenburg, Göteborg Energy has also showed how a local company, can stimulate the local interest for wind energy by initiating and starting local wind energy co-operatives.

NUTEK is Sweden's central authority for matters concerning the growth and renewal of industry and the long-term development of the energy system. It is NUTEK's concern that the Swedish supply of energy should be safe, efficient and environmentally friendly. NUTEK regards the supply, use and efficient marketing of energy as an integral part of a well-balanced future energy system.

It is also our task to make a contribution to the establishment of good conditions for business and industry, and to ensure that the energy system develops in efficient, safe and environmentally acceptable ways. We do this by financing industrially related research and by supporting the development of industrial enterprises, regions and the energy system.

The Swedish Energy System has a history of changes and today, once again, we are confronted with a change of balance in the energy supply system. We are now seeking ways to abandon a system heavily dependent on nuclear power and the question is not only how we can do this, but what are the alternatives?

This, and other questions, had to be resolved. Therefore a commission consisting of members from all parties in the Swedish Parliament was formed. Their report was released in December of last year.

An obvious national objective is to improve and increase the use of renewable energy. This is where NUTEK enters on stage. Our role in the adjustments of the energy system is that of a central energy authority. Our activities aims at the promotion of safe, efficient and sustainable supply and use of energy. NUTEK is responsible for coordinating energy research that primarily focus on renewable energy sources, and for implementing the government's energy polices.

NUTEK's support of energy-related research, development and demonstration aims to make a major contribution to developing a cost-efficient, environmentally and flexible energy system that will, in the long run, promote economical growth.

Activities within the field of energy supply has concentrated on developing renewable sources as bioenergy, wind and solar energy. Large efforts aim at an increased use of biofuels, which have a potential to claim a substantial part in the Swedish energy system.

Renewable energy, especially bioenergy, is cost-competitive on the heating market, since fossil fuels are levied with energy- and emission taxes. Hydropower and nuclear power are still the dominant sources for electricity production and the demand for new production capacity has so far been low.

The market for wind power and other electricity production forms has undergone major changes due to the deregulation of the electricity market that took place the 1st of January this year. The aim for this new act is to introduce competition on the electricity market thus creating conditions for efficient pricing and a more open trade in electricity. Competition in production and trade in electricity enables buyers to choose freely between different vendors on the market.

Discussions regarding the environmental impacts of electricity production has led to an increased interest in wind power. The new regulations give consumers an opportunity to demand electricity produced in an environmentally acceptable manner. As a consequence, the Swedish State Railways (SJ) made the decision to buy electricity produced by wind power through their supplier Sydkraft.

The deregulated electricity market also put focus on the cost efficiency of the production facilities. In order to safeguard smaller producers special regulations have been stipulated for an adjustment period of five years. Companies delivering power in one given area are obligated to purchase their electricity from a power generation plant located within the region and capable of delivering a maximum of 1,500 kW. Thus, the delivery concession gives small scale power producers a guaranteed market for their output. It is NUTEK's job to oversee and make sure that those rules are followed on the new market.

The possibilities of introducing wind power on a large scale in Sweden are sufficient from a wind supply perspective. The potential for wind power on land is estimated to be between 3 and 7 TWh, whilst the potential at sea can reach up to 20 TWh. Studies show that Sweden as a whole could produce wind power up to 4 TWh without putting pressure on other parts of the energy power system's efficiency or tapping into the need of additional power. How much wind power can be generated and what percentage it could fill of the total electricity production in Sweden is mainly subject to:

1. The cost efficiency of the wind power plants compared to other forms ways to produce electricity.
2. The possibility of finding suitable sites.

The overall goal for the Swedish Wind Energy Research Programme is to develop knowledge within the wind energy area which can support users and Swedish wind energy producers in their effort to manufacture and introduce wind energy at efficient costs into the Swedish Energy System.

In order to increase the possibilities for electricity produced from wind power converters, research efforts involve the development of cheaper wind power plants. One applied goal is to find methods that can be used for developing more flexible and lighter machines in the future. One example of such a machine is Nordic 1000 with a capacity of 1 MW owned by Vattenfall.

The **siting** of new electricity power plants always places high demands on the level of consideration against the surroundings. As with other constructions wind power plants need building permits. The leave to appeal has in many cases become a laborious process due to partly, the unfamiliarity at handling such a new production system that a wind power plant is, and partly, the construction of such plants tend to conflict with other interests on how to manage the land.

As a government agency NUTEK is responsible for pointing out to local authorities areas suitable for wind power plants in order to facilitate the land use planning. The planning process aims to locate good wind conditions without coming into conflict with local interests.

Apart from research, NUTEK administrate the Swedish wind energy investmentprogramme. Total government funding for this programme amounts to 340 million SEK, and the total sum had been reserved for use by the early spring 1996.

The support toward wind power has meant that the amount of wind turbines has increased from 38 in 1991 with a total effect of 4,7 MW to 223 as of March 1996 with a total effect of 68,4 MW.

Within the investment programme a technology procurement process, regarding wind power plants under taken. The technology procurement process is based on an initiative from NUTEK. Five Swedish wind turbine operating companies have decided to combine their procurement activities in an effort to raise the cost effectiveness of future energy conversion systems. The Swedish Wind Turbine Buyer Consortium has been formed for that specific purpose.

Let me conclude this presentation by saying a few words about how I look at the energy field in the future

Energy and environmental issues are of vitale importance for the development of the society and will be even more in focus in the future. The risk for climate change must be taken very seriously and the development of future energy markets must take this into account.

One of the greatest challenges for the future will be to co-ordinate the energy supply and environmental considerations with a promising economical growth. Supplies of

electricity and other forms of energy must be guaranteed according to competitive terms both in the short and long term.

The outlet of environmentally hazardous emissions must, for many different reasons, be restricted. Environmental issues will be a major defining factor for regulations in future energy systems. Adjustments to the Energy System must therefore be done in such a way that bears consideration to climate issues on a global level.

Wind Energy represents in many ways the future, is renewable and produces electricity without any emissions to the air.

Internationally the large increase of the number of windturbines shows in many ways that wind energy now can compete with other forms of electricity production. So far there has been a need for different subsidies. But the cost of wind turbines of today are in the same range as other new electricity production forms and the deregulation of electricity markets in Scandinavia has shown an increased interest for environmentally acceptable electricity production such as wind energy.

But the use of wind energy resource is depending on how well it can be an integrated part of both the electricity system and as an accepted part of the landscape. I hope this conference will give answers to these problems and that we all can se a positive future for wind energy, and with these words I would like to say ...

Thank you

Appendix 1-20, Föredrag

Appendix 1

Measured and Modelled Local Wind Field in Mountainous Terrain

Ann-Sofi Smedman, Hans Bergström, Ulf Högström

MEASURED AND MODELLED LOCAL WIND FIELD IN MOUNTAINOUS TERRAIN

Ann-Sofi Smedman and Hans Bergström
Department of Meteorology, Uppsala University
Box 516, Uppsala, Sweden

ABSTRACT. The flow regime over a frozen, snow-covered lake surranded by high mountains is studied in a field experiment and simulations with a numerical boundary layer model.

1. INTRODUCTION

Large scale exploitation of wind energy requires siting of wind turbines not only in flat coastal areas, but also in more complex terrain such as rough mountainous regions. Partly this is due to shortness of suitable locations in less complex terrain, but partly also to the expected increase in wind energy potential with increased altitude. Very favourable wind conditions have for example been found on the top of low fells in northern Finland, with average wind speeds close to what would be expected in the free atmosphere. Wind conditions in mountainous terrain are, however, generally highly complex. Much care has to be taken when siting wind turbines in such areas, as the wind potential may vary considerably over rather short distances. Also turbulence and shear conditions may be rather severe as compared to conditions in more homogeneous terrain. As atmospheric turbulence and wind shear are recognised as a primary source for loads on horizontal axis wind turbines, this is also a reason why one has to be very careful when siting wind turbines in rough terrain.

Terrain forcing is an important factor in establishing mesoscale circulation patterns in mountainous areas. For a number of theoretical and practical reasons it is important to know for example the interaction of winds in a valley with winds at higher levels. The prediction of wind energy potential in a valley requires the ability to relate local valley circulation to ambient synoptic conditions. To be able to calculate long term statistics of wind speed and direction at a certain site in complex terrain, it is necessary to develop an understanding of the mechanisms responsible for the observed behaviour.

In mountainous regions a multitude of local wind regimes are bound to occur and generalisations of results from one site to other areas are difficult. Nevertheless, detailed studies of the physical mechanisms causing the wind regime at one particular location is likely to give results that can be used to explain similar phenomena in seemingly very different geographical settings.

2. DATA AND INSTRUMENTATIO

A field experiment was conducted during the time period 15 March to 15 April 1994 on Lake Torneträsk in the north of Sweden (Figure 1). Lake Torneträsk is surrounded by high mountains. During this campaign, the stratification close to the ground was more or less stable at all times. The depth of the ice on the lake was about 100 cm with a 10-30 cm layer of snow. The ground surrounding the lake was also covered by snow. As confirmed by measurements at the various sites in the area, this situation resulted in very uniform surface temperature conditions.

Instrumentation during the field experiment included: (i) a 12-m mast on the lake (T in Figure 1) with profile instrumentation at four levels together with turbulence measurements at one height. Net radiation was also recorded. The turbulence instrument employed is the Gill Solent Sonic Anemometer, which has been recalibrated in a big wind tunnel. As a result of this calibration, corrections for flow distortion have been applied. (ii) Four 3.5-m high masts were placed at four locations shown in Figure 1: Tornehamn (Th), Abiskosoulo (A), Jiebrensullut (J) and Roggenjarga (R). The masts were equipped with the MIUU wind package, which consists of a combination of a small cup anemometer and a wind vane. The instrument is described in [1]. At the site A, pressure was also recorded. Profile data were usually sampled every second minute and the sampling rate for the turbulence instrument was 21 Hz. (iii) Pibal trackings and radio soundings were carried out at the tower site (T) and at ANS simultaneously on selected days. (iv). Routine meteorological measurements were performed at the ANS station.

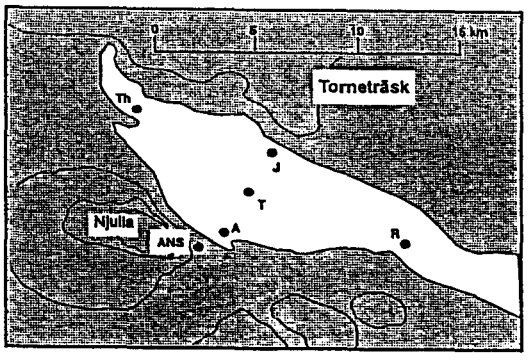

Figure 1. Schematic picture over the lake

3. RELATIONS BETWEEN THE GEOSTROPHIC WIND AND THE WIND REGIME OVER THE LAKE

Whiteman and Doran [2] consider four mechanisms which are likely to create local winds in mountainous terrain. The first is thermal forcing. Temperature differences over heterogeneous terrain will create pressure gradients and thus local wind systems may occur. In our case the ground was covered by snow (~20 cm) and the surface temperature was observed to vary little in the area,

as already remarked. Thus thermally driven wind systems are not likely to develop over the lake.

The second process is strong downward transport of momentum from aloft, which would produce near-surface wind directions similar to the geostrophic wind direction. This downward transport could be caused by vertical turbulent mixing or by gravity waves and would be most likely to occur during unstable or neutral conditions in wide flat-bottomed valleys with low side walls [2]. Also this mechanism is considered to be ineffective during winter conditions with stable stratification over Lake Tometräsk.

The remaining two processes will both produce near-surface winds which will align with the lake axis. Winds would blow up or down the lake axis, depending on the direction of the geostrophic wind relative to that axis. The two possibilities are: (i) forced channelling and (ii) pressure-driven channelling. In the first case the ambient wind, which is assumed to be in geostrophic balance above the mountains, will be channelled by the valley side-walls. The near-surface wind direction and speed depend on the sign and magnitude of the component of the overlaying wind projected along the lake axis.

In pressure- driven channelling the winds over the lake are driven by the component of the pressure gradient along the lake axis. Those winds are often referred to as gap winds, in particular for cases when the resulting wind is relatively strong ([3], [4]). The combination of large-scale synoptic forcing, the configuration of the surrounding topography, and very small surface roughness may lead to the formation of gap winds over water. High gap winds are often observed in gaps along mountainous coasts of the eastern Pacific and the Gulf of Alaska [5], and were also observed to occur over Lake Tometräsk, [6]. This mechanism was also
used by Gross and Wipperman ([7]) for the Rhine Valley and by Whiteman and Doran ([2]) for the Tennessee Valley. Although pressure-driven channelling does occur within valleys, high gap winds are only likely to be present over surfaces with very low roughness such as water or snow-covered ice.

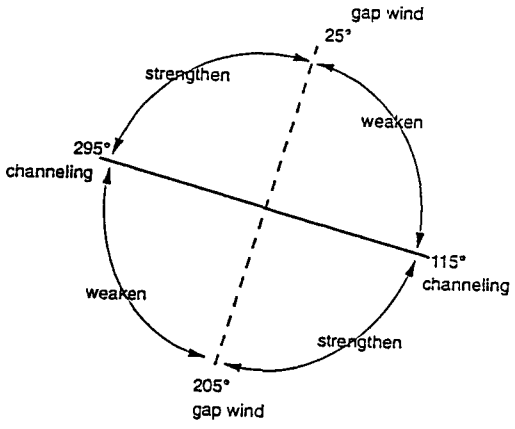

Figure 2. The sectors of geostrophic wind direction causing gap wind and forced channelling respectively.

Thus, both forced channelling and pressure-driven channelling would result in winds aligned with the lake axis. Wind direction reversal will occur when the geostrophic wind shifts across a line normal to the lake axis for forced channelling but across the lake axis for pressure-driven channelling.

In Figure 2 the direction of the lake (115°-295°) is indicated with a bold line and the line normal to the lake with a hatched line. Over the lake, winds from 115° can be caused by pressure-driven channelling for geostrohpic winds coming from 120°- 290°, i.e. when the synoptic pressure decreases along the lake axis from east to west, and/or by forced channelling for synoptic winds from 30°-200°. Geostrophic wind directions
between 300° and 110° are likely to result in pressure-driven channelling winds from 295°. The same wind direction over the lake is also likely to occur as a result of forced channelling by a geostrophic wind from between 210° and 20°. Thus for geostrophic winds in the two sectors 300° - 20° and 120° - 200° the two mechanisms act in the same direction and may reinforce each other. For the remaining sectors the two mechanisms operate against each other and are likely to cause relatively weak winds over the lake.

In Figure 3 the measured wind direction over the lake, Wd_o is given as a function of the geostrophic wind direction, Wd_g taken from analysed pressure fields. The solid lines in the figure indicate the locus of points that would be expected if pressure-driven channelling alone was responsible for the wind over the lake and the hatched lines show the same for forced channelling. The representing all cases during the 1994 measuring campaign with well defined wind direction over the lake and wind speed in excess of about 3 m s^{-1}. For a geostrophic wind direction between 0° and 115° two measurements indicate pressure-driven channelling whereas in the direction interval 115° to 20° data show that forced and pressure driven channelling determine the wind direction over the lake, both acting to give winds from 115°. Between 205° and 295° both mechanisms are working, but now in opposite direction. Finally from 295° to 25° pressure-driven channelling alone rules the surface wind direction. Note that all measurements of well defined wind over the lake is along the lake axis, either from around 115° or from around 295°. This result indicates that during wintertime conditions when lake Tometräsk is frozen forced and pressure-driven channelling are phenomena that exert great influence on the local wind regime. In Section 4 results from simulation with a numerical boundary layer model are used to generalise these results.

3.1 Forced channelling

As mentioned above winds over a valley, or in this case a frozen lake, can be forced down to the ground by the mountains surrounding the valley. The surface wind speed will depend on the magnitude and direction of the geostrophic wind but it will also be a function of stability and surface roughness. In a case of forced channelling the wind speed close to the ground will never exceed the over-laying wind speed. In Figure 4 a typical example of forced channelling is shown. The geostrophic wind direction is 280° and the wind speed 10 ms^{-1} . In the

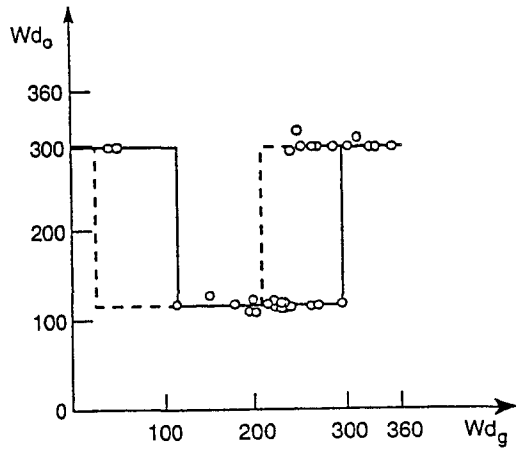

Figure 3. Measured wind direction over the lake. Wdo plotted as a function of geostrophic wind direction. The rings indicates measurements, the solid line: the locus of points expected in pressure-driven flow and the hatched line the same for forced channelling.

boundary layer over the lake the wind direction is close to 295°, the direction of the lake axis. The wind speed decreases gradually towards the surface, without any marked low level wind maximum.

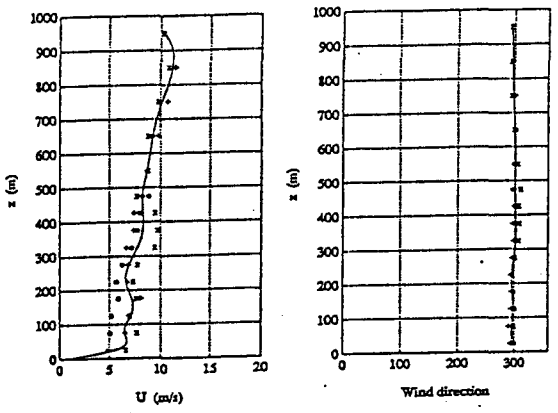

Figure 4. Examples of wind speed and direction profiles during forced channelling conditions.

3.2 Pressure -driven channelling (gap wind)

Pressure driven channelling or gap winds can be defined as an ageostrophic flow of air in a channel, accelerating under the influence of a pressure gradient parallel to the axis of the channel [4].

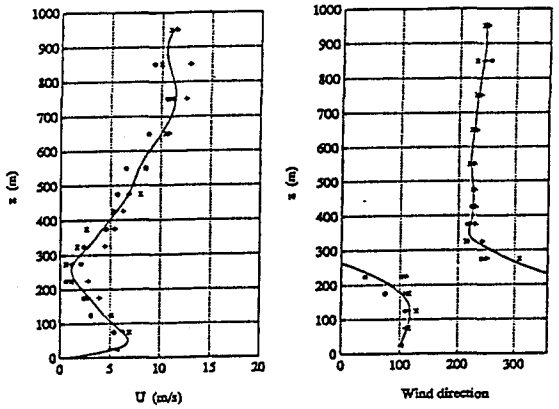

Figure 5. Examples of wind speed and direction profiles during gap wind conditions.

Figure 5 shows a set of three consecutive wind soundings over the lake during a situation with well developed (although not excessively strong) gap wind, which is seen to be very sharply confined to the lowest 200 m and with a wind maximum of ca. 7 m s^{-1} at around 50 m. At 250 m the wind drops to nearly zero. Above this height the wind direction is almost constant at 220°, increasing in speed linearly with height to about 12 ms^{-1} at 750 m.

5. NUMERICAL SIMULATIONS

The MIUU mesoscale model is a three-dimensional hydrostatic boundary layer model with terrain-following co-ordinates and second-order turbulence closure scheme [8]. Below the model is also validated against measurements in the Torneträsk area, before it is used as a tool to create a 'synthetic data base' for generalisation of the results discussed in the previous Section.

For validation the model was run for a simulated 24 hour period of time with input data chosen such as to simulate two cases with gap wind and one without. The geostrophic wind speed and directions were taken from analysed pressure fields, which in those cases agreed very well with pibal measurements. The initial potential temperature profiles were taken from the soundings. Starting with this boundary layer temperature profiles and the geostrophic wind speeds given above, the model was run with prescribed surface temperature taken from measurements.

Figure 6a shows the modelled gap wind structure over Lake Torneträsk (940412 at 1000 LST) in a line from ANS over site A, T and J. In Figure 6b the corresponding measured wind field is presented. The geostrophic wind is blowing from 205° with 10 ms^{-1}. Over the lake a gap wind from 115° has a maximum value of 6 ms^{-1}, at a height of 75 m. Above the low level jet there is a layer with almost no wind, and at higher levels the wind speed increases to 5-6 ms^{-1} and the direction is across the lake. Comparing the simulation with measurements, Figure 6 a and b, there is very good agreement for all three height intervals. There is, however a slight tendency for the model to give lower wind speeds close to the ground.

The overall impression from all simulations is that there is very good agreement between simulations and measurements both as regards the height and the strength of the gap wind.

4. A SYNTHETIC DATA SET

The model was run with a constant geostrophic wind speed of 10 ms^{-1} for 18 directions evenly distributed around the compass and for two stability conditions, near neutral and slightly stable. Note that both observations and simulations show that no gap winds develop in strongly stable conditions.

In Figure 7 the simulated wind speed at a height of 30 m is given in a hodograph representation as a function of geostrophic wind direction. The full circle represents a indicates near neutral stratification and the hatched curve slightly stable conditions. The axis of the lake is marked with a solid line. Starting with a geostrophic wind direction along the axis of the lake (295°), forced channelling alone is working and the highest surface winds are obtained for neutral stratification. Moving clockwise round the circle, the two 'stability curves' cross for an approximately northerly geostrophic wind direction. For a wind direction of 25° (the line normal to the axis of the lake) only pressure-driven channelling is acting and is most effective during slightly stable conditions. In the direction quadrant 25° - 115° the two mechanisms are counteracting and the resulting surface winds are low. Again for 115° (along the axis of the lake) forced channelling is giving the highest surface winds during neutral conditions. In the next quadrant (geostrophic winds from 115° - 205°) the two mechanisms work together. For 205°, pressure-driven channelling again gives the highest surface winds for slightly stable conditions.

To conclude, the model simulations show that a combination of pressure-driven channelling and forced channelling can explain the observed wind field close to the surface over the lake for most cases when the stratification is slightly stable (or near neutral) and the overlying wind is not too weak. Pressure-driven channelling will create the highest wind speeds during slightly stable stratification but is less effective during neutral and very stable conditions. On the contrary, forced channelling creates the highest wind speeds in near neutral conditions.

ACKNOWLEDGEMENT

This work was carried out within the JOULE I project 'Wind measurements and modelling in complex terrain' funded by EU contract JOUR-CT90-0067-C.Contributions was also given by the Swedish National Science research Council contract S-AA/fo 03556-314 and by the National Energy Administration (NUTEK) under grant P529-1.

REFERENCES

[1] Smedman, A.S., Lundin, K. Bergström, H. and Högström, U., 1991, Bound.-Layer Meteorol. 56, 295 - 307.

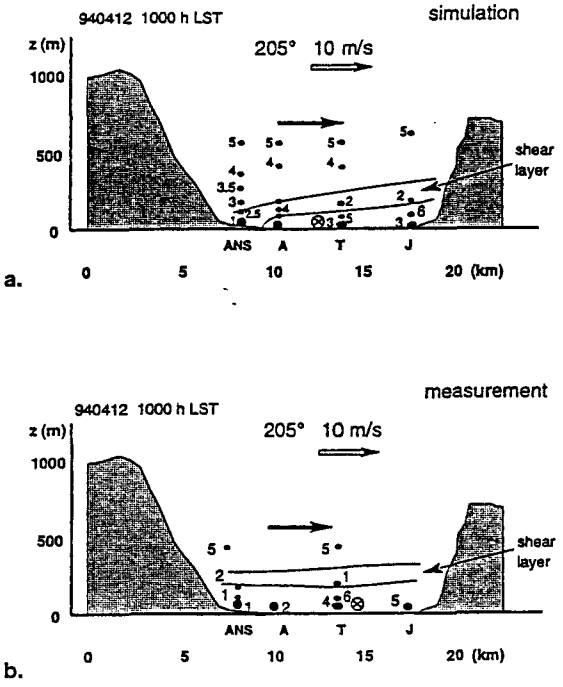

Figure 6. Modelled, Figure 6a, and measured, Figure 6b, wind field in a cross section from stations ANS to J (cf Figure 1) during a gap wind situation.

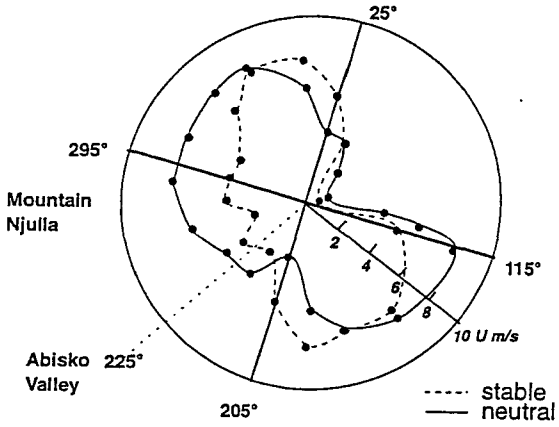

Figure 7. Hodograph representation of simulated wind speed over the lake as a function of geostrophic wind direction and for a geostrophic wind speed of 10 ms^{-1}. The full line denotes neutral and the hatched line stable air.

[2] Whitemann,C.D. AND Doran, J.C., 1993,. J. Appl. Meteorol. 32, 1669- 1682.

[3] Reed, T.R., 1931, Mon. Wea. Rev. 59, 373 - 376.

[4] J.E. Overland and Walter, B.A., 1981, Mon. Wea. Rev. 109, 2221 - 2233.

[5] Lackmann,G. M. and Overland, J.E., 1989, Mon. Wea. Rev. 117, 1817 - 1833.

[6] Smedman, A. and Bergström, H., 1995: Mon. Wea. Rev. 123 (8), 2319 - 2333.

[7] Gross, G and Wippermann, F., 1987,. J. Climate and Appl. Meteorol., 26 (10), 1293 - 1304.

[8] Enger, L., 1990, Atmos. Env., 24A, 2431 - 2446.

Appendix 2

Do Simple Models Give a Correct Description of the Wind Condition in a Coastal Area?

Birgitta Källstrand

DO SIMPLE MODELS GIVE A CORRECT DESCRIPTION OF THE WIND CONDITIONS IN A COASTAL AREA?

B. Källstrand
Department of Meteorology, Uppsala University
Box 516, S - 751 20 Uppsala
Sweden

ABSTRACT: When the surface conditions changes at a coastline, an internal boundary layer evolves, with a wind speed and turbulence intensity influenced by these new conditions. Aircraft measurements across the coastline, performed during near neutral conditions, are compared with a model and thirteen more simple expressions for the growth of an internal boundary layer (IBL). The majority of the expressions overestimate the IBL height, while other underestimate it. Some of the expressions give reasonably result close to the coast. The model gives good agreement, even for larger distances. The vertical potential temperature gradient turned out to be an important parameter for the growth of the IBL, even with this near neutral conditions.
Keywords: Coastal Sea Areas, Boundary Layer, Wind Speed, Meteorology.

1. INTRODUCTION

Many wind turbines are situated in coastal areas, to take advantage of the higher wind energy potential off shore. It is therefore of large interest how fast the wind conditions is changing moving inland.

The larger roughness and changes in the temperature conditions at the coastline, gives decreasing wind speed and increasing turbulence intensity. An internal boundary layer (IBL), where the meteorological conditions are influenced by the conditions over land, evolves. A schematic illustration of the physical situation, studying onshore wind, is shown in Figure 1. The height of the IBL grows inland with distance from coast, until an equilibrium height is reached.

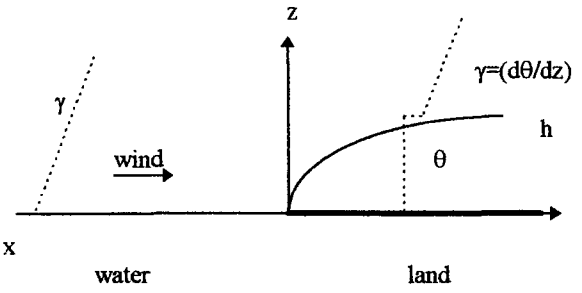

Figure 1: Schematic illustration of the growth of an internal boundary layer. θ=potential temperature, (where $\theta = T(1000/p)^{2/7}$, T=temperature and p=pressure) and h=IBL height.

The development of internal boundary layers have been studied in numerous investigations and there are also a large number of field experiments (e.g.[1] and [2]), theoretical expressions for the IBL growth, (e.g.[3]) and a number of more or less complex numerical models (e.g.[4] and [5]). A review is found in [6].

A common feature in most of these measurements and numerical studies, is a cold sea and a warmer land surface. In this study, the measurements used are carried out in autumn. Here, the sea surface is warmer than the land surface (about 1-2 °C). There is slightly stable conditions over sea and slightly unstable conditions over land, but the stratification can be regarded as near neutral.

2. DATA

The Department of Meteorology at Uppsala University, Sweden, has carried out a number of field experiments on the Baltic coast. One area where measurements has been performed is in the southeast of Sweden (see Figure 2), e.g. [7], [8] and [9]. The measurements in this comparison were part of an extensive measuring program performed in September and October 1990.

Aircraft measurements giving wind, temperature, humidity and fluxes of momentum and sensible and latent heat were performed. These airborne measurements were taken with an instrument package mounted on a Sabreliner 40A aircraft (operated by the Swedish Defence Material Administration, available for atmospheric research on a rental basis). The measurement system, calibration and accuracy estimations are described by [10]. Evaluation of the slant profile data and a discussion of the potential errors generated by that analysis are found in [8].

Ground based measurements, consisting of profile and turbulence measurements on a 25 m tower, radiosoundings and pilot balloon measurements, were performed on the small island Utlängan (see Figure 2). The instrumentation and measurements are described in [8].

Two cases, of the eleven occasions with aircraft measurements, are studied in this investigation. They consist of several flight legs flown over the same track but at different altitudes, from 50 to 500 m, to cover the vertical profiles of meteorological parameters in the boundary layer. The flight legs cross the shoreline - half flown over sea and half over land. The flights start and end with slant profiles, from a height of about 50 m and up to about 1600 m. Three of the four vertical profiles are flown over the sea (see Figure 2). The first of these two flights was flown on September 24, between 1340 and 1505 local time and the second on September 25, between 940 and 1110 local time. The approximate heights for the flight legs are for the first flight 50, 100, 150, 200, 300 and 400 meter and for the second flight 50, 100, 150, 200, 250, 350 and 450 meter. The flight area was chosen so the track was perpendicular to the coast and the wind direction was towards

land (Figure 2). The vertical potential temperature gradient, γ, over the sea is small and so is the surface heat flux, $(w'\theta')_0$, over both land and sea. These conditions are very common in autumn at our latitudes.

Isoplots of wind speed is found by combining data for a specific latitude (or longitude) from flight legs at different heights to profiles, and then plot the data profiles as a function of latitudes (or longitudes). This gives a picture of the variation of wind speed, both as a function of height and as a function of distance from coast. This procedure implies stationary conditions during the flights. The distance from the coast is calculated in the mean wind direction, taken from the aircraft measurements.

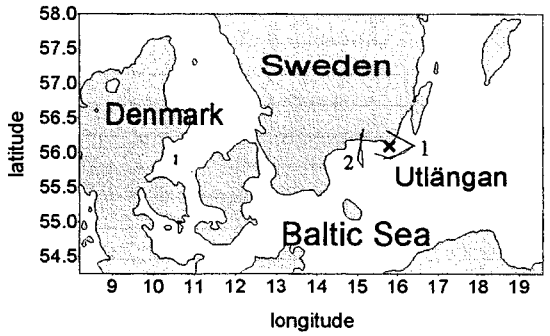

Figure 2: Map over the area where the measurements were performed. The lines shows the flight tracks. 1: 24 September, 1990 and 2: 25 September, 1990. The cross shows the island Utlängan.

3. THE GB MODEL

A model describing the growth of near-neutral and convective internal boundary layers by [4] is used, in a somewhat simplified version:

$$U_h\left(\frac{h^2 g}{2Bu_*^3\theta}+\frac{1}{u_* C\gamma}\right)\frac{dh}{dx}=\frac{1}{\gamma}\quad , \qquad (1)$$

where U_h=wind speed at the top of the IBL, u_*=friction velocity, g=acceleration of gravity, and B=2.5 and C=1.3 are constants. (Remaining parameters, see Figure 1.)

This equation is used iteratively to calculate the IBL growth. The most important difference between Eq. (1) and the original model is that $(w'\theta')_0$ is neglected, since that parameter is very small in our measurements. Although this model (hereafter called GB model) is a model for both near-neutral and convective IBL growth, the comparisons found in the literature, between this model and measurements, is mainly with more or less convective conditions, [4], [1] and [11]. According to [4] the model cannot be used for: (1) the development of stable internal boundary layers or (2) situations when the upwind air is neutral or unstable stratified. Here, the conditions is near neutral both upwind and downwind. The potential temperature gradient, with γ=0.0001 Km^{-1} as smallest, is more than a magnitude smaller than any value in the comparisons mentioned. Also, $(w'\theta')_0$ is smaller in our data and values of other parameters differ too.

4. COMPARISON BETWEEN GB MODEL AND DATA

In Figure 3 and 4 comparisons between contour plots of wind speed, as a function of height and distance from coast, and modeled IBL growth (Eq. 1) are shown for the two cases, 24 September and 25 September, respectively. For both flights, it is a significant decrease in wind speed at the coastline, illustrating the growing IBL. A large wind speed gradient clearly shows the limit for the influence of the land conditions. Over a distance of 20 kilometres, from

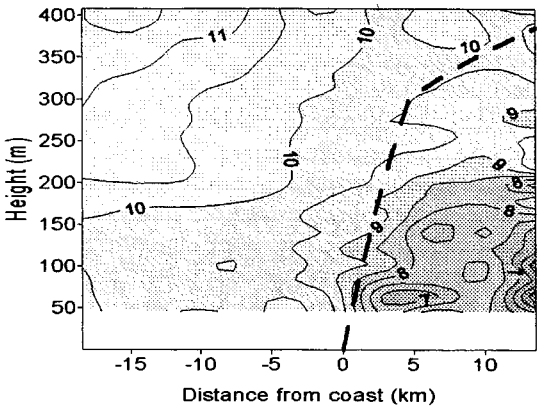

Figure 3: Wind speed as a function of height and distance from coast for 24 September, 1990. The dashed line is predicted IBL height (Eq. 1), with γ=0.0002 Km^{-1} for 0-300 m, γ=0.002 Km^{-1} above.

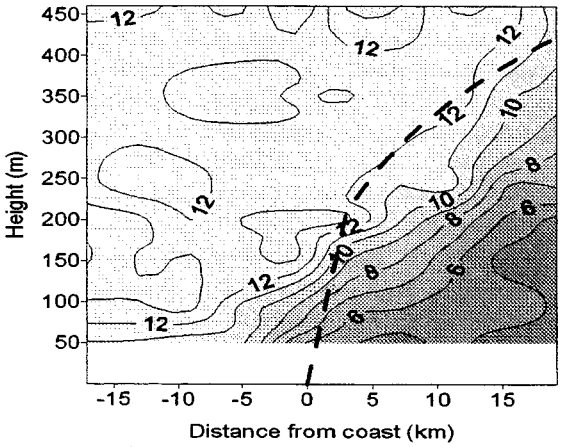

Figure 4: Wind speed as a function of height and distance from coast for 25 September, 1990. The dashed line is predicted IBL height (Eq. 1), with γ=0.0001 Km^{-1} for 0-200 m, γ=0.001 Km^{-1} above.

10 km upwind to 10 km downwind the coastline, the wind speed at 25 September decreases from 11 m/s to 5 m/s, i.e. more than a halving of the wind speed. For the 24 September the corresponding decrease is 2 m/s, from 9.5 m/s to 7.5 m/s. There also seems to be upstream effects, especially in the second flight, decreasing the wind speed upwind the coastline. This is in agreement with a climatological study of this part of the Baltic Sea by [12]. Possible factors affecting the upstream wind speed decrease is e.g. the curvature of the coastline and islands situated upstream.

The height of the IBL can be defined in different ways, e.g. where (1) $\partial u/\partial z$ or (2) $\partial\theta/\partial z$ has a discontinuity.

From isoplots of different parameters (here exemplified with wind speed, Figure 3 and 4) a graphically comparison of the form and height of the IBL, between measurements and model result, was performed. Note that there are no measurements below 50 meters height. The comparisons show a generally good agreement between measurements and predicted IBL height. Although the calculated height, in average, shows an even better agreement than the exact form of the IBL, the result fulfill the expectations.

5. IBL EXPRESSIONS

There are a number of formulas for the growth of the (coastal) IBL in the literature. A test of thirteen more or less simple expressions, with a limited number of parameters, is performed here. The model (Eq. 1) agreed well with the measurements, in spite of the relatively small heat flux, the small γ and the "reversed" temperature difference. This comparison is performed to see how less complex expressions handle these meteorological conditions. Most of them involve both physical and empirical considerations, but they are derived in different ways and use different simplifications. The majority of them are compared with one or more data sets. (See Table I. The abbreviations for the different expressions from Table I are used in the following text.)

6. COMPARISON OF DIFFERENT FORMULAS WITH THE GB MODEL

We have seen that the used version of the model by [4] agree well with our measurements. It is therefore possible to use that result as a starting-point for the comparison of the expressions in Table I. Choosing this starting-point, the result of this test is presented as a comparison of calculated IBL growth for all expressions, using the GB model as a reference. The calculated IBL heights for the 25 September, 1990, is shown in Figure 5. The GB model is drawn with a broad line and all expressions are marked with an abbreviation of the name of respective author(s) (see Table I).

In our measurements, both $(w'\theta')_0$ and γ is small. The expressions including the term $(x\cdot|T_L\text{-}T_W|\ /\gamma)^{1/2}$ or $(x\cdot(w'\theta')_0\ /\gamma)^{1/2}$, i.e. Ra, We, Ve and Pl, thus includes the ratio between two small quantities. All these expressions give a larger or smaller overestimation of the IBL height. This result could be expected, since γ is the parameter with the most extreme values here. Also the VdH formulation gives a large overestimation of the IBL height. The VdH equation, and also the SH83 expressions, include parameters related to the vertical temperature variations, and is sensitive to the exact value of those parameters. Both SH83 versions overestimate the IBL height, but the "form" of these curves resemble the GB model result. The difference between the two SH83 versions is quite small, which confirms the assumption that neglecting the $(w'\theta')_0$ term has a minor influence on the IBL growth for our cases.

Three of the expressions, i.e. E, Wo and SH78, involve the roughness length, z_0. SH78 use the roughness indirect, since the constants depend on z_0 and stability. Together with the expression by B, these four formulas has a larger exponent (0.7-0.8) than the majority of the expressions, which have a $x^{0.5}$ dependence. Both the E and Wo equations give IBL heights that agree well with the GB model close to the coast, but give a too fast growth for larger distances. The equation by B has the same form as the two equations previously discussed, but gives to small values of the IBL height. The SH78 expression, on the contrary, gives far too high values of the IBL height.

Table I: Expressions for IBL growth, used in the comparison described in section 5 and 6.

Expression	Authors
$h = 8.8\left(\frac{x}{U_m\delta}\right)^{1/2}$ U_m = mean wind speed in IBL, δ = temp. diff., top to bottom of marine surface - based inversion	VdH: Van der Hoven (1967) (from [3])
$h = \frac{u_*}{U_m}\left(x\frac{\lvert T_L-T_W\rvert}{\lvert\gamma\rvert}\right)^{1/2}$, T_L, T_W = surface temp. for land and water, respectively.	Ra: [13]
$h = \frac{u_*}{U_m}\left(\frac{2\lvert T_L-T_W\rvert x}{\gamma(1-2F)}\right)^{1/2}$, F=1/7	Ve: [14]
$h = \left(\frac{4(w'\theta')_0 x}{\gamma U_h}\right)^{1/2}$	Pl: Plate (1971) (from [3])
$h = \left(\frac{2(w'\theta')_0 x}{\gamma U_h}\right)^{1/2}$	We: [15]
$\begin{cases} h = 0.1x & (x \le 2000\text{m}) \\ h = 200 + 0.03(x-2000) & (x > 2000\text{m}) \end{cases}$	Ha: [16]
$h = z_{01}\left[0.75 + 0.03\ln\left(\frac{z_{02}}{z_{01}}\right)\right]\left(\frac{x}{z_{01}}\right)^{0.8}$ z_{01},z_{02}=roughness length upstream and downstream, respectively.	E: Elliot (1958) (from [17])
$h = 1.91x^{0.5}$	Hsu: [18]
$h = ax^b$, a,b tabulated	SH78: [19]
$h = \left(5\frac{u_*^3\theta x}{g\Delta U_m}\right)^{1/2}$, Δ = temp. jump at the top of IBL	SH83a: [20]
$\frac{dh}{dx} = \frac{1}{U_m}\left(A\frac{(w'\theta')_0}{\Delta} + B\frac{u_*^3\theta}{g\Delta h}\right)$	SH83b: [20] (used iteratively)
$h = z_{or}\,0.28\left(\frac{x}{z_{or}}\right)^{0.8}$, z_{or} = the larger of z_{01} an z_{02}	Wo: [21]
$h = 0.2x^{(0.78-0.33z/L_a)}$, $L_a = -\frac{u_*^3 T_0}{gk(w'\theta')_0}$,k=0.4	B: [5], (modified version after [1])

Finally, two of the expressions depend only on the distance: Ha and Hsu. Both formulas give almost the same IBL heights as the GB model close to the coast, but for larger distances the Hsu equation gives too low heights, while the formula by Ha gives a too fast IBL growth. These expressions are formulated with the intention to be simple. According to [16], this kind of formula, in contrast to several of the other expressions, do not 'blow up' (i.e. produce very small or very large values of the IBL

height) for extreme values of certain parameters. Since both $(w'\theta')_0$ and γ is small in our cases, this sensitivity becomes important. This may explain why the two simplest expressions give relatively good results here, in comparison to some of the other formulas.

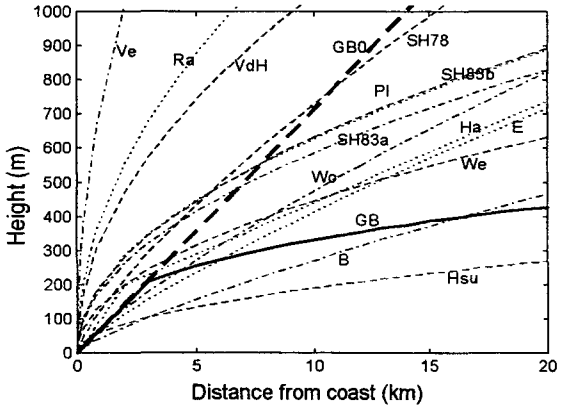

Figure 5: Comparison of different IBL expressions with the GB model, for 25 September, 1990. GB model (broad lines) with: γ as in Figure 4 (full line) and with γ=0 (dashed line).

It is important to be careful in drawing general conclusions about the different expressions from this comparison. This is a case study, with two quite special cases. But, the comparison do say something about the sensitivity of the expressions for the values of the involved parameters and, at least for some of the expressions, of the limited range the expressions is valid within.

7. THE POTENTIAL TEMPERATURE GRADIENT

As illustrated in Figure 5, setting γ=0 in the GB model has a large effect on the IBL height. Taking the small values of the potential temperature gradient into consideration, the effect is even larger than might be expected.

The potential temperature gradient upwind also changes with height in our cases, for 24 September at 300 m and for 25 September at 200 m. Such a double structure of the marine boundary layer may be caused by several reasons, e.g. the conditions over land areas upstream, clouds or specific synoptic situations, and may therefore not be rare. Above the slightly stable boundary layer here, γ is a magnitude larger than below. Following [4], the value of γ used in the model is changed, when the IBL height reaches 300 m and 200 m, respectively. Using this change turned out to have large effect on the IBL growth. For the 25 September, using γ=0.0001 Km^{-1} for the whole IBL growth, in Eq. (1), gave an IBL of 710 m at 15 km from the coast, while using γ as in Figure 4 gave 420 m.

The potential temperature gradient also appear in some of the IBL height expressions in Table I. Using a changing γ in the We equation, calculating the IBL height iteratively, gives a form and height more like the GB model. At 15 km from the coast, this gives a height of 310 m, instead of 550 m. This further illustrate the sensitivity of the IBL growth on the value of γ.

8. CONCLUSIONS

The aircraft measurements used here showed a considerable decrease in wind speed close to the coast, starting upstream the coastline. The growth of an internal boundary layer is clearly seen from the isoplots of wind speed, giving a large wind speed gradient at that height. The majority of the expressions for the IBL growth tested in this comparison overestimate the IBL height, while other underestimate it. Some of the expressions give reasonably result close to the coast. The GB model agree well with our measurements, even for larger distances. The vertical potential temperature gradient, and the vertical change of that parameter, turned out to be important for the growth of the IBL, though the near neutral conditions. Finally, if further work was to be done on expressions for the IBL growth, this comparison shows that the way the potential temperature gradient is used in a formula, and the upstream effects, is important to study.

Acknowledgment: Discussions with S.E. Gryning, Risø National Laboratory, Denmark, are greatly appreciated.

REFERENCES

[1] D. Melas and D. Kambezidis: 1992, *Bound.-Layer Meteor.*, **61**, 247.
[2] P. Durand, S. Brière and A. Druilhet: 1989, *J. Atmos. Sci.*, **46**, 96.
[3] M. Stunder and S. Sethuraman: 1985, *Bound.-Layer Meteor.*, **32**, 177.
[4] S.-E. Gryning and E. Batchvarova: 1990, *Quart. J. R.. Met. Soc.*, **116**, 187.
[5] H. Bergström, P.-E. Johansson and A. Smedman: 1988, *Bound.-Layer Meteor.*, **42**, 313.
[6] J. R. Garratt: 1990, *Bound.-Layer Meteor.*, **50**, 171.
[7] A. Smedman, M. Tjernström and U. Högström: 1993, *Bound.-Layer Meteor.*, **66**, 105.
[8] M. Tjernström and A. Smedman: 1993, *J. Geophys. Res.*, **98**, 4809.
[9] B. Källstrand: 1993, Wind Energy Report WE 93:1, Dep. of Meteorology, Uppsala University, Sweden.
[10] M. Tjernström and C. A. Friehe: 1991, *J. Atmos. Oceanic Technol.*, **8**, 19.
[11] E. Batchvarova and S.-E. Gryning: 1994, *Bound.-Layer Meteor.*, **71**, 311.
[12] H. Bergström: 1992, Wind Energy Report WE 92:1, Dep. of Meteorology, Uppsala University, Sweden.
[13] G.S. Raynor, P. Michael, R. M. Brown and S. SethuRaman: 1975*J. Appl. Meteorol.*, **14**, 1080.
[14] A. Venkatram: 1977, *Bound.-Layer Meteor.*, **11**, 419.
[15] B. Weisman:1976, *Atmos. Env.*, **10**, 172.
[16] S. R. Hanna: 1987, *Bound.-Layer Meteor.*, **40**, 205.
[17] H. A. Panofsky, D. Larko, R. Lipschutz, G. Stone, E. F. Bradley, A.J Bowen, and J. Højstrup: 1982, *Quart. J. R.. Met. Soc.*, **108**, 215.
[18] S. A. Hsu:1986, *Bound.-Layer Meteor.*, **35**, 311.
[19] A. Smedman-Högström and U. Högström: 1978, *J. Appl. Meteorol.*, **17**, 942.
[20] A. Smedman and U. Högström: 1983, *Bound.-Layer Meteor.*, **25**, 271.
[21] D. M. Wood: 1982, *Bound.-Layer Meteor.*, **22**, 241.

Appendix 3

High Resolution Climatological Wind Measurements for Wind Energy Applications

Hans Bergström

HIGH RESOLUTION CLIMATOLOGICAL WIND MEASUREMENTS FOR WIND ENERGY APPLICATIONS

Hans Bergström
Department of Meteorology, Uppsala University
Box 516, S-751 20 Uppsala, Sweden

ABSTRACT: Measurements with a combined cup anemometer/wind vane instrument, developed at the Department of Meteorology in Uppsala, is presented. The instrument has a frequency response of about 1 Hz, making it suitable not only for mean wind measurements but also for studies of atmospheric turbulence. It is robust enough to be used for climatological purposes. Comparisons with data from a hot-film anemometer show good agreement, both as regards standard deviations and the spectral decomposition of the turbulent wind signal. The cup anemometer/wind vane instrument is currently used at three sites within the Swedish wind energy research programme. These measurements are shortly described, and a few examples of the results are given.
Keywords: Coastal sites, climatic conditions, anemometers, boundary layer, off-shore, wakes.

1. INTRODUCTION

The demand for wind data with high temporal resolution at heights of relevance to wind energy applications is large. The reason for this is not only to get a better knowledge about the wind energy potential, but also to increase the understanding of the turbulence structure of the wind in the atmospheric boundary layer. Such information is of great importance when estimating wind turbine load and fatigue. When judging the extreme load situations, it is also of great importance to know the behaviour of the wind during the most severe wind conditions. This includes not only knowledge of the highest wind speed, but also of the most extreme changes in wind speed and wind direction during a short period of time, say a few seconds. Thus it is important to measure the wind with a temporal resolution of 1 s or better, and to take measurements during as long periods as possible in order to reduce the statistical uncertainty in the estimates of the most severe wind situations during the lifetime of a wind turbine. Wind measuring periods of the order of several years are then desirable.

Within the Swedish wind energy research programme, such wind measurements are at present taken at three locations. At Alsvik on the island Gotland in the Baltic Sea, at Lyse on the Swedish west coast, and at Östergarnsholm 4 km east of the island Gotland.

At all sites wind measurements are taken with a high quality cup anemometer/wind vane instrument, allowing accurate measurements of the two horizontal wind components with a time resolution of 1 s. At the Östergarnsholm site, all three wind components are also measured using Solent ultrasonic anemometers.

2. TECHNICAL DESCRIPTION

At the Department of Meteorology in Uppsala a combined Cup Anemometer/Wind Vane (CAWiV) instrument has been developed. The instrument has ashort response time, making it possible to measure the turbulent fluctuations of the two horizontal wind components up to a frequency of 1 Hz. This is sufficient for wind energy purposes, and thus at a rather low cost makes it possible to take high quality measurements of the atmospheric turbulence structure.

A schematic picture of the instrument and a block diagram illustrating its components is shown in Figure 1. The wind speed is measured with a three-cup anemometer of the pulse type. The radius of the rotor is 4 cm, and the cups are conical in shape, made of plastic, and has a weight of 10 g.

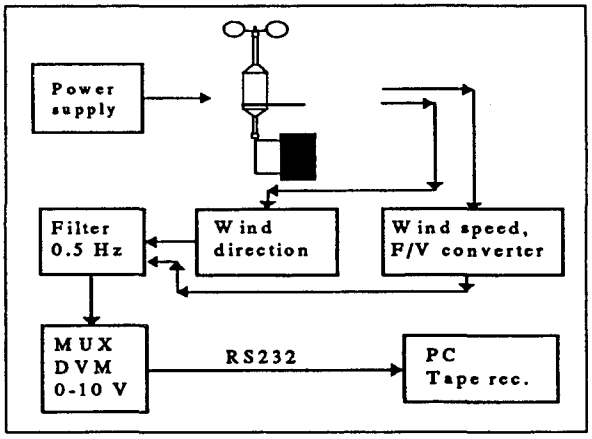

Figure 1: Schematic picture and block diagram of the cup anemometer/wind vane system.

A 40-slot disc connected to the shaft of the anemometer chops an infrared beam. The pulses are detected by an infrared sensitive photo transistor, and the pulse frequency is fed into an F/V converter, where the frequency is transformed to an analog voltage signal. This voltage is then a direct measure of the wind speed.

The wind direction part of the instrument consists of a potentiometer, sensing the position of a high performance wind vane, made of balsa wood. The size of the wind vane is 8 cm x 16 cm.

The complete instrument thus makes it possible to measure the two horizontal wind components with a high frequency resolution. Before storing data on cassette tapes at a sampling frequency of 1 Hz, in order to avoid aliasing

the analog signals are passed through electronic filters with their half energy points at 0.5 Hz.

Before taken into use, 16 anemometers of this type were calibrated in a wind tunnel. These calibrations showed that the mechanical parts of the anemometer (bearing, shaft, slot disc) gave practically identical wind response when compared using the same cups. Comparisons of the different cups also showed good agreement, all of them being within ±1.5% in measured wind speed.

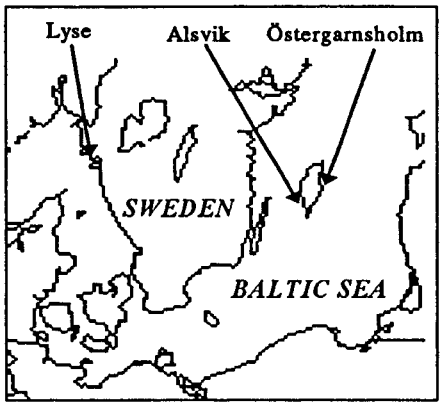

Figure 2: Map of southern Sweden showing the location of the three experimental sites.

3. FIELD PERFORMANCE TESTS

Data from the Alsvik site (cf. below) sampled with a frequency of 1 Hz was compared with turbulence data taken with a hot-film instrument sampled at 20 Hz. The comparison shows that the CAWiV instrument has negligible over-speeding, and is capable of measuring the variance of the longitudinal and the lateral wind components with high accuracy [1]. At 40 m the cup anemometer instrument catches 93% and 95% of the standard deviations of the longitudinal and lateral wind components respectively, compared to measurements with the hot film instrument. The remaining 5-7% are the contributions from frequencies between 1 Hz and 20 Hz. The losses can easily be corrected for by assuming the inertial subrange -2/3-slope to be valid above 0.5 Hz, and integrating over the higher frequencies to estimate the losses.

Spectral densities of the longitudinal and lateral wind components were determined using the FFT technique. Also spectra from the CAWiV instrument compare well with those measured with the hot film instrument, [1].

4. EXAMPLES OF APPLICATION

Wind measurements for wind energy applications are presently made at three sites in Sweden: Lyse at the Swedish west coast, Alsvik on the island of Gotland in the Baltic Sea, and Östergarnsholm, a small island 4 km east of Gotland. see Figure 2.

4.1 Alsvik

Measurements at Alsvik have been taken since April 1990. Two towers (M1 and M2 in Figure 3) are since June 1991 equipped with anemometers at 8 levels, (10, 18, 24, 31, 36, 41, 47, and 53 m), which are sampled with 1 Hz and stored on data cartridge tapes. Before June 1991 instruments were mounted at 7 heights from 3 to 41 m. The measurements also include temperature at five levels (3, 10, 18, 31, and 41 m) in tower M1.

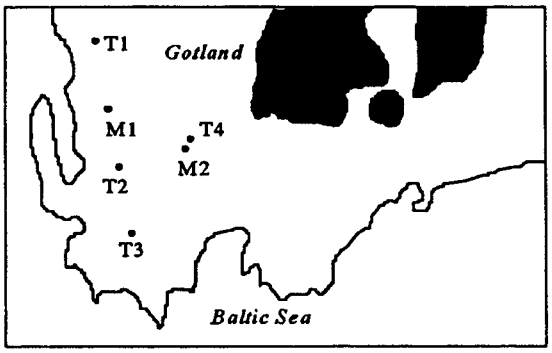

Figure 3: Map of the Alsvik site. Towers are marked M1 and M2, wind turbines are marked T1-T4. Shaded areas are covered with forests.

The Alsvik measurements are primarily intended for the study of wind turbine wakes at a number of distances from 1 to 9.6 rotor diameters downwind of the four 23 m diameter, 180 kW turbines located at this site, 50-200 m from the shore-line (T1-T4 in Figure 3). But they also give valuable information on the structure of the atmospheric turbulence, suitable for load and fatigue estimates, e.g. RFC (rain flow count) statistics of the wind speed and direction.

The site is very flat and the coastal area surrounding the turbines is mainly grassland, occasionally partly overed with small ponds when the water level of the Baltic Sea is high, making it difficult to accurately determine the exact location of the coast line. To the east of the site, towards the interior of the island, there are some forested areas with mainly 5-10 m high pines.

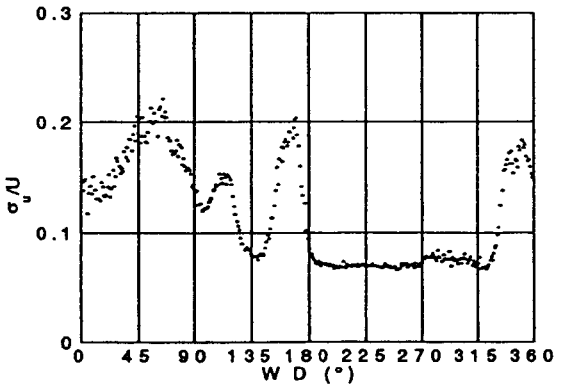

Figure 4: The turbulence intensity at Alsvik, tower M1, as function of wind direction (mean values in 1° sectors). The peaks around 110°, 165° and 345° are caused by upstream wakes.

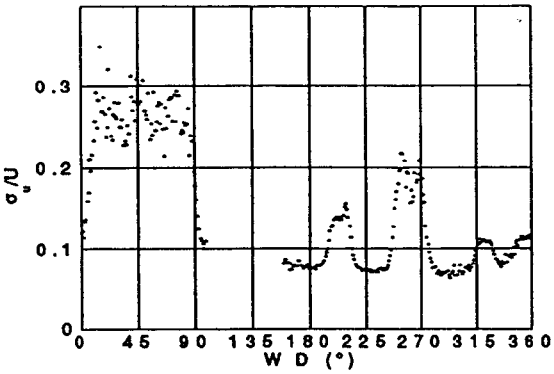

Figure 5: The turbulence intensity at Alsvik, tower M2, as function of wind direction. The peaks around 40°, 210°, 260° and 320° are caused by upstream wakes. In the sector around 120° the anemometers are downstream the tower.

The climatological influence from the four wind turbines upon the turbulence characteristics could e.g. be illustrated by looking at the wind directional dependence of turbulence intensity, σ/U (where σ=standard deviation of the wind, and U=mean wind speed). This is shown in Figures 4-5, where we can clearly see the influence from the wakes. The increased turbulence levels with winds from the forested areas with winds from the northeastern sector is also obvious. The turbulence intensities are here as a mean between 0.15 and 0.20, whereas the intensities with winds from the sea are only about 0.07 to 0.08.

The vertical gradients of mean wind speed may be devided into two parts, an asymetric and a symetric gradient, Γ_a and Γ_s respectively. Having three levels of wind measurements, z_1 - z_3 , these two gradients are defined around the heights z_2 as:

$$\Gamma_a = 0.5\left(\frac{U_3-U_2}{z_3-z_2}+\frac{U_2-U_1}{z_2-z_1}\right)$$

$$\Gamma_s = 0.5\left(\frac{U_3-U_2}{z_3-z_2}-\frac{U_2-U_1}{z_2-z_1}\right)$$

where U_1-U_3 are the mean wind speeds at there three heights. Thus the symetric gradient is the part of the total gradient that has opposite sign above and below the heights z_2, while the asymetric gradient is the remaining part. In the case of the wind speed varying linearly with height, the asymetric gradient will give the total wind gradient, while the symetric gradient will be zero. This partitioning of the gradient is useful in wind turbine design because the response of the turbine will be different for the symetric and the asymetric parts.

The variation of the mean asymetric and symetric gradients around the 31 m level of tower M1 are shown in Figure 6. In free sectors with no wakes, the symetric gradient is close to zero, while in sectors with wakes (cf. Figure 4) it becomes positive (minimum wind speed at 31 m). The asymetric gradient is usually around 0.05 s^{-1}, with values closer to zero within wake sectors.

The standard deviation of the asymetric gradient is about 0.04 s^{-1}, while it is only about 0.02 s^{-1} for the symetric gradient. Thus although the mean asymetric gradient is only 0.05 s^{-1} for winds from the sea, much larger values are expected to occur even on a 10 min average base. In Figure 7 the distribution of the asymetric gradient is shown. It has a broad maximum between 0.01 and 0.05 s^{-1}, with extremes around -0.1 and +0.2 s^{-1}.

The distribution of 1 s maximum and minimum asymetric gradients are shown in Figure 8. As they were deermined using wind data from 5 heights between 18 and 41 m, they should respresent extreme gradients which endeed would affect a wind turbine. The most extreme positive gradient corresponds a wind speed difference of 10 m/s over a vertical distance of 20 m.

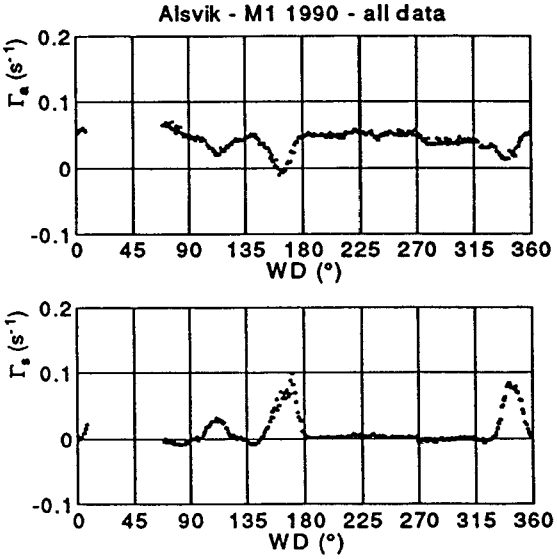

Figure 6: Asymetric and symetric gradients versus wind direction. Data from tower M1, 1990. The line give mean values in 1° sectors, while the vertical bars are the corresponding standard deviations.

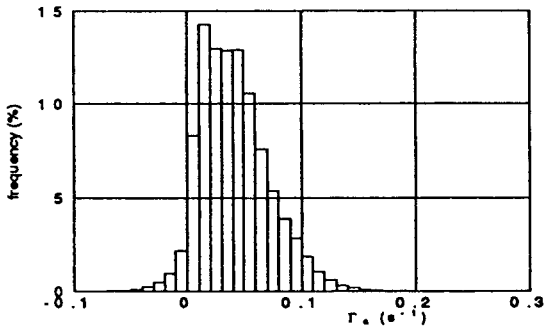

Figure 7: Distribution of the asymetric gradient. Data from tower M1, 1990.

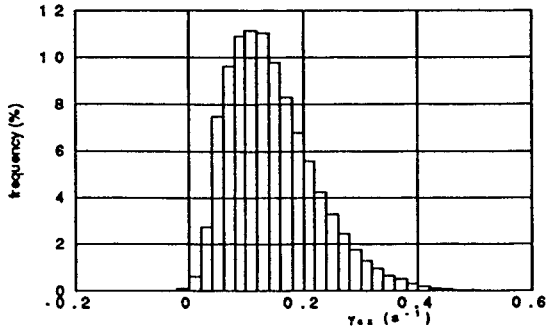

Figure 8: Distribution of maximum, γ_x, and minimum, γ_n, 1 s asymetric gradients. Data from tower M1, 1990.

4.2 Lyse

Since the autumn of 1992 similar 1 Hz. tower measurements are taken at the Lyse wind turbine site, using the same type of instruments. To be able to get undisturbed measurements from all directions, anemometers have been mounted at 7 heights (10, 23, 31, 40, 48, 57, and 64 m) on the northwestern side of the tower, and at 5 heights (32, 40, 49, 57, and 65 m) on the southeastern side. Temperature is measured at 5 heights (2, 10, 23, 40, and 64 m), and relative humidity and air pressure at 2 m.

The terrain at Lyse is, in contrast to the flat and rather homogeneous Alsvik site, much more heterogeneous. The coastal area to the east is rocky with peaks reaching 50 m a.s.l. within the nearest 1-2 km. Nearby islands to the west and southwest are 30 to 40 m high. Both the islands and the nearby mainland rocks have only sparse vegetation, with patches of grass and herbs, and only very few bushes and trees. Thus the roughness of the surface could be expected to be rather small, except for the heterogeneous rocky landscape itself.

A comparison between the turbulence at Lyse and Alsvik reveals that with winds from the sea sector, the more heterogeneous terrain at Lyse increases the turbulence intensity at 30 m from 0.08 at Alsvik to between 0.08 and 0.15, see Figure 9.

With easterly winds, i.e. from land, the turbulence intensities at Lyse are of the same order of magnitude as those at Alsvik, indicating that the turbulence intensity above a heterogeneous hilly terrain with sparse vegetation may be approximately the same as over flat, partly forested, terrain. The peak around 220° is caused by upstream islands at a distance of 0.5-1 km.

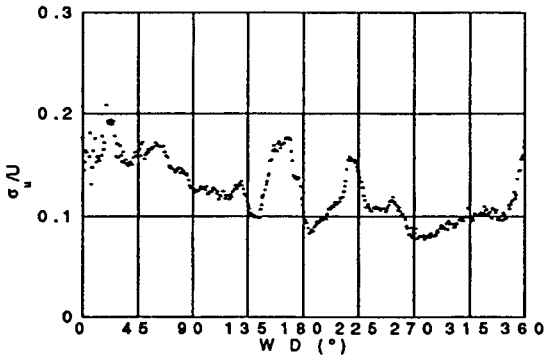

Figure 9: Turbulence intensity at Lyse, 32 m level, as function of wind direction. The peaks around 360° and 165° are caused by upstream wakes from nearby turbines.

4.3 Östergarnsholm

On the island Östergarnsholm 4 km east of Gotland in the Baltic Sea, meteorological measurements were started in May 1995. On a 30 m high tower wind and temperature are measured at 5 heights. The tower is located on the southern tip a the island, allowing a free over water fetch in a wide sector from northeast over east to southwest. In the western sector the water fetch is about 4 km, while for winds from the northern sector Östergarnsholm will locally affect the measurements. The site thus offers the opportunity to to take observations in a wide wind direction sector of the off-shore conditions.

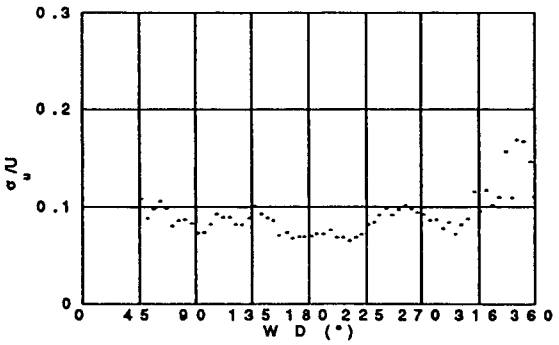

Figure 10: Turbulence intensity on Östergarnsholm, 30 m level, as function of wind direction.

This may clearly be seen in Figure 10, where turbulence intensity is plotted against wind direction. For winds from the sea, the intensity levels are between 0.07 and 0.09. In the sector around west-southwest, whith winds from Gotland, the turbulence intensity show maximum levels of about 0.10. Further to the north Östergarnsholm locally affects the turbulence levels.

5. SUMMARY

The field test reveals excellent performance of the CAWiV instrument. It truthfully records fluctuations in the two horizontal wind components of all scales up to the frequency limit 0.5 Hz set by the sampling frequency 1 Hz, and thus illustrates the possibility of using a relatively low cost instrument for high quality wind and turbulence measurements.

Within the Swedish wind energy research programme, the Department of Meteorology in Uppsala is presently taking wind measurements at three sites: Alsvik, Lyse and Östergarnsholm.

Site	*measurements started*	*amount of data*	*tower height*
Alsvik	April 1990	5 years	54 m
Lyse	June 1993	3 years	66 m
Östergarnsholm	May 1995	7 months	30 m

Also at the wind turbine site Näsudden on Gotland, winds are measured (by Vattenfall AB) on the 145 m high tower, but with a more slow responding cup anemometer system, only allowing data to be sampled with 0.1 Hz. The 0.1 Hz measurements started in 1993. Hourly mean wind data are available from the Näsudden tower since 1980.

Acknowledgement: The work was sponsored by NUTEK, Swedish Board for Industrial and Technical Development.

REFERENCES

[1] H. Bergström: Proccedeings European Community Wind Energy Conference, Travemünde 1993.

Appendix 4

Wind Characterisation for Design and Comparison with Standards, an Example from Lyse at the Swedish West Coast

Hans Ganander, Ingemar Carlen, Hans Bergström

Wind Characterisation for Design and Comparison with Standards, an Example from Lyse at the Swedish west Coast

Hans Ganander, Teknikgruppen AB, Box 21, S-19121 Sollentuna, Sweden
Ingemar Carlén, Division of Marine Structural Engineering, Chalmers Technical University, S-412 96 Gothenburg, Sweden
Hans Bergström, Department of Meteorological , Uppsala University, S-751 20 Uppsala, Sweden

ABSTRACT:The Lyse site at the Swedish west coast is an area with an archipelago of rocky islands to the west and an equally rocky mainland to the east. In between there are some open sea areas. As being a responsible project manager for the erection and the operation of a turbine at a site like Lyse, the question arises about characterisation of the wind for design or purchase of a wind turbine. Or in other words what wind turbine class has to used for the design, according to existing standards like for exemple IEC-1400.?

KEYWORDS:wind turbine class, extremes, design, certification

1. INTRODUCTION.

Since June 1993 meteorological measurements continuously measure wind speed and temperature at the Lyse site. After about two years an evaluation of all recorded data (95871 observations) started. Data from different wind direction sectors and for different stability situations were studied. Consequently it is possible to study in detail, and to quantify, the influence from quite different upstream conditions, in this type of heterogeneous coastal area. Thus e.g. mean wind profiles, turbulence intensities, and spectra are compared with results from 'ideal' sites with homogeneous surface conditions. There was also a possibility to test models of different complexity against the observations. This is of interest, because most wind descriptions for design assume homogeneous conditions and neutral stratifications as well was analysed in terms of common meteorological characteristics as mean wind speed, turbulence intensity and spectra. Wind structural parameters have therefore also been studied. They are called asymmetric and symmetric gradients and are used in design according to a method which is described in [1]. The large amount of continuously measured data has also made it possible to evaluate extreme value distributions. A presentation of this meteorological investigation is found in [2].

In the first part of this paper some results of the meteorological study are presented. Most of the results chosen are of interest for wind models for design purposes. The second part deals with aspects about the applicability of wind descriptions as in IEC-1400, regarding wind measurements of the Lyse site as an example.

2. SITE.

A map of the measurement site located at the Lyse Wind Power Station in the northern part of the Swedish west coast, is shown in Figure 1. This is a rather heterogeneous area, with an archipelago of rocky islands reaching typically 30 m to 50 m above sea level. Also the nearby mainland is non-homogeneous with many rocky parts with peaks and plateaus up to about 50 m in height.

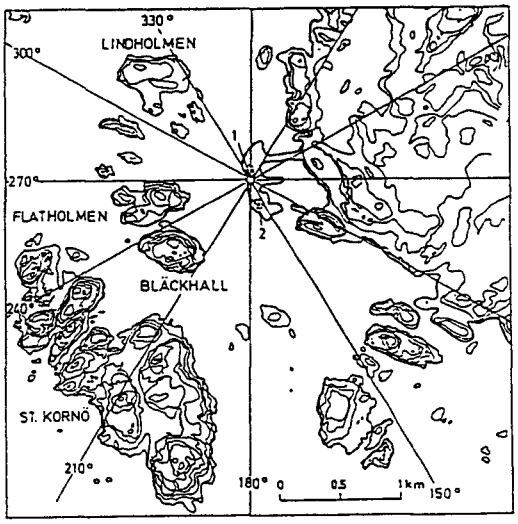

Fig 1 Map of the Lyse site

3. MEASUREMENTS.

The meteorological tower is 66 m high. It has been instrumented with combined cup/wind vane anemometers at 7 heights, giving information on mean wind conditions and turbulence characteristics of both longitudinal and lateral wind components. The upper five levels are equipped with two anemometers at each level, mounted on a northwest (308°) southeast (128°). The anemometers were calibrated in a wind tunnel. To get information about the thermal stability of the atmosphere, temperature is measured at five heights, using Pt-500 thermometers. At 2 m height air pressure and relative humidity are also measured.

Data is sampled on a PC (IBM compatible) with a time resolution of 1 s. It is temporarily stored on a hard disc for 3 days, and then a backup is made on a Wangtek 1 Gb steamer tape station.

4. SOME RESULTS OF THE EVALUATION

4.1. Turbulence intensity

The turbulence intensity (σ_u/U) of the two horizontal wind components (u and v), are often used as measures of the degree of turbulence in the atmosphere. Standard deviations and means are calulated per 10 min periods.

To illustrate how the heterogeneous surroundings influence the turbulence levels, the turbulence intensities have been averaged in 1°-sectors and plotted versus wind direction. The results are shown in Figure 2 for the u-component. Note the influence of the two turbines on turbulence intensities and on the gradient quantity in fig 3 as well.

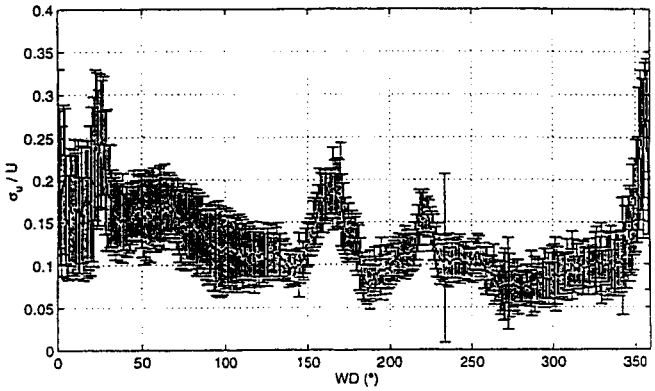

Fig 2 Turbulence intensity (10 min) of the longitudanal wind speed component u, versus wind direction (1 dgr)

4.3. Vertical wind gradient fluctuations

As wind observations were made once every second, it is, in analogy with the standard deviation of the wind speed, possible to determine the standard deviation of the vertical wind gradients using the individual 1 s measurements. The variation with wind direction of the standard deviations of the asymetric (ga) and of the symetric gradients (gs), σg_a and σg_s respectively, evaluated over consequtive 10 min periods, are shown in Figure 3 as mean values and standard deviations in 1° sectors of wind direction.

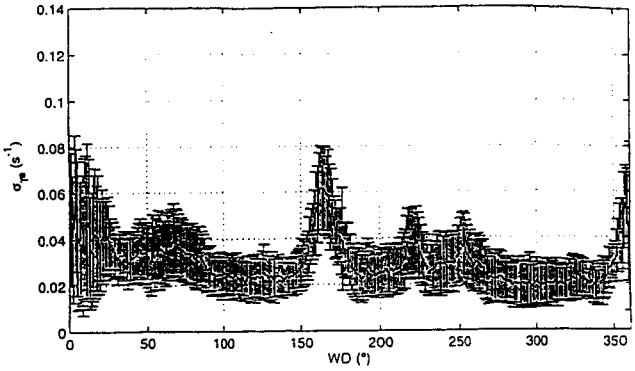

Fig 3 Standard deviations (10 min) of asymmetric vertical gradient (ga).

The behaviour of σ_u, the standard deviation of the longitudinal wind component, is rather well known, once the roughness length is known, at least simple homogenuous terrain. This is, however , not the case for the standard deviations of the asymetric and symetric gradients, why a relation to determine σg_a and σg_s from σ_u would be useful. In Figure 4 σg_a are plotted as function of σ_u for neutral stratification.

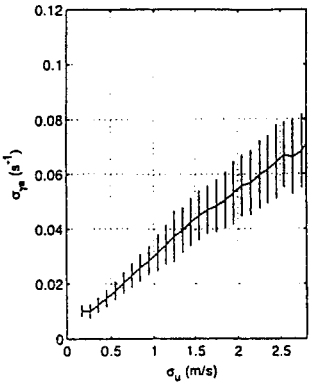

Fig 4 Standard deviations (10 min) of asymmetric vertical gradient versus σ_u, for neutral stratification.

Linear relations seem to be valid at least up to σ_u =2.8 m/s during neutral stratification. For other conditions it is found that linear relations are approximatively valid up to σ_u =2.2 m/s during stable stratification, and up to σ_u =1.5 m/s for unstable stratification. At larger σ_u -values, the relations with σ_ga seem to level off at constant values. Comparing the relations for the three stability classes, we find that $\sigma g_a / \sigma_u$ and $\sigma g_s / \sigma_u$ increase with increasing stability.

We may thus conclude that complete knowledge about σg_a and σg_s, may not be gained only through σ_u, but some consideration regarding the upstream conditions in heterogeneous terrain is also needed. But in most cases, it seems possible to determine σg_a and σg_s to within ±10-20% through empirical relations with σ_u, at least for σ_u -values less than about 1.5 m/s.

4.3 Extremes

Higher loading, in most aspects, is relatively more important for the designer. The reson is that fatigue damage is rather non linear. Behaviour of the wind in terms of variations (standard deviations) and extremes have therefore been investigated. Some of these results are shown below.

The variation of the 10 min averages of ga, versus wind direction is shown in Figure 5 for neutral stratification, where mean values and standard deviations for 1° sectors have been plotted. It can be observed that the standard

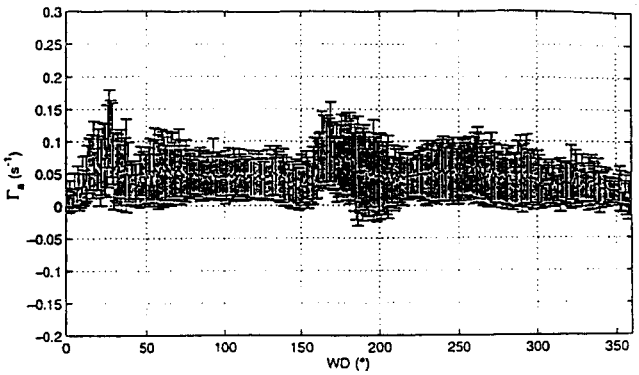

Fig 5 Mean values and standard deviations of the asymmetric gradient determined during 10 minutes

deviations are nearly of the same order as the mean values.

The frequency distributions of the standard deviation of the asymetric gradient during all 10 min periods with neutral stratification are shown in Figures 6

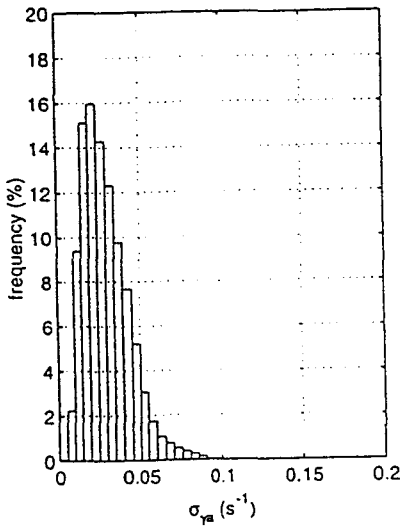

Fig 6 Frequency distribution of standard deviation of asymetric gradient over consequtive 10 min periods

The frequency distributions of the extreme 1 Hz asymetric gradient during all 10 min periods with neutral stratification are shown in Figures 7.

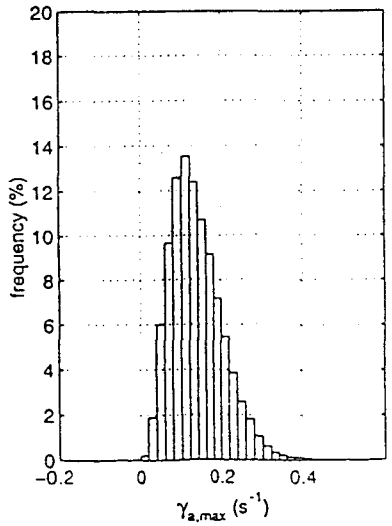

Fig 7 Frequency distribution of extreme 1 Hz max of asymetric gradient over consequtive 10 min periods

5. Summary of the meteorological study.

One conclusion of the analysis is that in spite of the rather heterogeneous surroundings with rocky terrain at various distances in all directions, the turbulence levels are by no means extremely high, when talking about **mean values**. Neither is the mean wind gradient extreme. Instead, the mean wind profile show a much smaller vertical gradient below 30 m than might have been expected even over the open sea, while above 40 m the wind gradient is somewhat larger than over the sea.

Comparisons with theoretical relations, for both mean wind profiles and profiles of turbulence intensity, show that the conditions above 40 m with wind directions from the land sector are about the same as the conditions over homogeneous terrain. The roughness length is of the order 0.1-0.2 m. With winds from the rocky islands in the western sector, the wind characteristics above 40 m are about the same, as in homogeneous areas with the roughness length 0.01-0.02 m.

The largest turbulence levels, except in the wake from the two wind turbines, have been found in a narrow sector around 220° with unexpectedly high turbulence levels and large mean wind gradients above 40 m, as well. The conditions in this sector are about the same as with winds from land as regards the turbulence levels, while the mean wind gradient is even larger, corresponding to a roughness length of 0.5 m. The cause for these rather extreme conditions in this narrow sector seems to be a combined effect of the upwind trajectory passing over the southeastern corner of the island Bläckhall, and further away passage over a main part of the larger island Stora Kornö.

The results of turbulence intensities also indicate large variations around the mean values. Standard deviations of 25-50% of the mean values are relatively common. The reason for these variations are not investigated yet.

An analysis of the 1 Hz vertical wind gradient values, divided into an asymetric and a symetric part, were also carried out. The gradients are evaluated at the height 49 m using simultanuous data from the height interval 32 m to 65 m. The result is that the standard deviations of these turbulent gradients, as an average, could be related to the standard deviation of the longitudinal wind component, but that variations in these relations were found to depend on the upstream conditions and also on the thermal stability. The distribution of the 1 Hz asymetric gradients showed that the difference in 1 Hz wind speed between the 65 m and the 32 m levels have an range between about -9 m/s and 16 m/s.

6. An extreme coherent event.

Due to the fact that the NWP400 turbine at the Lyse site has an event logging system and also measure some control system quantities, it was possible to find a situation with very unusual wind behaviour. The wind speed was about 15-20 m/s, coming from NE. Turbulence intensity was about 15-20 % and the turbine was running in stall at rated power. Examination of the logging information indicated an emergency stop and details of the 0.8 Hz sampled control variables made it clear that something extreme in yaw and/or teeter motions occurred. The meteorological measurements are continuously recorded, which made it possible to go into details regarding wind conditions at this occasion.

The result of this is presented in figure 8 below. They show during 5-7 seconds rather rapid and large changes

of wind direction. It is interesting to note that all ten (five shown in the fig.8) anemometers within the rotor area indicate the same time sequence. The average, at every sample, of all wind direction signals varies from 75° to 25° degrees during 3.5 seconds, indicating a wind direction change of 14 °/sec. These average quantities could be used as regarded as wind structural parameters, indicating coherent properties of the wind speed structures and changes.

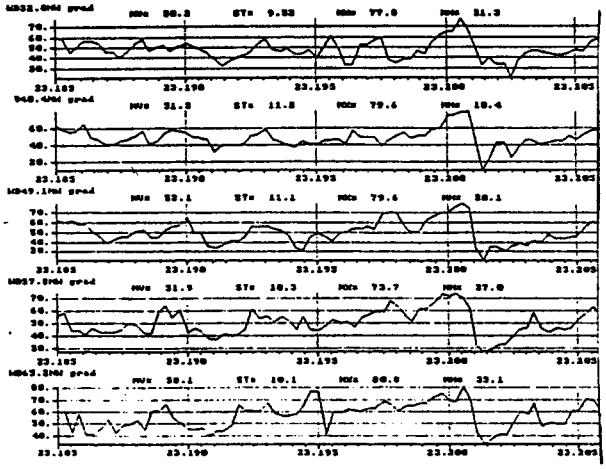

Fig 8 Time series of five wind direction signals at 32, 40, 49, 58 and 65 m heights.

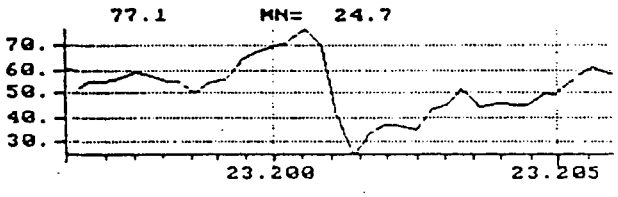

Fig 9 Averaged wind direction signal, showing a change 75° -> 25° during 3.5 seconds, approx 14 °/sec.

7. Comparing Spectra

Fatigue calculations are normally based on turbulence intensity models and spectra. The large variation of measured turbulence properties at the Lyse site, in different directions, have therefore been compared with IEC 1400-1. Figure 10 shows spectral densities, averaged over several sequencies for U = 10 m/s, z = 49 m, and near neural conditions. Sector 30° - 60°(dashed line) and 270° - 300° (dashdotted line), are compared with IEC 1400-1 (1996-2, Annex B, turbulence intensities A and B, Kaimal). Inertial subrange level for sector 30° - 60° corresponds closely to IEC 1400-1 (turbulence intensity B), while for the sea sector, 270° - 300°, this level is 5-6 times lower.

The following observations between measured spectra and those defined in IEC 1400 can be made:

- there is a relatively small difference between IEC spectra in comparison with measured spectra
- spectra for sea sector conditions or equivalent sites seem are rather low.

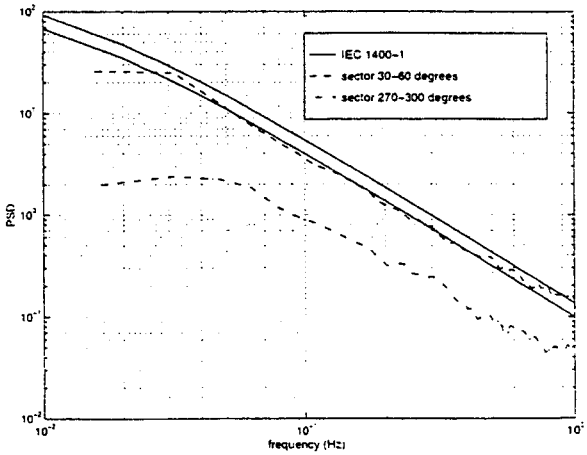

Fig 10.Comparison between two measured spectra and spectra according to IEC 1400-1.

8. Comments

Even if the concept of 'wind turbine class' according to the IEC code is accepted and used, results of these presented investigations arises many questions about the practical applicability of the code. Some of the questions are:

- how to find values of wind model parameters for fatigue design or for the determination of wind turbine class, reagrding different wind direction? Should weighted mean values be used or worst value or...?

- what does it mean that spectra for rough terrain are well described by the IEC code, while sea conditions or corresponding flat terrain are not?

- is there any description available, which defines the range of applicability of wind models in the IEC code? What is flat / complex terrain and/or what obsticals within what distances are important?

These are some of the questions that can be asked. Hopefully results presnted here will contribute to future R&D and cerification activities

9. References

[1]: Fatigue Design by using a modified RFC description of the wind. Hans Ganander and Hjalmar Johansson. AWEA National Conference, Honolulu, Hawaii, 1988.

[2]: Wind Measurements at Lyse Wind Power Station. Hans Bergström. Wind Energy Report WE 95:2, Department of Meteorology Upsala University

[3]: IEC 1400-1, Second Edition 1996-2. Wind Turbine Generator Systems Part 1, Safety Requirements. Modified by 88/7 (Butterfield) 102, 25 February 1996.

Appendix 5

Wake Effects in Alsvik Wind Park: Comparison Between Measurements and Predictions

Mikael Magnusson, K. Rados, K. Pothou

WAKE EFFECTS IN ALSVIK WIND PARK: COMPARISON BETWEEN MEASUREMENTS AND PREDICTIONS.

M. Magnusson[1], K.G. Rados[2] and K.P. Pothou[2]
[1]Department of Meteorology Uppsala University
Box 516, 752 42 Uppsala, Sweden
[2]Fluid section, National Technical University Athen
P.O. Box 64070, 15710 Zografou, Athens, Greece.

ABSTRACT: In this paper characteristic parameters in a wind turbine wake are studied. The data used are full-scale measurements from a wind farm in Sweden, Alsvik, and results from a numerical model calculated for the same site. The results are valid for neutral stratification. The model employs a particle-vortex approach at the rotor plane, a Navier-Stokes solver in the near wake and applies self preservation in the far wake. The parameters investigated are the relative velocity deficit at centre line and hub height, and the radial distribution of the turbulent kinetic energy.
Keywords: Wake, Measurements, Model, Turbulence

1. INTRODUCTION

To be able to obtain information of the wake effects in a wind farm numerical models have to be used.

For validations of the numerical models, tests against full-scale measurements have to be performed. Here some of the results derived with a numerical model are compared with full-scale measurements from the Alsvik wind farm in Sweden.

The measurements from the Alsvik wind farm have earlier been used to investigate how different parameters influence the wake flow e.g. in [1].

One result from these investigations is that the atmospheric stratification is affecting the flow. Another result is that the efficiency of the turbine is important for the development of the wake. It was also found that the best way to analyse the measured data is by using the transport time, t, downstream the turbine as parameter instead of the distance, x. With this method it was possible to derive an expression for the velocity in the wake as function of turbine data and site characteristic, see below.

The transport time, t, is calculated:

$$t(z) = \frac{x}{U_a(z)} \qquad (1)$$

where x is the distance downstream and U_a is the ambient wind speed at the height, z. This approach is also applicable on the model results, as the free stream velocity is known.

2. DESCRIPTION OF THE MODEL

The model is axisymmetric and assumes that the wake is decomposed into three regions: the rotor region the near-wake region and the far-wake region [2].

Figure 1 shows a schematic description of the different parts of the numerical model.

- rotor region
- near wake region
- far wake region

The flow around the rotor of a wind turbine is a rotational flow. Bound vorticity is generated on the blades as a result of their shape whereas, according to Kelvin's theorem, free vorticity must be shedded downstream the rotor plane. The vortices generated at the blades are treated with a three-dimensional vortex particle model, GENVUP=GENeral Unsteady Vortex Particle method [3].

The data calculated with the vortex model are used as inlet conditions for the near-wake region, together with the ambient flow data. The velocity distribution used is the one given by the analysis of the rotor region, whereas the inlet distributions of the turbulent kinetic energy k and the turbulent length scale L are modified in order to account for the specific ambient conditions [3].

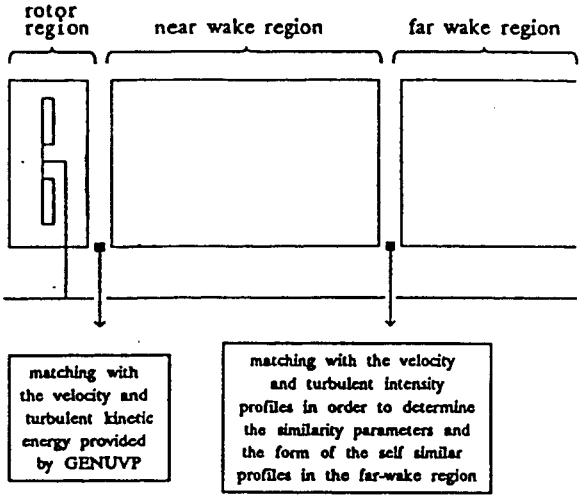

Figure 1: Schematic description of the model

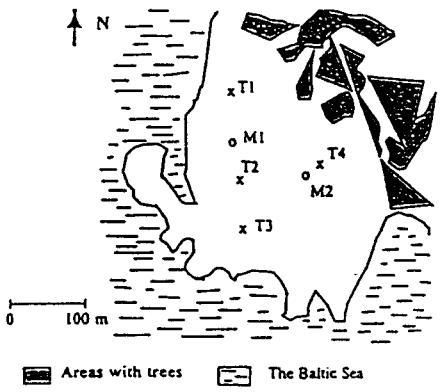

Figure 2: The site

As regards L, for $r > R$ (where R denotes the radius of the rotor) it is set equal to the ambient length scale L_α, whereas for $r < R$, local equilibrium between production and dissipation of k is used [2] This assumption was found to be the best choice according to the conclusions of a parametric analysis presented in [4].

With these boundary conditions the Navier-Stokes equations are solved with the AXI-NS code to obtain the velocity and turbulence intensity profiles in the near-wake region.

The velocity in the far wake is calculted with functions assuming self preservation

3. THE FULL-SCALE MEASUREMENTS AND SITE DESCRIPTION

The full-scale data in this paper are from measurements in a wind farm on the island Gotland in the Baltic sea. The wind farm consists of four 180 kW Danwin wind turbines. The hub height is 35 m and the rotor diameter is 23 m. The turbine starts to operate at 5 ms^{-1} and regulates due to stall at 12 ms^{-1}. At the site (see Figure 2) there are two 54 m meteorological masts located (M1 and M2). On both masts there are wind sensors at eight levels and also temperature sensors at five levels on mast M1. The data are sampled at a rate of 1 Hz. The wind sensor is a combined light-weight cup anemometer and wind vane, developed at MIUU (Meteorological Department, Uppsala University). The temperature profile consists of Pt-500 sensors in ventilated radiation shields. The measuring system is described in [5].

During a concentrated field effort in June 1991 turbulence measurements were performed on mast M2 at three levels. The turbulence instrument used was the MIUU instrument, which is described in [6]. It is basically a wind vane based three axial hot film system supplemented with dry and wet bulb temperature sensors. The sampling rate was 20 Hz.

4. RESULTS

4.1 Relative velocity deficit

In this section interest is directed towards the development of the relative velocity deficit at centre line and hub height as function of transport time downstream, for neutral stratification. The radial distribution is also studied for three transport times.

In this study C_T is calculated with the aid of the produced power. The assumption is that the relation between C_T and produced power is constant, hence, independent of the actual wind speed. The power produced must be divided into two classes depending whether or not the turbine is regulated.

Figures 3 to 5 shows radial distribution of the relative velocity at three times downstream the turbine. In figure 3 the model results (—) is larger at centre line compared to the measuremets (+). The measurements shows double peaked structure while the calculted values have maxima at the centre line. For the other two times studied the calculated relative velocity deficit is lower compared to the measurements at centre line. However the form of the distribution is satisfactory. The above difference at the centre line might be a result of the mixing velocity, which probably is higher in the model compared to what is found for the measurements. The time dependency of the relative

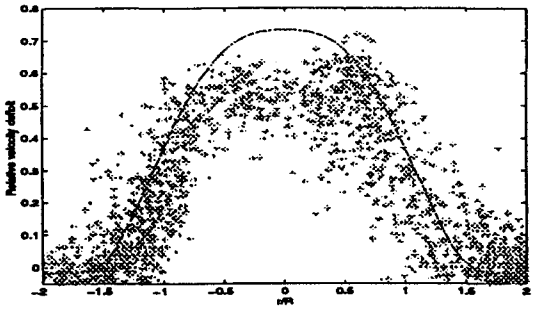

Figure 3: Radial distribution of the relative velocity deficit at 3s, $C_T = 0.8$

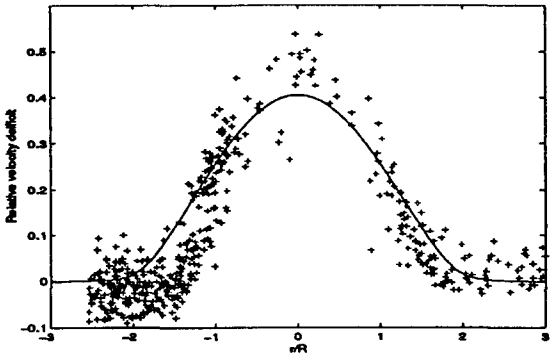

Figure 4: Radial distribution of the relative velocity deficit at 10s, $C_T = 0.8$

velocit at centre line and hub height is presented in figure 6 which shows a comparision at centre line of the relative velocity deficit between results from the numerical model (—). and measurements (*) for $C_T = 0.8$. From the figure it is seen that, for $t < 20\ s$, the numerical results are lower than measured, while the opposite is true for larger travel times, t.

An analytical expression has been derived for the relative velocity deficit time dependency for times larger than the time required to create one maximima at centre line, t_0.

$$\frac{\Delta U}{U} = 0.4 \ln\left(\frac{t_0}{t}\right) + C_T \qquad (2)$$

The curve corresponding to neutral stratification (....), $t_0 = 5.25\ s$, agree with the measured data and the slope of the curve in the range $5 - 15\ s$ is similar to that of the numerical curve in this range, $t = 15\ s$ is the approximate lower limit of the far wake.

4.2 Turbulent kinetic energy

The radial distribution of the turbulent kinetic energy, $k = \frac{q^2}{U_a^2}$ for three cases is presented in Figures 7 to 9. The general structure is that the measured

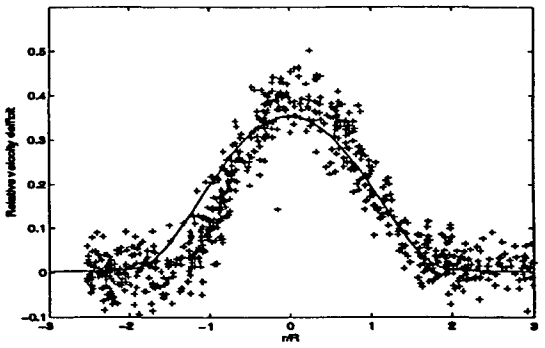

Figure 5: Radial distribution of the relative velocity deficit at 8.5s, $C_T = 0.65$

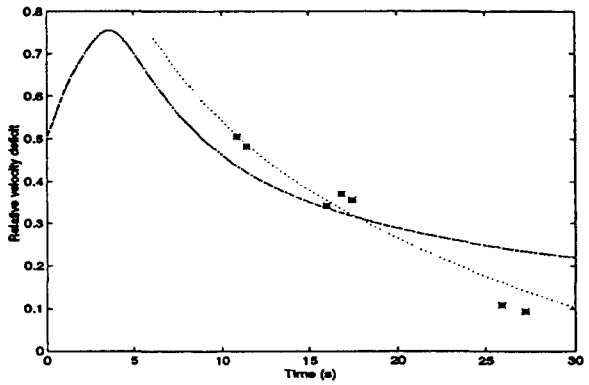

Figure 6: Calculated an measured relative velocity deficit as function of the time downstream the turbine. —: numerical model, ...: Eq 4, *: measurements, $C_T = 0.8$

values (+) are larger compared to the modelled values (—) at all times downstream. At 3.5 s, Figure 7, the model has maximum energy at $r = R$ and a minimum at $r = 0$. This behaviour is a result of the large reduction of wind speed in the middle sections of the blades. Large reduction of wind speed generates large shear, and at this time there has not yet been any considerable advection of turbulent energy towards the centre. The magnitude of the measurements is much higher than the predictions. This higher level is a result of the higher turbulent intensity in the ambient flow (0.13 compered to 0.07) and higher efficency of the turbine for the measured data. But the structure in the measurements does not contradict the shape derived from the model. At $t = 8.5\ s$ and $t = 17\ s$ (see Fig. 8 and Fig. 9) energy has been transported towards the centre. for the model, although the relative velocity deficit has a maximum at the centre line at this time, see Figure 4. The reason for this might be that the production of turbulent energy at the maiximum gradient is higher than the advection rate. The data from the measurements does not indicate a minima at the

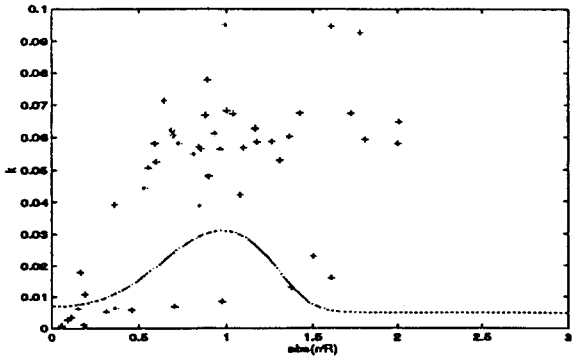

Figure 7: Radial distribution of the relative velocity deficitturbulent kinetic energy at 3s, $C_T = 0.8$

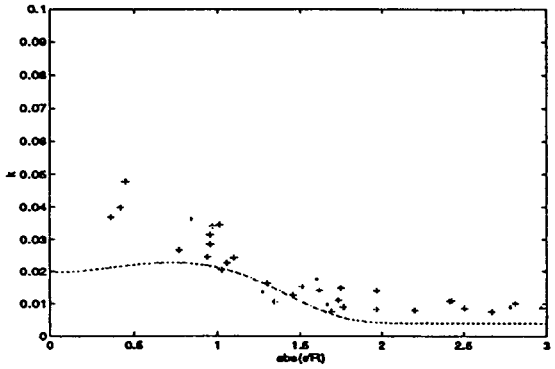

Figure 8: Radial distribution of the relative velocity deficitturbulent kinetic energy at 8s, $C_T = 0.8$

centre line, so the advection rate might be higher than found in the model. In Figure 9 after 17.5 s the peak value of turbulent energy is occuring at the centre line. Studying the lateral structure of k for the different times, it is found that the position of the maximum is moved towards the centre as the time increases. This is a consequence of the behaviour of the velocity distribution in the wake. Initially the maximum reduction is occurring approximately at the centre of the blade, and as the time develops the maximum is occurring at the centre line. The turbulent energy produced by shear is advected towards the centre.

CONCLUSIONS

Comparisons between full-scale measurements and numerical simulations have been performed. The relative velocity deficit at centre line and hub height is investigated, together with the turbulent energy The agreement is found to be relatively good for the near wake. In the far wake there is substantial difference. This could be attributed to the axisymetric character of the numerical model. The 3D effects of the atmospheric boundary layer

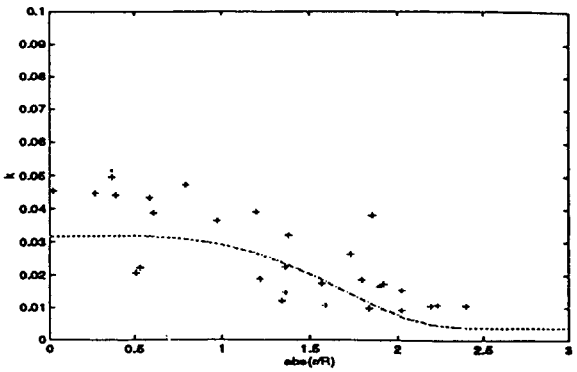

Figure 9: Radial distribution of the relative velocity deficitturbulent kinetic energy at 17s, $C_T = 0.8$

which is important for the far-wake are not taken into account by the model. However, an posteriori procedure for the influence of such effects is described in [4]. Nevertheless, where the relative velocity deficits are similar, the results for the turbulent kinertic energy also agree. This indicates that the energy transport in the wake is, as expected, strongly correlated to the relative velocity deficit.

Further work

The next step is a full 3D resolution of the wake for better understanding on one hand the 3D atmospheric boundary layer effects and on the other hand the influence of the atmospheric stratification which can indirectly be included in a 3D numerical model by the inlet conditions. Since the influence of the atmospheric stability is found to be rather important for the development of a wind turbine wake [1].

References

[1] M. Magnusson, A. Smedman, Wind Engineering vol. 18 (1994) No, 3.

[2] S.G. Voutsinas, K.G. Rados, A. Zervos, Proceedings ECWEEC 93 (1993).

[3] S.G. Voutsinas, M.A. Belessis, K.G. Rados, AGARD Conference Proceedings 552 FDP, 11 (1995)

[4] S.G. Voutsinas (ed.), Final report of Jour-0087 Project (1992).

[5] H. Bergström, K. Lundin, Proceedings ECWEC 93 (1993)

[6] U. Högström, J. Appl. Meteorology 21 (1982).

Appendix 6

A New Approach for Evaluating Measured Wake Data

Mikael Magnusson

A NEW APPROACH FOR EVALUATING MEASURED WAKE DATA

M. Magnusson
Department of Meteorology Uppsala University
Box 516 S-751 20 Uppsala

ABSTRACT: Wind turbine wakes have been studied by analysing a large set of atmospheric data, from a wind farm with four turbines sited on a flat coastal area. The results obtained have been generalized to allow tests against data from other full scale wind turbines as well as wind tunnel simulations. These comparisons are found to give very satisfactory results. The thrust coefficient is found to be a better parameter for description than wind speed, of wake characteristics beacuse it implicitly includes the effect of regulation. It is also found that down-wind travel time is more convenient to use than downwind distance in this context. The travel time to the end of the near wake region, i.e. to the point where a single velocity deficit peak first appears, is found to be inversely proportional to the rotational frequency of the turbine and to the turbulence intensity of the ambient air flow and proportional to the ratio of the wake radius and the hub height. For larger travel times, i.e. for the far wake region, it is found that the centre line relative velocity deficit decreases with the logarithm of the time traveled and is parametrically dependent on the time constant and the thrust coeficient
Keywords: Wake, Measurements, Stratification, Turbulence

1. INTRODUCTION

For large-scale exploitation of wind energy, it will be necessary to put wind turbines together in clusters or wind farms, as areas with suitable wind resources are limited. But in wind farms the turbines will always interfere with each other. The flow field behind a wind turbine is characterised by low wind speed, strong wind shear and a high degree of turbulence, and thus a second wind turbine placed behind the first one along the wind direction is likely to produce less energy than the undisturbed one, by an amount that will decrease with increasing distance. As wind shear and turbulence is recognised as two causes for dynamic loads on wind turbines, it implies that detailed knowledge of the flow field behind wind turbines is needed for planning of wind farms.

In this investigation wakes behind wind turbines in the Alsvik wind farm on the island of Gotland in the Baltic Sea have been analysed by using the time as the parameter determining the development of the relative velocity deficit.

2. SITE AND MEASUREMENTS

The Alsvik wind farm consists of four 180 kW Danwind turbines and is located close to the shore line on the West coast of Gotland. The site, which is presented in Figure 1, is a flat coastal strip covered with grazed grass and low herbs. Only data with wind coming from the sea ($200^o - 320^o$) is used in this investigation.

The four turbines are stall regulated, three bladed with a diameter of 23 m and a rotation speed of 42 r.p.m.. The hub height is 35 m. Cut-in speed is 5 ms^{-1} and the rated wind speed is 12 ms^{-1}.

Meteorological measurements have been performed at Alsvik since June 1990. There are two masts (M1 and M2 in Figure 1) whith a total height of 54 m. Wind speed and direction are measured at 8 heights on both masts and temperature at 5 heights on mast M1. Wind speed and direction are measured with a type of sensor developed at the Department of Meteorology in Uppsala (MIUU). The instrument is a combination of a small three cup anemometer and a very light wind vane . Wind speed and direction are

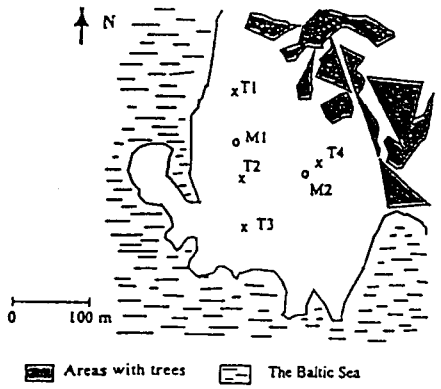

Figure 1: The site

sampled with 1 Hz. The instrument is described in [1]. Temperature is measured with 500 W platinum sensors.

The four turbines are marked T1-T4 in Figure 1. Wake profiles from turbines T1-T3 are measured on mast M2, while the undisturbed wind profile is recorded on mast M1. The distance from T1, T2 and T3 to mast M2 is 9.6D, 4.2D and 6.1D, where D is the rotor diameter (23 m).

2. DATA

In [2] the relative velocity deficit and the turbulence in the wake were studied as function of distance and stability. The relative velocity deficit is defined as $\frac{\Delta U}{U_a} = \frac{(U_a - U_w)}{U_a}$, where 'a' denotes the ambient wind speed and 'w' the wind speed in the wake. The stability parameter used was the Richardson Number, Ri.

$$Ri = \frac{g}{T_0} \cdot \frac{\frac{\partial \Theta}{\partial z}}{\left(\frac{\partial U}{\partial z}\right)^2} \qquad (1)$$

where T_0 is a reference temperature, g is the acceleration of gravity and Θ is the mean potential temperature.

It was found that the relative velocity deficit decreased with increasing distance from the turbine and increased with increasing stratification.

In the present investigation atmospheric stratification is divided into three stability classes: unstable (Ri<-0.05), neutral (-0.05<Ri<0.05) and stable (Ri>0.05). Richardson number was calculted using temperature and wind speed at 18 and 31 m.

The thrust coefficient is used for determine how well the turbine operates in the wind.

4. RELATIVE VELOCITY DEFICIT

4.1 Dependence of transport time and stability

Figure 2 a shows measurements of relative velocity deficit for unstable stratification as a function of distance and for $C_T = 0.84$. This is the usual way to plot relative velocity deficit but the data points are very scattered at each distance (4.2D, 6.1D and 9.6D). A more physical way to represent the variation of deficit is to use transport time behind the turbine instead of distance. The near wake is determined by the properties of the turbine but the diffusion of the wake downstream is settled by the ambient turbulence and the longer transport time the stronger influence of atmospheric turbulence. The transport time, t, at a fixed height, z,

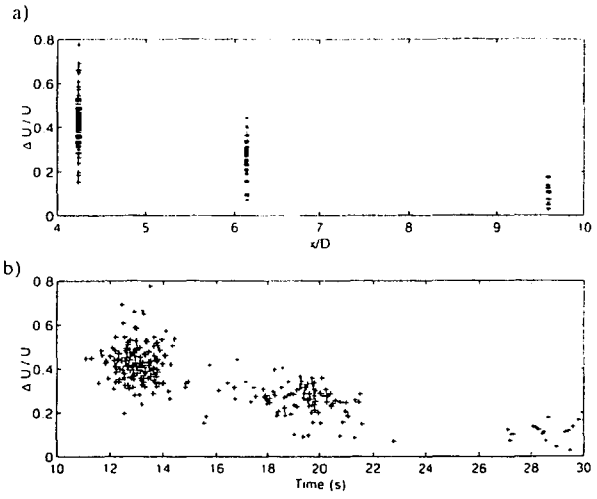

Figure 2: The relative velocity as function of a) distance and b) time

is calculated.

$$t(z) = \frac{x}{U_a(z)} \qquad (2)$$

Figure 2 b shows the same relative velocity deficit values as in Figure 2 a but as a function of transport time. There is still a rather large scatter, but the data points form a more continuos band. Taking the data at x = 6.1D with the standard deviation $\sigma \approx 0.075$, and dividing it in data intervalls of 1 s, it will range from 17 to 23 s. The mean of the standard deviations is in this case reduced to $\sigma \approx 0.06$. The mean of the relative velocity deficit at this distance is of the order 0.25.

By using time scale instead of length scale, yields a more contiuos pattern and also reduces the scatter. We conclude that the relevant parameter is the transport time instead of the distance.

In Figure 3 isolines of relative velocity deficit in unstable stratification are given as function

of height above ground and transport time for $C_T \approx 0.85$ in Figure 3 a and $C_T \approx 0.6$ in Figure 3 b. The relative velocity deficit is much larger for large C_T -values (low wind speeds) than for small (high wind speeds), because the turbine is working much more effectively at low wind speed, although the power production is less. In Figure 4 a and b the corresponding relative deficit values are given but for stable air. It is quite clear that the relative velocity deficit increases with increasing stability. The ambient turbulence is less effective to diffuse the wake during stable conditions, and the stability tends to suppress vertical motions.

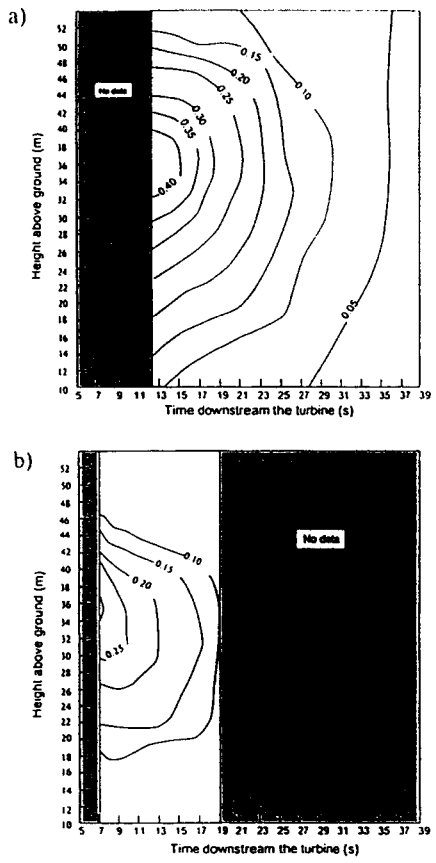

Figure 3: The relative velocity deficit as function of time, a) C_T=0.85 stable, b) C_T=0.85 unstable

4.2 Near wake

In the region closely behind the turbine the wake is mainly determined by the characteristics of the turbine, although atmospheric stratification also comes into play. In [3] theoretical calculations, supported by measurements, show that just behind the rotor the relative velocity deficit has two peaks, situated at the middle section of the blades. With increasing transport time behind the turbine

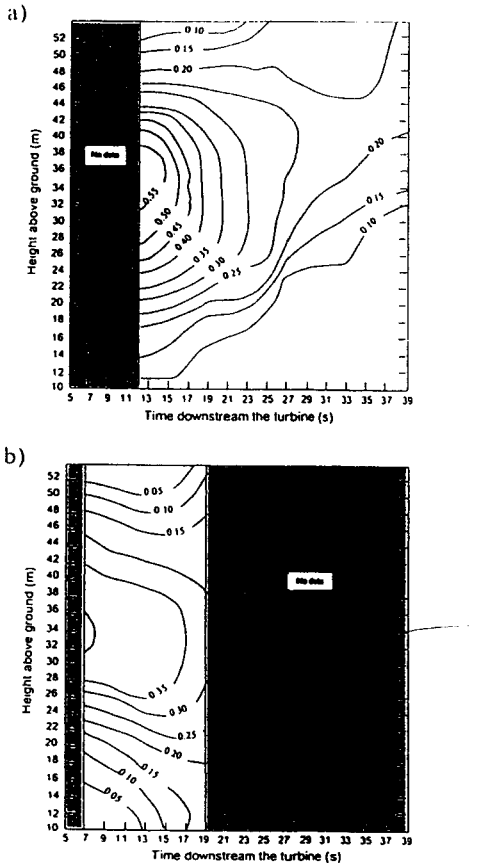

Figure 4: The relative velocity deficit as function of time, a) C_T=0.6 stable, b) C_T=0.6 unstable

momentum transport towards the centre gradually wipes out the two peaks and one maximum at the centre will occur, the time required is denoted t_0.

For neutral stratification t_0 can be expressed as

$$t_0 = \frac{1}{f} \cdot \ln\left(\frac{H}{z_0}\right) \cdot \frac{R}{H} \qquad (3)$$

where f is the rotational frequency, H the hub height, z_0 the roughness height and R the rotor radius.

For the Alsvik turbines t_0 is calculated to be approximately 5.25 s, with a z_0-value of 0.0005 for the sea sector at Alsvik.

4.3 Far wake

Beyond $t = t_0$ the relative velocity deficit decreases with downstream travel time. Initally at the time t_0 the relative velocity deficit is larger for larger C_T. An analytical expression can be derived by using the above results.

$$\left(\frac{\Delta U}{U}\right)_w = C_2 \cdot \ln\left(\frac{t_o}{t}\right) + C_T \quad t > t_o \qquad (4)$$

fitting this expression to data from Alsvik gives $C_2 = 0.4$. In Figure 5 $(\frac{\Delta U}{U})$ is given as function of transport time for the sites : a) Nibe, b) Sexbierum, c) Alta Nurra, d) wind tunnel measurements at TNO and e) Näsudden. The solid curves in all figures are Eq (4). The overall impression is that this equation fairly well describes the deficit decrease as a function of transport time. The site with largest difference between measurements and calculation is Näsudden. This is due to the fact that the averaging time is 30 min. The averaging time for the other full-scale sites is 1 min. (Nibe, Alta Nurra) and 3 min. (Sexbierum). Case studies at Alsvik show that longer averaging times gives lower relative velocity deficit, because of meandering of the centre.

Conclusions

The thrust coefficient, C_T of the turbine is found to be a better variable for description of turbine wake characteristics than wind speed, because it implicitly includes the effect of regulation on power output from the turbine.

The characteristics of the wake is found to be primarily a function of downwind travel time as opposed to travel distance as conventionally assumed. The scatter of the data points is found to be reduced when time instead of distance is used in the various expressions describing downwind development of the wake. This behaviour is thought to be due to the time of exposure of the developing wake to the turbulence in the ambient air flow being of decisive importance.

In the near wake the crosswind profile has two peaks, which gradually merge into a single centre line peak. The downwind travel time for this merge to appear, t_0, is found to be inversely proportional to the rotational frequency of the turbine and to the turbulence intensity of the ambient atmospheric flow and proportional to the ratio of the wake radius to the hub height.

For travel times $t > t_0$, i.e. for the far wake region, the relative centerline velocity deficit is found to be linearly related to $\ln(\frac{t_0}{t})$.

References

[1] H. Bergström, K. Lundin, Proceedings ECWEC 93 (1993)

[2] M. Magnusson, A. Smedman, Wind Engineering vol. 18 (1994) No, 3.

[3] M. Magnusson, Wind energy report WE 95:3, Dept. of Meteorology. UU.

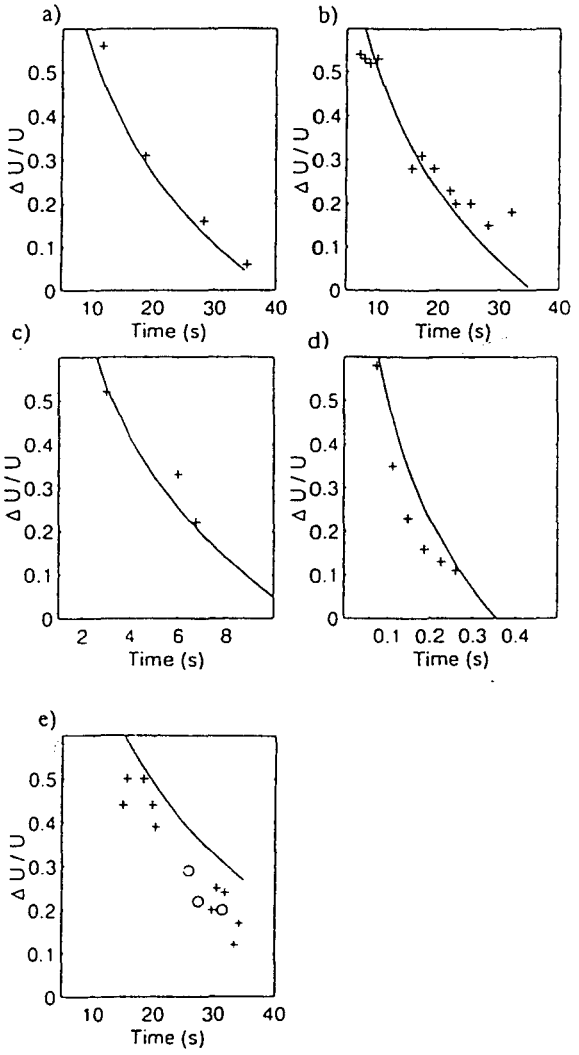

Figure 5: The relative velocity deficit as function of the time downstream the turbine for five sites. +: Tower measurements, o: Sodar measurements, –: Calculated using Eq.(2). a) Nibe, C_T=0.82, b) Sexbierum, C_T=0.75, c) Alta Nurra, C_T=0.85, d) TNO-Wind tunnel, C_T=0.87, e) Näsudden, C_T=0.8

Appendix 7

Calibration Procedures for Improved Accuracy of Wind Turbine Load Measurements

Jan-Åke Dahlberg och Hjalmar Johansson

Calibration Procedures For Improved Accuracy Of Wind Turbine Blade Load Measurements

1. **Jan-Åke Dahlberg**, FFA, The Aeronautical Research Institute of Sweden,
Box 11021, S-161 11 Bromma, Sweden, tel +46 8 6341000, fax +46 8 253481, jad@ffa.se

Hjalmar Johansson, Teknikgruppen AB,
Box 21, S-191 21 Sollentuna, Sweden, tel +46 8 359455, fax +46 8 969987

Abstract: External loads acting on wind turbine blades are mainly transferred via the hub to the rest of the structure. It is therefore a normal approach to measure the loads acting on the turbine by load measurements in the blade roots. The load measurement is often accomplished by measurements of strain on the surface of the blade or the hub. The strain signals are converted to loads by applying calibration factors to the measurements. This paper deals with difficulties associated with load measurements on two different wind turbines; one with strain gauges applied to a steel hub where a linear stress-load relationship is expected and the other with strain gauges applied to the GFRP blade close to the bearings where strong non-linearity's and temperature effects are expected. This paper suggests calibration methods to overcome these problems.

Keywords: Calibration, Load, Measurements, Blades,

Introduction

Part I, deals with load measurements on a three bladed, Danwin 180 kW, stall regulated WECS. The turbine under test is located in the Alsvik wind farm on the isle of Gotland in the Baltic sea. Strain gauge sensors were applied on the steel hub. The calibrations were performed by rotating the turbine slowly in low wind conditions. Comparisons of measured and calculated moments from the turbine in Alsvik showed large discrepancies. An explanation of the problems associated with the load measurements and calibration and recommendations to avoid these problems are presented.

Part II, deals with load measurements on the two bladed, 3000 kW, pitch controlled WECS, Näsudden II. The turbine under test is located on the Näsudden peninsula on the island of Gotland in the Baltic sea. Strain gauge sensors were applied on the GFRP blades close to the bearings. Play in the blade pitch bearings and other non linear deformations near the bearings influence negatively the linear relationship between external loads and the strains at the location of the gauges. A calibration method has been developed to overcome this problem. The method utilises measurements in well defined conditions, such as start in high steady wind speed in combination with corresponding structural dynamic simulations.

Part I:
Experiences from load measurements on the DANWIN 180 kW turbine in Alsvik

Background

An extensive investigation of the blade loads on a three bladed, stall controlled WECS has been carried out through continuos measurements since 1990. The turbine under test is located in the Alsvik wind farm on the island of Gotland in the Baltic sea. The hub is made of cast steel and has relatively long cylindrical root parts suitable for applying strain gauge sensors. Strain gauge sensors were applied on the steel hub, on all three legs, in planes 45° off the plane of rotation. The purpose for not aligning the bridges in pure in-plane and out of plane directions was to enable the blade gravity moment to be the applied calibration load, thus acting on both load components.

Calibration

The calibrations were performed by rotating the turbine slowly in low wind conditions. Figure 1 shows the measured and fitted output from one of the two components. The mass of the blades and the centre of gravity are well known. The calibration factors were then easily determined from the fitted sinusoidal output from the two components. Flap wise (out of plane) and edge wise (in plane) bending moments were composed from the two components of the measured signals.

Comparison with measurements

Comparisons between measured and calculated moments on Danwin 180 showed large discrepancies. The measured flap moments were far below the calculated values. Comparisons of the mechanical input power estimated from the edge wise bending moment (and rotational speed) and the corresponding output power from the generator indicated an efficiency of the transmission of more than 100%. In other words, also the edge moments seemed to be too low. However, the magnitude of the gravity moment turned out correct. These discrepancies put forth a question on the appropriateness of the used calibration procedure; Were the loads during calibration representative for the loads during normal grid connected operation?

Finite element analysis (FEM) of the hub

A comprehensive finite element analysis of the hub was performed in order to investigate these questions. A model of the hub, shaft and blade root was made, see Figures 2 & 3 The end of the primary shaft of the model was assumed to be fixed. Unity loads (six components) were applied to all blades in order to get the complete picture. The different load conditions from normal operation and calibration could easily be investigated by appropriate combinations of the unity loads. The analyse was made with STRIPE [1], a finite element program developed at FFA.

Correction matrix

From the calculated signals it was possible to derive a 6*6 matrix (below) which could be used to correct the measured flap and edge wise moments. The matrix accounts for sensitivity and cross talk correction factors for each component.

	Corr.	Matrix						Meas.
Flap 1	16.4	1.216	0.000	0.094	-0.068	0.094	0.068	10.7
Edge 1	20.6	0.000	1.131	-0.028	0.144	0.028	0.144	18.5
Flap 2	29.9	0.094	0.068	1.216	0.000	0.094	-0.068	19.8
Edge 2	8.6	0.028	0.144	0.000	1.131	-0.028	0.144	7.1
Flap 3	37.8	0.094	-0.068	0.094	0.068	1.216	0.000	29.4
Edge 3	-8.6	-0.028	0.144	0.028	0.144	0.000	1.131	-11.1

Figure 4 shows a comparison between measured and corrected signals from the slow rotating calibration. The calculated signals from the finite element analysis are very close and confirms the validity of the results from the FEM analysis.

Corrected measurements

Figures 5 and 6 show a comparison between measured and corrected signals from a measurement campaign. The measured mean flap and mean edge moments should be increased by up to 40%.

Figure 7 shows how a typical load spectra based on the old measured data and the new corrected data. The difference is significant.

Discussion and Conclusions from Part I

Load measurement is accomplished by strain measurements which is converted to loads by means of calibration factors. Loads in other parts of the structure may give rise to strain levels in the measured parts and consequently apparent loads (cross talk) in the part of interest. Although the hub in Alsvik seemed to be ideal for load measurements, the interaction (cross talk) was surprisingly strong. The measurements in Alsvik fortunately included all three blade roots thus enabling the cross talk to be taken into account.

The bending moments, during calibration by slow rotation, from each blade are balanced by each other and no torque is transferred into the shaft. During normal operation however, moments from the blades are balanced by the shaft. So the stress flow during normal operation is different from the stress flow during calibration.

To avoid these problems the following general conclusions can be drawn:

- Measure all major external loads that affect the structure.
- Use a calibration method that, as far as possible, resembles the load situation during measurement conditions.
- Evaluate the cross talk.

Part II:
A calibration procedure for the Näsudden-II strain bridges in the blade roots, where strong non-linear and temperature effects are present

The cylindrical (ϕ 2.5 m) blade roots at the Näsudden II turbine have 6 full strain bridges each, situated very near (0.6 m) the pitch bearings. As the strain gauges, by lack of space, have been bonded so close to the bearings, the bridge signals are not linearly depending on the blade loads in the whole loading range. The complex stress distribution near the pitch bearings makes, in general, all strain bridges sensitive to all types of loads (strong cross talk). The blade root material (GFRP) is rather anisotropic, making the bridge signals significantly influenced by the temperature.
As a consequence of these related conditions, the blade root bridges cannot be calibrated by slowly rotating the turbine rotor (loaded by its own weight) or by static loading the blades by external well-known forces. Instead the bridges must, if possible, be calibrated in or close to the real operating conditions, as described below:

A turbine start at steady high wind has been chosen from the continuous measurements at Näsudden, where the following steps can be observed:

1. the rotor accelerates up to 21 RPM by pitch control
2. the generator is connected to the net
3. the power is raised up to about rated power (3MW).

Based on the measured wind speeds at 38, 75 and 120 m height, pitch angle, rotor-speed and generated power, a corresponding turbine start has then been simulated by the computer program VIDYN [2]. The results are written as time series representing, among many other quantities, the blade root loads, rotor and pitch angles, rotor speed and generator power.

VIDYN is a program written by Teknikgruppen AB for simulations of horizontal axis wind turbines (HAWT). Its results have been verified against measurements from

many turbines at different operating modes and wind situations.

The characteristics of the procedure mean that the calibration of the blade root bridges is based on:

1. Measurements from a turbine start at steady high wind.
2. Simulation (program VIDYN) of a corresponding start at the same wind conditions.
3. Least Square Method: The composed measured signals are fitted to the VIDYN-computed quantities when the measured and simulated **rotor angles** are equal (after interpolation) and

   a) before generator net-connection: the **rotor speeds** are as equal as possible
   b) after generator net-connection: the **generator powers** are as equal as possible.

All samples from the start recordings have not been used in the curve-fitting computations, instead, limited periods have been chosen. Especially only a late period from the rotor acceleration phase was used due to the non-linearity's caused by the too close nearness to the pitch bearings. However, after the generator connection, all recorded samples have been used up to about 15 turbine rotations at full power.
The temperature influence on the strain bridge signals has been considered by including additional high wind start measurements (4 starts, May 96) at quite different temperatures in the same curve fitting computation. The rotor speed and its squared value have also been involved in the curve-fitting process for further increasing the calibration accuracy and reliability.
The calibration quality has been examined by computing the turbine power as the product of rotor speed and the computed edge-moment sum at the hub. The correspondence between the computed and measured power was quite good at these tests.
It is not possible to give a more detailed description of the calibration process due to space limitations in this paper. However 4 figures are shown below as an illustration to the method and the results. The numbered figures contain only time plots and represent the following:

8. Näsudden II measurements from the high wind speed start at 1995-08-09 21:40:30 - 21:44:24, have been used as input to the VIDYN program. From top to bottom the curves show:
   WS38 = wind speed at 38 m height in the met mast
   WS75 = at 75 m [m/s]
   WS120 = at 120m [m/s]
   Pitchvinkel = pitch angle [deg]
   Effekt = Power [kW]
   Gen.varvtal = generator speed [RPM] (Rotor speed = generator-speed/73.475[RPM])

9. Plotted results from VIDYN simulation
   Fi = rotor angle [deg]
   Fip = rotor speed RPM]
   Mflap, Medge, Mpitch = computed moments [Nm] at hub center
   Fflap, Fedge, Fnorm = computed forces [N] at hub center
   Pitch = Pitch angle [deg]
   Pgen = generator power [kW]

10. Additional measured quantities are shown from the related start (see fig. 8), and as can be seen especially from the blade root 1:
    Rotorlage = rotor angle [deg]
    Gen.varvtal = generator speed [RPM]
    Flapmom b1, Edgemom b1, Pitchmom b1 [mV]
    =signals from blade-fixed bridges, specially designed to sensing bending and torque moments in blade-root 1
    Tvarkr 1 b1, Tvarkr2 b1, Normalkr b1 [mV]
    = signals from bridges designed for sensing corresponding forces
    Pitchvinkel = Pitch angle [deg]
    Effekt = generated power [kW]

11. The results from the calibration are here shown for the root of blade #1, when applied to the start measurements. As can be seen, these curves coincide rather well with the corresponding VIDYN-curves in figure 9. (Unfortunately the two diagrams no 7 show opposite sign-definition).
    The curve no 9 (AxelEff) in figure 11 represents computed power, based on the measured and transformed edge moments and the rotor speed, see above. During synchronizing, before the generator net connection, this curve differs a lot from the underlying curve, which represents Pgen(=measured generator power).

Conclusions from Part II

It has been demonstrated that acceptable accuracy can be obtained from load measurements by combining information from measurements in well defined conditions with calculations. However, the general advice is: Never mount strain gauges for load measurements close to bearings.

References

[1] Andersson B., Falk U., Babuska I. Petersdorff, Reliable Stress and Fracture Mechanics analysis of Complex Components Using A *h-p* Version of FEM. International Journal for Num. Methods in Engineering, Vol. 38, 2135-2163, 1995

[2] Ganander H, Olsson B., VIDYN, Version 6, Time simulation program for wind turbines. 1994-12-14

Figures

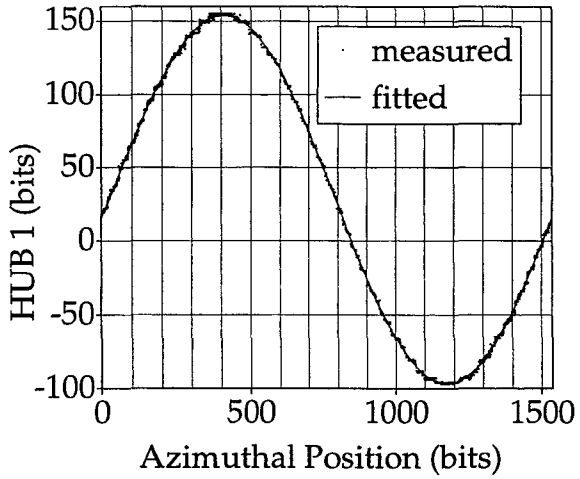

Figure 1 Measured and fitted output from the calibration.

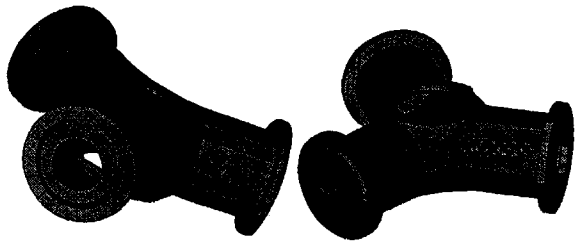

Figure 2 The FEM model of the hub.

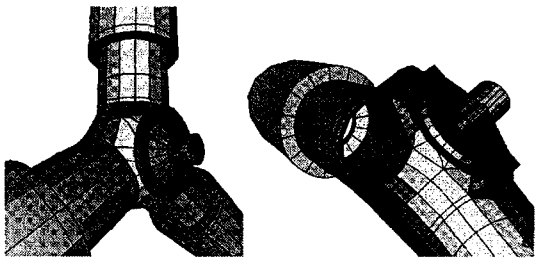

Figure 3 Complete model with blades.

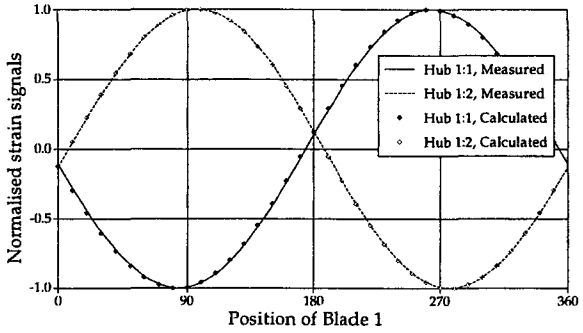

Figure 4 Measured and corrected signals from the slow rotating calibration

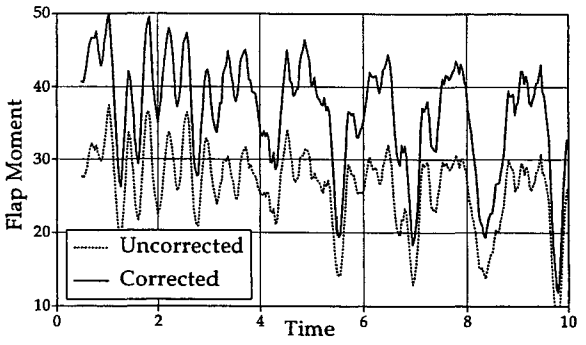

Figure 5 Comparison of measured and corrected flap moment.

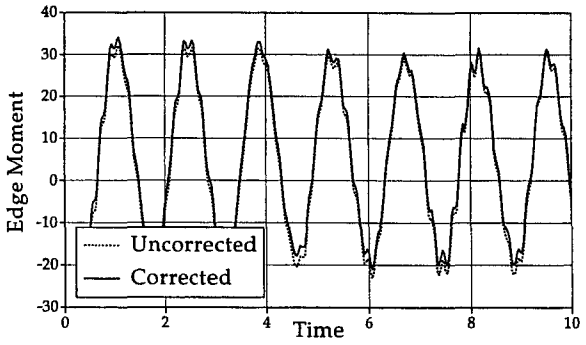

Figure 6 Comparison of measured and corrected edge moment.

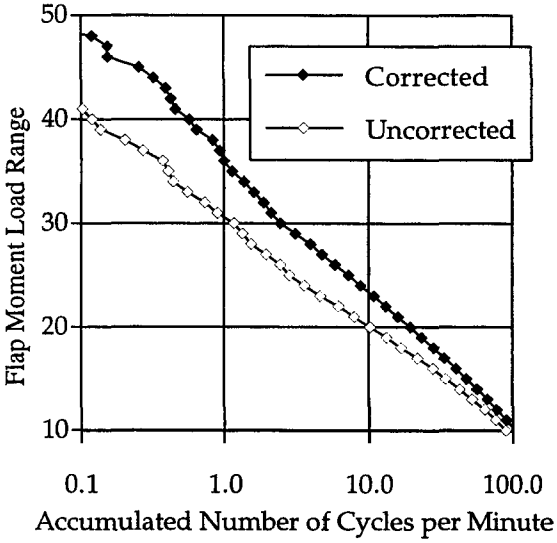

Figure 7 A typical load spectra based on the old measured data and the new corrected data.

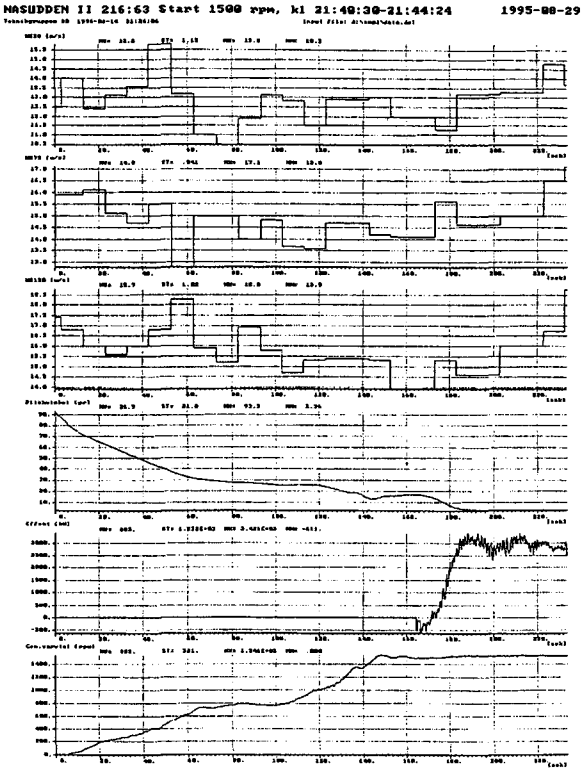

Figure 8. Measurements from start in high wind.

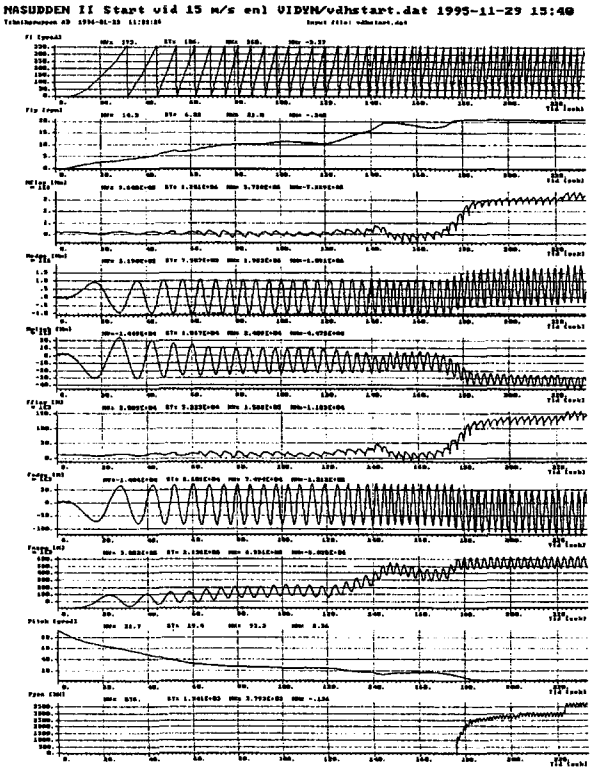

Figure 9. Results from VIDYN calculations.

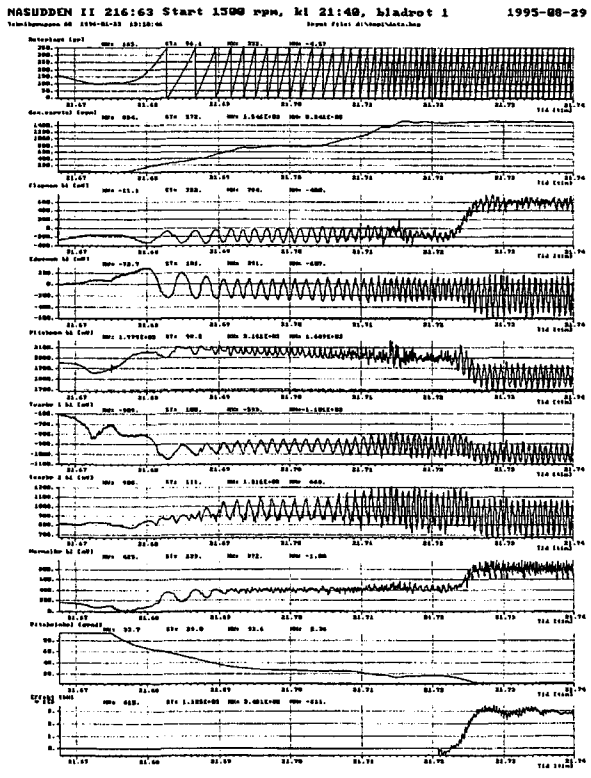

Figure 10. Additional measured quantities from fig 8.

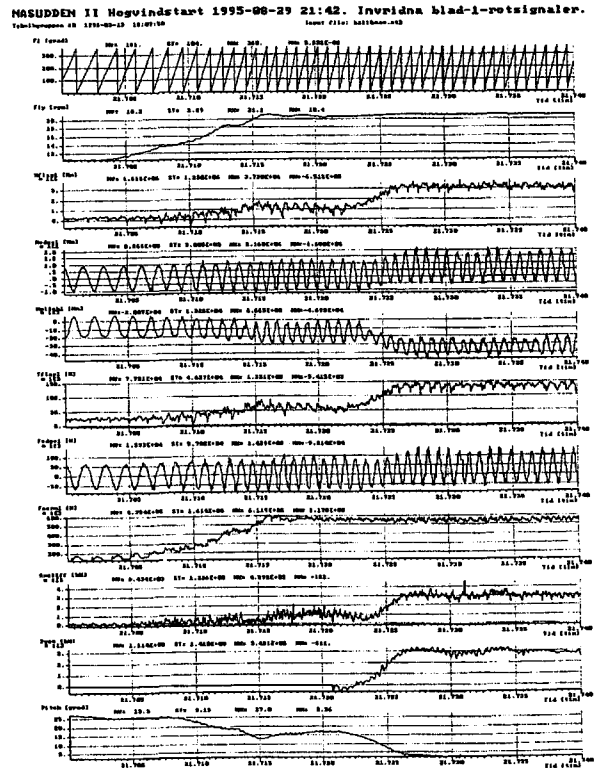

Figure 11 Results from calibration applied to the measurements.

Appendix 8

Load Prediction of Stall Regulated Wind Turbines

Anders Björck, Jan-Åke Dahlberg, Ingemar Carlén, Hans Ganander

Load Prediction Of Stall Regulated Wind Turbines

Anders Björck, Jan-Åke Dahlberg
FFA, The Aeronautical Research Institute of Sweden
Box 11021, S-161 11 Bromma, Sweden, tel +46 8 6341000, fax +46 8 25 34 81

Ingemar Carlén
CTH, Chalmers University of Technology, Division of Marine Structural Engineering
S-412 96 Göteborg, Sweden, tel +46 31 7721492, fax +46 31 7721541

Hans Ganander
Teknikgruppen AB
Box 21, S-191 21 Sollentuna, Sweden, tel +46 8 359455, fax +46 8 969987

Abstract: Measurements of blade loads on a turbine situated in a small wind farm shows that the highest blade loads occur during operation close to the peak power i.e. when the turbine operates in the stall region. In this study the extensive experimental data base has been utilised to compare loads in selected campaigns with corresponding load predictions. The predictions are based on time domain simulations of the wind turbine structure, performed by the aeroelastic code VIDYN. In the calculations a model developed by Stig Øye were adopted in order to include the effects of dynamic stall. This paper describes the work carried out so far within the project and key results.

Keywords: Load Prediction, Dynamic Stall, Wind Field Simulation, Load Simulation

1. INTRODUCTION

An extensive investigation of the loads on a three bladed, stall regulated WECS has been carried out through continuos measurements since 1990. The turbine under test is a 180 kW DANWIN, stall controlled, wind turbine located in the Alsvik wind farm on the isle of Gotland in the Baltic sea. The measurements include a range of operation conditions, such as very low turbulent flow when the wind comes from the open sea, and high turbulent flow when the wind comes from the interior of the island. Wake effects at different distances have been investigated thoroughly in previous projects. These investigations show that wake operation can create high loads that significantly exceeds the loads that occurs in high turbulent conditions and in complex terrain. However, the highest blade loads occur during operation close to the peak power i.e. when the turbine operates in the stall region. At these conditions both high flap load cycles and high edge load cycles of high frequency occur. In the current study the extensive experimental data base has been utilised to compare loads in selected campaigns with corresponding load predictions. The predictions are based on time domain simulations of the wind turbine structure, performed by the aeroelastic code VIDYN.

2. PROJECT GOAL

Dynamic simulation includes many key issues such as the structural description, integration methods, mode description, couplings, steady and unsteady aerodynamic stall models, wind description, etc. The objective has been to utilise the data base to compare loads in selected campaigns with corresponding load predictions. This is done as one mean of identifying if and where modifications in any of the many steps are necessary to be able to predict loads in the stall region.

3. INITIAL STEPS OF WORK

3.1 Wind field simulation

Wind fields were simulated using an in house code called SOSISB7. This code is based on conventional wind simulation technique, involving orthogonal decomposition of the spectral matrix, and inverse Fourier transform. The meteorological models used here were diabatic spectral densities (u- and v-components) proposed by Kaimal et. al. [1], and the diabatic logarithmic wind law (se for example [2]). Cross-spectral densities were modelled using a modified exponential coherence function. Model parameters, such as roughness length, Monin-Obukhov length, and coherence decrements, were fitted to the measured wind. These procedures were developed for neutral to moderately stable atmospheric boundary layer.

3.2 Selection of measured wind conditions

Several wind sequences below stall and in the stall region were selected from the database and analysed. Two wind sequences below stall were used to tune the structural model and one wind sequence above stall was used for the simulations in stall. The sequences below stall were selected because a good matching could be obtained with the simulated wind field.

3.3 Tuning the response of the structural model

The aeroelastic code VIDYN [3], developed by Teknikgruppen AB, is a simulation program for static and dynamic analysis of horizontal axis wind turbines. The method used for calculation is based of numerical inte-

gration of dynamic equations of the whole turbine system. Structural dynamic modelling of the DANWIN turbines in Alsvik turbine were done in the project "Dynamic Loads In Wind Farms II" [4]. The results from this project has been used as input to the current project. Further refinement of the structural model has led to, what we believe, a good structural description of the turbine. Finite element modelling of the blade has enabled an adjustment of the structural description of the blade. The stiffness in the yaw-system has been adjusted. A coupling between the rotation of the nacelle due to the side-to-side motions of the tower and the power fluctuations has been identified and implemented in the VIDYN code. Figures 1 and 2 shows comparisons of measured and calculated dynamic response of Flap and Edge moment for a moderate wind condition. The turbine rational frequency is ≈0.7 Hz. The agreement is very good.

4 AIRFOIL DATA

Two sets of data where used. An estimation of Aerofoil characteristics for NACA 63-2xx airfoils at a Reynolds number of around 2 million was made. Figure 3 shows this set which is called Aerodata 1. For the inner part of the blade a 3D correction was applied which is shown as the data for c/r=0.3. The first simulations in stall resulted in too low flap and edge moment vibration amplitudes compared to measurements so a second set of data called Aerodata 2 where also used. For this set of data, the 15% and 18% aerofoils were given $C_l(\alpha)$ characteristics to be more prone to stall induced vibrations. This set of data is shown in Figure 4.

5 MEAN POWER AND FLAP MOMENT

Figures 5 and 6 show the calculated mean power and flap moment compared to measurements. The agreement in power is best using Aerodata 2, but for the flap moment actually Aerodata 1 best reproduce the slope of the flap moment as function of the wind.

6 CALCULATIONS BELOW STALL

Calculations were done with different descriptions of the wind as function of space and time.

1.) Simulated wind field updated with 16Hz, as described in paragraph 3.1. The wind was given in a 22x22 matrix with a mesh width of 1.25 m. Both u and v-component. (Windfield484)
2.) Wind field created from the wind in the meteorological mast at five heights within the rotor swept area. The wind field is updated with 2 Hz. No transversal gradients or v component. (Windfield25)
3.) Wind input as the measured wind at three heights within the rotor swept area. The wind field is updated with 2 Hz No transversal gradients or v component. (Measured wind)
4.) Constant exponential wind shear and no time variation.

Results from the simulations below stall at a mean wind speed of 8.6 m/s with a turbulence intensity of 7% is seen in Figure 7 as Rain Flow Count spectra of the flap moment.

It is seen that the general agreement between simulations and measurements is good except when all time variation of the wind is excluded. The figure shows that the difference in load spectra by using the simulated wind field with both u and v-components compared to using the measured wind at three or five heights is small. The simulated wind field have statistical properties that matches the measured wind over a longer period than the 500 seconds of simulations that was used to create the load spectra. During these 500 seconds the simulated wind has a slightly larger mean wind speed and standard deviation than the measured. This has resulted in slightly larger load variation in the simulation and explains why the results with simulated wind show slightly larger load variations.

7 CALCULATIONS IN STALL

7.1 Dynamic stall model

The dynamic stall model of Øye [5] has been used. The calculations with the dynamic stall model were made with a non-dimensional time lag Tf=6. (Tf is non-dimensional with the half chord so that Tf is equivalent to $2 \cdot \tau_{fac}$ used in [5])

7.2 Selected sequence from measurements

Simulations and comparisons with measurements are shown for a 200 seconds long sequence. The wind speed is ≈15 m/s and the turbulence is ≈8%. This situation represents a fairly severe condition for the turbine with flap moment oscillations of an amplitude of 35% of the mean level. The measured yaw misalignment during the sequence is approximately 12 degrees.

7.3 Type of simulations

Simulations were done with several combinations of aerofoil data, types of wind input and at different yaw angles. In the subsequent paragraphs results are included to show the effect of:

- Aerofoil data and dynamic stall model
- Yaw angle
- Type of wind input

7.4 Effects of Airfoil data and dynamic stall model (Figure 8)

Calculations were first made with Aerodata 1. We had suspected that, without the inclusion of a dynamic stall model, large stall induced vibrations should occur in the calculations. However, for the chosen campaign the simulations showed no sign of large flap-vibrations. The load variation is substantially lower than found in the measurements. (A partial explanation to this is that this first calculations were made with zero yaw missalignment. As shown in paragraph 7.5 the yaw angle has a large influence on the loads.)

In order to investigate the influence of different static aerofoil data, a second set of aerofoil data was made up as described in paragraph 4.

With this set of data large vibrations occurred both in flap and edge during short time sequences of the campaign. These vibrations had an amplitude much larger than the measured flap moment amplitude.

The next step was to include the dynamic stall model. With the dynamic stall model applied (Tf=6) the stall-induced vibrations disappeared and the load variation drastically decreased as shown in Figure 8. With Aerodata 1 used, the inclusion of the dynamic stall model resulted in slightly increased loads. This can be explained by the fact that the lift-coefficient variation becomes larger when the dynamic stall model is applied (e.g. $C_{l,max}$ increases).

The results in figure 8 show that the choice of static aerofoil data and dynamic stall model has a large influence on the loads.

7.5 Effect of yaw misalignment (Figure 9)

The difference between the nacelle direction and the wind direction in the meteorological mast indicated a yaw angle of 12 degrees. Calculations were made with different yaw misalignment. Figure 9 shows load spectra for these calculations. It is seen that the yaw angle has a large effect on the simulated loads. For the simulations made with an yaw-angle of 12 degrees, the agreement between simulations and measurements are very good. The shown calculations are done using Aerodata 2 and TF=6. If Aerodata 1 was used the load variation became lower both with and without the dynamic stall model used.

7.6 Effect of wind input (Figure 10)

The calculation shown in figure 8 and 9 were made with the wind input from a simulated wind field. The calculations below stall, described in paragraph 6, showed that the use of a wind field with u and v-components compared to using the measured wind resulted in only small differences in the flap RFC spectra. However, at 15 m/s per second the method for describing the wind showed out to be important.

Figure 10 shows the flap RFC spectra for simulations with two different types of wind input.

1.) Simulated wind field in 22x22 points updated with 16Hz. Both u-and v-components.

2.) Wind input as the measured wind at three heights within the rotor swept area Only u-component. The wind field is updated with 2 Hz. (Measured wind)

Results from simulations with two realisations of the simulated wind with different random seeding are included.

It is seen that the calculation with the measured wind results in a large under-prediction of the load variation in comparison to using the simulated wind and compared to the measured flap moment variation.

8 CONCLUSIONS

The study shows that

- the selection of aerofoil data in combination with appropriate stall model is crucial for a realistic behaviour in stall.
- the description of the wind as input to the calculations is important and has a major influence on the simulated loads.
- in order to be able to compare the predicted loads with measured loads it is necessary to have a good knowledge of the yaw misalignment as it turned out to have a crucial influence on loads.

The results are encouraging and show that simulations with VIDYN agree well with measured loads.

This project will go on and include more severe conditions from the measured data base and simulate loads for:

- combined stall and wake effects
- combined stall and large yaw misalignment (>20°)

and to:

- evaluate other stall models
- study other quantities such as blade edge loads and tower loads.

REFERENCES

[1] Kaimal, J.C., Wyngaard, J.C., Izumi, Y. and Cote' O. R.,"Spectral Characteristics of Surface-Layer Turbulence", Quart. J. Roy. Meteorol. Soc. 98 , 1972 , 563-589

[2] Panofsky, H. A. and Dutton J. A. , "Atmospheric Turbulence-Models and Methods for Engineering Applications", Wiley, NY

[3] Ganander H., Olsson B., "VIDYN, Version 6, Time simulation program for wind turbines". 1994-12-14

[4] DLWF-II, Dynamic Loads in Wind Farms II, Joule Project JOU2-CT92-0094, Final Report, 960322.

[5] Øye, S. "Dynamic Stall-Simulated as Time Lag of Separation", IEA 4th symposium on aerodynamics for wind turbines. Rome, January 199, Edited by Ken MacAnulty, ETSU England.

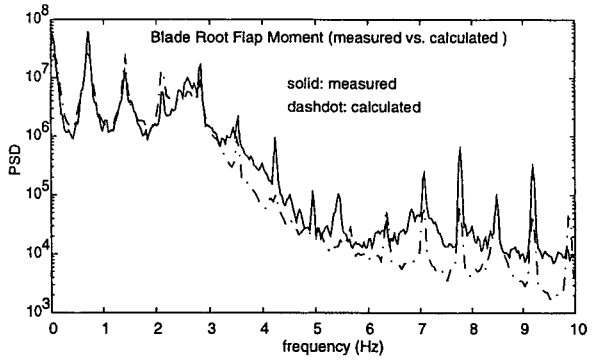

Figure 1. PSD of flap moment below stall

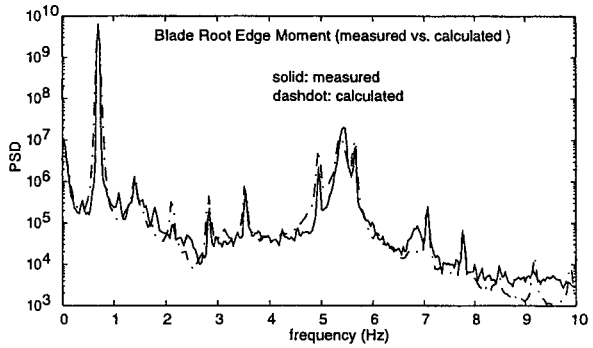

Figure 2. PSD of edge moment below stall

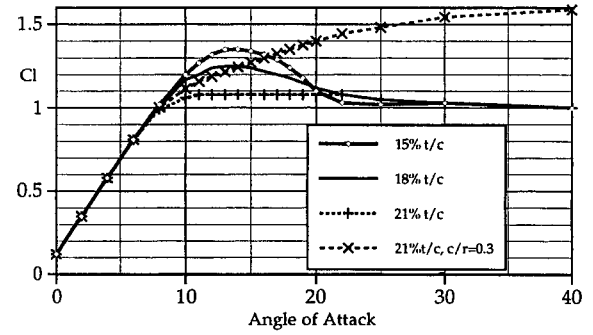

Figure 3. Airfoil data "Aerodata 1"

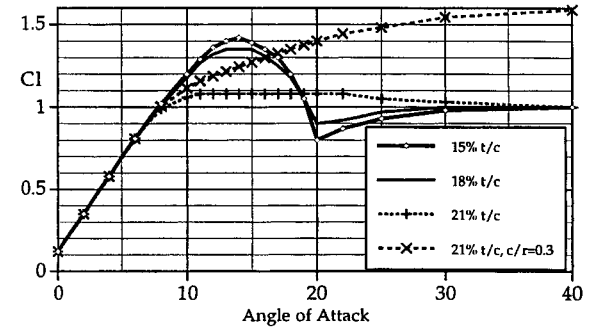

Figure 4. Airfoil data "Aerodata 2"

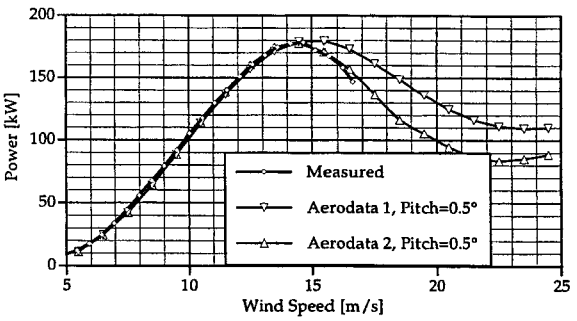

Figure 5. Measured and calculated power

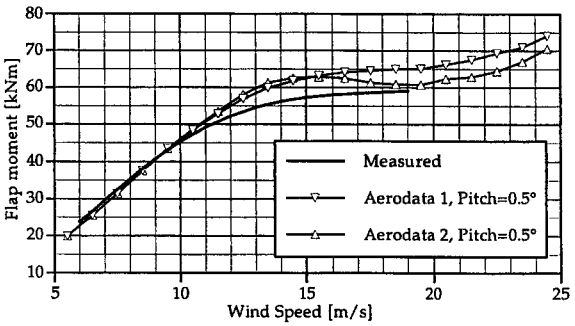

Figure 6. Measured and calculated flap-moment

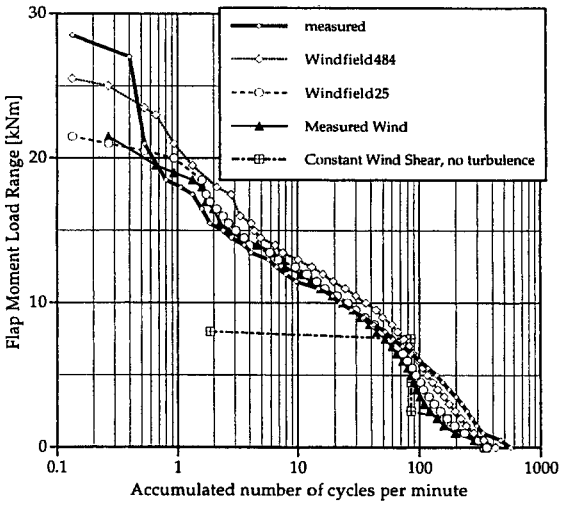

Figure 7. RFC Load spectra on measured and simulated flap-moment. Simulations with different types of wind input.

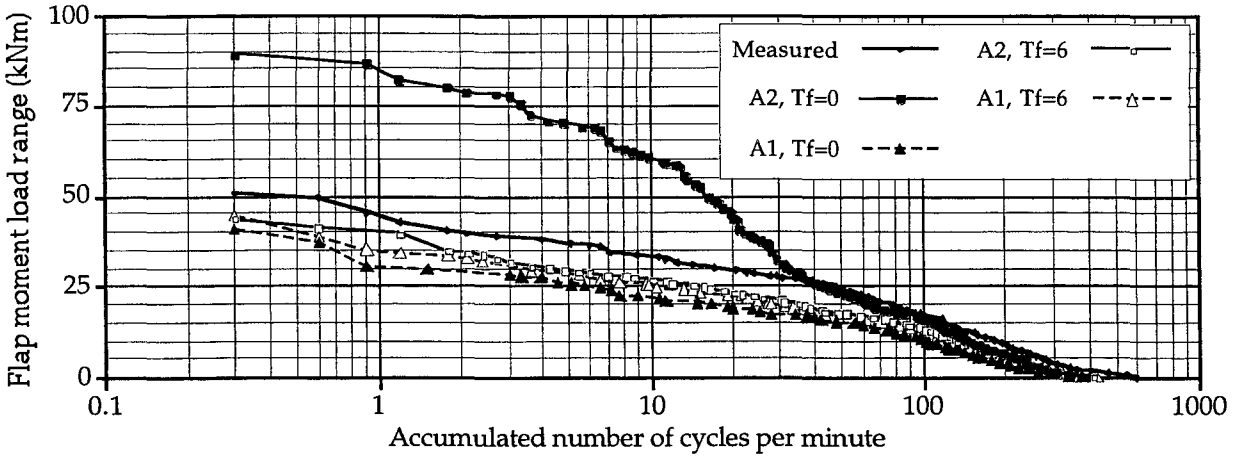

Figure 8. Comparison of measured and simulated flap moment load spectra. Different combinations of aerodata, with and without the dynamic stall model, Tf=0 is no dynamic stall model. (Measured Yaw angle=12°, Yaw angle in simulations=0°. Simulated wind field#1.)

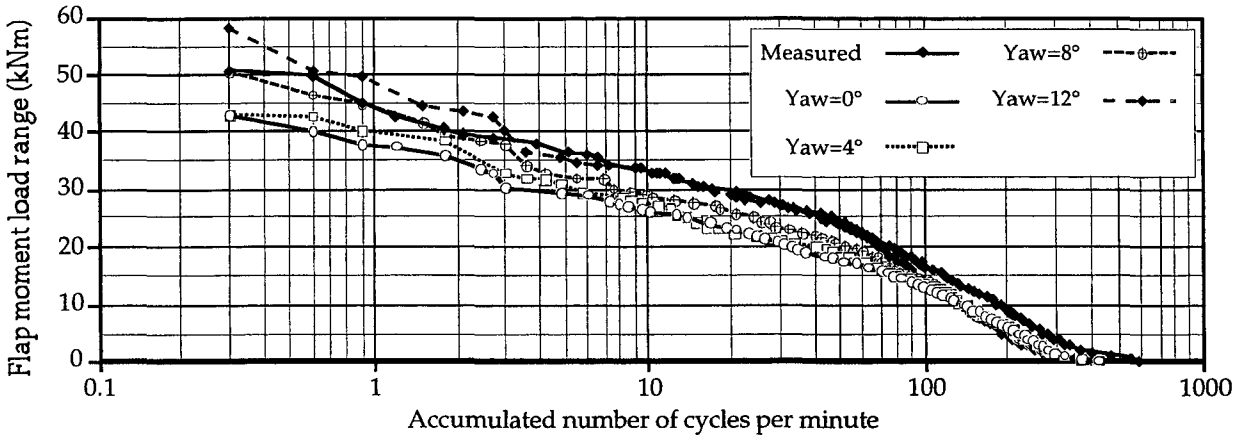

Figure 9. Comparison of measured flap moment load spectra (measured yaw angle ≈ 12°) and simulated load spectra for different yaw angles. (Simulated wind field#1, Aerodata 2 and dynamic stall model with Tf=6)

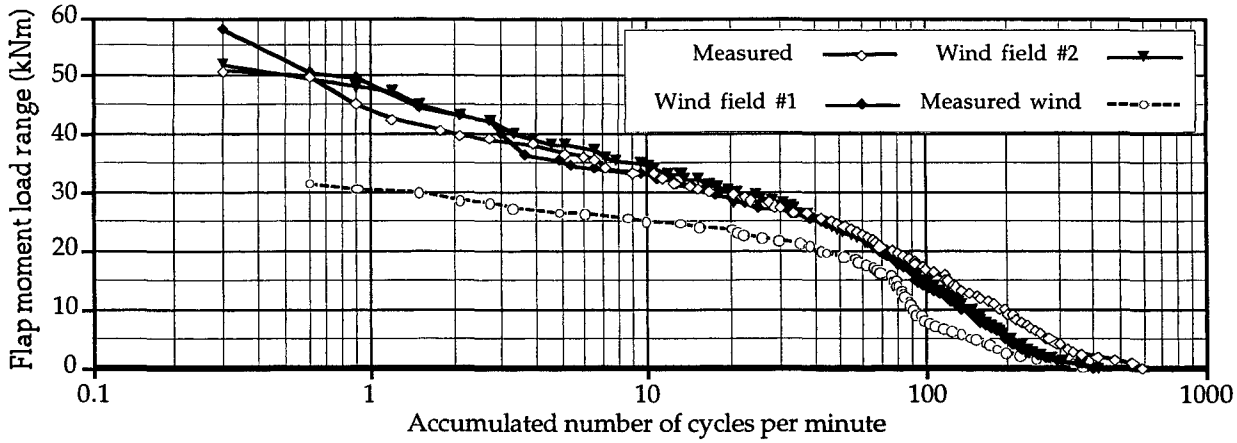

Figure 10. Comparison of measured and simulated flap moment load spectra Different wind input. Comparison of measured flap moment load spectra. (Yaw angle =12°, Aerodata 2 and dynamic stall model with Tf=6)

Appendix 9

Aerodynamical Errors on Tower Mounted Wind Speed Measurements due to the Presence of the Tower

Hans Bergström, Jan-Åke Dahlberg

AERODYNAMICAL ERRORS ON TOWER MOUNTED WIND SPEED MEASUREMENTS DUE TO THE PRESENCE OF THE TOWER

Hans Bergström[1] and Jan-Åke Dahlberg[2]
[1] Department of Meteorology, Uppsala University, Box 516, S-751 20 Uppsala, Sweden
[2] FFA, Aeronautical Research Institute, Box 11021, S-161 11 Bromma, Sweden

ABSTRACT: Field measurements of wind speed from two lattice towers showed large differences for wind directions where the anemometers of both towers should be unaffected by any upstream obstacle. The wind speed was measured by cup anemometers mounted on booms along the side of the tower. A simple wind tunnel test indicates that the boom, for the studied conditions, could cause minor flow disturbances. A theoretical study, by means of simple 2D flow modelling of the flow around the mast, demonstrates that the tower itself could cause large wind flow disturbances. A theoretical study, based on simple treatment of the physics of motion of a cup anemometer, demonstrates that a cup anemometer is sensitive to velocity gradients across the cups and responds clearly to velocity gradients in the vicinity of the tower. Comparison of the results from the theoretical study and field tests shows promising agreement.
Keywords: Anemometers, aerodynamics, velocity, wind speed, wakes,

1. INTRODUCTION

Measurements of loads on wind turbines and of meteorological conditions have been carried out at the Alsvik wind farm on the isle of Gotland in the Baltic sea. The measurements include wind speed data from two 54 m high triangular open towers, M_1 and M_2, placed 145 m apart, see Figure 1. The width (side) of the mast is 0.34 m. The anemometers in M_1 and M_2 are mounted on 1.2 m long booms with square cross section of 30x30 mm. The booms are directed such that they point towards the wind for wind directions 219° in M_1 and 310° in M_2.

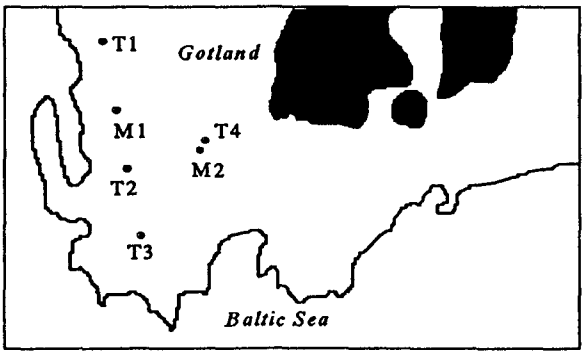

Figure 1: Map of the Alsvik site. Towers are marked M1 and M2, wind turbines are marked T1-T4. Shaded areas are covered with forests.

The analysis of the measured wind data indicates a large difference in wind speed between the two towers for wind directions where the anemometers on both towers should be unaffected by the wake of the tower or any other upstream obstacle. Figure 2 shows the measured ratio between the wind speeds from the two towers. The large dips are the velocity deficits in M_2 due to the wakes of upstream turbines. The wind speed in the sectors between the wakes is, however, expected to be the same at both towers. The measurements, however, show a variation in wind speed ratio of the order -5% to +2% for these sectors.

The reason for this could not be explained by different distances from the shore-line to the two towers, being of the order 50 m to tower M1 and 200 m to tower M2 for the sector 280°-300°. One could then expect the internal boundary layers to be about 5 m and 20 m high at towers M1 and M2 respectively. As we can see in Figure 2, the trend in wind speed ratio from about +2% at 180° to -5% at 300° is approximately the same at the heights 10 m, 31 m and 41 m, but at 41 m the anemometers on both towers will measure the conditions over the sea. Different upstream conditions is thus probably not the reason for the observed trend.

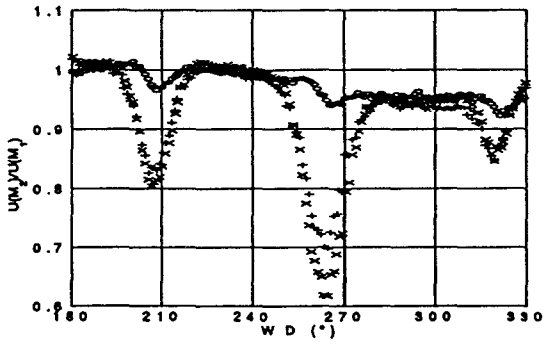

Figure 2: Ratio between measured wind speed in towers M2 and M1. Data from the period April 1990 to June 1991 has been used. Heights 10 m (o), 31 m (x), 41 m (+).

2. BOOM TEST IN FFA WIND TUNNEL

The possible influence on the measured wind speed of the boom on which the anemometers are mounted was

checked in FFA 10 m^2 low speed wind tunnel, see [1]. The anemometer was mounted on top of a very slender pole. A boom could be inserted from the side of the tunnel to simulate the presence of a boom. The boom was inserted on the side of the anemometer where the cups were moving with the wind. The vertical distance between the anemometer and the boom was 5.5 boom diameters. The rotational speed of the anemometer was repeatedly measured with and without the boom inserted, also with the boom inserted in the wind tunnel far away from the anemometer in order to check the influence on wind tunnel speed due to the presence of the boom.

The rotational speed of the anemometer without a boom inserted or with a boom inserted far away from the anemometer both gives measured values between 461.2-461.7 r.p.m.. The influence of the boom on the speed in the wind tunnel was thus negligible. The rotational speed of the anemometer with boom inserted beside the anemometer gives measured values between 466.0 and 466.8 r.p.m.. The ratio between the rotational speed with and without the boom at the anemometer is 1.011. It can therefore be concluded that the presence of the boom increases the wind speed by 1.1 % as measured by the cup anemometer.

The sensitivity of the boom position was examined by measurements with the anemometer pointing up or down. With the anemometer pointing upwards the boom is located on the side of the anemometer where the cups are moving with the wind, and with the anemometer pointing downwards the boom is located on the side of the anemometer where the cups are moving against the wind. The rotational speed of the anemometer with the anemometer pointing upwards give measured values of 468.0-468.1 r.p.m.. The rotational speed of the anemometer with the anemometer pointing downwards give measured values of 462.2-462.9 r.p.m.. The ratio between the rotational speed with the anemometer upwards and downwards is 1.012.

The conclusions, based on the combined results from the wind tunnel experiment are that the presence of the boom, in any direction, could only cause wind speed deviations in the order of 1 %, as measured by the cup anemometer. The relatively large deviations experienced at Alsvik could therefore not be explained by the presence of the boom only.

3. ASSESSMENT OF TOWER EFFECTS ON THE FLOW AROUND A TOWER

Another possible cause of the measured differences at Alsvik could be tower effects or interference between tower and anemometer. The presence of the tower influences the flow field. Disturbances in the flow field have mainly two causes: 1) The "solid body" displacement caused by the tower. 2) The wake behind the tower. The speed will be reduced in front of and increased beside the tower. It is assumed that the aerodynamic force of the tower only acts in the flow direction (drag). Any side force (lift) generated is neglected. The flow field can be estimated by means of simple 2D flow modelling based on potential flow including solid body effects (source-sink) and wake flow (source). Figure 3 shows the tower cross sectional layout, the coordinate system used and velocity

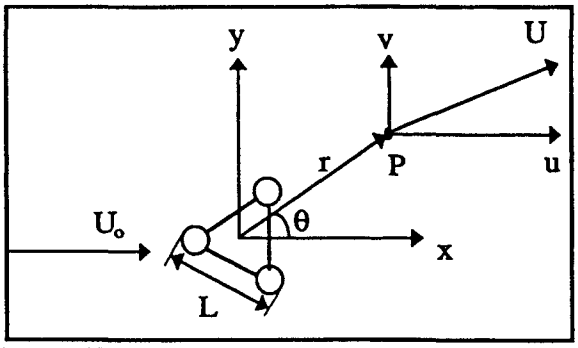

Figure 3: Tower cross section with definitions of coordinate systems and wind vector.

components. The velocity components u and v at a point P are obtained by summing the components from the two considered cases: solid body flow and wake flow.

	Free stream	Wake flow	Solid body flow (doublet flow)

$$\frac{u_{tot}}{U_0} = 1 + \frac{C_d \times L}{4 \times \pi} \times \frac{x}{r^2} - \frac{a^2 \times \cos(2\Theta)}{r^2}$$

$$\frac{v_{tot}}{U_0} = \frac{C_d \times L}{4 \times \pi} \times \frac{y}{r^2} - \frac{a^2 \times \sin(2\Theta)}{r^2}$$

$$U_{tot} = \sqrt{u_{tot}^2 + v_{tot}^2}$$

Necessary inputs to the calculation are the width of the tower (L), the drag coefficient (C_d), the radius (r) and the angle (Θ). To account for the solid body disturbance the tower is represented by a fictitious cylinder with radius (a). Details are given in [1].

3.1 Estimation of the drag of the mast

The drag coefficient, C_d, for the entire tower is estimated by an area weighted summation of the drag coefficients for projected individual parts. The drag coefficient for cylindrical parts is set to 1.2 and for sharp-edged plates to 2.0. The C_d value obtained by summation amounts to 0.7, and can be regarded as an upper bound for the C_d of the tower. The total drag coefficient will, if shadowing effects are taken into account, probably be lower. In this context the tower is considered to be an evenly diffused object seen at a distance. In reality local effects such as the proximity to a corner, etc. must be included.

3.2 Assessment of tower effects on the flow around the Alsvik tower

Figure 4 shows calculated local relative wind speed versus position around a tower with a drag coefficient of 0.6 and for 9 different distances r. Note that the position angle differs from (Θ) in the formulas above. In Figure 4 the angle is zero when the boom is pointing against the incoming flow. A positive angle is obtained when the mast is turned counter clockwise as seen from above. The radius of the fictitious solid body was assumed to be to 0.12 m. The calculations indicate that the wind speed in

front of the tower is reduced by maximum 4.7 % and increased by maximum 2.6 % at the side of the tower for r=2L. These numbers are reduced to 1% or less for r>6L.

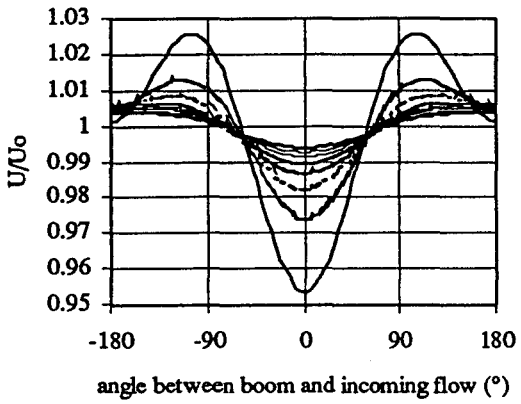

Figure 4: Local relative wind speed ratios versus position around the tower for 9 values of distance to the tower: r=2L to r=10L, giving values closer to 1 for an increased r.

4. SIMPLIFIED PHYSICS OF A CUP ANEMOMETER

The cup anemometer usually consists of three cups but can, in a simplified way of looking, be treated as a device with two cups on each side of the vertical shaft of rotation. The cups, usually shaped as hollow half spheres or cones, turn different faces towards the incoming wind. The drag coefficient for the cups depends on which side of the cup which is facing the stream. The incoming wind flow creates forces on each side of the shaft. An ideal anemometer will run with no torque on the shaft. The anemometer will then, for each wind speed, adjust the rotational speed so the forces on each side of the shaft are equal.

The following equilibrium equation can be written for the forces acting on the cups:

$$\frac{(U-\omega \times r)^2}{2} \times \rho \times A \times r \times C_{d1} =$$

$$= \frac{(U+\omega \times r)^2}{2} \times \rho \times A \times r \times C_{d2}$$

The magnitude of the forces depends on the square of the relative wind velocity ($U \pm \omega r$), the density ρ, the projected area (A), the radius from the axis of rotation to the centre of the cup (r), and the drag coefficient (C_{di})on each side.

A typical drag coefficient value for a half-sphere with the opening against the stream is 1.4 and 0.4 with the convex side against the stream. This would give a drag ratio, C_{d1}/C_{d2}, of 3.5.

4.1 A cup anemometer exposed to a linear velocity gradient

As the forces on each side of the anemometer is proportional to the square of the flow speed approaching the cups, the anemometer will strongly respond to variations in wind speed across the projected area. A cup anemometer will, for instance, respond to the velocity gradients in the vicinity of a tower.

Assume that the cup anemometer is exposed to a linear velocity gradient giving a speed increase ε on the side where the cups are moving with the wind flow and a speed decrease of the same value where the cups are moving against the wind. The errors in wind speed as measured by the cup anemometer due to the velocity gradient will for ε=0.002 give a 0.7 % too high wind speed output, and correspondingly 0.7 % too low wind speed output for ε=-0.002. Anemometers with high drag ratios (C_{d1}/C_{d2}) will be less sensitive to velocity gradients. For a given velocity gradient anemometers with small diameters will be less sensitive to a velocity gradient.

5. COMBINED TOWER AND SHEAR EFFECTS ON A CUP ANEMOMETER

The velocity distribution of the flow in the vicinity of a tower is not uniform. The velocities vary with distance to the tower and a cup anemometer will respond to these velocity gradients. The flow will be symmetric around a symmetric tower, but the anemometer is asymmetrical and will respond differently on the two sides of the tower. Figure 5 shows the calculated anemometer response due to the tower effect, velocity gradient effect and combined tower & velocity gradient effects, for the conditions at Alsvik. The radius from the axis of rotation to the centre of the cup is 0.04 m.

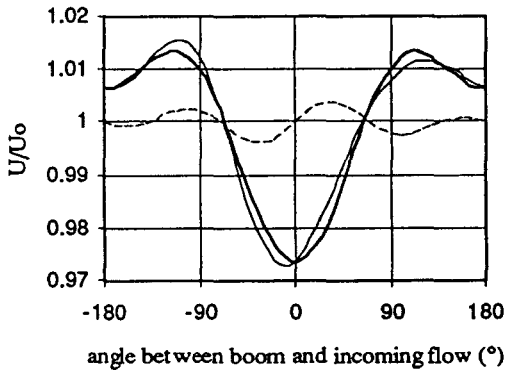

Figure 5: Calculated cup anemometer response due to tower effects (thick line), velocity gradient effects (dashed line), and combined tower & velocity gradient effects (thin line).

5.1 Comparison of measurements and theory

Figure 6 shows a comparison of the ratio between measured wind speed from the two towers at Alsvik and corresponding calculated wind speed ratios. The calculations take tower and velocity gradient effects on the wind speed measurements into account. The boom effects derived from the wind tunnel test are, however, not included due to the fact that the wind tunnel test only covered two angles ±90°.

From Figure 6 it is clear that the calculations rather well represents the general conditions at the site. Both the increased velocity ratios in the sector 225°-255° as well as

the decreased velocity ratios in the sector 290°-320° are well represented by the calculations.

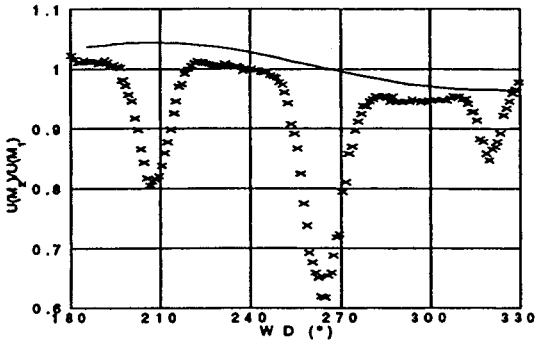

Figure 6: Ratio between measured wind speed on towers M2 and M1 (31 m), together with the theoretical results taking account of tower and anemometer effects(full line).

6. A FIELD COMPARISON BETWEEN TWO TYPES OF ANEMOMETER MOUNTINGS

At an agricultural site with dominantly open fields and a homogeneous fetch over 1-5 km, measurements were taken with two anemometers at 2 m height. Both anemometers were mounted on horizontal booms, of which one was mounted on a triangular tower like at Alsvik, and the other on a pole with 50 mm diameter. Both booms pointed in the direction 305°, see Figure 7.

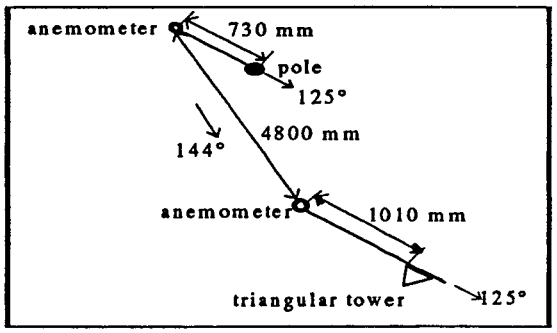

Figure 7: Sketch of the experimental setup during the field comparison between two anemometer mountings.

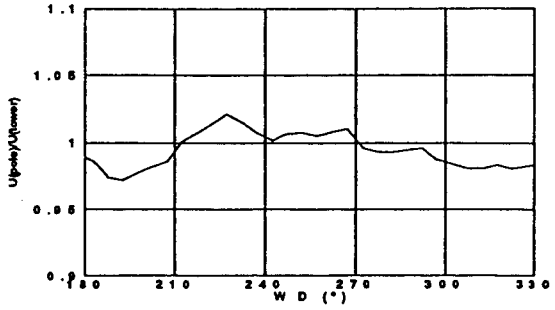

Figure 8: Ratio between wind speed measured on the pole and on the tower.

The resulting wind speed ratio between the wind measurements on the pole and on the tower respectively are shown in Figure 8. It can be seen from the figure that these results do not agree the measurements at Alsvik. Here the tower mounted anemometer measures a higher wind speed as compared with the pole mounted one when the wind direction is along the boom, i.e. the anemometer is on the upwind side of the tower, while for wind directions when the anemometer is beside the tower, the measurements on the pole give the higher wind speed. Also the magnitude of the wind speed ratio is here within ±2%, whereas at Alsvik the ratio varied between -5% and +2%.

The reason for this apparent disagreement is not obvious, and a thorough investigation has not yet been made. But one explanation may be that the disturbance on the wind field around a pole is larger than one might expect. Results in [2] show that wind speed ratios may amount to +11.3% at a distance of 4 diameters beside a pole. Although the distance in our case is much larger, about 14 diameters, it might be possible to explain the observed wind speed ratios between 0.98 and 1.02 in the same way as above for the Alsvik data.

7. POWER CURVES

It is of course extremely important to have accurate wind measurements when determining power curves for wind turbines. Oppositely power curves may be used as indications of aerodynamical errors due to the presence of the tower. This has been done for 3 MW wind turbine on Näsudden, Gotland. Comparing power curves using wind data from two 30° sectors centered around 245° and 305°, with the booms pointing towards 240°, one may conclude that the differences are large. Assuming the same power performance for both sectors, it is possible to determine the errors in wind speed necessary to explain the differences. They amount as a mean over the whole power range to 6.4%. This is of the same order of magnitude as the theoretical calculations give using C_d=0.8 and r=2.5L.

8. CONCLUSIONS

The present study shows that not only the boom effects but also the tower effects and anemometer response to velocity gradient effects have to be taken into account to minimize errors in wind speed measurements.

Comparisons with field data from two sites show that great care has to be taken when wind speed data accurate to within ±1% are needed. Theoretical calculations indicate that booms reaching at least the distance 6L from the tower are needed to accomplish this.

REFERENCES

[1] J.-Å. Dahlberg: Mast, Boom & Velocity Gradient Effects on Cup Anemometers, FFAP-V-009, The Aeronautical Research Institute of Sweden, 1996.

[2] G. C. Gill, L. E. Olsson, J. Sela and M. Suda. Bulletin of American Meteorological Society, 1967, vol. 48, no. 9, 665-674.

Appendix 10

Methods to Predict Fatigue Lifetimes of GRP Wind Turbine Blades and Comparison with Experiments

Andreas Echtermeyer, C. Kensche, P. Bach, Maria Poppen, L. Lilholt, S. Andersen, P. Brøndstedt

METHOD TO PREDICT FATIGUE LIFETIMES OF GRP WIND TURBINE BLADES AND COMPARISON WITH EXPERIMENTS

A.T. Echtermeyer[1], C. Kensche[2], P. Bach[3], M. Poppen[4], H. Lilholt[5], S.I. Andersen[5], P. Brondsted[5]

[1] Det Norske Veritas Research AS, (DNV), P.O. Box 300, N-1322 Hovik, Norway
[2] Deutsche Forschungsanstalt für Luft- und Raumfahrt (DLR), Pfaffenwaldring 38-40, 70569 Stuttgart, Germany
[3] The Netherlands Energy Research Foundation (ECN), Westerduinweg 3, 1755 ZG Petten (N.H.), The Netherlands
[4] The Aeronautical Research Institute of Sweden (FFA), P.O.Box 11021, S-16111 Bromma, Sweden
[5] Riso National Laboratory, P.O. Box 49, DK-4000 Roskilde, Denmark

This paper describes a method to predict fatigue lifetimes of fiber reinforced plastics in wind turbine blades. It is based on extensive testing within the EU-Joule program. The method takes the measured fatigue properties of a material into account so that credit can be given to materials with improved fatigue properties. The large number of test results should also give confidence in the fatigue calculation method for fiber reinforced plastics.

The method uses the Palmgren-Miner sum to predict lifetimes and is verified by tests using well defined load sequences. Even though this approach is generally well known in fatigue analysis, many details in the interpretation and extrapolation of the measurements need to be clearly defined, since they can influence the results considerably. The following subjects will be described: Method to measure SN curves and to obtain tolerance bounds, development of a constant lifetime diagram, evaluation of the load sequence, use of Palmgren-Miner sum, requirements for load sequence testing.

The fatigue lifetime calculation method has been compared against measured data for simple loading sequences and the more complex WISPERX loading sequence for blade roots. The comparison is based on predicted mean lifetimes, using the same materials to obtain the basic SN curves and to measure laminates under complicated loading sequences.

Keywords: Glass Reinforced Plastics, Fatigue, Palmgren-Miner sum, WISPERX

1 INTRODUCTION

No widely accepted method to predict fatigue lifetimes of composite structures exists today. One reason is that the micromechanical failure mechanisms are poorly understood or need too many parameters to be described. Therefore, it is currently not possible to base a fatigue failure method on basic physical principles. Simple methods based on the linear Palmgren-Miner sum (1) lack a physical meaning for composite materials. However, if checked carefully the Palmgren-Miner sum can be used with a safety factor as an engineering approach. Designers have to predict fatigue lives keeping these shortcomings in mind.

Table 1: Materials

Material Code	Glass Layup	Matrix, Manufact. Method
A	0/90	Epoxy, Prepreg
B	0/90 WR 90% II* CSM on surfaces.	Polyester, Hand layup
C	0/±45	Epoxy Hand layup
D	0/±45	Polyester Hand layup

*Woven roving with 90% of fibers in the load direction.

The method suggested here is compared against experimental results of four materials. An overview of the materials is given in Table 1. Material A was investigated by Sahu and Broutman and details about its properties can be found in Ref. (2). Material B was investigated by Riso (3), FFA (4), IPM (5), and DNV (6). Materials C and D were investigated by DLR (7) and ECN (8,9) respectively.

2 FATIGUE LIFETIME CALCULATION

2.1 Obtaining constant amplitude fatigue design curves and tolerance bounds

Standards do not exist for most fatigue tests of composites. However, good experience has been obtained with various test methods (10). Fatigue lifetimes are usually presented as SN curves (Wöhler diagrams), showing number of cycles to failure for a given stress level. For composite laminates it is more convenient to represent the data as εN curves, showing the cycles to failure for a given initial strain amplitude. (Since composites loose stiffness with increasing cycle numbers, the strain increases with increasing number of cycles at a constant load amplitude.) If for a design SN fatigue data are needed, such data can be easily calculated from εN curves using the relationship "stress equals Young's modulus times strain" $\sigma = E\,\varepsilon$, as long data are in the linear range.

Various fit methods are used to describe fatigue results, e.g. fitting the data to a straight line in an ε vs. $\log_{10} N$ plot, in and $\log_{10} \varepsilon$ vs. $\log_{10} N$ plot, or as a Weibull curve in a $\log_{10} \varepsilon$ vs. $\log_{10} N$ plot. In most cases a log-log representation has yielded good results. In particular for high cycle numbers this method seems to give the best results (11,12). The difference between the

mean values of a Weibull fit and a log-log fit seems to be small (13). In this work data are described by a linear $\log_{10} \varepsilon$ vs. $\log_{10} N$ fit:

$$\log_{10} N = \log_{10} K - m \log_{10} \varepsilon \qquad (1)$$

Linear regression analysis of data pairs (ε,N) by this model will lead to least-squares estimates of the intercept $\log_{10} K$ and the slope m. Values for K and m are listed in Table 2.

Table 2: Parameters describing the fatigue mean properties.

		B	C	D
R =	$\log_{10}$K	0.5371		1.707
0.1	m	10.350		11.214
R =	$\log_{10}$K	0.9905	4.374	3.759
-1	m	11.677	9.574	10.236
R =	$\log_{10}$K	-0.2168		-0.6856
10	m	11.678		23.162

"Run out" specimens and static test values were not used for the fatigue analysis, because such measurements cannot be directly related to a fatigue analysis (12). ("Run out" specimens are specimens which did not fail, but testing got stopped.)

The European CEI directive on wind turbine blades requires that a 95% tolerance bound with 95% confidence has to be used for design (14). The 95/95 tolerance bound should be obtained according to proper statistical procedures where N is the dependent variable and ε is the independent variable. Details about the procedure can be found in Ref. (15,13). Note that the curve describing the tolerance bound with a confidence has an approximate hyperbolic shape and is not parallel to the mean curve. Figure 1 shows the fatigue lifetime curves for material B as an example.

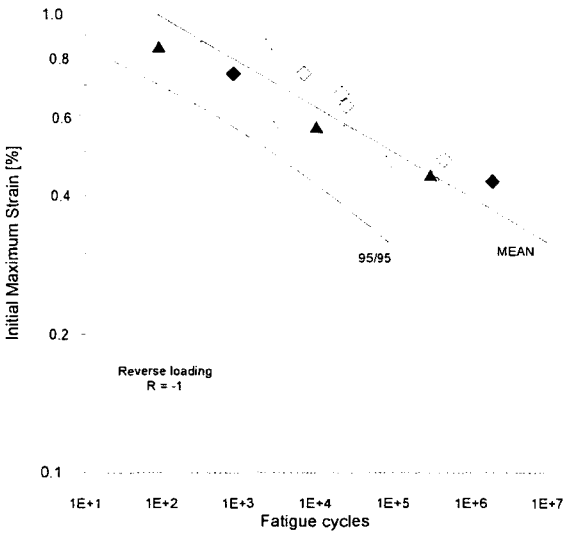

Figure 1: SN curves of laminate B (R= -1), based on a small number of specimens.

2.2 Constant lifetime diagram

Mean stresses have to be considered when performing a fatigue analysis for FRP structures. Constant lifetime diagrams are commonly used to obtain fatigue lifetimes for a given stress amplitude and mean. Fatigue data are often only available for three R-ratios, R=10, -1, and 0.1. These represent three lines in the constant lifetime diagram, other values have to be interpolated. Linear extrapolations are mostly used, giving the constant lifetime diagram a triangular shape. Some data confirm that this is a good approach (9,16), however, the extrapolations add another element of uncertainty to the fatigue life predictions.

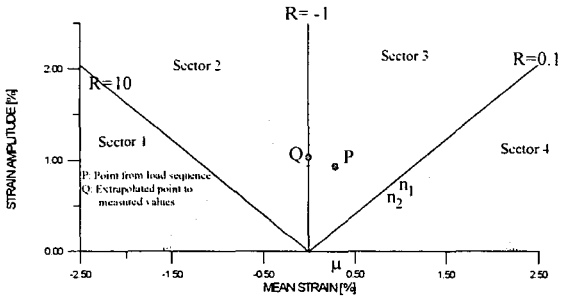

Figure 2: Schematic of a constant amplitude life diagram. The drawing illustrates the description in Section 2.2 describing how the fatigue life for a strain amplitude α at mean μ (described by point P as an example) can be found.

The exact method to carry out the linear extrapolation in a constant lifetime diagram is generally not specified and tends to vary from investigation to investigation. In order to gain experience with fatigue lifetime predictions, it is important to compare results based on the same method. The following linear extrapolation method was used here:

- The constant lifetime diagram was constructed as a strain amplitude vs. mean strain diagram. Note this is equivalent to the more commonly used presentation in stress-space.
- The diagram was based on fatigue curves measured at the R-ratios R=10, -1, and 0.1. In addition the static tensile and compressive strains at failure were needed.
- The constant lifetime diagram could be divided into four sectors. The sectors are shown in Figure 2. Within each sector constant life lines were drawn for lifetimes of 1, 10, 100, 1000, ... cycles. These lines are assumed to be straight.
- For sectors 1 and 4 all lines were connected to the static tensile and compressive strains at failure. Very little data are available to justify this extrapolation. Most materials are also seldom used in these sectors. If a material is used in this sector a careful analysis should be made. Otherwise it is recommended to use reduced static values to obtain the constant lifetime diagram.
- One constant lifetime diagram was constructed based on mean constant amplitude fatigue data.

From this diagram the mean expected number of cycles to failure $N_{\mu}^{exp}(\alpha, \eta)$ could be obtained.

- Another constant lifetime diagram was constructed based on constant amplitude fatigue data representing the 95/95 tolerance bound. From this diagram the expected number of cycles to failure $N_{95/95}^{exp}(\alpha, \eta)$ with 95% tolerance and 95% confidence could be obtained.
- The expected number of cycles to failure for a given α, η was obtained by linear extrapolation to the nearest R line in the constant life diagram (17).
- If fatigue data at other R-ratios exist an equivalent approach with more sectors can be used.

2.3 Evaluation of the load sequence

The load sequence was analyzed by Rainflow counting (30). The number of load cycles n_i at an amplitude α and mean η was obtained for all combinations of α and η present in the particular loading sequence. Rainflow counting is considered to be the most conservative method considering mean values and amplitudes.

It should be noted that substantial uncertainties can exist in the load sequence. Usually conservative load sequences are used for the fatigue analysis, thereby including an extra unknown factor of safety in the analysis. A more proper fatigue lifetime analysis could take the uncertainties of the loads into account (18) in a more rational way.

2.4 Use of Palmgren-Miner sum and requirements for load sequence testing

Possibly the most critical issue in a fatigue analysis is how to calculate the expected fatigue life for a given load sequence based on measurements from constant amplitude loading. One method that has been used in most fatigue calculations is the linear Palmgren-Miner sum (1). There is no physical reason why this method should be applicable to composite materials, but its simplicity makes it very attractive.

Lifetimes are *often* predicted quite accurately, but since there is no physical reason for the Palmgren-Miner sum approach, it should be used with great caution. Considering the lack of any better method it is proposed here to use the linear Palmgren-Miner sum modified by a factor γ to the summation, or rather to define failure to take place whenever the Palmgren-Miner exceeds a level of γ instead of the usual threshold of 1.0.

This *Palmgren-Miner sum* method assumes that fatigue failure will occur when the sum of applied load cycles n_i at an amplitude α and mean η divided by the expected total number of cycles to failure N_i^{exp} at amplitude α and mean η becomes equal to or greater than γ.

$$\sum_{i=1}^{K} \frac{n_i(\alpha,\eta)}{N_i^{exp}(\alpha,\eta)} = \gamma \qquad (6)$$

The total number of combinations of α and η in the loading sequence is K. The load cycles n_i at an amplitude α and mean η are obtained from the rain flow analysis, the expected total numbers of cycles N_i^{exp} at amplitude α and mean η are obtained from the constant lifetime diagram. The value of the threshold γ has to be chosen in such a way that it approximately accounts for the model uncertainty associated with the Palmgren-Miner sum. This will be described in the next section. Note that ideally the threshold γ should be 1.

The expected number of cycles to failure for a given load sequence is:

$$N_{\mu}^{tot} = \frac{\gamma \sum_{i=1}^{K} n_i(\alpha,\eta)}{\sum_{i=1}^{K} \frac{n_i(\alpha,\eta)}{N_{\mu,i}^{exp}(\alpha,\eta)}} \qquad (7)$$

The 95/95 tolerance bound for the number of cycles to failure for a given load sequence is:

$$N_{95/95}^{tot} = \frac{\gamma \sum_{i=1}^{K} n_i(\alpha,\eta)}{\sum_{i=1}^{K} \frac{n_i(\alpha,\eta)}{N_{95/95,i}^{exp}(\alpha,\eta)}} \qquad (8)$$

Equations 7 and 8 are both based on the assumption that no uncertainties are related to the number of load cycles n_i at each of the K combinations of α and η in the representation of the load sequence.

2.5 Load sequence testing

Due to the uncertainties in the Palmgren-Miner sum it was found to be necessary to perform at least one load sequence test to estimate the threshold γ. The load sequence should be representative of the application. It should contain typical peak loads and load sequences. Specimens should be tested using the load sequence for different maximum strains. Results of the tests can be plotted as maximum strain of the load sequence vs. number of cycles.

The threshold γ can be found by comparing experimental data with predictions according to equations 7 and 8. The predicted curves were plotted together with the data. If 50% of the data lie above the mean curve and 95% of the data lie above the tolerance curve, the chosen γ is acceptable for that material and similar loading sequences. Note, that a lower γ has to be chosen if this requirement is not fulfilled and a higher γ can be chosen if more than 50% of the data lie above the mean curve.

In the ideal case γ can be 1, but not larger. If γ has to be less than 0.1 it is very doubtful whether the Palmgren-Miner sum is the proper way to describe the material behavior.

3 COMPARISON WITH EXPERIMENTS

To gain confidence in the fatigue lifetime calculation method described in Section 2, it was compared against experimental results. Experimental

results are presented for load sequences of different complexity.

3.1 Two-Stress level cumulative damage tests

An extensive fatigue study on cross-plied glass reinforced epoxy (Scotchply 1002) was carried out by Sahu and Broutman (2). They determined the SN curve of the material at R=0.05 and performed two-level cumulative damage tests.

The data showed that for high-low stress cumulative damage tests the Palmgren-Miner sum was either greater or very close to 1. with one exception. For low-high stress cumulative damage the sum was less than 1 for ten out of twelve cases. This is an indication of a sequence effect. i.e.. the material behavior and occurrence of failure depend on the order in which the load cycles are applied. The Palmgren-Miner sum approach used here cannot account for the sequence effect. A longer experimental fatigue lifetime compared to Palmgren-Miner prediction was also found by Bach (19) for specimens loaded in a high-low stress cumulative damage test.

While these results show that Palmgren-Miner sum has its limitations for loading sequences with a pronounced sequence effect. they also give an estimate of the error when using Palmgren-Miner sum. If one would choose $\gamma = 0.25$ in equations 6-8, the Palmgren-Miner sum can be used as a simple method to predict the lifetimes for this loading sequence. This approach may suffice for engineering purposes.

3.2 Block testing at constant R-ratio

Block testing at constant R ratio R=0.1 (3) and at three R ratios R=0.1, R=-1, and R=10 (6) was carried out on material B. The load blocks are described in Tables 3 and 4 respectively. The analysis of fatigue lifes of both load sequences did not require any constant lifetime extrapolation since all R ratios were tested. but extrapolated values from the εN curves have to be used.

The block test sequence was run for different specimens at various maximum loads exposing the specimens to different maximum strains. Test results are shown in Figures 3 and 4 together with the predicted lifetimes according to the procedure of Section 2.

The lifetimes of material B can be predicted quite well for both loading sequence using Palmgren-Miner sum with the ideal value of γ=1.

Table 3: Load Sequence of the Block Testing at R = 0.1. Loads are given in % of the maximum load of the test.

Minimum Load (%)	Maximum Load (%)	Number of Cycles
3	30	50000
5	50	50000
7.5	75	20000
10	100	500
7.5	75	20000
5	50	50000

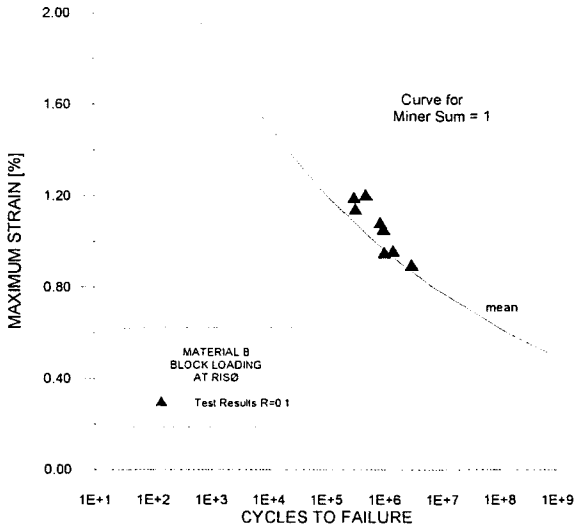

Figure 3: Comparison of predicted and measure fatigue life under the block loading sequence shown in Table 3. Calculations are made for the Miner sum = 1.

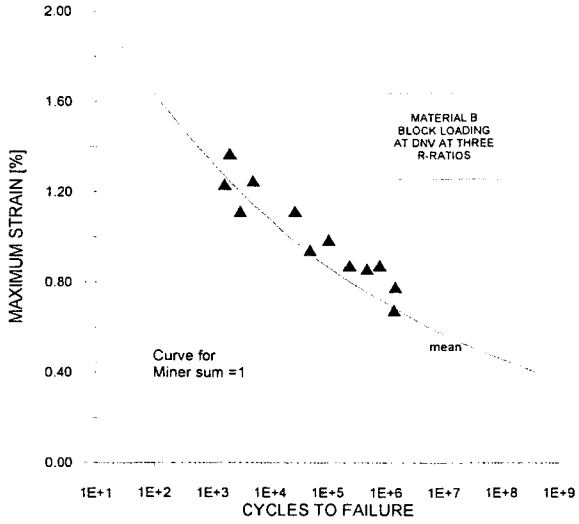

Figure 4: Comparison of predicted and measure fatigue life under the block loading sequence shown in Table 4. Calculations are made for the Miner sum = 1.

Table 4: Load Sequence of the Block Testing at three R ratios. Loads are given in % of the maximum load of the test.

Minimum Load (%)	Maximum Load (%)	Number of Cycles
10	100	50
-10	10	50
-30	-3	50
-50	50	50
10	100	50
-30	-3	50
-10	10	50

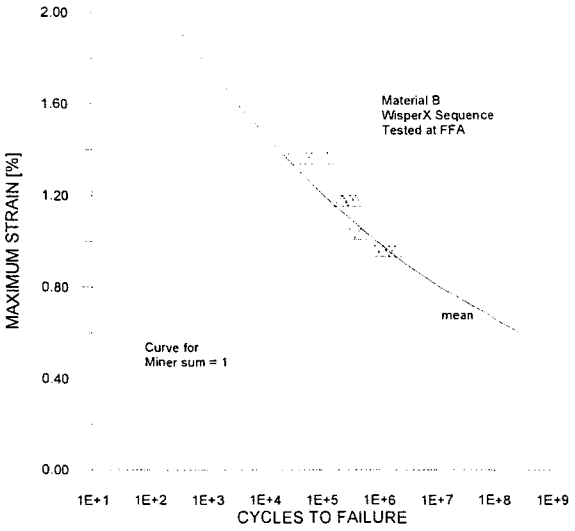

Figure 5: Comparison of predicted and measured fatigue life under the WisperX loading sequence for material B. Calculations are made for the Miner sum = 1.

3.4 WISPERX load sequence testing

A further test to check how well fatigue lifetimes can be predicted is to compare predictions with experiments for loading sequences that resemble the service loads closely. The WISPERX load sequence describes typical loads on wind turbine blade roots (20). Testing materials with typical load spectra is also common practice in other areas, in particular for aeronautical applications.

Tests using the WISPERX load sequence were performed for material B at FFA (21), for material C at DLR (7), and for material D at ECN (8,9). All these materials are glass fiber reinforced plastics. Experimental results and lifetime prediction curves are shown in Figures 5 to 7.

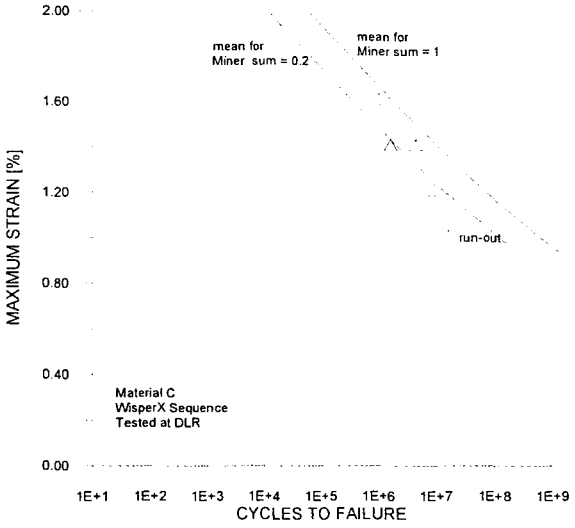

Figure 6: Comparison of predicted and measured fatigue life under the WisperX loading sequence for material C. Calculations are made for the Miner sum = 1 and Miner sum = 0.2.

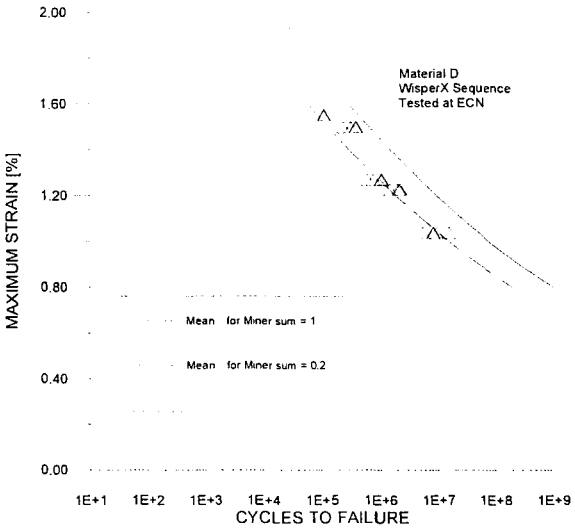

Figure 7: Comparison of predicted and measured fatigue life under the WisperX loading sequence for material D. Calculations are made for the Miner sum = 1 and Miner sum = 0.2.

The results show again that lifetimes of material B can be well predicted by the Palmgren-Miner sum = 1. However, lifetimes for materials C and D can only be predicted by a Palmgren-Miner sum = 0.2.

4. DISCUSSION

4.1 Fatigue lifetime predictions

If the Palmgren-Miner sum and the procedure of Section 2 were the ideal method to predict fatigue lives of GRP the sum should always be the same for all loading conditions and for all GRP laminates. The test results show that fatigue of material B under a couple of load conditions can indeed be modeled by using a Palmgren-Miner sum of 1. However, for the other materials the results deviated from the ideal value of 1, ranging from 0.2 up to 1.6. Table 5 shows the best Palmgren-Miner sum values at failure for the experiments reported here.

Table 5: Best values for Palmgren-Miner Sum

Material	Load Sequence	Ideal Palmgren-Miner Sum γ
A	Two Blocks	0.25 - 1.6
B	Table 3	1
B	Table 4	1
B	WISPERX	1
C	WISPERX	0.2
D	WISPERX	0.2

A range of 0.2 to 1.6 for γ is not satisfactory if one wants to understand the fundamental mechanisms governing fatigue of GRP. However, from an

engineering point of view this range can be acceptable. In fact, a similar range is observed for metals and Palmgren-Miner sum is frequently used for these materials.

The results indicate, that a γ=0.1 should be a safe choice for most cases. However, since the Palmgren-Miner sum value at failure can vary for different laminates and for different load sequences it is highly recommended to check how well the procedure described in Section 2 applies for a chosen material and a typical load sequence of the application. This check will ensure that the method works for the γ chosen. If the load sequence of the application is fairly well known and the test sequence is representative for the application, the load sequence tests could be used to document that a γ larger than 0.1 could be used. It seems that lifetimes of material B could be predicted by a γ=1 if used in wind turbine blades, for which the WISPERX spectrum is representative. Lifetimes of materials C and D should be predicted using γ=0.2, if the WISPERX spectrum is representative for the application.

It should be noted that for all materials the experimental data seem to follow a slightly different slope than predicted by the fatigue lifetime calculations when exposed to WISPERX loading (see Figures 5-7). Whether this is a systematic problem that may influence the long term life predictions should be investigated in the future.

The lack of representatives of the Palmgren-Miner sum is accounted for by the threshold factor γ that is used to define failure and that is determined from the mean values of the lifetime measurements. The variability of materials data and the confidence in these measurements is represented by the 95/95 tolerance bounds of the fatigue curves. Life predictions based on these tolerance bounds are much less than the predictions based on the mean levels (17). However, it is still important to distinguish between the uncertainty and bias in the Palmgren-Miner model and the uncertainty in the materials data themselves.

4.2 Large structures and components

For safety critical structures it may be necessary to perform fatigue testing of components or the full scale structure in addition to testing of small specimens. One reason for testing large structures is the uncertainty about size effects. Large scale tests are also used to document resistance to mixed stresses and buckling. Such tests, especially when performed under realistic load sequences, are very time consuming and expensive. Performing constant amplitude tests on these structures can save some time and the total lifetime can then be calculated by the Miner-Sum approach as described above (22). However, it should be clearly kept in mind that the structure or component should always be exposed to the maximum service stresses in such tests. If constant amplitude tests are performed at stresses below the maximum service stresses, the high stresses that may shorten the service life will not be simulated. Therefore, in the case of proof tests by constant amplitude loading, some defined loads should be added that go up to the maximum design load. The occurrence of these high loads should be as often as expected in the service life.

4.3 Comparison with other design codes

The method to predict fatigue lives presented here takes explicitly the properties of the materials into account. The test effort is high, but the method should represent the actual properties of the materials.

Two European fatigue design codes for wind turbine blades are used today (23,24). Both codes are based on the static strength of the material assuming general fatigue constant lifetime diagram for all materials, normalized by the static strength. Fatigue lives are then calculated by the Palmgren-Miner sum using the general fatigue properties. The safety factors are not explicitly given and they are not based on standard deviations of the material. A comparison between life predictions by the codes and experiments showed that the codes predict fatigue lives in a conservative way (9). However, if the codes are used to predict mean fatigue lives by omitting the safety factors of the codes, the codes will sometimes be non-conservative, i.e. they will lead to overprediction of the fatigue lives. This shows that direct tests of a specific material should be done to ensure its safe use in fatigue applications.

5 CONCLUSIONS

- A detailed fatigue analysis method has been given, based on constant amplitude fatigue data, the Palmgren-Miner sum, and testing with a typical load sequence.
- Load sequence testing is essential for fatigue predictions, because the Palmgren-Miner sum at failure is not necessarily 1 for all materials and load sequences. For the four materials investigated here, the Palmgren-Miner sum at failure was 1 for only one material, while for the three others it was 0.2.
- The method described here requires extensive testing of a material. But it should also give a high level of confidence in the fatigue predictions.
- Due to the lack of knowledge of the basic fatigue mechanisms the empirical fatigue lifetime prediction described here should be applied with caution. In addition, effects of specimen size and mixed stress states in large structures should be considered. Provided these limitations are taken into account, the fatigue lifetime prediction method described here can be used for non-constant load sequences.

6 ACKNOWLEDGMENTS

The authors want to thank the European Commission, the Norwegian Research Council (NFR), and the Netherlands agency for energy and the environment (NOVEM) for financial support of the project.

REFERENCES

1 Miner. M.A.. Cumulative Damage in Fatigue. Journal of Applied Mechanics 12. Nr.3. pp. A159-A164. 1945

2 Broutman. L.J. and Sahu. S.. "A New Theory to Predict Cumulative Fatigue Damage in Fiberglass Reinforced Plastics" Composite Materials: Testing and Design. ASTM STP 497. American Society for Testing and Materials. pp. 170-188. 1972

3 S.I. Andersen. P. Bronsted. P. Toft. "Constant Load Fatigue and Variable Load Fatigue Properties of Industrial Produced Glass Fibre Reinforced Polyester Materials for Wind Turbine Blades" Riso National Laboratory. Final Report of the Joule Project "Development of Advanced Blades for Integration into Wind Turbine Systems" (1996)

4 M. Poppen. S.-E. Thor. "Static and Constant Amplitude Fatigue Tests of Glass Fibre Reinforced Polyester Materials for Wind Turbine Blades". The Aeronautical Research Institute of Sweden (FFA). Report FFA TN 1995-44 (1995)

5 J. Andersons et. al.. Institute for Polymer Mechanics. (IPM) Riga. Final Report of the Joule Project "Development of Advanced Blades for Integration into Wind Turbine Systems" (1996)

6 Echtermeyer. A.T.. "Fatigue testing of Industrially Produced Glass-Polyester Laminates for Wind Turbine Blades". DNV Research Report 95-2050. (1995)

7 Kensche. C. W.. "High Cycle Fatigue of Glass Fibre Reinforced Epoxy Materials for Wind Turbines. Deutsche Forschungsanstalt fur Luft- und Raumfahrt. DLR-Forschungsbericht 92-17. (1992)

8 Bach. P.W. "High Cycle Fatigue Investigation into Windturbine Materials". European Community Wind Energy Conference. 6-10 June 1988. Denmark

9 Bach. P.W.. Joosse. P.A.. van Delft. D.R.V. "Fatigue Lifetime of Glass/Polyester Laminates for Wind Turbines". Proceedings of the European Wind Energy Association Conference and Exhibition. Thessaloniki. Macedonia. Greece. October 10-14. (1994)

10 R. Mayer (ed.) "Design of Composite Structures Against Fatigue - Applications to Wind Turbine Blades". Mechanical Engineering Publications Ltd.. Suffolk. UK (1996)

11 van Delft D.R.. Rink H.D.. Joose. P.A.. Bach. P.W. "Fatigue Behaviour of Fibreglass Wind Turbine Blade Material in the Very High Cycle Range", Proceedings of the European Wind Energy Association Conference and Exhibition. Thessaloniki. Macedonia. Greece. October 10-14. (1994)

12 A.T. Echtermeyer. B. Engh. L. Buene. *Influence of matrix and fabrics on fatigue of FRP. in Design of Composite Structures:*"Design of Composite Structures Against Fatigue - Applications to Wind Turbine Blades" R. Mayer (ed.) . Mechanical Engineering Publications Ltd.. Suffolk. UK (1996)

13 A.T. Echtermeyer. E. Hayman. K.O. Ronold. *Comparison of Fatigue Curves for Glass Composite Laminates, in Design of Composite Structures:*"Design of Composite Structures Against Fatigue - Applications to Wind Turbine Blades" R. Mayer (ed.) , Mechanical Engineering Publications Ltd.. Suffolk. UK (1996)

14 CEI. "Wind Turbine Generator Systems - Part 1: Safety Requirements". International Standard 1400-1. International Electric Commission. Geneva. Switzerland. 1994

15 Ronold. K.O. and Echtermeyer. A.T.. "Estimation of Fatigue Curves for Design of Composite Laminates". accepted to be published. *Composites Part A*. 1996.

16 Hahn. H.T.. "Fatigue of Composites" in Delaware Composites Design Encyclopedia. Vol. 1. pp. 73-130. 1989

17 Echtermeyer. A.T.. "Method to Predict Fatigue Lifetimes of Glass Reinforced Plastics for Wind Turbine Blades". DNV Research Report 95-2056. (1995)

18 Ronold. K.O.. Wedel-Heinen. J.. Christensen. C.J.. Jorgensen E.. "Reliability-Based Calibration of Partial Safety Factors for Design of Wind-Turbine Rotor Blades against Fatigue". Proceedings of the European Wind Energy Association Conference and Exhibition. Thessaloniki. Macedonia. Greece. Vol. II. p.927-933. October 10-14. (1994)

19 Bach. P.W.. "High Cycle Fatigue Investigation into Windturbine Materials". Proceedings of the European Community Wind Energy Conference EWEC 88. editor W. Palm. Stephens Ass.. Bedford. England. p. 337. 1988

20 ten Have. A.A.. "WISPER and WISPERX final definition of two standardized fatigue loading sequences for wind turbine blades". NLR report NLR TP 91476. (1991)

21 Poppen. M.. Thor. S.-E. "Fatigue Life Time Predictions of GFRP Material for Wind Turbine Blades - Comparisons with WISPERX tests". FFA-The Aeronautical Research Institute of Sweden. Report FFA-TN-1995-46. (1995)

22 Kensche. C.W.. "Influence of Composite Fatigue Properties on Lifetime Predictions of Sailplanes". XXIV OSTIV Congress. Omarama. New Zealand. (1995). Technical Soaring Vol. 19. No. 3. pp. 69-76. (1995)

23 Rademakers. L.W.M.M. et. al. Voorstel tot wijziging technische criteria met betrekking tot de vermoeiigseigenschappen van vezelversterkte kunststoffen. (in Dutch) DE-Memo-91-58. 1991

24 Germanischer Lloyd. Regulations for the Certification of Wind Energy Conversion Systems. Hamburg. 1993

Appendix 11

Joule II - Dynamic Stall and 3D Effects

Anders Björck, Sven-Erik Thor

Dynamic Stall and 3D Effects

A. Björck, S-E Thor
FFA, The Aeronautical Research Institute of Sweden,
P.O. Box 11021 S-161 11 Sweden, tel: +46 8 634 10 00, Fax: +46 8 25 34 81 email:bka@ffa.se

Abstract: The JOULE II project "Dynamic Stall and 3D Effects" started in January 1994 and was completed in September 1995. The objective of the project has been to increase the understanding of the three-dimensional and unsteady aerodynamics of stall controlled HAWT's. The objectives have also been to develop "engineering models" - suitable for inclusion into aero-elastic codes. The project included the participation of 13 parties within Europe. This paper describes an overview of the work carried out within the project and key results.

Keywords: Blade Aerodynamics, Dynamic Stall, Pressure Distribution, Stall Rotation Effects

1. INTRODUCTION

The use of 2D steady state aerofoil data in strip theory including aeroelastic effects will result in unsatisfactory predictions of wind turbine loads at high wind speeds and when operating in yaw. The maximum power for stall regulated turbines is generally under-predicted using 2D wind tunnel data. To achieve the correct power level and blade bending moments it is therefore common practice to apply empirical corrections to 2D airfoil data. In addition, the amplitude of blade oscillations relies heavily on the aerodynamic damping. When the blade is stalled, the aerodynamic damping is small and the blade would be undamped and oscillate heavily if it was not for 3D and unsteady dynamic stall effects. In order to correctly simulate the loading and performance of a wind turbine operating in stall, it is today clear that dynamic stall and 3D effects have to be included in aeroelastic calculations.

2. PROJECT GOAL

The objective of the project has been to increase the understanding of the three-dimensional and unsteady aerodynamics of stall controlled HAWT's. The objectives have also been to develop "engineering models" - suitable for inclusion into aero-elastic codes - for dynamic stall and 3-D effects.

3. OUTLINE OF THE PROJECT

The project has included 13 parties in Europe. FFA has been the technical coordinator of the project. The other participants have been: Risø and Tech. Univ. of Denmark in Denmark, ECN, NLR and Delft Univ. of Technology in the Netherlands, Univ. of Bristol, Garrad Hassan, Imperial College and Cranfield University in England, Nat. Tech. Univ. of Athens and CRES in Greece and Univ. du Havre in France.

A more comprehensive description of the project and results can be found in the project report [1].

The project was divided into three tasks: Experiments, calculations and development of engineering models.

Full unsteady 3D viscous flow calculations on a rotating blade were outside the scoope of the project and the work with calculations were therefore divided into steady 3D and unsteady 2D calculations.

Measurements on several rotating and non-rotating wind turbine blades were used to analyse 3D effects. From these experiments, aerodynamic section coefficients as function of angle of attack were determined. These data were used for comparison with calculations and for comparison with expected 2D characteristics. Measurements on rotor blades carried out in a wind tunnel and field rotor measurements under conditions with low wind turbulence provided information on "quasi-steady" 3D flow. Risø field rotor measurements during turbulent conditions and during yawed operation provided unsteady $C_n(\alpha,t)$ data that were used for comparison with Navier-Stokes calculations and simulations with the dynamic stall models

4. THREE-DIMENSIONAL EFFECTS

4.1 Inner part of the blade

All experiments of the project show a stall delay for the inner part of the blade.

An analysis of the 3-D boundary layer equations by Snel [2] has shown that convection terms containing radial derivatives are of higher order than remaining terms. Neglecting radial derivatives allows a simplified system of equations which can be solved in a 2-D sense. This is used by NLR in the viscid/inviscid strong interaction code ULTRAN V. Further, neglecting the radial pressure gradient, the analysis of NLR [3] shows that the main effects of rotation scales with the ratio of local chord to local radius, c/r.

The ULTRAN V "quasi 3D" calculations [3] show a stall delay and increased lift at angles of attack past the 2-D stall, as seen in experiments.

Calculations were in the project also made with a 3D Navier-Stokes code EllipSys by Denmark Technical University. Figure 1 shows these calculations for a constant chord non-twisted blade. Results for different radii are compared to 2D calculations with the same code and aerofoil. For small radii, the 3D lift coefficient of the rotating shows a large stall delay compared to the 2D case in the same way as predicted by NLR.

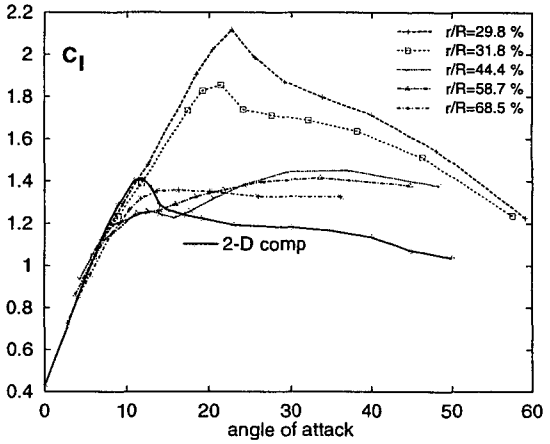

Figure 1. 3D Navier-Stokes calculations.

Looking at angles of attack past 2D static stall a "triangular shaped" pressure distribution, quite different to 2D pressure distributions at equivalent angles of attack, have been measured on several rotating blades.

Such pressure distributions also were the result of calculations in the project. Calculations with two different codes are shown in Figure 2. The Figure shows calculations by NLR and DTU for the same rotor as in Figure 1 at an angle of attack of 19.3 degrees. It is seen that both codes give similar results. For the 2-D case, flow separation occurs at around 30% x/c following a flat pressure region to the trailing edge. The flow is separated also for the rotating case. However, for the rotating case, no constant pressure region is found. The flow in the rotating cases of Figure 2 is also associated with significant radial flow directed outwards in the separated region (not shown in the Figure).

Calculations with viscous/inviscid interaction and Navier-Stokes codes thus show promising results. The increased normal force coefficient in stall has been caught by these two different types of code. The observed triangular shape of the suction side pressure distribution for stalled flow on rotating blades has been captured by both these methods. The ULTRAN V code does not model the full full 3D flow field but includes the effect of rotation. However, both codes qualitatively give the same result indicating that the main cause for the stall-delay and increased 3-D post stall lift coefficients is the effect of rotation, with Coriolis forces occurring in the separated 3-D boundary layer flow.

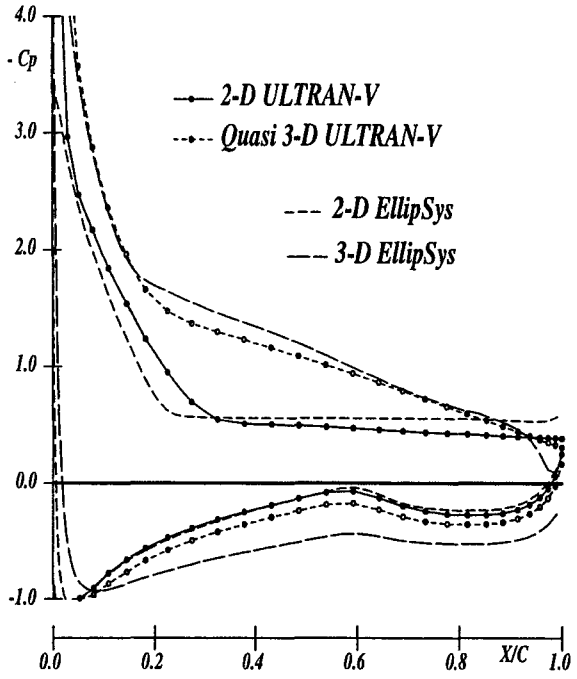

Figure 2. Calculated pressure distributions for a rotating blade compared to calculated 2D pressure distributions at the same angle of attack at an r/R of 35%.

4.2 Reynolds number scaling of rotational effects

The integral boundary layer equations show that the Coriolis term in the momentum equation scales with the boundary layer thickness. For larger Reynolds numbers the boundary layer thickness will become smaller and the viscous effects become less dominant. Therefore the radial flow becomes less and the Coriolis force will be smaller with increasing Reynolds number. The effect of rotation will thus not only scale with c/r but also with Reynolds number. This is an important finding and leads to the conclusion that the effects of rotation will be smaller as the turbine size increases. 3-D effects derived from experiments on relatively small turbines may not therefore be directly applicable for larger turbines.

4.3 Outer part of the blade

At larger values of r/R the effect of rotation on increased $C_{n,max}$ decreases but measurements show that the stall characteristics can differ from that measured during 2D tests. 2D measurements of aerofoils generally show a drop in C_n above $C_{n,max}$. Local instantaneous damping of flapwise motion can be written as proportional to the derivative $\partial C_n/\partial\alpha$. For unsteady motion the $C_n(\alpha)$ curve will differ from the character attained during a slow change of α. However, even if a dynamic stall model is applied the result will be dependent on the static data used as input. Hence the importance of stall and post stall data.

The time averaged $C_n(\alpha)$ at 70% r/R from Risø measurements on a LM 8.2 m blade shows a post stall behaviour

where all regions of negative $\partial C_n/\partial\alpha$ are absent. The tests of FFA on a non-rotating and a rotating blade at 75 % r/R both show a drop in C_n past $C_{n,max}$ even though the drop is slightly smaller for the rotating case.

In Figure 1 it is seen that C_l around α for static stall is lower for r/R larger than 44% but that the post stall level of C_l around is larger.

No firm conclusions could be drawn in the project regarding how 3D effects affect the stall behaviour at the important outer radial half of the blade. It, however, seems as if the general trend is that the drop in C_l (or C_n) past the stall angle of attack is smaller on rotating blades than during 2D measurements.

5. DYNAMIC STALL

Different aspects of dynamic stall were investigated by calculations with 2D Navier-Stokes solvers and with the ULTRAN V viscid-inviscid interaction code with effects of rotation included [1].

5.1 Pitching aerofoil versus pitching inflow

Studies on the importance of the type of type motion, e.g. pitching aerofoil versus pitching inflow, were carried out. A first conclusion is that the actual physics of the dynamic stall mechanism does not really depend on the generation mechanism of the unsteadiness at least not in the range of reduced frequencies for wind energy applications.

5.2 Dynamic variation of the relative velocity

Simultaneous with angle of attack variation there is often a variation in the velocity relative to the aerofoil. Risø has developed an "fgh-method" for dynamic stall.

$$C_n = C_{n,stat} + f \cdot \frac{c}{W}\frac{d\alpha}{dt} + g \cdot \left(\frac{c}{W}\right)^2 \frac{d^2\alpha}{dt^2} + h \cdot \frac{c}{W^2}\frac{dW}{dt}$$

The f-, g- and h functions were determined by application of a systematic optimization algorithm such that the best fit between simulations and measurements was obtained. The model was then applied to different schematic α– and W variations. Dynamic stall loops became slightly different depending on whether the W variation was in phase or counter-phase with α. Calculations were also made with an unsteady Navier-Stokes solver but these results showed a much smaller influence of a dynamic variation of W. No firm conclusion could thus be drawn, but it is recommended that this subject is studied further.

6. ENGINEERING MODELS

Engineering models were developed in order to incorporate dynamic stall and 3-D effects in aero-elastic codes with aerodynamic models of "strip theory" type

6.1 Dynamic stall

Five different dynamic stall models were applied to simulate the aerodynamic forces taken from two types of tests. The models were the Øye model used by DTU, The Beddoes model used by Garrad Hassan, the Onera model used by ECN, a new time-lag model by ECN and the fgh-model used by Risø.

The dynamic stall models were applied to simulate the aerodynamic forces taken from two types of tests:

- 2-D tests on aerofoils used on many wind turbines.
- Measurements of C_n on a blade section at 68% r/R from the Risø field rotor test with LM 8.2 meter blade.

The agreement between measurements and simulations with the engineering models was reasonably good. The simulations showed that the dynamic stall models both seem applicable to different types of aerofoils as well as they reasonably well predict the measured dynamic stall characteristics on a real rotor.

An example which shows the good comparison with measurements is shown in Figure 3 which shows $C_n(\alpha,t)$ from the Risø field rotor test and simulations with the Risø fgh-method.

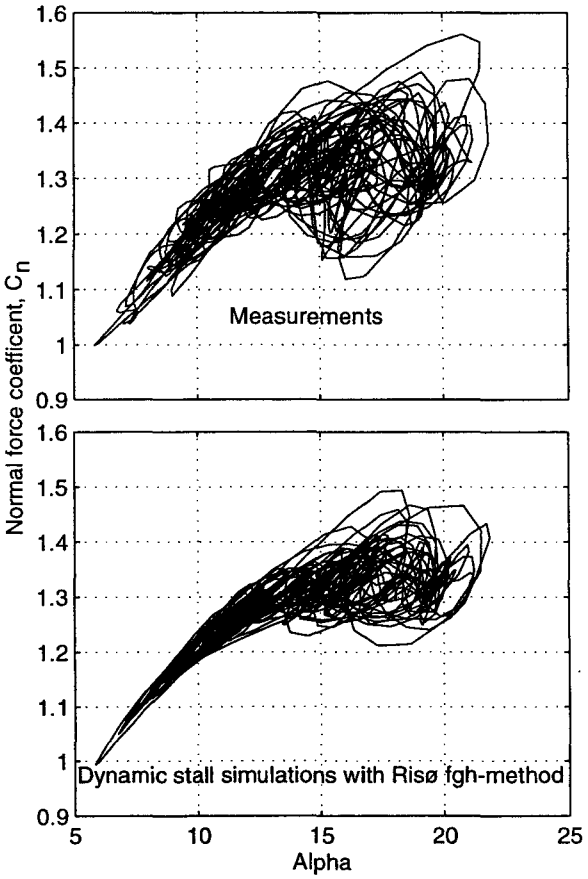

Figure 3. Measured and simulated dynamic stall.

6.2 3D effects

Two different methods to correct 2D data for rotational effects were developed. Garrad Hassan applied an angle of attack delay applied together with the dynamic stall method and ECN extended their 3D lift correction method with a drag correction part [1].

In the project, Garrad Hassan carried out calculations of power in different ways to study the effect of the 3D models. Calculations were made in the following ways:

1). Steady state performance calculations with static data (2D qs calc).
2.) Power curve taken as the mean power from simulations with an aeroelastic code with turbulent wind and with steady aerofoil data (2D qs sim.).
3). As 2 but with a dynamic stall model applied (2D unsteady sim.).
4). As 3 but with the Garrad Hassan 3D correction added and finally (GH 3D 2D un-steady sim.).
5.) As in 1 with the ECN 3D correction method applied (ECN 3D, qs calc.)

The result is shown for the turbine of the NREL combined experiment in Figure 4. The Figure shows that applying the 3D correction methods substantially improves predictions but further more that dynamic stall alone has a large effect on the mean power curve. It is thus important to separate 3-D effects from unsteady effects, and when using data from field rotor measurements to validate 3-D correction methods the effect of unsteady aerodynamics should be separated.

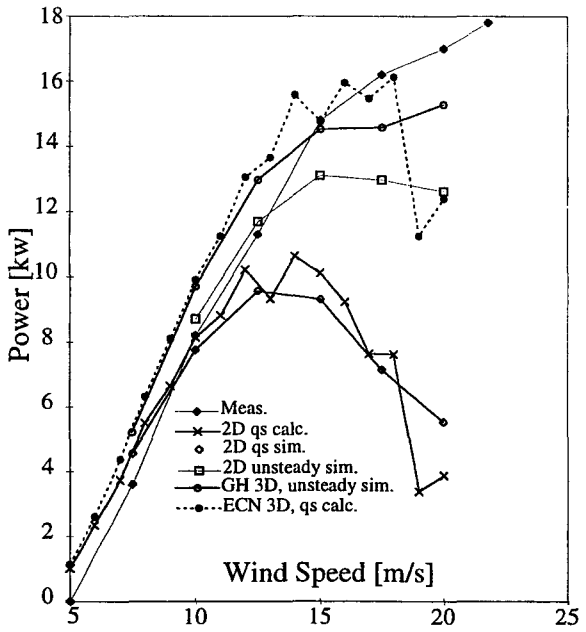

Figure 4. Measured and calculated power curves.

6. CONCLUDING REMARKS

The project has lead to improvements in the capabilities of calculating the viscous flow around wind turbine blades. Separated three-dimensional flow was for some cases well predicted and certain aspects of dynamic stall were investigated. Still, Navier-Stokes solutions are shown to be highly sensitive to the choice of turbulence models. The 3-D solutions were obtained with course grids and rather simplified boundary conditions. In order to increase the possibility to understand the 3-D viscous flow, both in general and for specific new designs, it is recommended that further work related e.g. turbulence models for Navier-Stokes methods is done.

It is recommended that the engineering dynamic stall models are further validated using data from more experiments. It is also recommended that improvements, for e.g. the calculation of the unsteady drag, are done. The influence of a varying relative velocity is also recommended to be studied further.

A further validation of either the engineering models or Viscous calculations will also require more experimental data not yet available.

ACKNOWLEDGEMENTS

The "Dynamic stall and 3D project" was funded by the European Commission under contract JOU2-CT93-0345 and partly by national agencies or participants.

REFERENCES

[1] A. Björck, "Dynamic Stall and Three-dimensional Effects, Final report for the EC DGXII Joule II Project, JOU2-CT93-0345", FFA TN 1995-31, Januari 1996, The Aeronautical Research Institute of Sweden

[2] H. Snel, "Scaling laws for the Boundary layer flow on rotating wind turbine blades", IEA 4th symposium on aerodynamics for wind turbines, Rome 1991, Edited by K.F McAnulty, ETSU-N-118

[3] J. Bosschers, "Influence of Blade Rotation on the Sectional Aerodynamics of a Wind Turbine Blade", NLR Contract Report CR 95290 L, September 1995.

Appendix 12

Survey of variable speed operation of wind turbines

Ola Carlson, Jonny Hylander, K. Thorborg

SURVEY OF VARIABLE SPEED OPERATION OF WIND TURBINES

O. Carlson, J. Hylander, K. Thorborg
Department of Electrical Power Engineering
Chalmers University of Technology
S-412 96 Göteborg, Sweden
Phone: +46 31-772 16 37, Fax: +46 31-772 16 33
E-mail: ola.carlson@elkraft.chalmers.se, jonny.hylander@elkraft.chalmers.se

ABSTRACT: During the last five years the production and operation of variable-speed wind turbines have advanced from a few experimental machines to a serial production of at least 10 MW of installed capacity of variable speed machines per week. The rated power of serial wind turbines is today around 600 kW and for the prototypes up to 3000 kW. Variable speed operation of wind turbines can be obtained with several different types of electrical generating systems, such as synchronous generators with diode rectifiers and thyristor inverters or induction generators with IGBT-converters, for the wide speed range. For the narrow speed range the wound rotor induction generator with a rotor cascade or a controlled rotor resistance is preferable. The development of permanent magnetic material and the reduction of costs of the power electronic components have opened a possibility of designing cost-effective wind turbines with a directly driven generator. Pitch control together with variable speed will make it possible to limit the power variation within a few percent, 2 to 5 %, of the rated power.
Keywords: Converters, Control, Electrical Generators, Variable-Speed Operation.

1. INTRODUCTION

Variable speed operation of wind turbines, connected to the utility grid, has been discussed for the last 20 years. To achieve a wide speed range of the turbine speed the most common way is to disengage the frequency of the generator from the frequency of the grid. This separation of frequencies is usually made by static electronic converters. Other types of variable speed systems have also been considered, such as hydraulic systems and variable ratio gearboxes. The electrical system is preferable due to high efficiency and low maintenance. The breakthrough for the electrical variable-speed systems has come during the last years mostly due to the development of static electronic valves such as Insulated Gate Bipolar Transistors (IGBT). This component is easy to control and the power rating is increasing every year.

The speed range can also be narrow, a 10 % rise of the nominal speed. With this design the speed variation is achieved by a controlled rotor resistance or a rotor cascade of the induction generator [1].

During the last five years the production and operation of variable-speed wind turbines have advanced from a few experimental machines to a serial production of at least 10 MW of the installed capacity of variable speed machines per week. The rated power of serial wind turbines is today around 600 kW and for the prototypes up to 3000 kW.

In [2] there are 36 wind turbine manufactures with 87 different models listed which can be classified according to Table I.

The three main manufactures of variable speed machines are Enercon and Kenetech with a wide speed range and Vestas with a narrow speed range. These three companies have a large part of the wind turbine market.

Table I: Different types of wind turbines.

Stall control Constant speed	Stall control Variable speed	Pitch control Constant speed	Pitch control Variable speed
59	2	18	8

2. ADVANTAGES OF VARIABLE SPEED OPERATION

A wind turbine which operates with variable speed has the well known advantages of decreasing the mechanical loads and especially the loads in the drive train of the wind turbine. This smoothing of torque and power is achieved by speed variations on the turbine. The power of a pitch-controlled, constant speed, turbine of 12 kW with a rotor diameter of 12 meter is shown in Figure 1. This can be compared with the same wind turbine but with variable speed operation (Fig. 2). As can be seen, the maximum power is reduced from 25 to 13 kW.

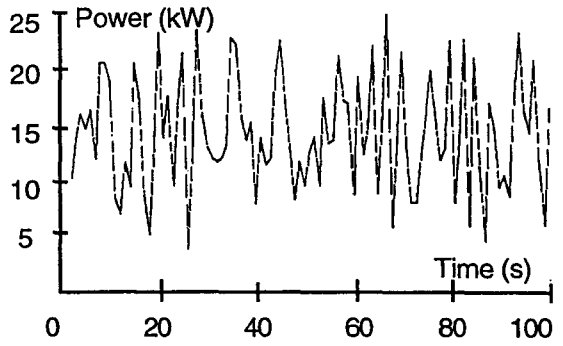

Figure 1: Power at constant speed operation.

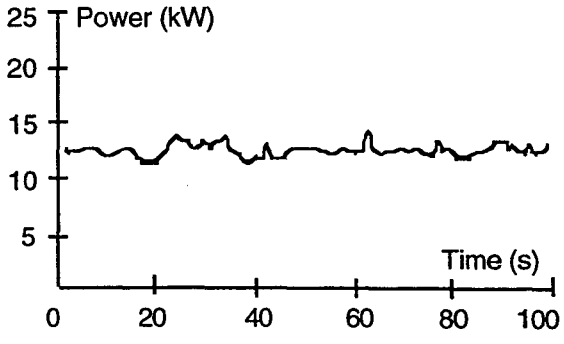

Figure 2: Power at variable speed operation.

With a wide speed range design, the noise will also be decreased due to the reduction of the operating speed at low wind speed conditions.

The energy production increases by 2-6 %, depending on the location, due to higher aerodynamic efficiency, i.e. optimal C_p-λ operation, and also due to lower losses in the electrical generating system.

There is also a possibility to avoid rotational speed which is triggering mechanical resonances in the wind turbine. Active damping of resonances in the drive train is also possible. In [3] it is shown that active damping in the drive train will decrease the amplitude of the drive train resonance considerably.

With variable speed operation the power quality from a wind turbine can be increased due to the elimination of flicker on the output voltage. Two different phenomena occur between the grid and the wind turbine. Stationary voltage variations emanate from starting and stopping the turbine, and voltage fluctuations emanate from power fluctuations. According to the flicker curve in the IEC 868 Standards, stationary voltage variations are allowed to be as large as 3%, while voltage variations occurring, for example, at 1 Hz may be only 0.7%. The X/R ratio of the grid has a significant impact on the minimum short-circuit ratio, to fulfil the standard, at the point of common connection (PCC). X in the ratio stands for the reactance of the grid and R stands for the resistance of the grid. The X/R ratio for a standard grid on the countryside is around 1. The short-circuit ratio is the ratio between the grid short-circuit power and the rated power of the wind turbine. Calculations of a constant speed wind turbine reveal that the minimum short-circuit ratio is determined by the stationary voltage variations, if the X/R ratio of the grid is low at the PCC, less than 2.3. At higher X/R ratios, the minimum short-circuit ratio is determined by voltage variations caused by fluctuating power (Fig. 3) [4].

By variable speed operation the power fluctuating is eliminated and thereby it is possible to connect the wind turbine to a weaker grid with less short-circuit power. The flicker problem is often the driving task in the integration of wind turbines. If the reactive power consumption of the electrical generating system is controlled, even more wind turbines can be installed on a weak grid [5].

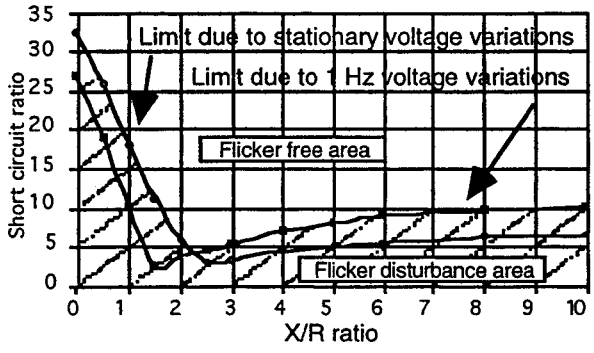

Figure 3: Minimum short-circuit ratio at different grid X/R ratios to avoid flicker caused by stationary voltage variations and 1 Hz variations.

3. GENERATORS

Today, most wind turbines use an induction machine as a generator. The induction machine operates at almost constant speed but has the advantage of being well enclosed and almost maintenance-free. The small operating speed variation with an induction machine gives a well needed damping of the wind turbine. In some wind turbine designs, two induction machines are used. The larger, high-speed machine, is used at higher wind speeds and more out-put power. The smaller machine, with a lower rated speed, is used at low wind speeds and lower out-put power. The two machines can be combined in a single machine. The winding can in this machine be switched so that two operating speeds will be possible. The drawbacks of the induction machine are that it consumes reactive power and that electrical transients occur during switching-in. The reactive power consumption can be compensated with capacitors, and several "soft-start" equipments are available, which reduces the transients. However, in variable speed operation, the small speed variation and reactive power consumption, make the converters unnecessarily complicated.

The conventional synchronous machines, with their constant speed, are not suitable to use in wind turbines without extra damping of wind-induced transients. In variable speed operation the damping can be provided by controlling the generator torque by the converter. With a synchronous machine a simple diode-equipped rectifier can be used. The rectified out-put power of the generator is supplied to the grid via a controlled inverter (Fig. 4).

The magnetic field in the synchronous machine can be created with a conventional field-winding or by using modern permanent magnets. With permanent magnet excitation a compact low-weight, low-speed, multiple pole, directly driven synchronous machine will be possible to design. The cost reduction of power electronic components and control equipment will in the future reduce the total cost of variable speed systems with synchronous machines.

Power electronic equipment creates harmonics. These harmonics will, if uncontrolled, produce harmonic torques in the generator and contribute to voltage variations and harmonic currents in the grid. The harmonics will besides give extra losses in the generator. Usually the power of generator is derated about 20 % when connected to a converter. The harmonic problem can with modern control methods be mastered.

4. CONVERTERS

In a variable-speed system the frequency of the generator is not the same as that of the grid and therefore two converters are needed: a rectifier converting the variable frequency ac into dc, and an inverter converting the dc into ac at grid frequency.

The converters can be characterized by their valves: non controllable (diodes), controllable (thyristors) and turn-off valves (GTO, IGBT). With diodes only rectification is possible. With controllable valves the converter can operate in the rectifying as well as in the inverting mode. Thyristors can control active power, while turn-off valves can control both active and

reactive power. It goes without saying that the price tag follows the converter's performance, which in short is:

RECTIFIER

Diodes: Uncontrollable dc, uncomplicated, robust.

Thyristors: Controlled dc, facilitating electrical damping of synchronous generator, but increases losses. Damping should preferably be performed by control of the inverter.

GTO, IGBT: Controlled dc and reactive power, and the flow of power can be reversed. Asynchronous machines can therefore be used, and they can furthermore start up as motors being supplied from the grid.

INVERTER

Thyristors: Burdens the grid with variable reactive current and low order harmonic currents. Relatively uncomplicated.

GTO, IGBT: Controlled power factor. Output voltage contains high order (usually not harmonic) voltage overtones. Connected to grid via inductors or filters . The current overtones can be kept low. Autonomous operation possible. The converter is quite complicated, especially with GTO.

The choice of a system depends on acceptable cost and desired performance. Ruggedness, complexity and expected reliability should also be considered.

Figure 4 shows an attractive system with low generator and rectifier losses and high power quality, i.e. controllable reactive power and low harmonic currents to the grid from the inverter.

The IGBT or similar future gate *voltage*-controlled valve devices will sooner or later replace the gate *current*-controlled GTO, which today is used for high power and/or voltage that is in the MVA and kV regions. A rough measure of the rated output power of a three-phase IGBT inverter bridge with 1200 V, 600 A valves is

$$S = \sqrt{3} \cdot U \cdot I = \sqrt{3} \cdot \frac{1200}{2} \cdot \frac{600}{2} = 312\,\text{kVA},$$

and for a future generation with 2000 V, 1000 A valves S will be about 800-900 kVA. Devices, or better valve bridges or modules, may be connected in parallel to increase the output power.

New technologies are coming resulting in, say 4000 V, 1000 A devices, i.e. S @ 1.7 MVA, and that would definitely mean the end of the GTO epoch.

5. ELECTRICAL SYSTEMS

The choice of electrical system, for the wide speed range, can be divided into two almost independent choices. The generator and rectifier must be chosen as a combination and the inverter can be chosen almost independently of the generator and rectifier used.

5.1 Choice of generator and rectifier

The cost comparison of the generator/rectifier alternatives is clear. The synchronous generator with diode rectifier has much lower total cost than the induction generator with force-commutated rectifier. The difference in total cost is large not only because of the high price of the force-commutated rectifier, but also because of its high losses. The advantages of the induction generator system is that it can be used for motor start of the turbine [6].

5.2 Choice of inverter

The comparison of the total cost of the inverter and its losses clearly shows that the thyristor inverter is the least expensive choice. Even with a substantial reduction of the IGBT inverter cost, the thyristor alternative will be cheaper because the difference in losses is not likely to be reduced much. However, the increasing demands on power quality may make the thyristor inverter less attractive in the long run. The IGBT inverter can even improve the power quality of the grid.

5.3 Efficiency of electrical systems

If a comparison of the efficiency of different electrical systems is to be carried out, it is important that the average efficiency of the systems is compared and not the rated efficiency. The calculation of the average efficiency is carried out by calculating the average power of the turbine, P_{tav}, and the average losses of the electrical system, P_{dav}. The average power and losses are calculated by using the probability density distribution of the wind speed and the power as well as the losses as a function of the wind speed [7]. The average efficiency can then be calculated as

$$n = 1 - P_{dav} / P_{tav}$$

Three different systems with the rated power of 500 kW have been investigated and compared. These are;

- a conventional constant speed system with a step-up gear and a directly grid-connected induction generator.
- a variable speed synchronous generator with a frequency converter.
- a directly driven variable speed permanent-magnet generator with a frequency converter.

Table II: Average and rated efficiency of the systems.

	Low-wind speed site	Medium-wind speed site	High-wind speed site	at Rated load
Induction generator	82.0 %	87.3 %	89.7 %	93.8 %
Synchronous generator	84.0 %	86.8 %	88.1 %	90.6 %
Directly driven generator	86.4 %	88.8 %	89.9 %	91.6 %
Average wind speed	5.3 m/s	6.6 m/s	7.8 m/s	—

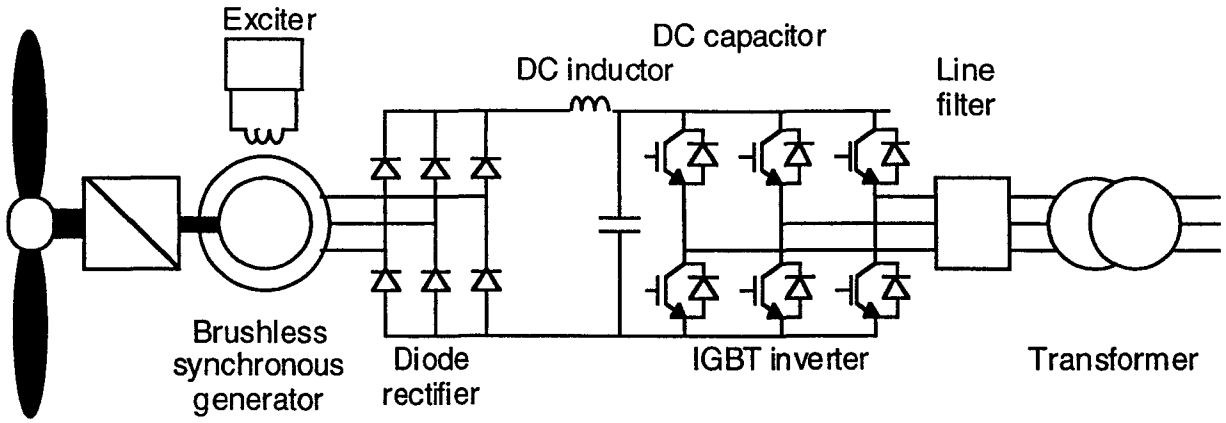

Figure 4: The proposed system for variable speed wind turbines. Synchronous generator and diode rectifier for low losses and low cost. IGBT inverter for high power quality.

6. CONTROL

The goal of the control of a wind turbine is operation at optimal C_p-λ in low-wind conditions and above rated wind speed to operate at rated power output. By a wide speed range of variable speed operation it is possible to achieve optimal C_p-λ operation. To operate, with a smooth output power at rated power requires variable speed of at least a 10 % variation and a pitch control of the turbine.

6.1 Pitch control

Pitch control together with variable speed will make it possible to limit the power variation within a few percent, 2 to 5 %, of the rated power. This can be compared with the standard constant speed systems which have power variations of +/- 30 to 60 % of the rated power.

6.2 Stall control

Variable speed operation with stall control is not so common; a few prototypes are running today. Of course optimal C_p-l operation is obtained, but it is difficult to control within the allowed limits of power variations. Test results show that it is possible to limit the power variations to a maximum of +/- 20 % of the rated power.

7. CONCLUSION AND FUTURE DEVELOPMENT

The current research and the impact of power electronics on power engineering indicate that within five years it will be possible to design a cost-effective wind turbine that will have a PM directly driven generator with a diode or an IGBT rectifier and an IGBT inverter. The main reasons for the electrical system are high efficiency, a good power quality, the possibility to control the power output and to avoid gearbox problems. The variable speed is also very important for noise reduction. The wind turbine will have pitch control and will be designed to act in a soft way, i.e. small movements instead of loads on the mechanical parts and thereby it will be possible to make a weight reduction in the design. All this altogether will make the wind turbines of tomorrow more cost-effective compared to the wind turbines of today.

8. ACKNOWLEDGEMENT

The authors would like to thank our colleagues Åke Larsson and Anders Grauers for their contributions regarding the power quality and systems efficiency. The financial support given by the Swedish National Board for Industrial and Technical Development is gratefully acknowledged.

REFERENCES

[1] Hylander, J., "Stator current frequency spectra and the torque pulsations in induction machines with rotor converter cascades", Technical report No. 163, Department of Electrical Machines and Power Electronics, Chalmers University of Technology, Göteborg, Sweden, (1986).

[2] Petersen H., and Lundshager P., "Beskrivelsen og vurdering af udenlansk vindmølleteknik", Energistyrelsen, J.nr. 51171/93-0045, Denmark, (1995).

[3] Carlson O. and Ulén E. "Torque control of synchronous and induction generators for variable speed operation of wind turbines", EUWEC '96, Göteborg, Sweden, (1996).

[4] Larsson Å, "Flicker and slow voltage variations from wind turbines", (1996), submitted to the 7th international conference on harmonics and quality of power, October 16-18, 1996, in Nevada, U.S.A.

[5] Svensson J. "Possibilities by using a self-commutated voltage source inverter connected to a weak grid in wind parks", EUWEC '96, Göteborg, Sweden, (1996).

[6] J. Svensson, A. Grauers, and O. Carlson, "Preliminary study of an electrical system for wind power plants with variable speed", Report nr: R-93-07, Department of Electrical Machines and Power Electronics, Chalmers University of Technology, Göteborg, Sweden, (1993).

[7] Grauers A. "Efficiency of three wind energy generator systems", IEEE Power Engineering Society, Winter Meeting 1996, Paper no: 96 WM 047-1EC, (1996).

Appendix 13

Generators for Gearless Wind Energy Converters

Anders Grauers

GENERATORS FOR GEARLESS WIND ENERGY CONVERTERS

Anders Grauers
Department of Electric Power Engineering
Chalmers University of Technology
S – 412 96 Göteborg, Sweden

ABSTRACT: This paper discusses some design alternatives for directly driven generators, and one specific generator type is investigated for a wide range of rated power. First, the specification for a directly driven generator is presented, then different design alternatives are discussed. A radial-flux permanent magnet generator for frequency converter connection has been chosen for a more detailed investigation. The design, optimization and performance of that generator type are presented. Generators from 30 kW to 3 MW are designed and compared with conventional four-pole generators with gear. It is found that a directly driven generator can be more efficient than a conventional generator and gear and have a rather small diameter and a low active weight.

KEYWORDS: Generators, Direct drive, Power Electronics, Performance.

1 INTRODUCTION

The interest in directly driven generators for wind turbines is increasing because they make the gear unnecessary. Without the gear, the wind energy converter can be cheaper, lighter and more efficient. Some different alternatives of electromagnetic design of the generators have been proposed, for instance: radial-flux generator [1,2]; axial-flux generator [3]; and transversal-flux generator [4].

Which generator type that is the best one is not clear, there is a need for further comparison of different design options. The papers mentioned above do not include fully optimized generators and, therefore, the achievable size and performance of the generators should be further investigated.

The purpose of this paper is to discuss some of the design alternatives in order to choose a generator type that can lead to a small, light and efficient generator. This paper also presents the size, efficiency and active weight of optimized directly driven generators from 30 kW to 3 MW of the chosen generator type. A brief comparison with conventional four-pole induction generators and gears is also made. Another paper discusses the optimization of the chosen generator more in detail [5].

2 GENERATOR SPECIFICATION

The specification for the directly driven generators in this paper is shown in Table 1. The rated torque of a directly driven generator is determined by the turbine power and speed. Out of data for 25 wind energy converters from 30 kW to 3 MW an approximate function for the rated torque and rated speed has been determined.

Table 1 The specification of the directly driven generators, P_N is the rated power.

Rated torque	$71.1\ \text{Nm}\left(\frac{P_N}{1\ \text{kW}}\right)^{1.23}$
Rated speed	$134\ \text{rpm}\left(\frac{P_N}{1\ \text{kW}}\right)^{-0.23}$
Winding temperature	≤ 130°C
Peak torque	≥ Rated torque

The required peak torque of the generator depends on the type of wind energy converter in which it is used. Stall-controlled turbines or turbines with electrical braking need a generator that transiently can produce a higher torque than the rated one. Pitch-controlled wind turbines without electrical braking do not require the generator to produce a high peak torque. The generators discussed in this paper do not have to produce a peak torque higher than the rated one. If that is required, the generator can be expected to be slightly larger than what is shown in this paper.

3 SOME DIFFERENT DESIGN ALTERNATIVES

A directly driven generator has to produce a large torque because of the low shaft speed. The size and the losses of a generator are to a large extent determined by the required torque. Therefore, directly driven generators can be very large and heavy and have a low efficiency. To avoid these unfavourable features, the generator must be of an efficient type with a high force density in the air gap.

3.1 Electrical excitation or permanent magnets

Almost all large generators are electrically excited, i.e. the flux density is generated by a current in a field winding. However, permanent magnets are increasingly used because they eliminate the need of a field winding and the losses due to the field current.

The pole pitch is important for the thickness of the stator and rotor yokes and for the length of the end windings. (The pole pitch is the distance between the magnetic north and south poles on the rotor surface.) If the pole pitch is small, the end windings are short, which leads to low resistive losses. A short pole pitch also leads to a low weight of the iron core. Therefore, the pole pitch should be small in a low-speed generator.

The pole pitch is also important for the field winding. However, a decreasing pole pitch increases the losses and weight of the field pole. As the pole pitch is decreased, the no-load field current cannot be decreased and the rotor pole has to be higher to make room for the field winding, which is illustrated in Figure 1. Since the number of poles increases as the pole pitch decreases, the total field winding losses increase. The pole pitch of an electrically excited directly driven wind turbine generator should not be smaller than about 0.1 m. A larger pole pitch is preferred to reduce the field winding losses.

Permanent magnets allow a smaller pole pitch than field windings do. The equivalent magnetizing current that a

permanent magnet produces is proportional to the thickness of the magnet. As the pole pitch is decreased, the magnet thickness remains constant, which is shown in Figure 1. The minimum pole pitch is only limited by mechanical considerations and by the leakage flux between the magnets. A pole pitch of 50 mm, or even smaller, is possible. Since a small pole pitch is preferred in low-speed wind turbine generators, to limit the weight and losses, permanent magnet excitation is chosen for the investigated generator.

3.2 Frequency converter or direct connection to the grid

To connect the generator directly to the grid requires that it generates 50 or 60 Hz voltages and that oscillations between rotor and grid are damped. Because of the minimum pole pitch, the diameter of an electrically excited 50 Hz generator has to be large. The diameter has to be at least 3 m for a 30 kW generator, 5.5 m for a 300 kW generator and 9 m for a 3 MW generator. These diameters will lead to expensive generator structures. Therefore, electrically excited generators should not be connected directly to the grid.

Permanent magnets allow a smaller pole pitch than electrical excitation does. 50 Hz can be generated with a reasonable diameter, less than half the diameters presented above. However, a generator with a small pole pitch cannot damp oscillations efficiently with damper windings. The oscillations can be damped by mechanical dampers [6] but that leads to a complicated mechanical design. Therefore, also permanent magnet generators should be connected to a frequency converter.

To use a frequency converter between the generator and grid, does not only solve the problems of connecting a generator directly to the grid, but also improves the performance of the wind energy converter. The turbine can operate at variable speed, which increases the energy production slightly and decreases the noise at low wind speeds. Torque peaks in the turbine shaft can be eliminated and the grid interference can be reduced. The investigated generator is designed for frequency converter connection.

3.4 Diode or transistor rectifier

The rectifier will have a very important influence on the rated power and peak power that can be produced by a generator. The two main types of rectifiers are: the cheap and efficient diode rectifier; and the more expensive and not as efficient self-commutated transistor rectifier. The reactance of the generator consumes reactive power. If the rectifier cannot supply that reactive power, the terminal voltage and active power will be reduced. A generator can be made smaller, if it is allowed to have a high reactance, than if a low reactance is required. In Figure 2 the output powers of a three-phase permanent magnet generator with the two types of rectifiers are shown. The generator reactance is 0.5 per unit.

The transistor rectifier allows a higher power than the diode rectifier does at equal current. About 35 % higher rated power can be achieved with the transistor rectifier if the reactance of the generator is 0.5 p.u. Diode rectifiers should not be used with higher reactance than 0.5 p.u. while transistor rectifiers can be used for generators with up to about 1.2 p.u. reactance. The difference in peak power is even larger than the difference in rated power. If the current is not limited, the generator can always produce about 2.5 times higher peak power if it is connected to a transistor rectifier instead of to a diode rectifier, but at about twice as high current.

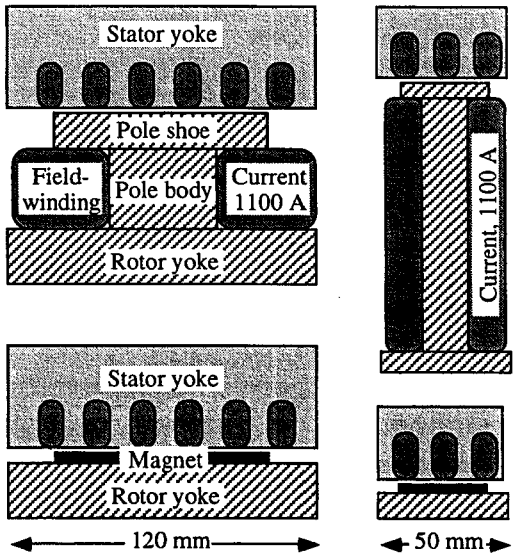

Figure 1 Electrical excitation and permanent magnet excitation with two different pole pitches. The no-load field current and the magnet height are almost the same for all pole pitches.

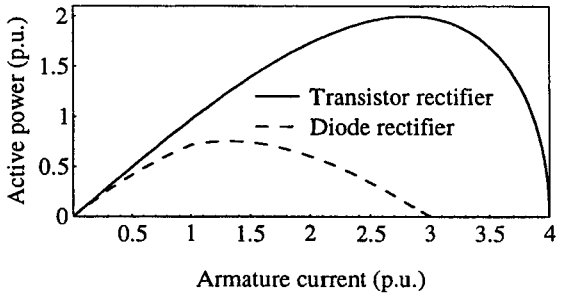

Figure 2 The output power as a function of current for a generator with a reactance of 0.5 p.u.

The cost of the generator can be assumed to be much higher than the cost of the converter. Therefore, the reduction of the generator size that can be achieved, if a transistor rectifier is used, will probably pay the extra cost of the transistor rectifier. The losses will remain almost the same at the generator rated current no matter which rectifier is used. Since a transistor rectifier allows a higher power, it will make the generator more efficient. The increase in generator efficiency at rated load will be in the same order as the difference in efficiency between a diode rectifier and a transistor rectifier. A transistor rectifier is chosen for the investigated generator.

4 GENERATOR DESIGN

The generator type chosen for this investigation is a three-phase radial-flux permanent magnet generator connected to a frequency converter with self-commutated transistor rectifier and inverter. The winding is a two-layer winding in semiclosed slots and the magnets are made of NdFeB.

A generator design method has been developed for the investigated generator type [7], including the optimization of the generator. The design method is based on conventional analytical functions for the generator performance and a lumped parameter thermal model. The

mechanical structure has not been investigated in detail but its influence on the optimization has been studied.

4.1 Average losses

The efficiency included in the optimization is the average efficiency (i.e. the energy efficiency, not the efficiency at rated load). The average efficiency is for this type of generator higher than the efficiency at rated load. The reason for the high average efficiency is that the largest part of the losses at rated load is resistive losses in the windings. As the current decreases with decreasing power, the resistive losses decrease rapidly, proportionally to the current in square. Since a wind turbine operates at partial load most of the time, the average losses are much lower than the losses at rated load, as illustrated in Figure 3. The average efficiency is discussed more thoroughly in [7,8].

4.2 Optimization

The cost function for the optimization includes the cost of the active part of the generator, the cost of the losses and an estimation of the cost of the generator structure. The effect of the cost function on the design of a 500 kW directly driven generator is discussed in detail in [5]. The three different costs are plotted as functions of the diameter in Figure 4. It can be seen that the cost of the active parts, the losses and the structure all increase as the diameter decreases below 2 m. The cost of the structure is only a rough estimation, but it is still clear that the diameter can not be much lower than 2 m. Because the cost of losses and the cost of the active part do not change much at large diameters, the cost of the structure will be the limiting factor for the maximum diameter. The optimum diameter will be between 2 and 3 m almost independently of the cost of the structure as long as it is assumed that the cost of the structure increases more than linearly with the diameter.

4.3 Generators from 30 kW to 3 MW

The generator design method has been used to calculate the size and performance of the generators for turbines between 30 kW and 3 MW. The generators are all optimized using the cost function described in [7]. The air gap diameter, stator length, pole pitch, winding temperature, air gap flux density, teeth flux density and slot height are optimized. The winding temperature is limited to 130°C according to the specification, but may be lower.

The air gap diameter and stator length of the generators are shown in Figure 5. The outer diameter and length are larger but the outer diameter will still be of about the same order as the width of a normal nacelle for all these generators.

The average efficiency and efficiency at rated load of the generators are shown in Figure 6. The average efficiency is calculated for a wind energy converter on a site where the capacity factor is 25 %. The efficiency increases with increasing power as for conventional four-pole generators. The optimum temperature of the winding is low for the small generators and increases with increasing rated power. Only the 3 MW generator reaches the temperature limit. The consequence is that small generators, although they have lower efficiency, are easier to cool than large ones.

The active weight of the generators is plotted in Figure 7. It increases almost linearly with the rated power. The costs for the active part, cost of the losses and the cost of the generator structure also increase almost linearly with the rated power. The cost of the structure is only a rough

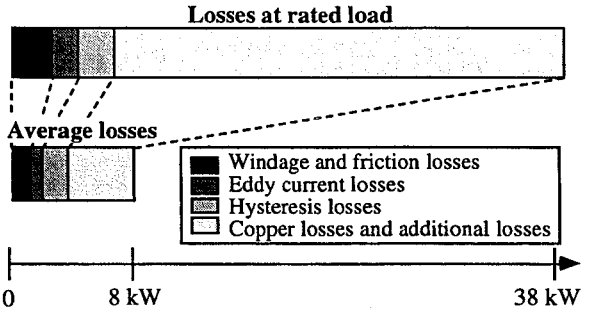

Figure 3 The different types of losses at rated load and the average losses for a 500 kW generator.

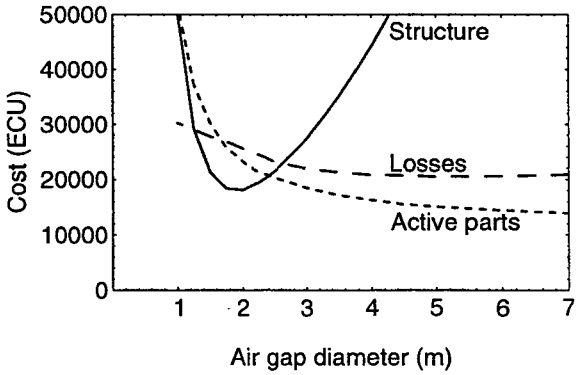

Figure 4 The cost functions for the active parts, the structure and the losses as a function of the diameter for a 500 kW generator.

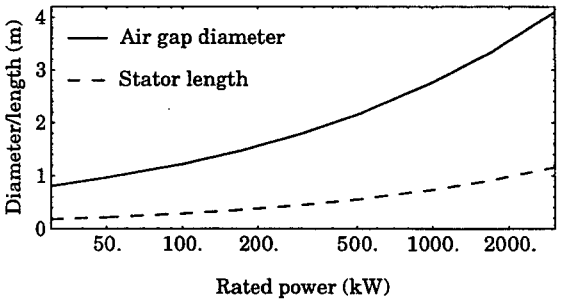

Figure 5 The diameter and length of the generators.

estimation, but the results show that the specific cost (cost/kW) of the active part of the generator and the specific cost of the losses will be rather equal for generators of all the investigated powers.

The reactance of the optimized generators increases as the rated power increases, from 0.76 p.u. for a 30 kW generator to 1.05 p.u. for a 3 MW generator. The small generators will be capable of producing a torque higher than the rated torque transiently but for the large generators that capability is limited.

Nothing in this study indicates that there is an upper or lower power limit beyond which the directly driven generator is not feasible.

5 COMPARISON WITH CONVENTIONAL GENERATORS AND GEARS

In Table 2 the weight and efficiency of grid-connected four-pole induction generators with gears and directly driven generators with frequency converters are

presented. The frequency converters for the directly driven generators have an efficiency of 96 % at rated load and their average efficiency is 95.6 %. Since the generator structure has not been investigated in detail the total weight of the directly driven generators is not known, only the weight of the active part of the generators is presented.

The comparison shows that directly driven generators with frequency converters are slightly more energy-efficient than a directly grid-connected induction generator with gear. The average efficiencies of directly driven generators are higher although their efficiencies at rated load are lower. These figures do not include the difference in energy production between a variable speed turbine and a constant speed turbine. The difference in produced energy will, therefore, be larger than the difference in average efficiency. The active weight of the directly driven generators is 2 to 4 times lower than that of the gears and induction generators. The total weight can be assumed to be of the same order for both systems.

6 CONCLUSIONS

To achieve a high efficiency, low active weight and a small diameter the generator should be made with permanent magnets and connected to a self-commutated rectifier. It is difficult to design a directly driven generator that can be connected directly to the grid.

The reactance of the generator limits the possible output power. To be able to utilize a generator well the rectifier has to supply the generator with reactive power. If a high peak torque is required, the generator may have to be larger than if it is only required to produce the rated torque.

Directly driven generators from 30 kW to 3 MW can all be made with a diameter equal to the width of a normal nacelle. The average efficiency of a directly driven generator can be higher than the efficiency of a conventional generator and gear but the full load efficiency is lower.

From this study of the active part of the generator there seems to be no upper or lower power limits beyond which directly driven generators are not feasible.

Table 2 Four-pole induction generators and gears compared with directly driven generators with frequency converters.

	Directly driven gen. and frequency converter		Grid-connected generator and gear	
Rated power (kW)	Average efficiency (at rated load) (%)	Active generator weight (kg)	Average efficiency (at rated load) (%)	Total weight (kg)
30	88 (87)	210	81 (89)	440
220	90 (89)	1300	87 (93)	4700
500	90 (90)	2700	88 (94)	7400
3000	91 (91)	14000	90 (94)	53000

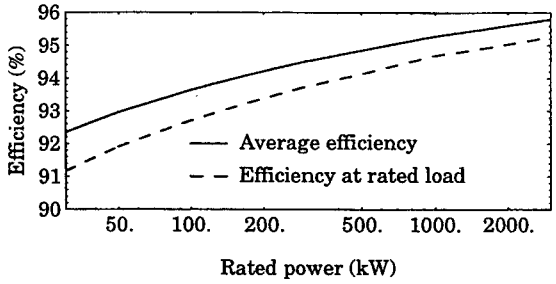

Figure 6 The efficiency of the generators.

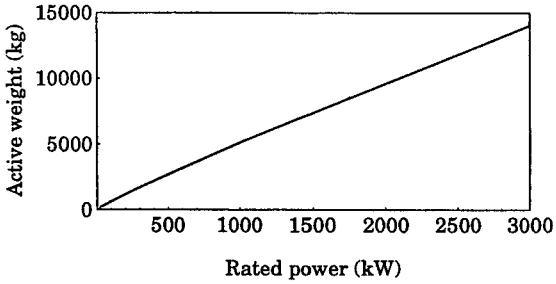

Figure 7 The active weight of the generators.

REFERENCES

[1] E. Spooner, A. Williamson, "Permanent-magnet generators for wind power applications", *International Conference on Electrical Machines (ICEM'92)*, Manchester, U.K., 15-17 Sept. 1992.

[2] P. Lampola, "Electromagnetic and thermal design of a low-speed permanent magnet wind generator", *Stockholm Power Tech Conference*, Stockholm, Sweden, June 18-22 1995, vol. Electrical machines and drives, p. 211-216.

[3] Honorati O et al., "Gear-less wind energy conversion system using an axial-flux PM synchronous machine". *European Wind Energy Conference (EWEC'91)*, Amsterdam, The Netherlands, October 14-18, 1991, Proceedings Part I, p. 814-818.

[4] Weh H et al., "Directly-driven permanent-magnet excited synchronous generator for variable speed operation". *European Wind Energy Conference (EWEC'88)*, Herning, Denmark, June 6-10, 1988, Proceedings p. 566-572.

[5] A. Grauers, "Directly driven wind turbine generators", *International Conference on Electrical Machines (ICEM'96)*, Vigo, Spain, 10-12 Sept. 1996.

[6] A. Westlake et al., "Damping the rotor angle oscillations of a permanent magnet wind generator", Proceedings of *UPEC*, 1993, Stafford UK

[7] A. Grauers, *"Directly driven permanent-magnet generator for wind turbines"*, Göteborg, Sweden, Doctoral thesis, Chalmers University of Technology, (To be published in 1996).

[8] A. Grauers, "Efficiency of three wind energy generator systems", *IEEE Power Engineering Society 1996 Winter meeting*, 21-25 January 1996, Baltimore USA, paper 96 WM 047-1 EC

Appendix 14

Rotating Transformers in Wind Turbine Applications

Jonny Hylander

ROTATING TRANSFORMERS IN WIND TURBINE APPLICATIONS

J. Hylander Ph.D.(*), S. Engström M.Sc.(**)

(*)Chalmers University of Technology
S-412 96 Göteborg, Sweden
(**) Ägir konsult AB
Drottvägen 2
S-181 31 Lidingö, Sweden

ABSTRACT: The power consumption of rotating electrical components is often supplied via slip-rings in wind turbines. Slip-ring equipment is expensive and need maintenance and are prone to malfunction. If the slip-rings could be replaced with contact-less equipment better turbines could be designed. This paper presents the design, some FE calculations and some measurements on a prototype rotating transformer. The proposed transformer consists of a secondary rotating winding an a stationary exciting primary winding. The results indicate that this transformer could be used to replace slip-rings in wind turbines.
Keywords: Wind Turbines(HAWT), Electrical Components, Electrical Systems

1. INTRODUCTION

In operation of wind turbines some rotating parts, such as pitch control or other actuators, need power supply. The electric power is usually supplied via slip-rings. Slip-ring equipment is expensive and need maintenance and are prone to malfunction. If the slip-rings could be replaced with contact-less equipment better turbines could be designed.

To supply rotating parts with electric power is a common procedure in electric machine design. In nearly all larger synchronous machines, the rotating field windings is supplied by induction from a stationary stator. The principle with induction can be adapted to larger axial diameters and used in wind turbines, as suggested in [1]. Some interesting design problems now occurs, as the axial diameter is usually less in synchronous machines than the diameter of the low speed shaft in a wind turbine. The rotating speed is also usually much lower.

2. PRINCIPLE OF OPERATION

The principle of operation can easily be understood if figure 1 is studied. A short simple U-shaped iron core is used. The stationary primary winding on the U-core creates a magnetic flux which is guided under a rotating secondary winding. The primary circuit only covers a segment of the secondary coil. To reduce the air-gap, the secondary winding is mounted on thin transformer iron strips, which is wound on the shaft. The width of the layer of strips determines the air-gap. The frequency in the secondary winding is exactly the same as in the primary winding, independent of the speed of rotation. The rotating secondary winding supplies the rotating equipment.

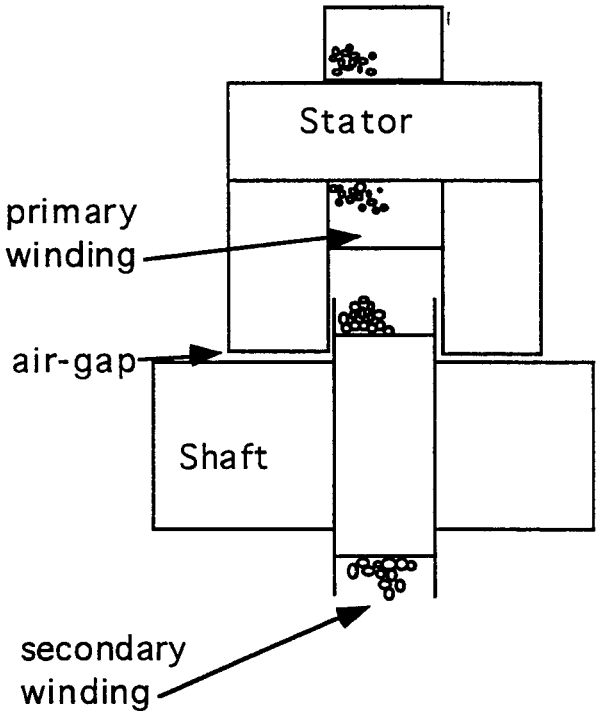

Figure 1: Principle of operation.

3. DESIGN OF A PROTOTYPE

Traditional transformer calculations [2] gives the dimensions and the characteristics of the prototype. The calculations were based on available material in our laboratory. As a stator, a C-shaped laminated transformer core was used. The length of the core was 49 mm. The magnetic strip which was used in the secondary rotating core had a width of 30 mm and the height of the layers was 14 mm. With elementary transformer design, an initial guess of the winding turns N were determined with:

$$U = 4.44 \cdot \hat{B} \cdot f \cdot A_{fe} \cdot N.$$

The magnetic flux density B was chosen low, 1 T. The iron area A_{fe} was given by the available materials.

The conductor copper area was determined from the rated currents and a maximum allowed current density of 4 A/mm^2.

In order estimated the leakage reactances a finite element calculations of the magnetic fields [3] were done. Compared with a normal transformer, without air-gaps, the leakage reactances are higher.

A plot from the magnetic field calculations, with the transformer in no-load operation, is shown in figure 2.

The details of the calculations is presented in [4].

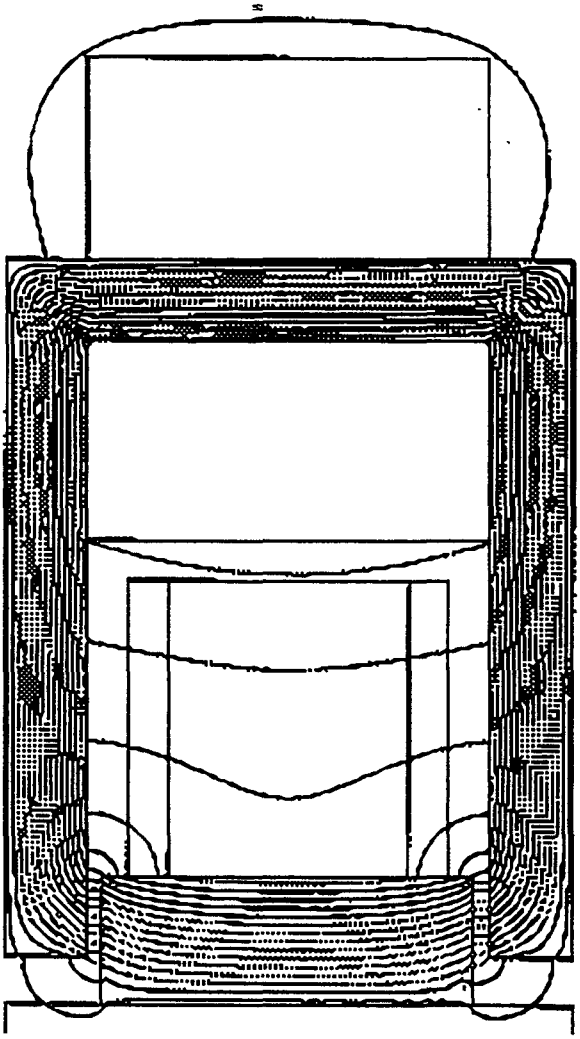

Figure 2: Calculated magnetic field lines.

4. PROTOTYPE CONSTRUCTION

The prototype rotor core was wound on large diameter shaft in the laboratory, see picture in figure 3 below. The shaft was connected to a dc-machine acting as a prime mover. In order to measure the voltage and the current in the rotating secondary winding, the rotor was equipped with slip rings.

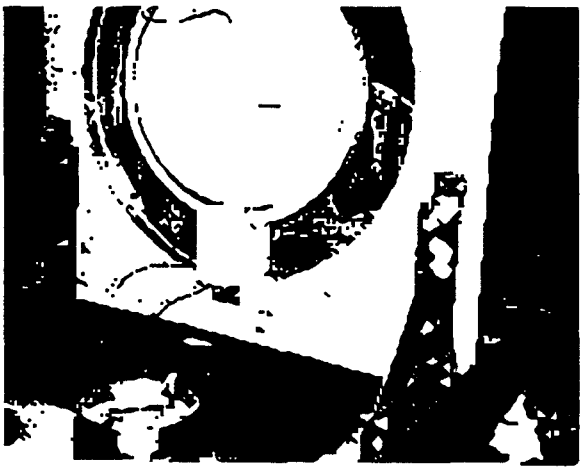

Figure 3: The prototype during construction.

5. MEASUREMENTS

With the prototype mounted on the dc-machine several measurements were done. Independent of the rotating speed, the voltage of the secondary winding is 21 V at 220 V supply on the primary stationary winding. This is lower than expected from the initial calculations, the design voltage was 24 V dc rectified. With the winding loaded, the voltage drops significantly due to the leakage. Especially the secondary leakage reactance is very high. The secondary voltage was increased by loading the secondary circuit with capacitors during some load tests. The capacitors can be chosen so that they compensate for the voltage drop over the leakage reactances.

5. MODIFIED DESIGN

In order to use the rotating transformer in a wind turbine, the design must be modified.

The rated power of the transformer is proportional to the air-gap area. The rated power can be increased by increasing the air-gap area by using multiple stator segment mounted on the rotor or using a larger part of the circumference. The rotor leakage reactance can be reduced by modifying the rotor magnetic circuit. This can be done in several ways, such as using other rotor core materials. Finally, the air-gap requirements is less in radial than axial directions due to different mechanical

tolerances. By modifying the magnetic circuit so that this is obtained, less magnetising current is needed.

7. CONCLUSIONS

The calculations and the tests on the prototype indicate that it is possible to design a rotating transformer, which can supply electric energy to rotating parts in a wind turbine. The operation of the transformer is independent of the speed of the turbine. The leakage reactances of the rotating transformer will however be high. By capacitor compensation the influences of the leakage reactances can be reduced.

An other drawback with the proposed design is the air-gap. Due to mechanical tolerances in the axial direction of the wind turbine, the air-gap must be large. With a large air-gap, the transformer needs a high magnetising current. If the air-gap can be reduced, the transformer performance will increase.

8. ACKNOWLEDGEMENTS

The financial support given by the Swedish National Board for Industrial and Technical Development is gratefully acknowledged.

REFERENCES

[1] Engström, S., "Roterande transformator för navhydarulik" (in Swedish), Specification, Nordic Wind Power, 1994-03-23.

[2] "Elkraftteknik" (in Swedish), Chalmers University of Technology, 1995.

[3] Lowther, D.A, Silvester, P.P., "Computer-Aided Design in Magnetics", Springer-Verlag, 1986.

[4] Hylander, J., "Roterande transformator för vindkraftverk", Report nr: R-95-03, Department of Electrical Machines and Power Electronics, Chalmers university of Technology, Göteborg, Sweden,(1995).

Appendix 15

Possibilities by Using a Self-Commutated Voltage Source Inverter Connected to a weak grid in Wind Parks

Jan Svensson

POSSIBILITIES BY USING A SELF-COMMUTATED VOLTAGE SOURCE INVERTER CONNECTED TO A WEAK GRID IN WIND PARKS

Jan Svensson M. Sc.

jan.svensson@elkraft.chalmers.se
Department of Electric Power Engineering
Chalmers University of Technology
S-412 96 Göteborg, Sweden

ABSTRACT: In this paper the hybrid wind farm connected to a weak grid is investigated. By combining different electrical wind power plant systems a cost-efficient solution is obtained. The point of common connection voltage level can be controlled by injecting reactive power from a phase-compensating capacitor battery and a voltage source inverter (VSI). If the short-circuit impedance ratio is lower than 1, the demanded reactive power injection to keep the voltage at nominal level is unrealistic. For short-circuit impedance ratios of 2 or higher the demanded reactive power level is acceptable. When using both induction generators and thyristor inverters the reactive power injector VSI size should be about 0.2 pu. If the hybrid farm consists of THYs, IGs and VSIs and the active power is equally shared between the systems, the VSI had to be scaled up by 5% to handle both active and reactive power.

Keywords: Electrical systems, Reactive power, Grid, Control.

1. INTRODUCTION

To successfully install wind turbines on a weak grid, a knowledge of the wind turbine impact on the grid is essential. The most common electrical system of commercial wind power plants is the induction generator (IG) directly connected to the grid. A major drawback is that the reactive power flow and thus the grid voltage level cannot be controlled. Another drawback associated with fixed speed system is that the blade rotation causes voltage fluctuations of a frequency of 1 to 2 Hz on the grid [1]. This fluctuation problem is not solved by using several turbines; on the contrary, if several identical wind turbines are installed in a wind park, the rotors can synchronize with each other and the power fluctuations are superimposed in phase [2].

With variable-speed wind turbines several advantages can be achieved compared to the directly connected IGs. Such as lower noise, increased average efficiency [3], reduced power fluctuation between the wind turbine and the grid and less dynamic stresses on the mechanical structure of the plant. However, the disadvantage is a higher cost of the electrical system [4].

Today the thyristor inverter (THY), also named grid-commutated inverters, is the cheapest solution to transmit the power into the grid. However, the grid voltage can still not be controlled since the power factor depends on the active power. If the grid is weak, voltage distortion will occur [5]. Another problem is injected current harmonics into the grid, which results in voltage distortion.

The self-commutated voltage source inverter (VSI) is a grid-friendly converter [6]. The harmonics injected into the grid are now of a much higher order and can much easier be filtered. The reactive power can now be chosen freely. However, some drawbacks are high cost, lower efficiency than with the THY and a limited maximum size of the inverter [4].

A conventional wind park connected to a weak grid can give rise to voltage variations. Today the solution is to build a stronger grid. To equip all the wind turbine electrical systems with VSI would also be a solution, but a rather expensive one.

In this paper a solution is proposed which combines the technical and economical advantages of different systems, the hybrid wind farm. The farm consists of wind turbines with constant speed using directly connected IG as well as variable-speed electrical systems. One of the variable-speed electrical systems has a VSI connected to the grid, the others have THYs. The VSI is used to reduce harmonic distortion and voltage variations. Important factors are the short-circuit ratio, SCR, and the ratio between the reactance and the resistance of the grid, SCIR (Short-Circuit Impedance Ratio).

2. THE SYSTEM CONFIGURATION

The hybrid wind park consists of wind turbines that have directly connected IGs, variable-speed electrical systems using THYs and one or a few VSIs. In Figure 1 the hybrid wind park configuration is shown. The variable-speed system uses synchronous generators (SG) and a diode rectifier to obtain high efficiency and low cost [4]. The grid strength is governed by the grid impedance consisting of a resistance R_N and an inductance L_N. The no-load grid rms-phase voltage is denoted E_N The grid at the farm, called point of common connection (PCC), has the rms-phase voltage E. The THY DC-link voltage yields u_{dc}. The VSI rms-phase voltage is denoted U.

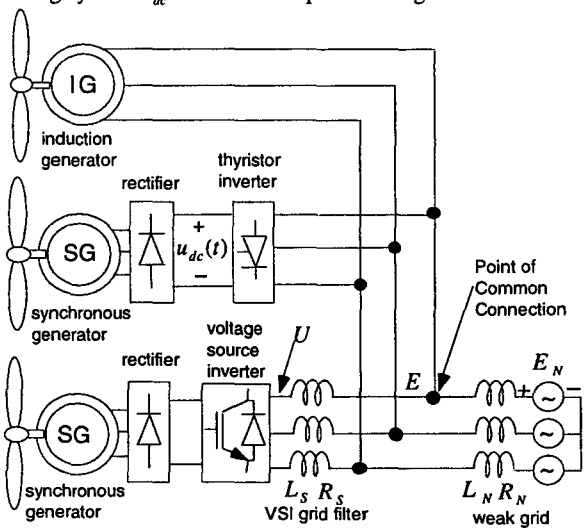

Figure 1: The hybrid wind park configuration.

For the variable-speed system with the THY, two DC-link voltage control strategies are investigated. Apart from using the conventional control strategy of constant flux (CF) in the SG a proposed strategy is investigated. The idea is how to get optimal efficiency (OPT) for the SG [7].

3. VOLTAGE VARIATIONS DUE TO WIND VARIATIONS

Since the reactive power injected by IG and THY into the grid cannot be controlled, the voltage level of the PCC will vary. The two different control methods of the THY will also affect the grid voltage differently. Figure 2 shows the reactive power as a function of the active power for the IG and the THY.

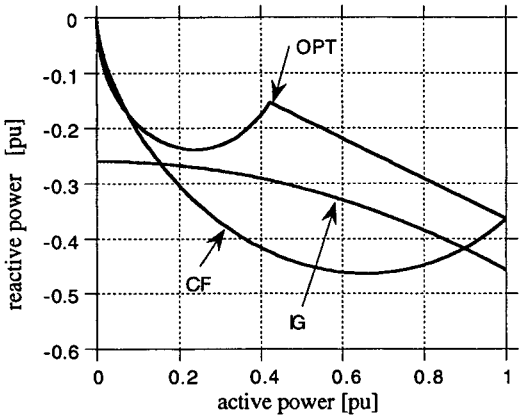

Figure 2: The reactive power as a function of the active power for the IG and the THY. The THY uses CF- and OPT-modes.

For a typical IG the reactive power varies from approximately –0.25 pu to -0.45 pu at rated active power. The reactive power of the THY goes from 0 to –0.38 pu when the advance angle is 20°. The CF-mode has the largest reactive power span, 0.45 pu. The reason for the different reactive power functions for the two types of THY controls is that the DC-link voltage is higher in the OPT-mode for median wind speeds. In Figure 3, the DC-link voltage and the resulting reactive power are plotted as a function of the wind speed.

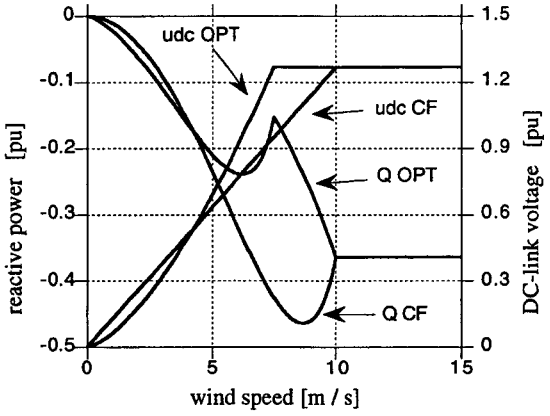

Figure 3: The THY DC-link voltage and the reactive power as a function of the wind speed and for the CF- and OPT-modes.

3.1. The voltage fluctuation

Here, the voltage fluctuation of the PCC with weak grid is analysed. In Figure 4 and Figure 5 the voltage fluctuation caused by the IG and the THY is presented for the SCR of 10. For a low short-circuit impedance angle (SCIA) the grid is mainly resistive and a high SCIA means that the grid is mainly inductive. As can be noted SCIA strongly governs the voltage level, especially at high active power levels. Low SCIA increases the voltage at PCC and for high SCIA the voltage at PCC decreases. The voltage fluctuation is minimized if the SCIA is about 40° to 60°.

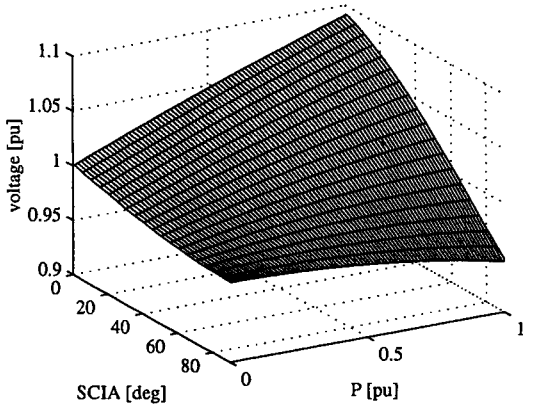

Figure 4: The PCC voltage level variation due to the SCIA and the active power from the IG. The SCR is 10.

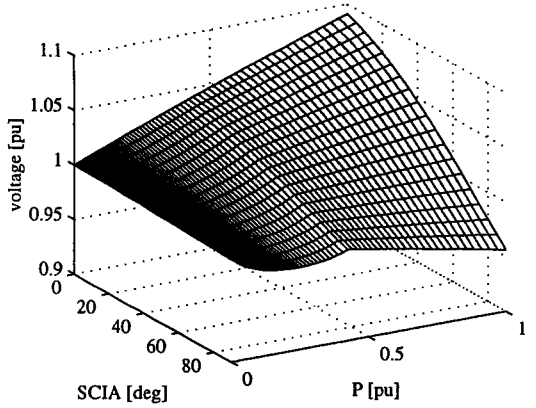

Figure 5: The PCC voltage level variation due to the SCIA and the active power from the THY. The SCR is 10 and the minimum advance angle is 20°.

4. VOLTAGE CONTROL OF THE GRID

The voltage level of the grid is used to control the reactive power injected to the grid. This can be done stepwise by a capacitor battery or continuously by controlling the reactive power from a VSI, shown in Figure 6. Usually one or two capacitor stages are used at wind turbines.

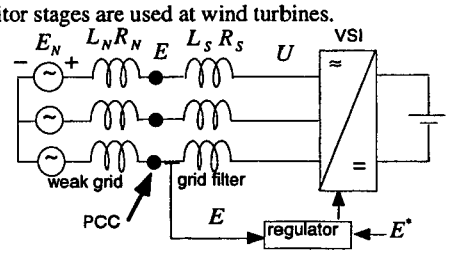

Figure 6: The method to control the voltage level of the grid.

5. REACTIVE POWER REQUIREMENTS

The reactive power, injected into the grid, needed to keep the PCC voltage at nominal level is investigated in this section. The SCR is 10 for every combination and the SCIR has the values of 0.5, 2.5, 10 and 20. The base power, 1pu of the wind farm is the total nominal active power of the wind farm. The seven variants investigated of the hybrid wind farm electrical system are presented in Table I.

Table I: The different electrical system formation in the hybrid wind farm.

Variant	Type of electrical system
A	VSI
B	IG + VSI reactive power injector
C	THY(CF) + VSI reactive power injector
D	THY(OPT) + VSI reactive power injector
E	IG+THY(CF) + VSI reactive power injector
F	IG+THY(OPT) + VSI reactive power injector
G	IG+THY(OPT)+VSI

To control the voltage at PCC all variants, A to G, have a capacitor battery, in some cases an inductor, which injects a constant value of reactive power to the grid. Furthermore, a VSI is used in every variant to actively control the voltage level at PCC by injecting reactive power. For the variants A and G the existing VSI is used. But, for the other variants, B to F, a VSI that only operates as a reactive power injector is used. In the G alternative, the VSI delivers one third of the total farm active power and also injects reactive power to the grid.

The capacitor battery is designed to deliver the mean demanded reactive power. The remaining part of the required reactive power is handled by the VSI. In this way, the VSI can be dimensioned as small as possible.

If the hybrid farm contains THYs, the capacitor battery can be designed as a tuned filter to remove harmonic currents from the grid.

The injected reactive power required for the different farm and grid configurations is shown in Figures 7 to 10. As shown, the reactive power demands changes substantially depending on the grid and the farm configuration. In some cases the demanded reactive power is inductive. The results are summarized in Table II for the different farm and grid constellations; the max and min reactive power; the size of reactive battery and the size of VSI are tabled. The VSI scale factor is also tabled, i.e. how much larger the VSI must be to handle both active and reactive power instead of only active power.

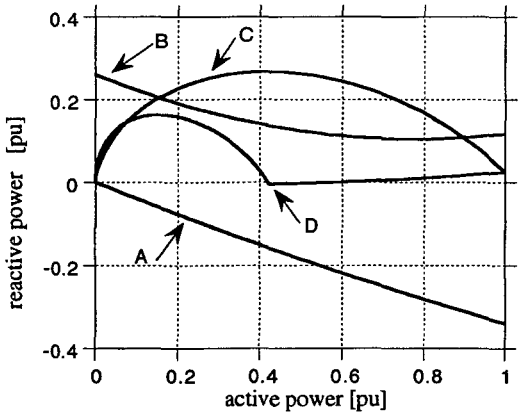

Figure 7: The injected reactive power required to maintain nominal PCC voltage. SCR is 10 and SCIR is 2.5. The electric system configurations are shown in Table I.

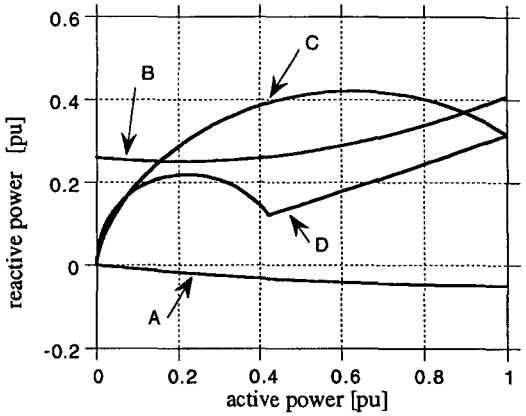

Figure 8: The injected reactive power required to maintain nominal PCC voltage. SCR is 10 and SCIR is 10. The electric system configurations are shown in Table I.

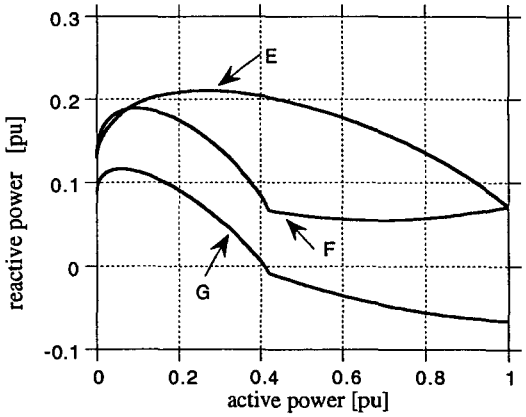

Figure 9: The injected reactive power required to maintain nominal PCC voltage. SCR is 10 and SCIR is 2.5. The electric system configurations are shown in Table I.

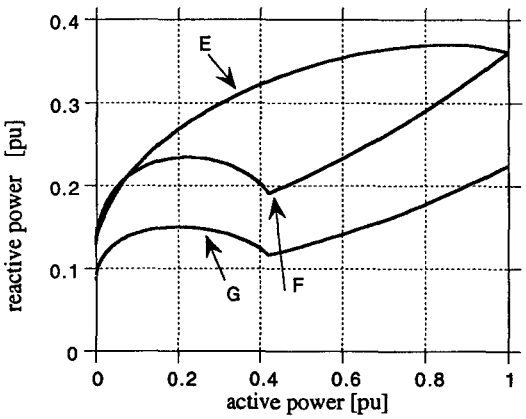

Figure 10: The injected reactive power required to maintain nominal PCC voltage. SCR is 10 and SCIR is 10. The electric system configurations are shown in Table I.

When the reactive power demand is almost constant due to active power variation, the size of the VSI can be minimized. For low values of SCIR, 0.5 and below, the required size of VSI becomes large and thus expensive. For these low SCIRs the cost of keeping a constant voltage will probably be unrealisticly high. However, the SCIR is usually high enough, at least for transmission lines with a capacity of 50 MVA or higher. The reactive power demand is approximately the same for SCIR of 10 and above. The SCIR of 10 to infinity is the same as SCIA of 84° to 90°. In Figures 4 and 5 the voltage variations at high SCIAs are almost the same. For the IG and VSI injector, variant B, and low SCIR, no capacitor battery should be used to compensate the IG reactive power if the PCC voltage level is to be controlled. Of course the grid current will increase, leading to increased transmission losses due to the increased reactive current.

When comparing the different modes of the THYs it is found that the CF-mode demands a larger VSI injector. Also the capacitor battery needs to be larger than that for the OPT-mode. But, when adding IG to the system, variants E and F, the two systems get the same characteristics, since, the reactive characteristics of the IG and the THY are smoothing each other.

The VSI injector size is maximum 0.21 pu when the VSI only is used as a reactive power injector for the hybrid farm and the SCR is 10 and the SCIA is 2.5 or higher.

When the hybrid farm consists of IG, THY, VSI and each subsystem takes one third of the active farm power, case G, the VSI only needs to increase about 5% to eliminate the voltage variation. The capacitor battery is approximately 0.10 pu.

If SCIR is larger than 2 it will be no problem to control the voltage at the PPC.

6. CONCLUSION

In this paper a hybrid wind farm connected to a weak grid has been investigated. It is shown that the voltage can be kept constant utilizing a VSI and properly sized capacitor battery providing that SCIR is higher than approximately 2. If SCIR is lower than 1, the reactive power needed to keep the voltage constant becomes unrealistically high.

The VSI injector size is maximum 0.21 pu when the VSI only is used as a reactive power injector for the hybrid farm and the SCR is 10 and the SCIA is 2.5 or higher.

The most advantageous configuration is the variant G, where the hybrid farm consists of IG, THY, VSI and each subsystem takes one third of the active farm power. The VSI only needs to increase about 5% to eliminate the voltage variation. The capacitor battery is approximately 0.10 pu.

Table II: The demanded reactive power to maintain the nominal voltage level at PCC.

Variants	SCIR 0.5	SCIR 2.5	SCIR 10	SCIR 20
A: MinQ [pu]	-1.98	-0.42	-0.050	-0.0125
MaxQ [pu]	0.66	0.12	0.035	0.0196
Q(C or L) [pu]	-0.66	-0.15	-0.007	0.0035
Q(VSI) [pu]	1.32	0.27	0.042	0.016
VSI scale	66%	3.6%	≈0%	≈0%
B: MinQ [pu]	-1.1439	0.1036	0.2498	0.2574
MaxQ [pu]	0.26	0.2598	0.4079	0.4576
Q(C or L) [pu]	-0.44	0.1817	0.3289	0.3575
Q(VSI) [pu]	0.70	0.0781	0.0790	0.1001
C: MinQ [pu]	-1.2374	0	0	0
MaxQ [pu]	0.0391	0.2670	0.4206	0.4529
Q(C or L) [pu]	-0.5991	0.1335	0.21	0.2264
Q(VSI) [pu]	0.6382	0.1335	0.21	0.2264
D: MinQ [pu]	-1.2374	-0.0042	0	0
MaxQ [pu]	0.0568	0.1632	0.3145	0.3642
Q(C or L) [pu]	-0.5903	0.0795	0.1572	0.1821
Q(VSI) [pu]	0.6471	0.0837	0.1572	0.1821
E: MinQ [pu]	-1.1906	0.0709	0.1299	0.1299
MaxQ [pu]	0.1353	0.2103	0.3698	0.4139
Q(C or L) [pu]	0.5277	0.1406	0.2498	0.2719
Q(VSI) [pu]	0.6630	0.0697	0.12	0.1420
F: MinQ [pu]	-1.1906	-0.0548	0.1299	0.1299
MaxQ [pu]	0.1446	0.1888	0.3612	0.4109
Q(C or L) [pu]	-0.5230	0.1218	0.2455	0.2704
Q(VSI) [pu]	0.6676	0.067	0.1157	0.1405
G: MinQ [pu]	-1.32	-0.066	0.0866	0.0866
MaxQ [pu]	0.0932	0.1159	0.2243	0.2739
Q(C or L) [pu]	-0.6172	0.0249	0.1554	0.1803
Q(VSI) [pu]	0.7104	0.0910	0.0688	0.0937
VSI scale	138%	3.6%	2.1%	3.9%

7. REFERENCES

[1] F. Santjer and G. Gerdes, "Netzrückwirkungen, verursacht durch den Betrieb von Windkraftanlagen am Netz," *DEWI Magazin*, pp. 35-41, August 1994.

[2] A. Stampa and F. Santjer, "Synchronisation von netzgekoppelten Windenergieanlagen in einem Windpark," *DEWI Magazin*, pp. 80-86, August 1995.

[3] A. Grauers, "Higher electrical effiency with variable speed," presented at ECWEC, pp. 656-658, Travemünde, March 1993.

[4] O. Carlson, A. Grauers, J. Svensson, and Å. Larsson, "A comparision between electrical systems for variable speed operation of wind turbines," presented at EWEC '94, pp. 500-505, Thessaloniki, Oktober 1994.

[5] K. Thorborg, *Power Electronics - in Theory and Practice*. Lund, Sweden: Studentlitteratur, 1993.

[6] J. Svensson, "Voltage Angle Control of a Voltage Source Inverter — Application to a Grid-Connected Wind Turbine," presented at EPE, pp. 539-544, Sevilla, Spain, September 1995.

[7] A. Grauers, "Synchronous generator and frequency converter in wind turbine applications: system design and efficiency," Chalmers University of Technology, School of Electrical and Computer Engineering, Göteborg, Sweden Technical Report No. 175L, May 1994.

Appendix 16

Torque Control of Synchronous and Induction Generators for Variable Speed Operation of Wind Turbines

Ola Carlson, Eskil Ulén

TORQUE CONTROL OF SYNCHRONOUS AND INDUCTION GENERATORS FOR VARIABLE SPEED OPERATION OF WIND TURBINES

O. Carlson and E. Ulén
Department of Electrical Power Engineering
Chalmers University of Technology
S-412 96 Göteborg, Sweden
Phone: +46 31-772 16 37, Fax: +46 31-772 16 33
E-mail: ola.carlson@elkraft.chalmers.se

ABSTRACT: The aim of this paper is to investigate variable speed electrical systems. Synchronous generators with diode rectifiers and line-commutated thyristor converters are compared with induction generators with force-commutated transistor converters and scalar control. The system characteristics are examined regarding possible speed of response (bandwidth) of the torque control, including the sensitivity to disturbances for the drive train and also the possibility to get damping of the drive train resonance. Analyses, simulations and laboratory tests with a 40 kW machine set-up have been performed. The investigation shows that the system with synchronous generator is well suited for wind power applications. A rapid standard DC-current regulator is included in the torque control and can be used for damping of the resonance. The torque control has a bandwidth up to about 3 Hz and the DC-volt controller up to about 1 Hz. The system with induction generator with scalar control (no transformations) is more difficult to control. A linear approach is only possible up to about 1.5 Hz. In this region it turns out that the behaviour can be visualized as an added inertia on the generator side that can be rather big.
Keywords: Converters, Control, Electricity Generators, Variable-Speed Operation.

1. INTRODUCTION

During the last decade researchers and wind turbine manufacturers have been working on electrical systems for variable speed wind turbines. The wellknown advantages of wind turbines with variable speed are reduction of noise, optimal C_p–λ operation, a well controlled torque in the drive train and thereby the possibility to damp resonance and avoid speeds causing resonance. For the wide speed range the synchronous as well as the induction generators with frequency converters are the most common systems. For prices and efficiencies of the systems see articles in [1,2,3]. The aim of this paper is to investigate the torque control of induction and synchronous generators for variable speed operation.

2. GENERATOR CONTROL AND DRIVE TRAIN BEHAVIOUR

2.1 Short drive train analysis

The drive train behaviour is very much influenced by the generator torque control. Figure 1 shows a scheme with three different inertias.

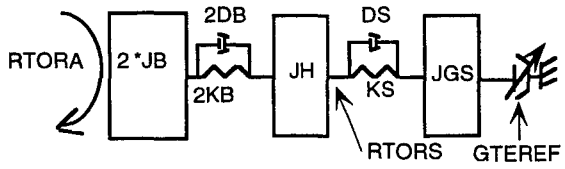

Figure 1: Model of the drive train.

The main goal is to get the control dependent only on the generator torque reference GTEREF and to get an acceptable damping of the resonances. Two resonances can be distinguished, in the following called blade resonance ωB (S mode) and drive train resonan ωG. For frequencies < the lowest resonance (stiff system) the following transfer functions can be calculated, if generator torque is supposed to be independent of speed

$$\frac{RTORS}{RTORA} = \frac{JGS}{jT + JGS} \cong \frac{JGS}{JT} \quad if \quad JGS << JT \qquad (1)$$

$$\frac{RTORS}{GTORE} = \frac{jT}{jT + JGS} \cong 1 \quad if \quad JGS << jT \qquad (2)$$

$$JGS = N^2 \cdot JG \qquad (3)$$

As JGS << 2JB + JH = JT a strong damping of disturbances from the aerodynamic torque is obtained.

Where: RTORS = Torque in shaft
RTORA = Aerodynamic torque
GTORE = Generator torque
JGS = Inertia of generator (turbine side)
JG = Inertia of generator

JT	=	Inertia of turbine	JH	=	Inertia of hub
JB	=	Inertia of blade	N	=	Gear ratio
DS	=	Damping of shaft	KS	=	Shaft spring
DB	=	Damping of blade	KB	=	Blade spring

For frequencies ≥ the lowest resonance JGS << JT, and if the blade resonance is considerably greater than the drive train resonance, they can approximately be treated separately and are as follows (Fig. 2).

$$\omega G = \sqrt{\frac{KS}{\frac{JGS \cdot JT}{JGS + JT}}} \cong \sqrt{\frac{KS}{JGS}} \qquad (4)$$

$$\omega B = \sqrt{\frac{KB}{\frac{JB \cdot JH}{2JB + JH}}} \qquad (5)$$

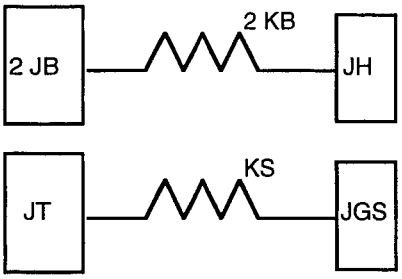

Figure 2: Drive train resonance ωG and blade resonance ωB.

The torque control could be used to damp the drive train resonance. It is difficult to damp the blade resonance However, as this frequency normally is considerably higher than the drive train resonance it will interfere very little with the drive train behaviour.

3. LABORATORY TEST EQUIPMENTS

Laboratory tests with a 40 kW machine set-up have been performed. The test arrangement consists of a dc-motor for aerodynamic torque, a flywheel for the simulation of turbine inertia and a soft shaft between the flywheel and the generator as a drive train. Both synchronous and induction generators with converters have been tested. For the experimental set-up the following picture could be used (Fig. 3).

Where: DCMC = DC- motor torque
GTORM = Mechanical torque
IDCREF = Reference of DC-current

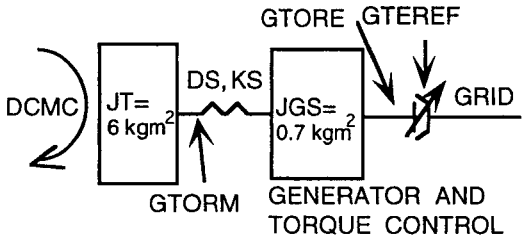

Figure 3: Scheme used for the experimental set-up.

4. SYNCHRONOUS GENERATOR

4.1 Analysis of synchronous generator

Figure 4 shows a simplified picture of the synchronous generator, diode rectifier and thyristor inverter.

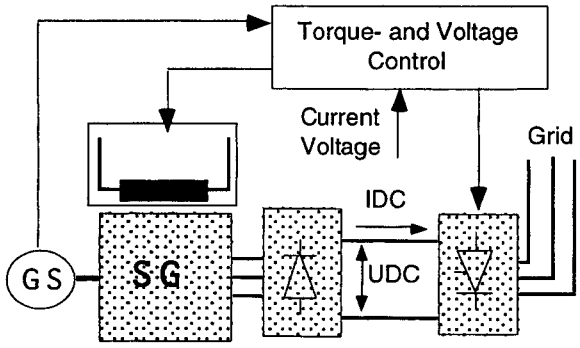

Figure 4: Generator and power electronics.

Two control systems are necessary. The field current is used to regulate the dc-voltage, UDC, and the dc-current, IDC, to regulate the electrical torque, GTORE. Different windings are used for these regulations and they are therefore only slightly dependent on each other. The electrical torque is also rather independent of the generator speed, GS.

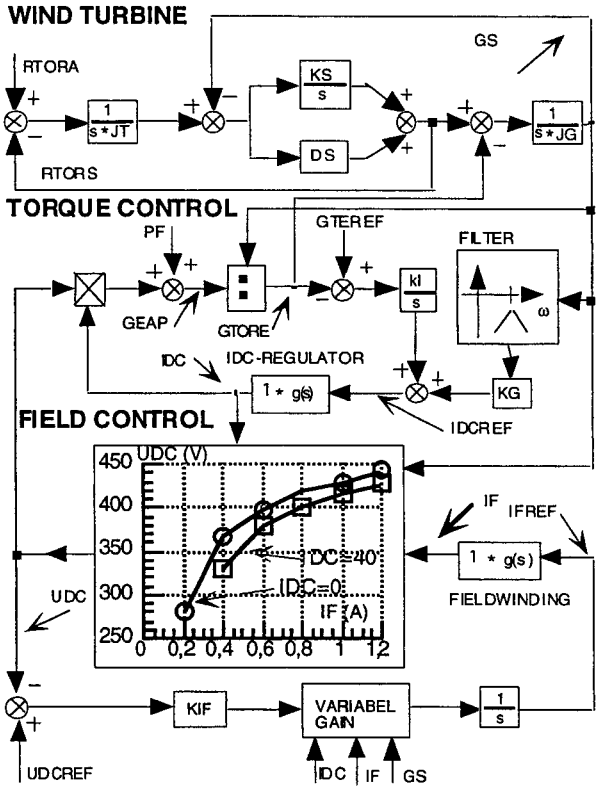

Figure 5: Control scheme for the synchronous generator with converter.

Figure 5 shows the complete control scheme. A machine model with parameters from the experimental set-up is also included in order to be able to make simulations to guide the laboratory tests and measurements.

In the torque control a standard IDC-regulator of the thyristor inverter is included. The transfer function was selected to be of second order with a time constant of 0.01 sec. In order to get a torque control, the following calculations are made:

$$GTORE = (IDC \cdot UDC + PF)/GS \qquad (6)$$

In the field control a transfer function from IFREF to IF was determined to be of second order with a time constant of 0.03 sec. and relative damping of 1. The function UDC = f(IF,IDC) at 1200 rpm has been measured (Fig. 5).

This function is very non-linear and it turns out that the gain ΔUDC/ΔIF varies between 50-1000 in the range. A variable gain depending on IF, IDC and GS has therefore been determined to compensate for this variation. Feed forward from GS to GTORE is included via a band-pass filter in order to get the damping of the resonance. The generator torque is supposed to be independent of generator speed.

4.2 Measurements on the synchronous generator

Figure 7 shows response from steps in DCMC, GTEREF and UDCREF. It can be seen that only about 12 % of DCMC disturbance reaches the drive train, and damping of the drive train resonance is obtained, compare figures 7b and 7c. The damping of the resonance frequency of 30 rad/sec leads to specific demands on the speed sensor and signal processing. The UDC-control works properly (Fig. 7d).

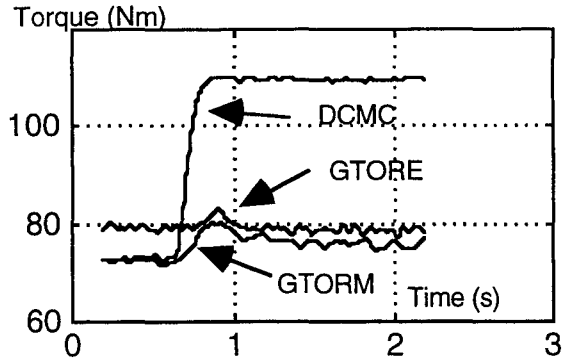

Figure 7a: Measurements of step response in DC-motor torque.

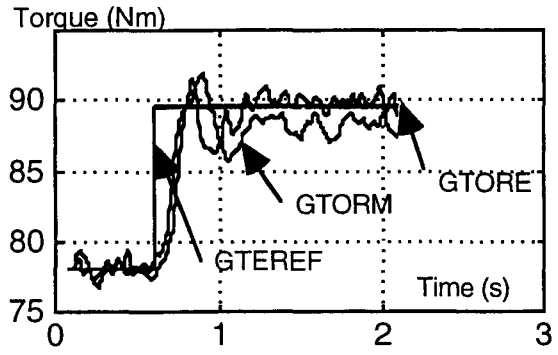

Figure 7b: Measurements of step response in generator torque reference, with damping in the control.

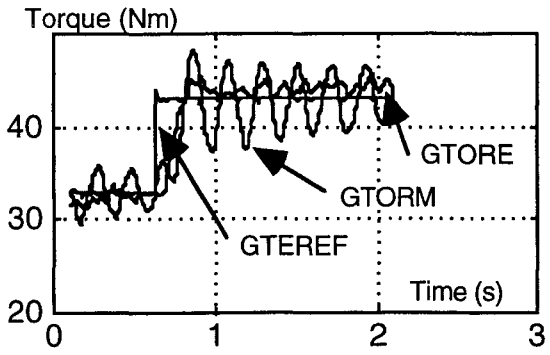

Figure 7c: Measurements of step response in generator torque reference, without damping in the control.

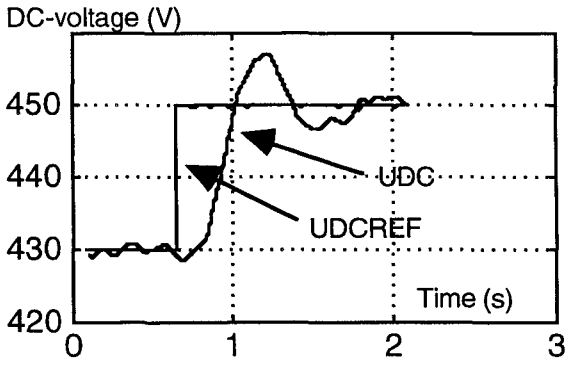

Figure 7d: Measurements of step response in DC-link voltage.

5. INDUCTION GENERATOR

5.1 Analysis of induction generator

In an induction generator torque and field are developed in the same windings and they are therefore dependent on each other. The torque is also very dependent on the speed because of the fact that max torque is developed by a speed change in the slip range (about 1 % of max speed). These facts will complicate variable speed applications [4]. Figure 8 shows a scheme for generator and torque control.

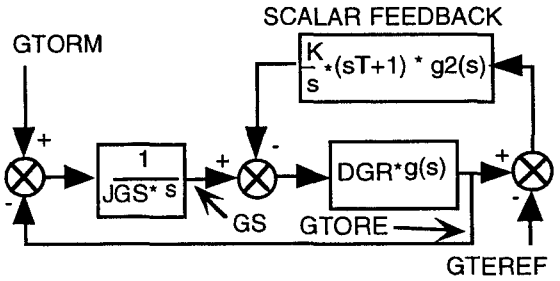

Figure 8: Scheme for generator and torque control.

In this report so called scalar control is used. This means that direct feedback without any transformations is used. This method is simple and only a crude knowledge of the model is used. However, limited performance is obtained. It turns out that a linear model shown in Figure 8 can in our case only be obtained for frequencies < 10 rad/s. For higher frequencies it is referred to the measurements. An integration is included in the feedback loop. For frequencies < the bandwidth (K*DGR) the following equation is valid.

$$\frac{GTORE}{GS} \cong \frac{s}{K} \cdot \frac{1}{s \cdot T + 1} \qquad (7)$$

This means that GTORE is dependent on generator acceleration. For low frequencies the control acts as an added inertia on the generator side equal to 1/K. This means that JG in (Eq. 3) should be replaced by JG+1/K. This will increase the sensibility to disturbances on the drive train. The slip slope DGR is usually very big because a small slip is wanted. Therefore, the value of K is very limited. The added inertia can therefore be rather large compared to generator inertia. For frequencies > 1/T there will be a proportional feedback that damps the drive train resonance. Feed forward of the generator acceleration can be used to get better performance. This acceleration can

be derived by differentiation of the generator speed. This will, however, be a very noisy signal so, a low pass-filter with a time constant of 0.25 seconds is needed. The negative gain in the feed forward loop, Ka, has the dimension of negative inertia. Another method is to get a higher gain at low frequencies by means of a so called lag/lead-filter.

5.2 Measurements of induction generators

Figure 9 shows an example of step responses and frequency diagrams. The value K=0.2 has been used, which gives an added inertia of 5 kgm^2. It can be seen in figure s9a and 9b that for frequencies<10 rad/s the turbine disturbances will be reduced to about 50 % on the drive train shaft. With an acceleration feed forward the disturbances will be even more reduced (Fig. 9c) for very low frequencies. The example with Ka=-6 means that also the generator inertia is compensated (motor action).

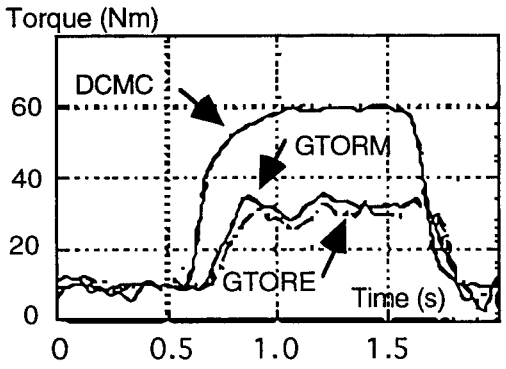

Figure 9a: Measurements of step response in the DC-motor torque with K=0.2.

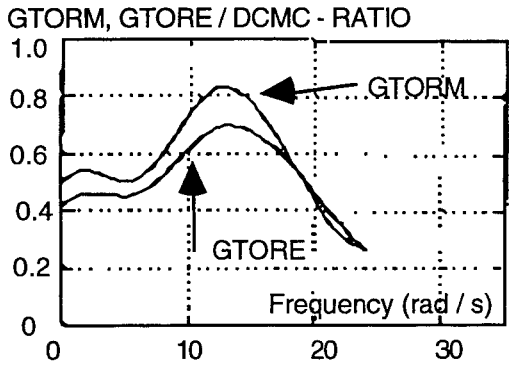

Figure 9b: Measurements of GTORM/DCMC and GTORE/DCMC - ratio with K=0.2.

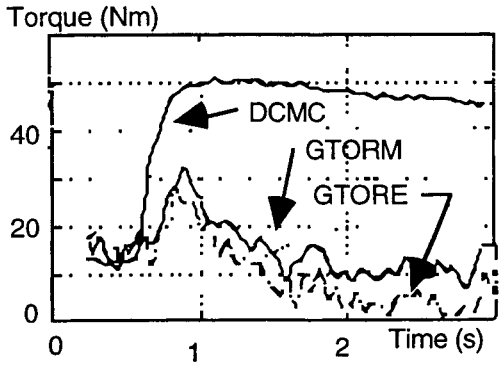

Figure 9c: Measurements of step response in the DC-motor torque with Ka=-6 and K=0.2.

6. CONCLUSION

The torque of a synchronous generator with separate magnetization depends very little on speed. Also the DC-current regulator that is included in the torque control can easily be very rapid. It can be used for the damping of rather high drive train resonances, in this case about 5Hz. Feed forward of the generator speed via a high-pass filter is used. Certain demands on speed sensor and signal processing must be fulfilled. The torque control has a bandwidth up to about 3 Hz. In the voltage control loop the gain is in a very non linear manner dependent on a field current and also on DC-current and speed. A three-dimensional linearization is therefore included in order to get acceptable gain. A bandwidth up to about 1 Hz is obtained. In wind turbine applications the turbine inertia is normally much bigger than the generator inertia. A significant damping of disturbances from the turbine to the drive train is therefore obtained. A synchronous generator with separate magnetization and a standard DC-current controller is therefore very attractive for wind power applications.

The induction generator torque depends in this study heavily on generator speed. Torque and field are developed in the same windings and are therefore very dependent on each other. With scalar control (no transformations) only limited performance is possible to obtain. A linear approach is possible only up to about 1.5 Hz. An integrator should be included in the feedback loop and the torque will therefore depend on the generator acceleration for low frequencies. That can be visualized by an added inertia on the generator side, that can be rather big. The damping of disturbances from the turbine will therefore be less. However, the damping of the drive train resonance is included in the control if a PI-regulator is used. For very low frequencies better performance can be obtained by means of acceleration feed forward (can be obtained by a filtered derivation of the generator speed) or higher gain at low frequencies in the feed back loop. The negative gain in the acceleration feed forward has the dimension of negative inertia and it is possible to compensate also for the generator inertia (motor action).

8. ACKNOWLEDGEMENT

The financial support given by the Swedish National Board for Industrial and Technical Development is gratefully acknowledged. The authors would like to thank Magnus Ellsén for his valuable laboratory work.

REFERENCES

[1] Carlson O., et al. "Survey of variable speed operation of wind turbines", EUWEC '96, Göteborg, Sweden, (1996).

[2] Grauers, A., "Synchronous generator and frequency converter in wind turbine applications: system design and efficiency", Technical report No. 175L, Chalmers University of Technology, Göteborg, Sweden,(1994).

[3] Carlson O., et al. "A comparison between electrical systems for variable speed operation of wind turbines", EWEC '94, Thessaloniki, Greece, (1994).

[4] Carlson O., et al. "Stall control with variable speed and an induction generator", ECWEC '93, Travemünde, Germany, (1993).

Appendix 17

Yaw Control for Active Damping of Structural Dynamics

Tommy Ekelund

YAW CONTROL FOR ACTIVE DAMPING OF STRUCTURAL DYNAMICS

Thommy Ekelund
Control Engineering Laboratory
Chalmers University of Technology
S-412 96 Göteborg
SWEDEN
Phone + 46 31 772 3717
Fax + 46 31 772 3730
E-mail te@control.chalmers.se

ABSTRACT: Yaw torque control for reduction of structural dynamic loads in a two-bladed wind turbine is investigated. The models are obtained using rigid-body mechanics. Linear quadratic control theory is utilized for design and analysis. The analysis of two simple examples, where the teeter angle and the tower lateral bending motion are regarded, shows that a time-varying controller has some advantages compared with a time-invariant controller.
Keywords: Yaw Control, Teeter, Lateral Bending, Two-bladed rotor.

1. INTRODUCTION

Most medium to large size wind turbines use a yaw servo to align the turbine with the wind. Typically the motor is activated when the misalignment exceeds a given threshold. Hence, the actuator does not operate continuously, but at discrete events. During these events it usually goes with constant speed. The nacelle is, however, locked to the tower most of the time.

An alternative strategy is to use the yaw servo continuously. Added compliance and the possibility to manipulate the structural dynamics to reduce loads are the main advantages with this concept. There are of course other means to make the yaw system compliant, passively, using mechanical devices for damping. The disadvantages with continuous yaw control are the need for measurement and possibly increased wear of the actuator. How efficiently the control system can decrease structural loads is related to the maximum torque and bandwidth of the yaw control servo.

The first part of this paper is general, and deals with modeling and controller design. Later, two design examples, where the controller is designed to decrease the teeter angle or the lateral tower load of a two-bladed wind mill, are given.

2. THE MODELS

Mathematical equations describing the interaction between different parts of a wind energy converter can be obtained from rigid-body mechanics. The most important external forces on the system are the aerodynamic forces on the blade and the actuator forces from generator, pitch and yaw motors. The blade forces depend on the speed and direction of the wind as experienced by the blade. This means that there is an inherent feedback mechanism from turbine motion to aerodynamic force, which of course is utilized when controlling the aerodynamic power.

Lagrangian mechanics is a convenient method to derive the equations of motion. In contrast to Newtonian mechanics, the constraint forces do not have to be considered. The details of these derivations are not presented here; the methods are given in any text book on the subject, see [2] or [5] for a wind turbine example.

The resulting equations are nonlinear and, in case of more than a few degrees of freedom, extremely complex. In a dense matrix form the equations of motion can be stated as

$$\mathbf{H}(\mathbf{q}(t))\ddot{\mathbf{q}}(t) + \mathbf{C}(\dot{\mathbf{q}}(t),\mathbf{q}(t))\dot{\mathbf{q}}(t) + \mathbf{B}\dot{\mathbf{q}}(t) + \mathbf{K}\mathbf{q}(t) + \mathbf{G}(\mathbf{q}(t)) = \mathbf{F}(\mathbf{q}(t),\mathbf{w}(t),\mathbf{u}(t))$$

where $\mathbf{q}(t)$ is a column vector with the generalized coordinates. The first term represents the forces of inertia, where the inertia matrix $\mathbf{H}$ is symmetric and positive definite. The other terms originate from, left to right, Coriolis plus centripetal forces, viscous damping, strain forces and gravity forces. The right hand side contains all control $\mathbf{u}(t)$ and aerodynamic forces that depend on the wind speed $\mathbf{w}(t)$.

A state realization of the system can be obtained by choosing the state vector as $\mathbf{x}(t) = \begin{bmatrix}\dot{\mathbf{q}}(t) & \mathbf{q}(t)\end{bmatrix}^T$. General methods for controller design are based on linear models. Therefore the nonlinear equations are linearized. If the rotor speed is assumed constant, the resulting system becomes periodically time-varying.

$$\mathbf{M}(t)\ddot{\mathbf{x}}(t) + \mathbf{C}(t)\dot{\mathbf{x}}(t) + \mathbf{K}(t)\mathbf{x}(t) = \mathbf{G}(t)\mathbf{u}(t) + \mathbf{n}(t)$$

The mass $\mathbf{M}$, damping $\mathbf{C}$, stiffness $\mathbf{K}$ and input $\mathbf{G}$ matrices should not be confused with the matrices in the nonlinear equations. The last term $\mathbf{n}(t)$ represents the disturbance from the wind speed. The state realization of the linearized system are

$$\dot{\mathbf{x}}(t) = \begin{bmatrix} -\mathbf{M}(t)^{-1}\mathbf{C}(t) & -\mathbf{M}(t)^{-1}\mathbf{K}(t) \\ \mathbf{I} & \mathbf{0} \end{bmatrix}\mathbf{x}(t) + \begin{bmatrix} \mathbf{M}(t)^{-1}\mathbf{G}(t) \\ \mathbf{0} \end{bmatrix}\mathbf{u}(t) + \mathbf{M}(t)^{-1}\mathbf{n}(t)$$

The so called Floquet method deals with the stability of this type of systems. This and other methods for

analysis of wind turbine stability are given in [4]. In this study the linear equations have been discretized, assuming time-invariance between the sample instants. The sampling frequency is chosen to one percent of the rotor frequency, or 3.6° in angular domain. The reason for the last step is to facilitate numerical calculation of control law and simulation. It is also straightforward to transform a discrete periodic system into a discrete time-invariant system. This can be done by increasing the state vector to include a full period, which in our case means increasing the model order a factor 100. Below a wind power plant with four degrees of freedom has been simulated, nonlinear and continuous versus linear and discrete. It illustrates how well the discrete model describes the original nonlinear.

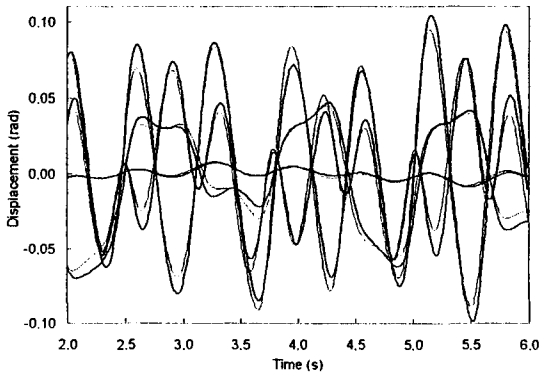

Figure 1: The generalized coordinates of a fourth order model simulated with nonlinear and continuous (thick) versus linear and discrete (thin) model. The computational time differs a factor 1200.

3. CONTROLLER DESIGN

Linear quadratic (LQ) control methods [1] are used for design and analysis. These methods can deal with time varying systems. The control signal, yaw torque, is calculated as $\mathbf{u}(t) = -\mathbf{L}(t)\mathbf{x}(t)$, where the control law $\mathbf{L}(t)$ is a row vector of same length as the state vector. The control law is derived to minimize a scalar criterion that is quadratic in the state variables

$$V(\mathbf{L}) = E\left\{\mathbf{x}(t)^T \mathbf{Q}_1 \mathbf{x}(t) + \mathbf{u}(t)^T \mathbf{Q}_2 \mathbf{u}(t)\right\}$$

The cost matrices $\mathbf{Q}_1$ and $\mathbf{Q}_2$ are chosen to penalize deviation from the operating point and control effort respectively. How to chose the cost parameters is not always obvious from logical reasoning, especially if the model order is high. The control law that minimizes the discrete version of the criterion is derived from the solution to a discrete Riccati equation, which is a nonlinear matrix difference equation. The stationary periodic solution is calculated numerically. Hence, an analytic expression of the control law is not obtained.

An LQ-controller uses feedback from all state variables. Nevertheless, measurement of all state variables is usually not required. The state vector can be estimated, with for example a Kalman filter, from measurement of a subset of the state variables. This part of the design procedure is not carried through here. An important question in that context is which variables to measure. For instance it would be advisable to measure rotor position and make the control law dependent on this rather than absolute time; it is rotor position, rather than time itself, that is relevant for the feedback gain. In an implementation it is most likely better to sample with respect to angle instead of time. Another alternative is to use the rotor position as scheduling parameter in a time-invariant nonlinear controller. Here the LQ control theory is used as an instrument to gain insight on how to control the process, rather than deriving a fully operational controller.

For comparison an alternative, more conventional solution, is studied. It is a PD controller with feedback of the yaw angle and angular velocity. The controller has the transfer function, from yaw angle to yaw torque, $G_{PD}(s) = K(K_D s + 1)$. This of course equivalent to PI controller if the yaw angular velocity is taken as input. Here it is referred to as a passive concept, since it is dynamically similar to a mechanical suspension system. Note that is obvious that the result with this solution never can compare to the result with the LQ-controller, since it is constant and only uses yaw motion in the feedback.

4. TWO DESIGN EXAMPLES

The yaw torque affects, more or less, every structural mode, since all modes are dynamically coupled. The interactions with many of these loads are however too weak to be exploited for load reduction in a feedback loop. Here two simple examples, where the coupling to the yaw motion is apparent, illustrate the benefits of using a time-varying controller.

4.1 A teetered hub

This example is based on a rigid-body model of a two-bladed turbine with two degrees of freedom: the teeter and yaw angles. The rationale for having a teetered hub is to reduce hub loads originating from the wind gradient; the external load results in teeter motion instead of internal loads [3]. Nevertheless, there may be an interest in keeping the teeter motion under control; there have been failures as a result of too excessive teeter motion, where the blade bumped into the tower.

There are two main physical causes for the teeter angle being affected by the input. The first is the inertia of the rotor with respect to the teeter axis. This coupling is strongest when the rotor is horizontal, and vanishes in vertical position. The second cause is the gyroscopic torque, following from the rotation of the turbine being orthogonal to the applied yaw torque. The resulting gyroscopic torque is horizontal and perpendicular to the drive shaft. Consequently the interaction is strongest when the turbine is vertical. Then the teeter shaft is aligned with the gyroscopic torque. Note that the second phenomenon demands turbine rotation in contrast to the first.

A control law, where yaw and teeter motion are given the same cost in the LQ-criterion, has been derived. Figure 2 shows how the four elements of the control law vary during one revolution. Note the difference between the periods of the yaw and teeter feedback. The first is used by the controller to decrease the yaw motion. Since most terms in the yaw dynamics are periodic with 180°

turbine rotation, due to symmetry, so is the feedback. Likewise the teeter feedback is designed to reduce the teeter angle. These dynamic relations, and therefore also the feedback gain, are periodic with a full turn, due to the anti-symmetry of the rotor orientation after 180°. (The new orientation is equivalent to changing sign on the teeter angle.) The anti-symmetry also leads to a gain that changes sign with a period of 180°, whereas the yaw feedback is strictly positive. This shows that a time-invariant feedback of the teeter angle is ineffective teeter damping.

From the control law it can also be seen that the teeter angle gain is largest when the turbine is close to vertical, which occurs at 0° and 180°. This indicates that the gyroscopic torque is the dominating interaction of the two previously discussed.

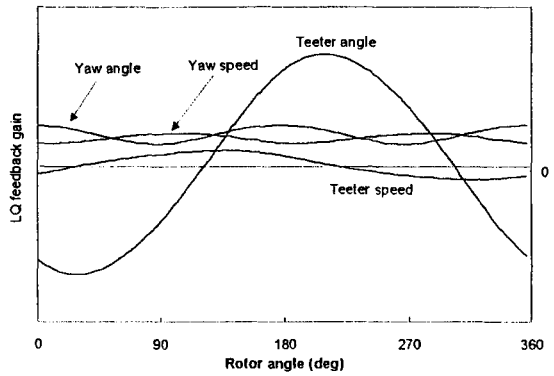

Figure 2: Control law gain, for the four states, during on revolution.

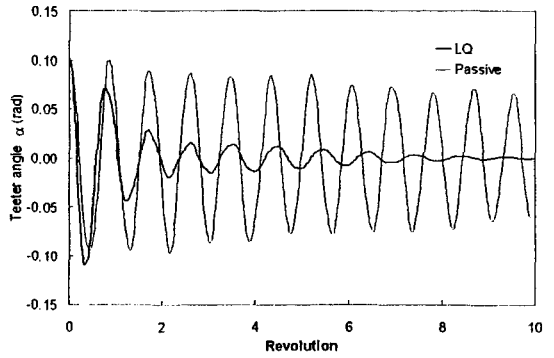

Figure 3: Teeter motion is reduced with the periodic LQ-controller.

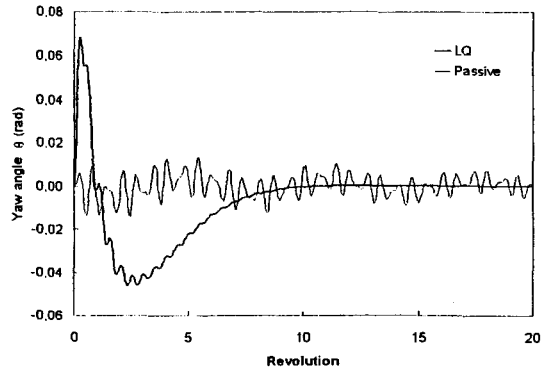

Figure 4: The yaw angle has a larger transient, but decreases faster with LQ control.

The simulations of an impulse response, (initial value of 0.1 radians for the teeter angle), show that the periodic LQ-controller increases the relative damping. In these simulations the external excitation has been left out. The control torque and the yaw angle experience a larger transient with the LQ-feedback, but the envelope decreases far more quickly.

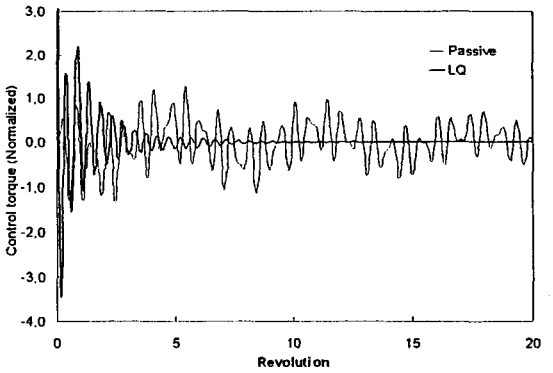

Figure 5: The torque envelope decreases more quickly with LQ-cont.

4.2 Lateral bending

This example also uses a fourth order model, but with the tower lateral bending and yaw angle as degrees of freedom. The interaction between these modes is due to the fact that the center of gravity, of the nacelle together with the turbine, is not placed on the yaw axis. This interaction is sometimes referred to as "fish tail" movement.

As in the previous example, the LQ-control law is derived with the same cost on both angles. In this case the control law elements all follow the same pattern; they are periodic with 180° and the maximum gain occurs when the rotor is approximately horizontal, (90° and 270°). The period being one half rotation follows from the symmetry of the two-bladed rotor. The locations of the maxima are a consequence of the inertia of the rotor, with respect to the yaw axis, being largest when it is horizontal; increased inertia means larger coupling between the two modes.

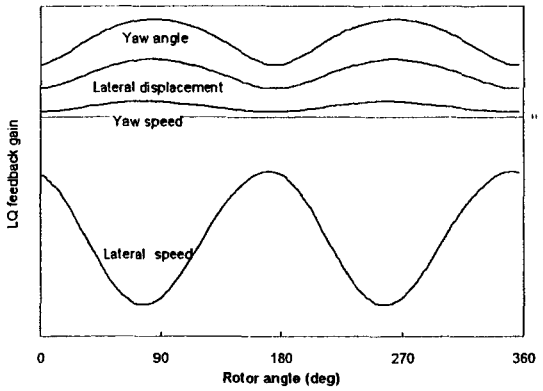

Figure 6: Control law gain, for the four states, during on revolution.

The periodic LQ-controller thus is more efficient than a time-invariant controller, since it uses the opportunities, when the inertia is large, to get as much as possible out of the control signal. However, in contrast to the teeter example, the feedback gains do not change sign. This indicates that a time-invariant controller could be

used. It should, for example, be reasonable to use the mean gain in a control law in case of state feedback.

The amplitude of the optimal gain, is a function of the inertia of the rotor: zero inertia makes the system, and hence the control law, constant. Therefore one can conclude that the benefit from a periodic control law in this case is directly related to the inertia of the turbine.

The simulations once again show that the periodic LQ-controller provides additional damping to the system. Also, as before, the yaw torque and its angle have larger transients but decrease faster than the passive, PD-controlled, system.

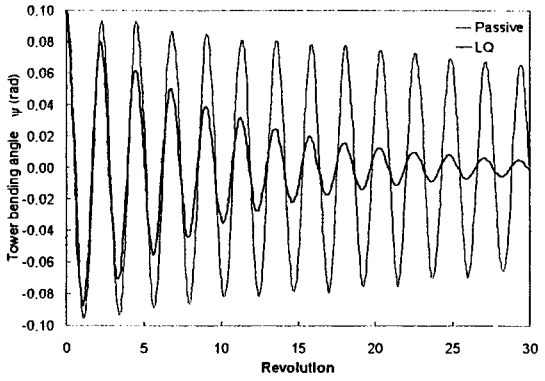

Figure 7: Tower motion is reduced with the periodic LQ-controller.

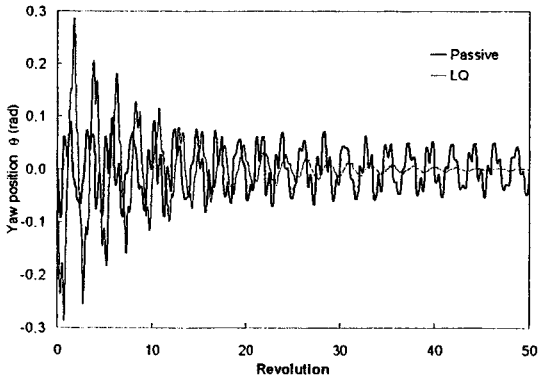

Figure 8: The yaw angle has a larger transient, but decrease faster with LQ control.

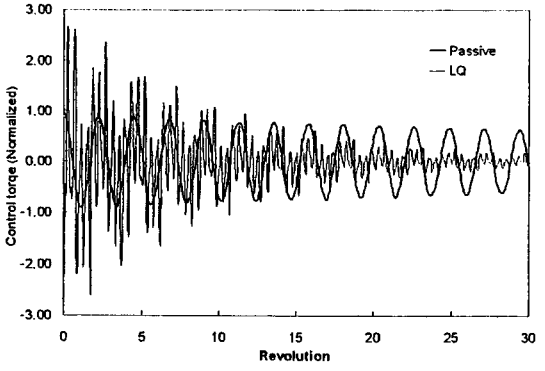

Figure 9: The torque envelope decreases more quickly with LQ-contr.

5. CONCLUSIONS

This theoretical study of yaw control for reduction of structural loads, in a two-bladed wind turbine, shows that a periodically time varying control law can give increased structural damping. The periodically time-varying controller can also be viewed as a nonlinear controller where the rotational angle of the turbine is used as scheduling parameter. When controlling the teeter angle, it was shown that the rotor position had to be considered. In control of the "fish tail" motion it is beneficial to take the rotor position into account, especially in case of a rotor with large inertia. This motion can however be reduced with conventional time-invariant control, which has been shown in practice [6].

The physical parameters of the examples have been chosen quite freely, to make the analysis clear and simple. In future work they should be more realistic. The importance of different parameter values and cost parameters should also be investigated. This is however a complicated problem due to the large number of parameters. Another important issue that has not been addressed is the influence of disturbances.

Linear quadratic optimal control theory has been used mainly as a convenient and powerful tool for analysis of two simple examples. The implementation of a controller of this type requires a state observer. When designing the observer, the choice of measured variables must be done. The design of an optimal controller can, however, be done independently from the design of the state observer, according to the separation theorem [1].

In an implementation it is not likely that the yaw torque can be controlled directly, hence the actuator dynamics need to be modeled and considered in the controller design.

REFERENCES

[1] Anderson, B.D.O. and J.B. Moore (1989). "Optimal Control, Linear quadratic methods". Prentice Hall, USA ISBN 0-13-638651-2.

[2] Meirovitch Leonard (1989), "Dynamics and Control of Structures", John Wiley & sons, USA, ISBN 0-471-62858-1.

[3] Freris L.L. ed. (1990), "Wind Energy Conversion Systems", Prentice Hall International (UK) Ltd, ISBN 0-13-960527-4.

[4] Dugundji J. and J.H. Wendell (1983), "Some Analysis Methods for Rotating Systems with Periodic Coefficients", American Inst. of Aeronautics and Astronautics Journal, Vol. 21, No 6, pp 890-97.

[5] Garrad A.D. and D.C. Quarton (1986), "Symbolic Computing as a Tool in Wind Turbine Dynamics", Journal of Sound and Vibration, Vol 109(1), pp 65-78.

[6] Ulén Eskil (1993), "Wind Tunnel Tests of a Ø 5.35 m Yaw Controlled Turbine", The Aeronautical Research Institute of Sweden, Report no: FFA TN 1993-20.

Appendix 18

Improving Acceptance in Wind Power Planning

Karin Hammarlund

IMPROVING ACCEPTANCE IN WIND POWER PLANNING

Karin Hammarlund
Department of Social and Economic Geography
University of Lund
Sölvegatan 13
S-223 62 Lund
Sweden

ABSTRACT: This paper presents important factors and planning procedures for public acceptance of wind power. Opinion surveys in Sweden show that acceptance is connected to the concept of utility rather than the aesthetic values. If wind turbines are confined by the authorities to marginal areas, they will not earn their rightful place in the landscape by being of use. A positive attitude in general promotes a positive experience of the effects of wind turbines. It is therefor essential to establish a sense of cooperation between the project management and the public. An open dialogue and continuous information will increase the possibilities for acceptance of future development. We must establish new codes of practice in permit processing because policies today contains ideological and practical contradictions between development and preservation of landscapes.

Keywords: public perceptions/ acceptability, planning, codes of practice, permit processing.

1. INTRODUCTION

This work aims at creating a good understanding of the prime factors involved in relation to public acceptance of wind power and establish what procedures are suitable for creating mental space and public acceptance for/of wind energy production.

A very complex scenario reveales itself under the denomination "social aspects". The number of alternatives offered in an energy system are connected to how we organize our societies and strive to increase the quality of our lives. Thus, when studing the acceptance patterns concering wind energy, we must illuminate what conditions makes it possible for people to accept wind power in their immediate surroundings. Further, wind energy seem to be of prime interest when it comes to the authorities ambitions of attuned development. Hence, public acceptance has since the introduction of windenergy in Sweden been an important discussion in permit processing. In general people seem to have a positive attitude towards wind energy, being a clean source of energy. However, problems with public acceptance might arise at the site of location. Opinion surveys in Sweden (1,2,3,4), show that acceptance is connected to the concept of utility rather than the estetic values resting within a specific geographical setting.

Competing land use interests along with cultural, environmental and recreational values enhanced by authorities in the permit procedures, might confine wind turbines to marginal areas. These areas will not comply with the wind conditions necessary to maximize the utility appraisment of wind power.

Wind power locations must apply to the swedish legislation on environmental protection, nature conservation and natural resources. The inventories of natural and cultural values in the swedish landscapes show that very few optimal sites are available for wind turbines. Hence, Sweden like other European countries have reached a situation where we must *create* space for the production of wind energy. I will argue that it is mostly a matter of communication and information in order to creat mental space in the minds of people and authorities.

2. OPINION OF WIND POWER

2.1 The NIMBY-syndrome

When reviewing the results from different surveys of attitudes after location (table I), it is evident that the experienced effects on the landscape are closely related to the personal attitude toward wind energy in general. This conclusion seem to stand in some opposition to the existens of a NIMBY-syndrome (not in my back-yard).

The NIMBY-syndrome has been studied concerning the location of nuclear power plants, waste disposal plants and off-shore oil extraction (5,6,7). To conclude the experiece of a NIMBY-syndrome in connection to wind power locations it can be said that: People seem to have a positive attitude towards wind power in general, but negative reactions and opposition occur when a wind farm location is planned in the near by environment.

However, a positive attitude in general toward wind energy promotes a positive experience of the effects of wind power after location. Hence, if the public persist in their positive opinon of wind power throughout the planning and construction phase, you have the prerequisite of positive establishment of wind power.

2.2 Information

The negative recations towards wind turbines could more truly be depicted by the words fear or misgivings. Hence, the correct planning and treatment of these misgivings decide the outcome of a project. In this context "timing" is of prime importance. Throughout the planning process of a wind power construction it is essential to inform the public. Preferably through a continuous dialogue which makes it possible to treat questions as they arise.

Examples of important information:

- the purpose of the project
- general description of the project in comprehensible terms
- timetable
- what qualities this source of energy has in comparison to other energy sources
- what advantages are directly observable

- how advantages and disadvantages can be evaluated in an environmental impact study (EIS).

2.3 Integration

It is not impossible to actively integrate the public opinion and preferences in the planning process and in the evaluation of the project. Such integration might reveal simple solutions to otherwise amplified problems. The possibility to influence the process of change in ones own neighbourhood might be of greater importance than the adjustment of the project to anticipated aesthetical preferenses.
Recommendations for aesthetic adjustment to the superior characteristics of a specific site do however constitute the inital position for wind power planning.

3. OPINION SURVEYS

3.1 Aim, sites and questions

The common aim of the performed opinion surveys has been to present the publics attitudes and experiences from each site, Tabel I and II.

Table I: Facts about opinion surveys

region/year	participants	method
a)Skåne1988	63	questionnaire
b)Blekinge 1990	95	questionnaire
c)Sweden 1992 (wind turbine owners)	30	interview
b)Blekinge 1993	50	interview
d)Bohuslän 1995	50	interview

Table II: Some facts about the wind turbines, letters refer to opinion surveys tabel I.

site/installed	output	supplier
a)Vallby/1988	150kW	Vindsyssel
b)Nogersund/1990	220kW	Vestas
d)Lysekil/1992	400kW	Nordic
d)Lysekil/1992	450kW	Bonus

The questions of each survey has been focused on the following aspects of wind power siting:

- visual impact
- disturbance/problems
- experiences of noise
- information
- discussions
- changes in attitude
- general experiences
- future development.

3.2 General results

Inspite of fears and hesitations among the concerned public during the introduction phase of each wind power project, the vast majority had a positive disposition.

By comparing ones conceptions of wind power in general with experiences of an operating wind turbine, most fears and hesitations turn in to curiosity. This curiosity gets triggered by the wind turbine itself. And in those cases where continuous information has been provided by the operators the curiosity among the public has been reinforced. The prerequisite of this positive development is ofcourse that the turbine is in operation as much as possible.

In this context it has been obvious that after location the public is more concerned about production statistics than the visual impact. One reason for this is that the turbine must be of some use in order to earn its rightful place in the neighbourhood. Hence, all discussions about experienced disturbance and visual impact must be interpreted with a strong connection to the utility. On a direct question about how ones attitude toward a wind turbine would change if it was possible to make private use of the produced energy, most persons would say "it's a different matter". This answer indicates the ability to accept changes that are directly experienced as being for the better. What could be better than renewable and clean wind power production for ones own household?

3.3 Noise and disturbance

No disturbance was experienced on flora, fauna or television signals at either site. Noise disturbance was reported from a few summer residents in the opinion survey in Bohuslän 1995. No link was established between the reported disturbance and living distance from the site. Surrounding rocks and cliffs may play a part in how the noise is experienced at this particular site. However, there is a connection to be observed between reported disturbance and a negative attitude in general.

It is evident that people can detect the sound from a wind turbine at long distance, but the reactions and experience of this sound vary greatly. Some people argue that it is most of the time impossible to distinguish the turbine sound from the sound of the wind. However, if the preconceptions of the sound are connected to alot of hesitations and misgivings, it is possible that the irritation threshold is set at a very low level. This situation indicates the importance of stressing concepts like "the sound from a wind turbine" as opposed to "the noise from a turbine" in the information to and discussions with the public.

Further, it is important to integrate the results from opinion surveys with noise measurements in order to grasp the true situation (8). In this context it is possible to argue that set noise standards are unusable since the personal disposition have a strong effect on our experiences of the sound from a wind turbine.

3.4 Changes in attitudes

Only one two-stage survey has been carried out, Blekinge 1990 and 1993. In this study a majority was very concerned about potential impacts prior to the construction. Opinions had altered significantly in 1993. Opinion surveys in Greatbritain (9,10,11) show the same result:

- despite worries about turbine noise and visual appearance prior to the construction of a wind turbine or wind farm, most local people are in favour after construction
- attitudes tends to become more positive once people have experienced operational turbines or farms. Many people feel that the environmental benefits in a wider context outweigh any perceived disadvantages at a specific site.

The swedish surveys indicate that if the public feels that it is possible to influence the development of ones surroundnings the willingness to accept changes improves. Hence, if people hold a negative attitude towards a wind power project it is possible to change this through an open dialogue. The dialogue should continue through all stages of the project either by way of written information or meetings. This is also a way to ensure that the most concerned public receives rapid and correct information. If this process works well, and the operator manages to bring about a sense of cooperation around the project, the result will be more than *just* acceptance, it will be engagement. This engagement might prove essential to further development of a site.

4. FUTURE DEVELOPMENT

4.1 How we value the landscape

Looking at the permit processing of wind power in Sweden, it is obvious that there are problems with assessment of impacts on the landscape. In a certain context wind power development might be seen as an important step towards a sustainable development of the landscape, with its physical and cultural values. In another context wind power might be seen as a threat to vacation environments and leisure activities, as well as to a magnificent view.

In Sweden the southern coastal areas are the most suitable for wind energy production on land. These areas experience intense land use competition and at the same time they are of great natural and cultural value. The most valuable areas have been classified as being of national interest. The classification device for such areas are comprehensive inventories and *evaluations*.

The aim for the continued swedish wind power planning is to give wind power priority in certain areas (12). The criterion for this priority could be based on technical, functional, environmental and social *points of view*. As is obvious in this context the future of wind power development lays in the right evaluations and points of view.

It is possible that swedish wind power might never obtain enough land in order to constitute a true complement in our energy system. The reason for this might be that we are not trained to look at the landscape as a totality of resources and *values*. It is easy to communicate about issues in words, figures and pictures, but to convert these symbols into wide ranging real and purposeful actions in the landscape is a quite different matter. The management of our landscapes has to do with the understanding of how abstract knowledge can be turned in to action on the ground (13).

4.2 Legislation and planning

"To imagine that legislation which is enforced from a certain date also controls events from that date is simply a convenient juridical fiction". (Torsten Hägerstrand, A look at the political geography of environmental management. 1986, p. 2).

Policy concerning the use of a landscape contains ideological and practical contradictions between development and preservation. Landscapes created by past forms of environmental use, or lack of use, will cease to exist if they are preserved from human contact (14).

Management plans demarcating national interests immediately turn obsolete as incalculable numbers of small actions pile up to major changes in space over time.The major formal ways by which the state can express its will in order to directly influence the behavior of the local actor involves legislation, taxation, subsidies, economic policy, information campaigns, but their ability to influence development is always uncertain. There is always a world of quite unforeseen reactions. Some laws might be impossible to obey because of the nature of real world situations. Hence, to be able to judge the effects and side effects of management operations we need the perspectives of the concerned actors (13).

4.3 Environmental impact assessment (EIA)

To some people an EIA seems out of place in a wind power context, since the effects of a wind turbine are marginal in comparison to other forms of energy production. However, an EIA might be the instrument most suitable for an integration of the technical, economic, environmental and social aspects of a wind power project.

The EIA should be made at a early stage of the project, as it is intended to be both a workning method for environmental considerations during planning and design, and the basis for decision making. This is an instrument which puts considerable emphasis on establishing an early contact with authorities and the public in order to up date and complement management plans (12).

It will be of great importance to investigate and develop the methods for environmental impact assessment including the social impacts of wind power locations.

4.4 Time geography

Time-geography constitutes a foundation for a general geographical perspective. Applying such a perspective on wind energy development in Europe the main task

will become to structure those mechanisms responsible for how individuals, authorities and governments structure the number of alternatives available in an energy system. The number of alternatives offered are connected to how we choose to organize our existence and strive to increase the quality of our lives. In this context it becomes essential to study the relationships responsible for making some choices possible and others impossible.

Research on time geography has shown that the individual at a certain point in time can handle only a limitied amount of alternative options and possible actions. When a choice has been made and yet a nother step in time has been taken, new options occur (15,16). By applying the time-geographic approach the primary aim will be to establish what mechanisms control the possible options of choice and acceptance.

So far, using the time geographic approach in analyses of the results from opinion surveys has revealed new connections. The fact that the physical space available for new development decreases as each new project occupy a certain amount of space does not strictly apply in a wind power context. The amount of options increases after the location of a wind turbine, due to the fact that most fears and hesitations among the public turn in to curiosity. Hence, after the correct choice of location and planning procedures, which makes it possible for the public to experiences wind power in a positive manner, new options for development occur.

Time geography can help us to structure those mechanisms which make certain choices possible and others impossible. Factors of great importance in this context are:

- the personal attitude
- available technology
- resources in the nearby environment
- the choice of other individuals
- the actions of authorities and organisations.

5. CONCLUSIONS

Working with a wind power project it is essential to have an understanding of the prime factors involved in 'planning for public acceptance'. Negative reactions towards a planned site has to do with misgivings and the fear of not being able to influence the development of ones own neighbourhood. By making sure that the most concerned public receives rapid an correct information through a continuous and open dialogue, there will be a sense of cooperation around the project. This cooperation might prove more important to future development, than adjustment of the project to anticipated aesthetical preferences.

Once the wind turbine/s are in operation it is possible for the public to compare preconceptions with direct experience. Most of the time experience will turn hesitations in to curiosity, and by providing production data this curiosity will be reinforced. Opinion surveys show that the public is more concerned about production figures after location than the visual impact. Hence, there is a concern that the turbine/s should earn their rightful place in the landscape by being of use. "It is easier to accept the sound of a turbine if I know it is producing for me"

By giving priority to other land use interests and by treating wind power as a threat to cultural, recreational and environmental values, authorities will confine wind turbines to marginal areas where they can be of little use. The future ability to look at the landscape as a totality in need of sustainable, renewable energy in order to survive will enrich the evaluations involved in permit processing. In this context it is important to understand that policies today already contains ideological and practical contradictions between development and preservation. Wind power might prove to be the least contradictory development of our landscapes.

REFERENCES

(1) K. Hammarlund, Vindkraft i Vallby. Institutionen för Kulturgeografi och ekonomisk geografi, Lunds Universitet (1988)

(2) K. Hammarlund, Havsbaserad Vindkraft i Nogersund. Karlshamnsverkets Kraftgrupp/Sydkraft (1990)

(3) K. Hammarlund , Varför satsar man på mindre och medelstor vindkraft i Sverige? Intervjuundersökning kring privata satsningar på mindre och medelstor vindkraft. KVAB (1992)

(4) K. Hammarlund, Havsbaserad Vindkraft i Nogersund. Karlshamnsverkets Kraftgrupp/Sydkraft (1993)

(5) K.R. Porteny, Allaying the NIMBY syndrome: potential for compensation in hazardous waste treatment facility siting. Haz Waste 1.(1984)

(6) M. O'Hare, "Not on My block you don't": facility siting and the strategic importance of compensation. Public Policy 25.(1977)

(7) G. Marks, D. von Winterfeldt, "Not in My Back Yard": Influences of motivational concerns on judgments about risky technology. J. of Appl. Psych. 69.(1984)

(8) J. N. Pinder, M. A. Price, Measurement of noise and assessment of likely disturbance due to noise from a 20 kW windturbine generator at Milton Keynes. University Southampton (1988)

(9) E. Esslemont, Cemmaes Windfarm. Sociological impact study: Final Report ETSU W/13/00300/REP (1994)

(10) B. Young, Attitudes towards wind power A survey of opinion in Cornwall and Devon. ETSU/W/13/00354/038/REP 1993.

(11) K. Bishop, A. Proctor, Love them or loathe them? Public attitudes towards wind farms in Wales. Report of research commisioned

by BBC Wales (1994)
(12) G. Grusell, E. Setzman, Common approach on how to get permission to put up wind turbines in European countries" (JOU2-CT92-0059) (1993)
(13) T. Hägerstrand, A look at the political geography of environmental management. Lund University (1993)
(14) K. Olwig, Nature's ideological landscape, the London research series in geography 5 (1984)
(15) T. Hägerstrand, Time-geography: focus on the corporeality of man, society and environment. The science and praxis of complexity. The United Nations University (1985)
(16) N. Thrift, An introduction to time-geography. no 13. Publ by Geo Abstracts Ltd Universty of East Anglia (1977)

Appendix 19

Comparison of Power Performance and Noise between Aeolus II and Näsudden II

A. Albers, C. Hinsch, J. Gabriel, H. Klug, G. Ronsten, B. Simonsson.

POSTER AWARD

On the occasion of the 1996 European Union Wind Energy Conference and Exhibition
20-24 May 1996, Göteborg, Sweden, the poster:

Comparison of Noise and Power Performance between Aeolus II and Näsudden II

by A. Albers, C. Hinsch, J. Gabriel, H. Klug, G. Ronsten and B. Simonsson

has been selected by the official jury as the winner of the

Poster Award

for the topic Aerodynamics, Wakes, Noise, Material and Fatigue

This outstanding scientific poster was deemed to be a particularly valuable contribution to this International Conference on Wind Energy.

The Conference Chairman

Prof. A. Zervos

The Poster Jury Chairman

S.-E. Thor

COMPARISON OF POWER PERFORMANCE AND NOISE BETWEEN AEOLUS II AND NÄSUDDEN II

A. Albers; C. Hinsch, J. Gabriel, H Klug
Deutsches-Windenergie-Institut (DEWI)
Ebertstr. 96,
D-26524 Wilhelmshaven

G. Ronsten
Flygtekniska Försöksanstalten (FFA)
P.O. Box 1102,
S-161 11 Bromma

B. Simonssen
KM Akustikbyrån
P.O. Box 7124,
S-171 07 Solna

ABSTRACT: The German Wind Energy Institute DEWI and the Aeronautical Research Institute of Sweden FFA perform comparing measurements at the 3 MW sister turbines Aeolus II and Näsudden II in the framework of WEGA II (CAN-Project). Results exist concerning the comparison of power performance and noise emission. Load measurements have been carried out but no comparing results are available yet. In the case of the Aeolus II interesting effects of different meteorological conditions on the power performance have been found. The project will continue till the end of 1996.
KEYWORDS: Performance, Meteorology, Noise, Operating Experience

1. INTRODUCTION

In 1993 two large wind energy converters Aeolus II and Näsudden II, each with a rated power of 3 MW, were erected in Wilhelmshaven, Germany and on the Island of Gotland, Sweden. The turbines incorporate almost identical geometric and aerodynamic features but different concepts for control strategy: At the Aeolus II a variable rotor speed concept is applied, while the Näsudden II has two fixed rotor speeds. The importance of these turbines for the further development of MW-scale WEC's is underlined by the fact that both WEC's, contrary to many other turbines of this size, have shown promising operational statistics since their installation. In the framework of WEGA II, DEWI and FFA are carrying out a comparison of the turbines, which includes measurements of power performance, noise emission and loads.
The tendency towards larger WEC's leads to an increasing interest in the relation between meteorological conditions and the power performance of these WEC's. The rotor of a MW-scale WEC covers a height range of about 50-100 m in which strong vertical wind speed gradients can occur. Therefore, the relations between the power performance of the Aeolus II and vertical wind shear, turbulence intensity and atmospheric stability have been investigated by DEWI.

2. DESCRIPTION OF THE WEC'S

The basic technical data of the Aeolus II and Näsudden II as well as the wind regime at both sites are illustrated in Table I. Both turbines have the same rotor geometry but different control strategies and towers. A new tower was designed for the Aeolus II, whereas the nacelle of the Näsudden II was put on the existing tower of its predecessor Näsudden I. However, because wind measurements are influenced by wake effects of nearby WEC's as well as mast effects, the values shown in Table I are only indicative for both sites.

Table I: Technical data of the turbines under investigation and wind statistics measured in 1994 and 1995. Measuring height 92 m (Aeolus II), 75 m (Näsudden II).

feature	Aeolus II	Näsudden II
manufacturer	MBB	Kvaerner Turbin
rotor orientation	upwind	upwind
number of blades	2	2
rotor diameter	80.5 m	80.5 m
hub height	92 m	78 m
rated power	3 MW	3 MW
generator	synchronous	asynchronous
rotor speed	variable, 14-21 min^{-1}	two fixed speed 14, 21 min^{-1}
power control	full span pitch	full span pitch
wind speed	8.0 m/s	7.9 m/s
wind potential	532 W/m^2	558 W/m^2
air density	1.236 kg/m^3	1.251 kg/m^3
mean wind direction	Southwest	Southwest
turbulence intensity	8 %	7 %

3. OPERATIONAL STATISTICS

The annual energy production of both turbines is given in Fig. 1. The larger energy output of the Näsudden II in 1994 and 1995 corresponds to the better wind potential. Due to the fact that the availability's of both turbines were below 100 %, the annual energy production in the years with complete measurements (1994, 1995) were lower than the theoretical energy output calculated from the measured power curves and the average wind speeds at the locations (Fig. 5). Furthermore, the measured wind speeds may not be fully representative for the conditions at the Aeolus II and Näsudden II: The investigated turbines and the wind speed measurements are influenced by the wakes of the surrounding WEC's and mast effects during different wind directions.

According to Fig. 2 and Fig. 3, the Aeolus II and Näsudden II have shown a high availability compared with other prototypes of this size. However, due to gearbox problems, the Aeolus II is since March 96 in its first longer period of breakdown. The gearbox is supposed to be repaired in June 96.

4. POWER PERFORMANCE

4 COMPARISON OF POWER PERFORMANCE

Generally the main uncertainty component in the determination of the power performance is the wind speed measurement. Even the uncertainties in the power curve measurement due to different procedures of anemometer calibration can be larger than the real differences in the power performance of the compared wind turbines [1], [2]. To eliminate these uncertainties, the anemometers used for the Näsudden measurements were recalibrated at DEWI and vice versa. In addition, the anemometers were calibrated at NLR[1] for verification. Further uncertainties in wind speed measurements result from:

- flow distortion of the massive masts,
- boom effects: the anemometers are mounted on booms, which influence the air flow at the anemometer. This is especially a problem at Näsudden because the distance between the mounting boom and the anemometer is relatively short.
- the large distance of about 850 m between the Aeolus II and the mast (correlation problems).

There are indications that these effects seriously influence the evaluated power curves. From this experience follows the recommendation to perform wind measurements for power curve determinations only on top of masts as suggested in the IEC standard [3]. If the wind speed is measured at different height levels covering the rotor, the anemometers should be mounted in a long enough distance from the mast and the mounting booms.

The power curves and C_p-curves of the Aeolus II and Näsudden II were evaluated according to the IEA [4] and IEC [3] recommendations and are compared in Fig. 4. The power curves are rather close with the differences within the uncertainties of the measurements. The shown high C_p-value of the Näsudden II at wind speeds below 5 m/s is due to an offset of the applied anemometer and does not reflect the real behaviour of the turbine. In the wind speed range of about 6-10 m/s the C_p-curve of the Näsudden II has a relative minimum in contrast to a smooth curve of the Aeolus II; the latter is achieved by adjusting the rotor speed to the wind speed. The relatively low cut out wind speed of about 20 m/s was chosen for safety reasons because of the design of the mechanical breaks.
From the power curve the annual energy production (AEP) was calculated according to the IEA recommendations [4] (Fig. 5). As expected from the power curves the calculated AEP's are almost equal.

5. INFLUENCE OF DIFFERENT METEOROLOGICAL CONDITIONS ON THE POWER PERFORMANCE OF THE AEOLUS II

5.1 Influence of Turbulence

The recorded data at the Aeolus II was classified according to the turbulence intensity. For each turbulence class a power curve was evaluated (Fig. 6) resulting in different calculated AEP's (Fig. 7).
When evaluating a power curve the measured power and wind speed is averaged over a period of usually 10 minutes. Because of the wind speed fluctuations and the non linearity of the power curve this time averaging process leads to an increase of the evaluated power curve where the power curve is concave and to an decrease of the evaluated power curve where the power curve is convex. This effect is evident from Fig. 6 and Fig. 8 and will grow with increasing turbulence intensity.

5.2 Influence of Vertical Wind Shear

From the wind speed measurements at the heights 32 m, 62 m, 92 m and 126 m a wind gradient weighted with its contribution to the rotor disk area was calculated and served as classification criteria for the recorded data at the Aeolus II. For each class of wind gradients a power curve and resulting AEP was calculated (Fig. 9).
Obviously for the applied wind speed distribution an increase of wind gradient leads to an increase of the AEP. This effect can be generally understood from the observations concerning the influence of turbulence intensity on the power performance discussed before: high wind gradients correspond to high spatial variations of wind speed over the rotor height. The spatial averaging effect of the rotor together with the nearly cubic increase of the power with wind speed result in a higher annual energy production similar to the effect of high turbulence.

5.3 Influence of Atmospheric Stratification

At the Aeolus II information about the actual atmospheric stability is derived from measurements of the vertical temperature gradient, i. e. temperature measured at 90 m and 2.5 m. A positive difference of the so called potential temperature $d\theta=\theta(90.0m)-\theta(2.5m)$ corresponds to a stable layer [5]. A potential temperature difference around 0 K indicates a neutral layer and a negative $d\theta$ correspond to an unstable layer. For each class of $d\theta$ a power curve was evaluated. The resulting AEP's have the tendency to decrease with increasing stability (Fig. 10).
The atmospheric stability strongly influences the turbulence intensity and the vertical wind gradient (Fig 11). Unstable conditions correspond to higher turbulence levels and relative low wind gradients, while lower turbulence and high wind gradients usually occur

[1] National Aerospace Laboratory - the Netherlands

during stable conditions. Because the turbulence as well as the vertical wind gradient effect the power performance, the observed dependence of the power curve on the stratification can probably be interpreted as an interference of both influences.

6. NOISE EMISSION

DEWI determined the noise emission of the Aeolus II and the Näsudden II for various wind conditions according to the IEA recommendations [6] by synchronous measurements of the electric power and the emitted noise. The wind speed at hub height was determined from the power curve and transferred to the wind speed at 10 m height by using a reference profile with a roughness length of 0.05 m. From Fig. 12 the correspondence of the emitted sound power level and the rotor speed is evident: For wind speeds lower than 6 m/s (at 10 m height) the Aeolus II is operated with a larger rotor speed than the Näsudden II and hence emits more acoustic noise. In the transition region of the Näsudden II, in which the Näsudden is operated either with a higher or lower rotor speed than the Aeolus II, the sound power level of the Aeolus II is between the values of the Näsudden II. Finally above the transition region the rotor speed as well as the sound power level of the Aeolus II remain slightly below the corresponding values of the Näsudden II.

7 CONCLUSIONS

Both, the Aeolus II and the Näsudden II have shown a high availability in their first years of operation compared with other prototype WEC's of similar size. The difference in power performance of both turbines is small and lies within the uncertainty of the measurements. For future power curve evaluations the wind speed ought to be measured preferably at the top of the mast or at a sufficiently large distance to the mast and mounting booms.

A significant influence of the atmospheric stability, vertical wind shear and the turbulence intensity on the power performance of the Aeolus II was found. The influence of such effects on the predicted AEP is in the range of 4 % and should be reflected in the recommendations for power curve measurements of (large) WEC's.

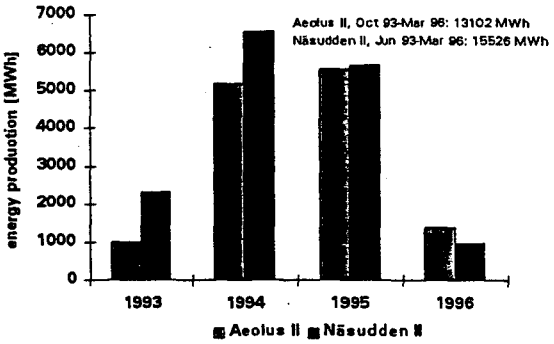

Figure 1: Annual energy production (energy to grid).

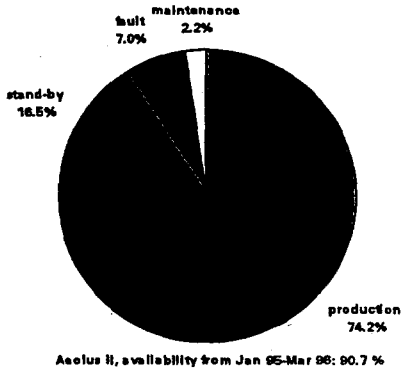

Figure 2: Operation modes of the Aeolus II from January 1995 till March 1996.

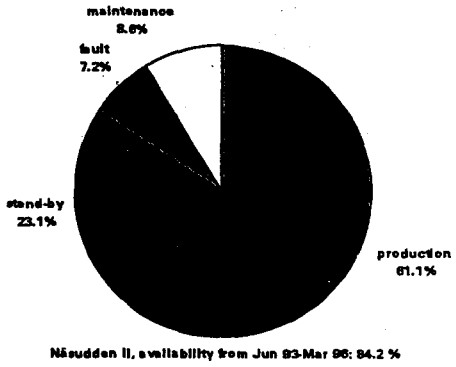

Figure 3: Operation modes of the Näsudden II from June 1993 till March 1996.

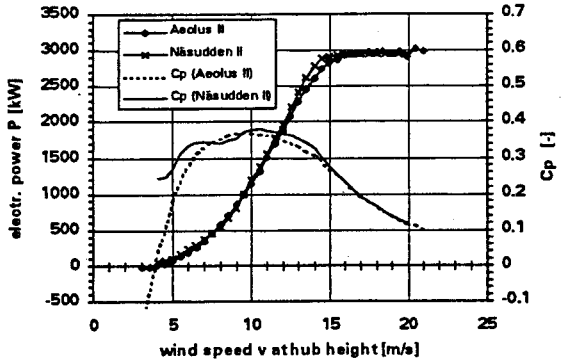

Figure 4: Comparison of power curves and C_P-curves based on the period October 93 till March 96 for the Aeolus II and January 94 till December 95 for the Näsudden II.

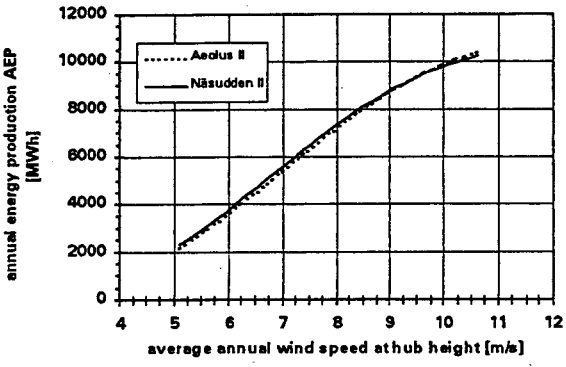

Figure 5: Calculated annual energy production as function of average annual wind speed (at hub height, turbine availability = 100 %). Wind speed distribution: Rayleigh.

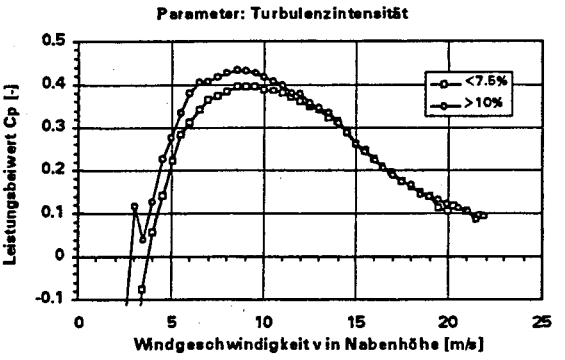

Figure 6: C_P-curves of the Aeolus II for different turbulence intensities[2].

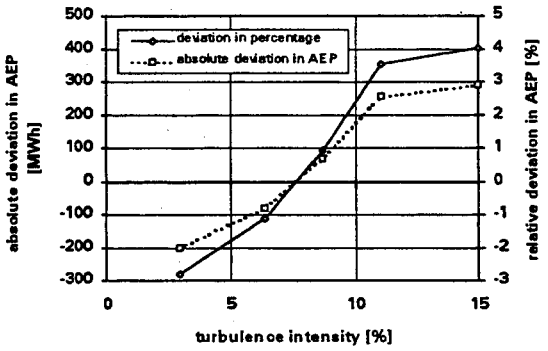

Figure 7: Deviations of calculated AEP's of the Aeolus II for different turbulence intensities from average value. Base: measured Weibull distribution at hub height of the Aeolus II.

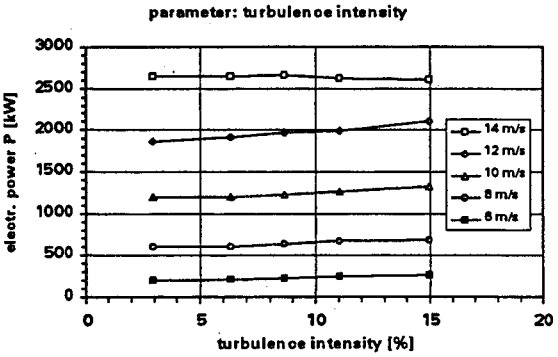

Figure 8: Electrical power of the Aeolus II as function of turbulence intensity for different wind speeds.

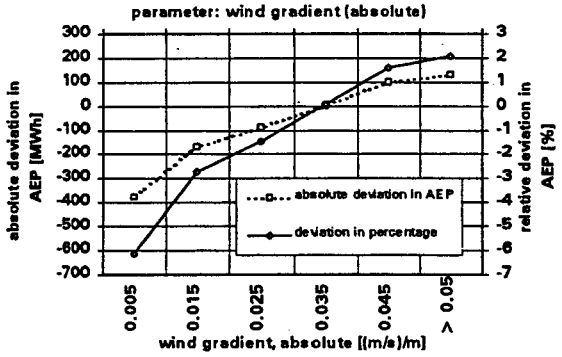

Figure 9: Deviations of calculated AEP's of the Aeolus II for different vertical wind gradients from average value. Base: Weibull distribution at hub height of the Aeolus II.

[2] The shown C_P-values are higher than in Fig. 4 because another anemometer calibration was used for the investigation of meteorological effects.

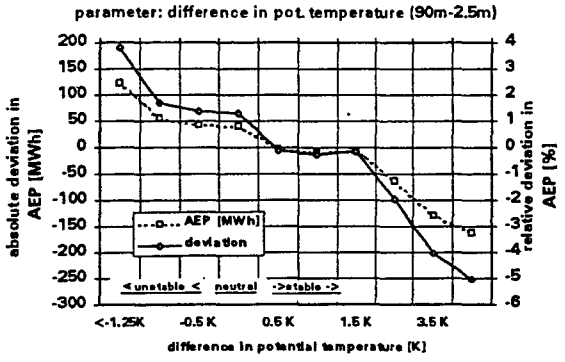

Figure 10: Deviations of calculated AEP's of the Aeolus II for different atmospheric stability from average value. Base: Weibull distribution at hub height of the Aeolus II.

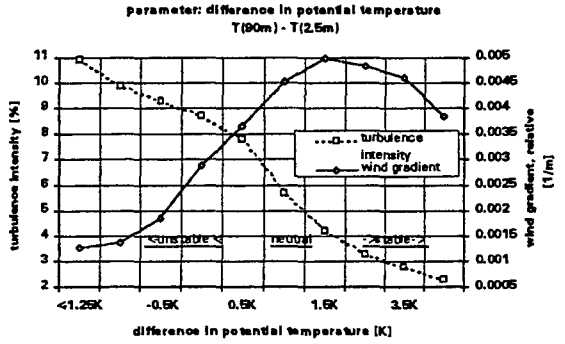

Figure 11: Turbulence intensity and wind gradient versus difference in potential temperature. Plotted is the relative vertical wind speed gradient, i. e. the wind speed gradient normalised by the average wind speed over the height.

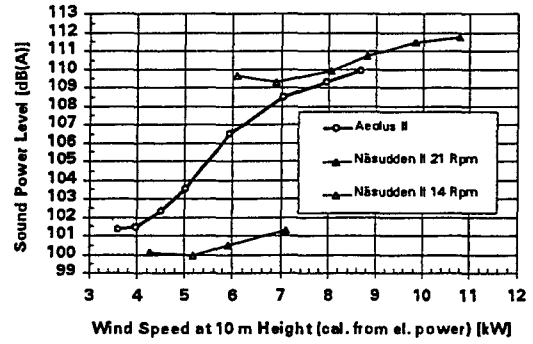

Figure 12: Emitted Noise versus wind speed at 10 m height. The sound power levels for reference conditions (8 m/s) are 109 dB(A) and 110 dB(A) for the Aeolus II and Näsudden II, respectively.

REFERENCES

[1] H. Klug, D. Westermann; Anemometer Calibration or „The answer is blowin' in the wind"; DEWI-magazine No. 7, 1995

[2] G. Ronsten; Technical data and calibration procedures for the SMHI-meteorological equipment of the Näsudden peninsular; FFA TN 1996-24, Stockholm 1996.

[3] IEC; Power Performance Measurement Procedure, IEC TC 88 WG 6,1994

[4] IEA; Recommended Practices for Wind Turbine Testing and Evaluation, 1. Power Performance Testing; 2. Edition 1990, Risø National Laboratory, DK 4000 Roskilde

[5] R. B. Stull; an introduction to boundary layer meteorology; Kluwer Academic Publishers, 1988

[6] IEA; Recommended Practices for Wind Turbine Testing and Evaluation, 4. Acoustics, Measurements of Noise Emission from Wind Turbines; 3. Edition 1994, Dept. of Fluid Mechanics Technical University of Denmark, DK 2800 Lyngby

ACKNOWLEDGEMENT

This work is sponsored by the National Board for Industrial and Technical Development, Sweden (NUTEK), and Vattenfall AB and cofunded by the European Commission under the contract Jou 2-CT93-0394. Thanks belong also to PreussenElektra and MBB for the allowance and support of the measurements at the Aeolus II.

Appendix 20

National Evaluation of Näsudden II, NEON

G. Tunell, A. Andersson, G. Olsson, G. Ronsten, H. Ganander, B. Göransson, B. Simonsson

NATIONAL EVALUATION OF NÄSUDDEN II, NEON

Georg Tunell, Vattenfall Utveckling AB, S-814 26 ÄLVKARLEBY
Anders Andersson & Göran Olsson, Vattenfall AB, Box 88, S-620 20 KLINTEHAMN
Göran Ronsten, FFA, Box 11021, S-161 11 BROMMA
Hans Ganander, Teknikgruppen AB, Box 21, S-191 21 SOLLENTUNA
Bengt Göransson, Kværner Turbin AB, Box 1005, S-681 01 KRISTINEHAMN
Bengt Simonsson, KM Akustikbyrån, Box 7124, S-171 05 SOLNA

Abstract: Vattenfall, the main electric utility in Sweden, is operating the Näsudden II turbine (3 MW, Ø 80 m) which was erected in October 1992 on the island of Gotland in the Baltic Sea. An evaluation program (National Evaluation of Näsudden II, NEON) is carried out by Vattenfall in co-operation with FFA, Teknikgruppen, Kværner Turbin and others. This paper presents results from the evaluation of power production, availability, power performance, structural behaviour, sub-system performance and noise emission. Comparisons with the 'sister' machine Aeolus II in Wilhelmshaven, Germany are carried out in the research program CAN (Comparison Aeolus II - Näsudden II) within WEGA II.

Keywords: Wind Turbines (HAWT), Large Machines , Performance, Reliability, Vibration, Control Systems, Noise

1. INTRODUCTION

The Näsudden II turbine is a modified and improved version of the earlier Näsudden I turbine. New features are two rotational speeds, increased rated power from 2 to 3 MW and the use of a load supporting bed plate. The 75-meter high tower from Näsudden I was kept unaltered. Among the components, the blades have undergone most changes. Instead of heavy steel blades the new ones are made of CFRP/GFRP, which have reduced the blade weight from 20 to 10 tons.

The main purpose of the Näsudden II project is to continue the development of large wind turbines based on the experiences of the Näsudden I turbine and prove that it is possible to increase the availability to a commercially acceptable level. For more details concerning Näsudden I see [1] and [2].

2. PRODUCTION & AVAILABILITY

Näsudden II was grid connected in mars 1993 and commercial operation started in July the same year.

The availability reached 92,6 % during 1994. The annual energy production from 1994 was as high as 6.740 GWh. This has shown that it is possible to reach commercially acceptable availability levels in large machines (even for a prototype).

The somewhat lower availability in 1995 (81,3%) is mainly caused by malfunctions in the yaw and control systems.

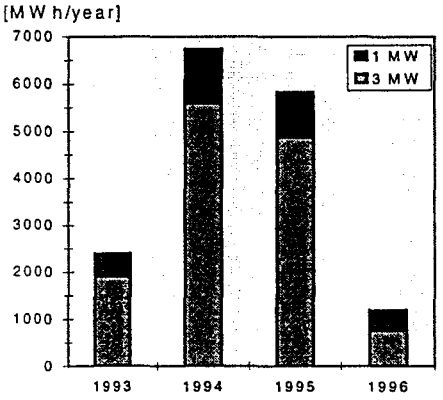

FIGURE 2.1: *Annual energy production; Näsudden II (1993 07 01 - 1996 04 30). 1 and 3 MW corresponds to the generator ratings.*

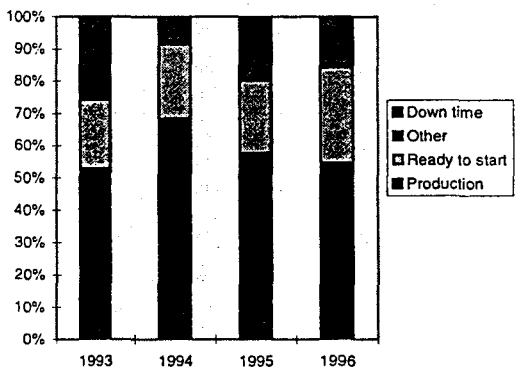

FIGURE 2.2: *Availability for Näsudden II (1993 07 01 - 1996 04 30).*

3. POWER PERFORMANCE

Näsudden II is located in Sweden on the Näsudden peninsula in the south-west corner of the island of Gotland. The winds from the Baltic Sea hit the peninsula's juniper bushes and farmland relatively undisturbed in a sector from 200° to 300°. The distance between Näsudden II and the meteorological tower is 226 m which equals 2.8 rotor diameters

The permitted measurement sector according to IEC [3] during 1994 was 214°-25°. The undisturbed sector decreased to 214°-264°, due to new neighbouring wind turbines during 1995. The black area, in Figure 3.1, marks this measurement sector. The mast influence on the anemometers makes it appropriate to utilise data only within the smaller measurement sector (214°-264°) also during 1994.

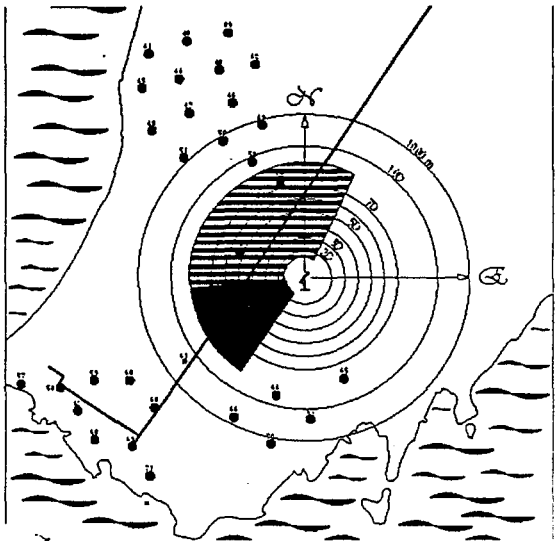

FIGURE 3.1: *Turbines within 20 D from Näsudden II (95 12 31).*

Table 3.1 contains a summary of the measured site parameters as well as production and energy yield (ratio = net production/wind energy contents) during 1994 and 1995.

TABLE 3.1: *Measured values at the Näsudden site.*

	1994	1995
Average wind speed 75 m height [m/s]	7,8	8,0
Ave. turbulence intensity all directions [%]	7,4	7,6
Ave. turbulence intensity (214-264 degrees) [%]	6,5	6,6
Ave. temperature [degrees C]	7,8	7,7
Ave. air density [kg/m^3]	1,24	1,24
Annual energy contents [MWh/m^2/year]	4,9	4,9
Actual production [MWh]	6740	5833
Energy ratio [%]	27,1	23,4

3.1 INFLUENCE OF MEASUREMENT SECTOR

Although the permitted measurement sector according to IEC [3] during 1994 was 214°-25° the resulting power coefficient vary dramatically due to, most probably, mast and boom effects.

The mast and boom effects may be of significant magnitude as reported by Dahlberg [4].

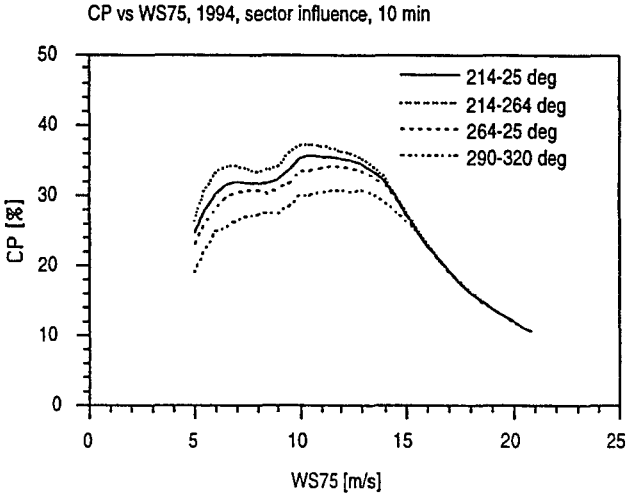

FIGURE 3.2: *Influence of measurement sector selection on power coefficient during 1994.*

3.2 POWER PERFORMANCE

The difference in power performance between 1994 and 1995 is most probably caused by the replacement of anemometers that took place in February of 1995 as no alterations were made to the control system during 1994 or 1995. The meteorological measurement system used at Näsudden is described by Ronsten in [5].

The power and thus the estimated annual energy production, is the net output to the grid, i.e. self consumption and transformer losses are subtracted.

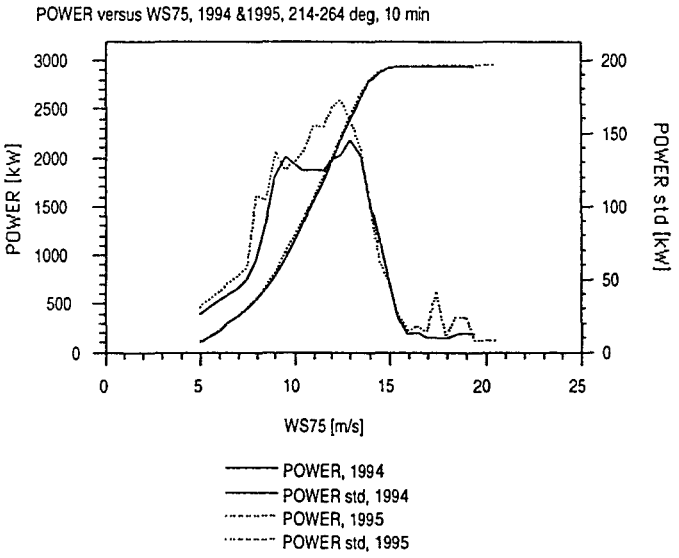

FIGURE 3.3: *Power performance during 1994 and 1995.*

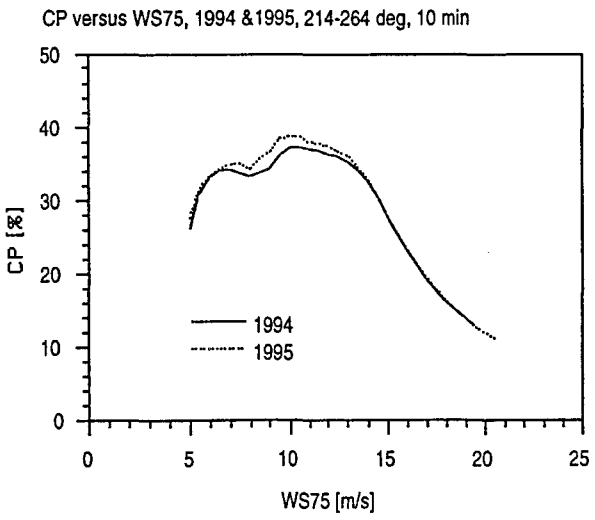

FIGURE 3.4: *Power coefficient during 1994 and 1995.*

TABLE 3.2: *Annual Energy Production, AEP (IEC).*

AWS	AEP-meas.	AEP-std. un-cert.	AEP-std. un-cert.	AEP-extra-polated	Comm-ent
[m/s]	[MWh]	[MWh]		[MWh]	
4	1020	321	32%	1020	
5	2174	506	23%	2175	
6	3766	699	19%	3770	
7	5607	854	15%	5648	
8	7426	951	13%	7604	
9	8990	994	11%	9456	
10	10171	997	10%	11069	Incomplete
11	10944	971	9%	12365	Incomplete

4. STRUCTURAL LOADS AND DYNAMICS

4.1. INTRODUCTION

Main objectives of this technical evaluation project is to

- understand the dynamic behaviour of the turbine
- verify computational tools
- identify and introduce possible improvements of the turbine
- gain experience and prepare for the next generation of wind turbines

These goals are set to be reached within the following evaluation activities:

- eigen-frequencies at high wind speeds with horizontally and vertically parked feathered rotor
- frequencies at normal steady operation
- loads and motions at normal operation as well as transients and extremes
- fatigue of main components

Some of these evaluations will also be used for comparison with measurements performed at Aeolus II, which is the German 'sister' turbine to Näsudden II. Two interesting features of the Aeolus II turbine are the variable speed concept and the soft tower.

4.2. MEASUREMENTS

The measurement system is built on a commercially available distributed measurement system. All signals are acquired continuously and stored to Video 8 tapes. Mechanical signals are sampled at 20 Hz, while the sampling frequency of meteorological data is 0.1 Hz. At low wind speeds, with the turbine at stand still, the sampling frequency of mechanical signals is reduced to 1 Hz. Full sampling capacity is also used when the turbine is parked at high wind speeds. Total amount of data per tape is ≈ 5 Gb. With about 50 signals and the used sampling frequencies tapes are being filled in approximately one month.

4.3. EVALUATED QUANTITIES

The structural evaluation is mainly based on strain gauges, and accelerometers. All six load components of each blade root are evaluated through strain gauges at the blade roots. This is also true for loads at the cylindrical steel adapter between the nacelle and the tower top. Accelerometers are used to measure all three translations and three rotations of the nacelle, which is regarded as rigid. Some position sensors are also used to indicate turbine, pitch and yaw angles.

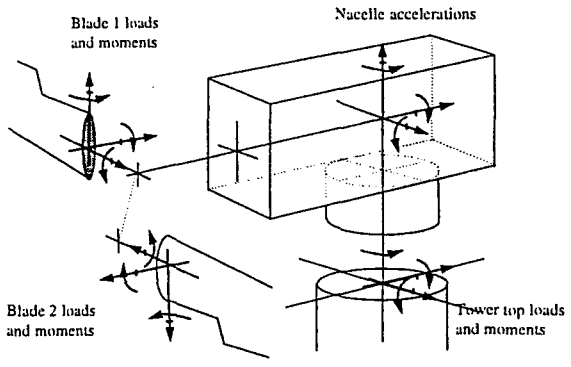

FIGURE 4.1: *Evaluated loads and accelerations at the two blade roots, nacelle and tower.*

This whole set of signals and load quantities makes it possible to get a rather complete picture of the load situation at the rotor centre. Comparing these loads with loads at the tower top and taking inertia influences of the nacelle into account makes it possible to obtain a good understanding of the dynamic coupling between the rotor and the tower.

A significant effort has been devoted to calibration of the load signals. Normal simple slow inching of the rotor could not be used for calibration due to the obvious non-linear behaviour of the signal to load relationship [6]. The gauges are, due to practical limitations, placed too close to the blade bearings. A

calibration method, using start up as well as shut down procedures, has been developed in order to enable calibration of all blade root signals.

Tower bending moment signals are calibrated by inching the nacelle. The shear loads are based on calculations of the strain gauges and the material properties.

Finally, the six accelerometers are directly used in six equations describing the translations and rotations along the chosen x -,y - and z - axes.

4.4. Preliminary results

The evaluation started formally in May 1995. Until now a great deal of work has been carried out calibrating load signals. Emphasis is set towards understanding and verification. Evaluation of different transients and extremes have high priority.

4.4.1 Frequencies

TABLE 4.1: *Eigen-frequencies at horizontal, feathered and parked conditions.*

Eigen freq. [Hz]	1,15	1,37	1,52	1,70	2,35	2,90	3,20
# cycles/ revoultion at 14 rpm	4,9	5,9	6,5	7,3	10,1	12,4	13,7
# cycles/ revoultion at 21 rpm	3,3	3,9	4,3	4,9	6,7	8,3	9,1
acc.x		1,35					
acc.y							
acc.z							
racc.x			1,55				3,20
racc.y							3,20
racc.z		1,35					
Myaw		1,40					
Mpitch							
Mroll							
Medge1		1,40					
Mflap1	1,15		1,55	1,70			
Mpitch1	1,15	1,35		1,70			
Fedge1			1,50				
Fflap1		1,35	1,55	1,70	2,35		
Fnorm1		1,35					
Medge2		1,40					
Mflap2			1,50	1,70			
Mpitch2	1,15				2,35	2,90	3,20
Fedge2						2,90	
Fflap2	1,15			1,70			
Fnorm2	1,15		1,50				
Clear peak				Weak peak			

Introductory activities were therefore concentrated on structural properties of the turbine, important for further calculations and analysis. Situations at high wind speeds with the turbine parked and feathered have been used for identification of the eigen-frequencies of the turbine at stand still. This is not ideal due to the above mentioned non-linear blade root signals, but some information could still be used.

4.4.2 Example of Extreme Dynamics

Two kinds of extreme dynamic events have been found. The first event leads to strong c-edge mode vibrations that seem to be initiated by a slipping yaw motions.

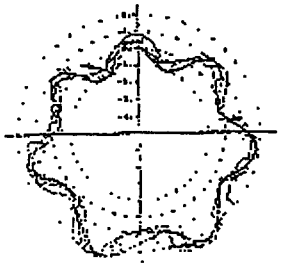

Polar Plot [0-360°]

Time Series [h]

FIGURE 4.2: *Time series and polar plot of C-edge vibration.*

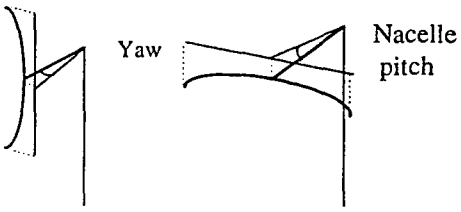

FIGURE 4.3: *C-edge coupling with nacelle yaw and pitch at two rotor positions.*

The second observed dynamic situation is a pure longitudinal vibration. All details about this vibration mode are not yet fully investigated.

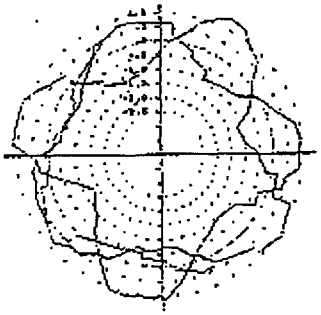

Polar Plot [0-360°]

Time Series [h]

FIGURE 4.4: *Time series and polar plot of longitudinal acceleration at top of tower.*

FIGURE 4.5: *Rotor and tower coupled vibration mode.*

4.5. CONTINUATION

This is the result of the mechanical evaluation up to now. The continued work is aiming towards understanding the extreme dynamic situations that have been found. The yaw properties and the relatively complex structural coupling between the nacelle and the tower are believed to be of key interest. The stiffness of the nacelle, including bearings and other coupling elements, is relatively low compared with the tower. This may explain the c-edge and yaw dynamics as well as the longitudinal vibrations.

5. CONTROL SYSTEM PERFORMANCE

Kværner Turbin AB has, as manufacturer of Näsudden II, been involved in the evaluation programme. The first task has been to investigate some properties of the control system.

5.1. POWER CONTROL

The turbine has full span pitch blade control. The blades are manoeuvred by means of a yoke and a rod actuated by a hydraulic servo cylinder. The evaluation has given the following results:

- The average power is close to rated 3 MW. The turbine is seldom stopped due to poor power control.
- There is a relatively large frequency component of 2P in the power spectrum as the rotor is two-bladed. This component is not regulated by the control system. The high slip asynchronous generator provides some damping of the 2P-component.
- Only a minor portion of the pitch system capacity is used at normal power control.

5.2. YAW SYSTEM

The yaw system consists of two hydraulic gear motors and four mechanical brakes. The turbine is yawed when the rotor misalignment reaches a limit value compared with the filtered wind signal. The brakes are released at yawing. Some of the results are:

- The yaw speed is 0.3° - 0.4°/second.
- The yaw system operates up to 120 times/day. This large number is probably caused by the poor measurement of wind direction.
- The average wind direction on the nacelle is compared with the wind direction at the meteorological mast and only small errors have been detected.
- The wind direction is followed sufficiently well.
- During certain situations, as shown in the diagram below, the brake is not able to hold the turbine in stand still. The turbine starts to oscillate, slips away and a yaw manoeuvre is initiated.

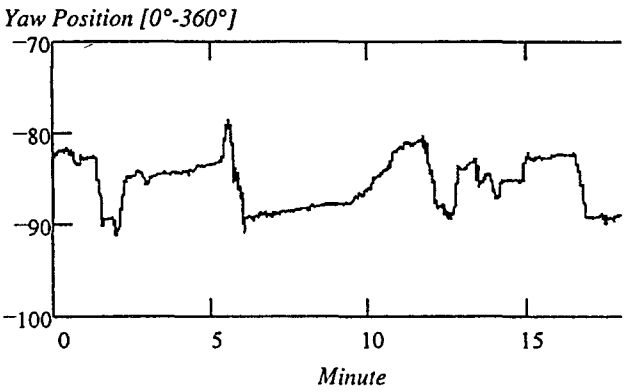

FIGURE 5.1: *Typical yaw behaviour.*

5.3. SPEED CHANGE

The turbine operates at two constant rotor speeds, 14 and 21 rpm. The generator ratings are 1 and 3 MW.

- During days with high winds, speed changes occurs 3 to 4 times/day.
- Total number of speed changes during 1995 was 855.
- The change of rotor speed takes about 120 s.
- The annual loss due to rotational speed changes is about 35 MWh, corresponding to 0.5 % of the total energy.

5.4. IMPROVEMENTS

Some improvements are suggested to increase the performance of the wind turbine:

- The 2P power signal could be controlled.
- The average capacity of the pitch system could be decreased.
- The time constant of the yaw control system can be increased to reduce the number of yaw manoeuvres.

6. NOISE EMISSION

Measurements of noise emission from the Näsudden II wind turbine have been carried out between April 18 - 19, 1995 at the sight on Gotland.

The apparent A-weighted sound power level for 21 rpm at 8 m/s is;

$L_{WA,\,ref}$ = **111 dB**

and estimated uncertainty of the apparent A-weighted sound power level is;

s= **0,7 dB.**

For 14 rpm the apparent A-weighted sound power level at 8 m/s is;

$L_{WA,\,ref}$ = **102 dB**

and estimated uncertainty of the apparent A-weighted sound power level is;

s= **1,2 dB.**

Corrections have been made for the background noise. The equivalent continuous A-weighted sound level from the wind turbine has been determined to 62 dB(A) at 118 m distance from the base of the wind turbine with a wind speed of 8 m/s. The measurements were made according to the Recommended Practices submitted to the IEA Programme for R&D on Wind Energy Conversion Systems.

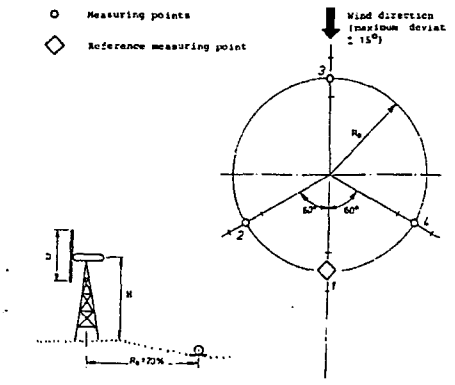

FIGURE 6.1: *Positions for noise emission measurements according to IEA [7].*

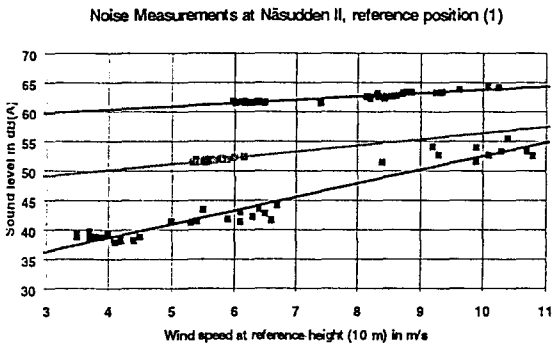

FIGURE 6.2: *Turbine noise levels for 21 rpm and 14 rpm in reference position (1) and background noise levels versus wind speed.*

At a distance of 240 m the noise decreased around 6 dB which for the lower rotational speed led to noise levels close to the background level.

TABLE 6.1: *Turbine noise level for 21 rpm and 14 rpm and backgrund noise in the different measurement positions in A-weighted sound levels, dB(A).*

Position	21 rpm	14 rpm	Background
1 (Reference)	62	53	48
2	64	55	49
3	64	57	48
4	65	56	47

REFERENCES

[1] The third generation of 3 MW wind turbines in Sweden, Pär Svensson, Bengt Göransson, EWEC 1994, Thessaloniki

[2] Evaluation of Loads measured at the two Swedish prototypes. Hans Ganander. EWEA 7-9 October 1986 in Rome

[3] IEC - TC 88 WG 6 - Wind Turbine Generator Systems, "Part 12 - Power Performance Measurements Techniques", CDV 2/8-1995

[4] Dalberg J-Å - "Mast, Boom & Velocity Gradient Effects on Cup Anemometers" FFAP-V-009, Stockholm, 1996

[5] Ronsten G. - "Technical data and calibration procedures for the SMHI-meteorological equipment at the Näsudden peninsula", FFA TN 1996-24, Stockholm, 1996

[6] Calibration Procedures for Improved Accuracy of Wind Turbine Blade Load Measurements, J.Å. Dahlberg, H. Johansson, EWEC 1996, Göteborg.

[7] Recommended Practices for Wind Turbine Testing and Evaluation, 4. Acoustics Measurement of Noise Emission from Wind Turbines, IEA 1994.

Utgivare	Beteckning		
Flygtekniska Försöksanstalten Box 11021 161 11 BROMMA	FFA 1996-36		
	Datum September 1996	Sekretess Öppen	Ex nr
	Dnr 306/94-23	Antal sidor 22 + App 1 t.o.m. App. 20 + docsida	
Uppdragsgivare	Projektnr	Beställning	
NUTEK 117 86 STOCKHOLM	VU-0073	P2939-1 Vindkonsortiet Dnr 8624-94-5646	

Rapportens titel

Vindkraftskonsortiet
FFA MIUU CTH

Sammanställning av föredrag vid EUWEC'96 i Göteborg

Författare

Sven-Erik Thor SE

Granskad av	Godkänd av

Sammanfattning

Den Europeiska Unionen arrangerar vart tredje år en konferens och utställning, European Union Wind Energy Conference and Exhibition, EUWEC. I år arrangerades EUWEC´96 i Göteborg. Vart tredje år arrangerar dessutom European Wind Energy Association, EWEA, sin vindenergikonferens. Konferenserna är förskjutna ett och ett halvt år inbördes. Det innebär att det i Europa arrangeras vindkonferenser var 18:e månad.

I denna rapport redovisas de svenska föredrag som har anknytning till vindkraftkonsortiet.

Nyckelord
Vindkraftskonsortiet, EUWEC´96, Vindkraft

Distribution

	NUTEK	VKK Styrelse	FFA
Antal ex/ex nr	1-10	11-25	26-70